Numerical Study of Pulsatile Flow through Stenosed Artery

Thesis submitted by Partha Goswami

Doctor of Philosophy (Engineering)

Department of Mechanical Engineering
Faculty Council of Engineering & Technology
Jadavpur University
Kolkata, India

2018

JADAVPUR UNIVERSITY
KOLAKATA-700032, INDIA

INDEX NO. 191/13/E

1. Title of the thesis:

Numerical Study of Pulsatile Flow through Stenosed Artery

2. Name, Designation & Institution of the Supervisors:

1. Dr. Dipak Kumar Mandal

Associate Professor, Department of Mechanical Engineering,

College of Engineering and Management, Kolaghat, Purba Medinipur

2. Dr. Nirmal Kumar Manna

Associate Professor, Department of Mechanical Engineering

Jadavpur University, Kolkata

3. Dr. Somnath Chakrabarti

Professor, Department of Mechanical Engineering

Indian Institute of Engineering, Science and Technology, Shibpur, Howrah

3. List of publication:

Journal Publications:

1. P. Goswami, D. K. Mandal, N. K. Manna, S. Chakrabarti, Study on the Effect of Steady, Simple Pulsatile and Physiological Pulsatile Flows through a Stenosed Artery, Heat and Mass Transfer (2014) 50 (10), 1343-1352

2. P. Goswami, D. K. Mandal, N. K. Manna, S. Chakrabarti, Wall Shear Stress Characteristics for the Progression of the Disease, Atherosclerosis, Journal of The Institution of Engineers (India): Series C (2015) 96 (3), 311-323

3. P. Goswami, D. K. Mandal, N. K. Manna, S. Chakrabarti, Analysis of Steady and Physiological Pulsatile Flow Characteristics in an Artery with Various Percentages of Restrictions, International Journal of Fluid Mechanics Research (2015) 42 (3), 260-280.

4. P. Goswami, D. K. Mandal, N. K. Manna, S. Chakrabarti, Analysis of Wall Shear Parameters of Physiological Pulsating Flow through Mild and Severe Arterial Stenosis and Correlation to Atherosclerosis, International Journal of Science and Technology (2016), 2(3), 40-54.

5. P. Goswami, D. K. Mandal, N. K. Manna, S. Chakrabarti, Numerical Investigation of Various Aspects of Plaque Deposition through Constricted artery, Journal of Mechanical Engineering and Sciences (under final review).

International Conference Publications:

1. P. Goswami, D. K. Mandal, N. K. Manna and S. Chakrabarti, Comparison of Steady, Simple Pulstile and Physiological Pulsatile Flow through a Stenosed Artery, Proc. of the International Conference on Advances in Mechanical Engineering and Its Interdisciplinary Areas, CEMK, Kolaghat, Purba Medinipur, India, 27-28 December, 2012, Paper ID: TF 14

2. P. Goswami, D. K. Mandal, N. K. Manna and S. Chakrabarti, Study on Shear Flow Characteristics in a Stenosed Human Artery for Initiation and Progression of Atherosclerosis, Proc. of 58th Congress Indian Society of Theoretical and Applied Mechanics (An International Conference), Indian Institute of Engineering, Science and Technology, Shibpur, Howrah, India, 18-21 December, 2013. Paper ID: 58-ISTAM-FM-FP-55

3. P. Goswami, D. K. Mandal. N. K. Manna and S. Chakrabarti, Numerical Simulation on Physiological Pulsatile Fluid Flow through a Constricted Artery of Human Being-From the Perspective of Womersley Number, Proc. of 22nd National and 11th International ISHMT-ASME Heat and Mass Transfer Conference, 28-31 December, 2013, IIT Kharagpur, India. Paper ID: HMTC 1300361

4. P. Goswami, D. K. Mandal, N. K. Mann and S. Chakrabarti, Fluid Dynamics Study of Physiological Pulsatile Flow through Stenosed Artery, Proc. of the 2nd International Conference on Advances in Mechanical Engineering and its Interdisciplinary Areas, 2-4 January, 2015, CEMK, Kolaghat, Purba Medinipur, India, Paper ID: TF 37

5. P. Goswami, D. K. Mandal, N. K. Mann and S. Chakrabarti, Analysis of Wall Shear Parameters of Physiological Pulsatile Flow through Mild and Severe Arterial Stenosis and Correlation to Atherosclerosis, Proc. of 3rd International Conference on Researches in Science and Technology, 30 July- 1 June, 2016, Nanyang Technological University, Nanyang Executive Centre, Singapore, Paper ID: GICICRST1604055

6. P. Goswami, D. K. Mandal, N. K. Manna and S. Chakrabarti, Investigation of Low and Oscillatory Wall Shear Stress in Realistic Pulsatile Flow through Stenosed Artery, Proceedings of the 1st International Conference on Mechanical Engineering, January 4 – 6, 2018, Jadavpur University, Kolkata India , Paper No. INCOM18-248, pages 341-344

National Conference Publication:

1. P. Goswami, D. K. Mandal, N. K. Manna and S. Chakrabarti, Study of Pulsatile Flow on Numerical Modeling of Early Atherosclerotic Lesions, Proc. of National Conference on Innovation in Mechanical Engineering, Singhad Institute of Technology, Lonavala, Pune, Maharashtra, India, 19-20 April, 2012, Paper ID ME-29.

4. List of Patents: NIL

5. List of Presentation in National/International Conferences/workshops:

Paper presentations:

1. P. Goswami, D. K. Mandal, N. K. Manna and S. Chakrabarti, Study of Pulsatile Flow on Numerical Modeling of Early Atherosclerotic Lesions, National Conference on Innovation in Mechanical Engineering, Singhad Institute of Technology, Lonavala, Pune, Maharashtra, India, 19-20 April, 2012, Paper ID: ME 29.

2. P. Goswami, D. K. Mandal, N. K. Manna and S. Chakrabarti, Comparison of Steady, Simple Pulstile and Physiological Pulsatile Flow through a Stenosed Artery, International Conference on Advances in Mechanical Engineering and Its Interdisciplinary Areas, CEMK, Kolaghat, Purba Medinipur, India, 27-28 December, 2012, Paper ID: TF 14

3. P. Goswami, D. K. Mandal, N. K. Manna and S. Chakrabarti, Study on Shear Flow Characteristics in a Stenosed Human Artery for Initiation and Progression of Atherosclerosis, 58th Congress Indian Society of Theoretical and Applied Mechanics (An International Conference), Indian Institute of Engineering, Science and Technology, Shibpur, Howrah, India, 18-21 December, 2013. Paper ID: 58-ISTAM-FM-FP-55

4. P. Goswami, D. K. Mandal, N. K. Mann and S. Chakrabarti, Fluid Dynamics Study of Physiological Pulsatile Flow through Stenosed Artery, 2nd International Conference on Advances in Mechanical Engineering and its Interdisciplinary Areas, 2-4 January, 2015, CEMK, Kolaghat, Purba Medinipur, India, Paper ID: TF 37

5. P. Goswami, D. K. Mandal, N.K. Mann and S. Chakrabarti, Analysis of Wall Shear Parameters of Physiological Pulsatile Flow through Mild and Severe Arterial Stenosis and Correlation to Atherosclerosis, 3rd International Conference on Researches in Science and Technology, 30 July- 1 June, 2016, Nanyang Technological University, Nanyang Executive Centre, Singapore, Paper ID: GICICRST1604055

6. P. Goswami, D. K. Mandal, N. K. Manna and S. Chakrabarti, Investigation of Low and Oscillatory Wall Shear Stress in Realistic Pulsatile Flow through Stenosed Artery, Proceedings of the 1st International Conference on Mechanical Engineering, January

4 – 6, 2018, Jadavpur University, Kolkata India , Paper No. INCOM18-248, pages 341-344

Poster presentation:

1. P. Goswami, D. K. Mandal, N. K. Manna and S. Chakrabarti, Study on Shear Flow Charecteristics in a Stenosed Human Artery for Initiation and Progression of Atherosclerosis, 22nd National & 11th ISHMT-ASME Heat and Mass Transfer Conference, 28-31 December, 2013, IIT Kharagpur, India, Paper ID: HMTC1300361

CERTIFICATE FROM THE SUPERVISORS

This is to certify that the thesis entitled "**Numerical Study of Pulsatile Flow through Stenosed Artery**" submitted by Shri PARTHA GOSWAMI, who got his name registered on 3rd July, 2013 for the award of Ph. D. (Engineering) degree of Jadavpur University, is absolutely based upon his own work under the supervision of Dr. Dipak Kumar Mandal, Dr. Nirmal Kumar Manna and Dr. Somnath Chakrabarti and that neither his thesis nor any part of the thesis has been submitted for any degree/diploma or any other academic award anywhere before.

_____ _____

1. Signature of the Supervisor
and date with Office Seal

2. Signature of the Supervisor
and date with Office Seal

_____

3. Signature of the Supervisor
and date with Office Seal

This thesis is dedicated to

our beloved twin sons

Priyan and Diyan

ACKNOWLEDGEMENT

I would like to express my special appreciation and thanks to my thesis supervisors Dr. Dipak Kumar Mandal, Dr. Nirmal Kumar Manna and Dr. Somnath Chakrabarti. They have not only showed me the art of doing research but also the science of being professional and human at the same time. It will not be possible for me to pen down without the deep gratitude I feel toward Dr. Mandal in a line or two. His gentle guidance and persistent encouragement will be treasured memories forever. The advice on my research from Dr. Manna is priceless. The interaction with Dr. Chakrabarti was the most important facets in my research. His valuable guidance helped me in writing this thesis. I want to express my thanks to Neptune Lab, Department of Mechanical Engineering, Jadavpur University and CFD Lab, Department of Mechanical Engineering, College of Engineering and Management, Kolaghat.

Heartfelt thanks go with love to my wife, Debasmita, for giving me encouragement and showing much needed patience. Finally, my parents, elder brother, my mother-in-law, my other family member, my colleagues and all the friends who helped me along the way, I extend my most sincere gratitude. I am filled with reminiscences of my father-in-law, who gave me the initial thrust. Unfortunately, he is not with us anymore to see my growing. My sincere thanks go to Dr. Nirmulendu Biswas and Mr. Tarun Kanti Paul, who always extended their help and best co-operation to me at the hours of need. I am also grateful to the authorities of West Bengal Power Development Corporation Limited, who were kind enough to allow me for carrying out my research endeavor. Finally, I am grateful to the authorities of Jadavpur University for giving me permission to pursue my PhD work and to submit my thesis in Jadavpur University.

Date:……..

Jadavpur University, Kolkata – 700 032

(*Partha Goswami*)

CONTENTS

ABSTRACT

A stenosis is a narrowing, restriction or constriction of the inner surface of the artery, usually caused by atherosclerosis. Atherosclerosis, a cardiovascular disease, occurs as a result of the buildup and infiltration of lipid streaks in artery walls, leading to plaques. Plaque is made up of fat, cholesterol, calcium, and other substances found in the blood. Over time, plaque hardens and narrows our arteries. Atherosclerosis can affect any artery in the body, including arteries in the heart, brain, arms, legs, pelvis, and kidneys. As a result, different diseases, coronary heart disease, carotid artery disease, peripheral artery disease and chronic kidney disease, may develop based on which arteries are affected. Atherosclerosis can lead to various complications like myocardial infarction, stroke, ulceration, thrombosis and aneurysm, thus affecting the human life span and quality of life of a large segment of population. The understanding of the development of atherosclerosis is of critical importance. The hemodynamic behavior of blood flow in arterial stenosis bears some important aspects due to engineering interest as well as feasible medical applications.

From the literature review, it is revealed that many investigators have contributed to the understanding for study of blood flow through stenosed artery and the knowledge in this field is still inadequate. Very few have considered the realistic shaped stenosis and physiologically realistic flow parameters. A systematic study considering all parameters is again missing. Keeping in mind the review of literatures, the present work is focused to carry out a systematic numerical study on the effects of different pulsatile flow profiles through axisymmetric bell shaped stenosis for various geometries of stenosis with respect to percentage of restriction and for flow parameters such as Reynolds number and Womersley number on fluid flow characteristics such as, wall pressure, stream line contour representing recirculation zone, peak time-averaged wall shear stress, low time-averaged wall shear stress and oscillatory shear index in details. In this thesis, an attempt has been made to study numerically on the flow characteristics of pulsatile flow through bell shaped stenosed artery at the stenotic zone and post-stenotic zone for the Reynolds numbers ranging from 50 to 200, Womersley numbers ranging from 5 to 12.5 and the percentage of restriction ranging from 30% to 70% (by diameter). Three different pulsatile profiles, i.e., simple pulsatile profile, physiological pulsatile profile and realistic pulsatile

profile, have been considered at the inlet of considered geometries of the modeled artery. The objective of the present work also includes investigation of the impact of the flow characteristics on the possibilities of initiation, progression and formation of the disease, atherosclerosis with respect to Reynolds numbers, percentage of restriction and Womersley numbers.

In the present work, the numerical solutions are obtained under the conditions of homogeneous, incompressible and Newtonian fluid through axially symmetric rigid stenosis. The blood flow has been considered as two-dimensional, laminar and pulsatile flow. The discretized forms of the governing equations (i.e. the continuity and Navier-Stokes equations in two-dimensional cylindrical co-ordinates (r,z)) have been obtained by a control volume formulation in non-uniform staggered grid. The equations have been solved numerically by the in-house CFD code developed using integral approach of the finite volume method following SIMPLER (Semi-Implicit Method for Pressure Linked Equations Revised) algorithm. The distributions of grid nodes have been considered in both coordinate direction allowing higher grid node concentrations in the region close to the wall and restriction. The third-order upwind scheme has been used for advective part. The discretized equations have been solved iteratively using line-by-line Tri-diagonal Matrix Algorithm (TDMA) with Alternate Direction Implicit (ADI) scheme.

From the simulation results, time-averaged wall pressure, time-averaged wall shear stress and oscillatory shear index have been computed. The streamline contours have also been plotted to investigate the flow fields. The detail study on the effect of Reynolds number, Womersley number and percentage of restriction for simple pulsatile flow has been made at first. The results of three different pulsatile flows are compared by evaluating the effect of Reynolds number, Womersley number and percentage of restriction on the flow characteristics.

The wall pressure drop strongly is influenced by types of pulsatile flow condition (simple pulsatile, physiological pulsatile and realistic pulsatile). The largest pressure drop is observed for physiological pulsatile flow condition while the realistic pulsatile flow condition has the least pressure drop. The chances of atherosclerotic plaque deposition are more for physiological pulsatile flow and less for realistic pulsatile flow. With an increase in Reynolds number, the wall pressure drop increases. Wall pressure drop increases slowly for mild to moderate stenosis, whereas from moderate to severe stenosis condition, this pressure drop increases markedly for all

pulsatile flow conditions. For all pulsatile flow conditions, the effect of wall pressure on Womersley number is not so evidenced.

At the time step t/T=0, for flow through mild stenosis, the smaller flow separation zone is found for simple pulsatile flow condition. The chance of development of atherosclerosis is more for physiological and realistic pulsatile flows in comparison to simple pulsatile flow at the said time step for the case of mild stenosis. At time step t/T=0, for flow through severe stenosis, lager flow separation zone is found for realistic pulsatile flow at low Womersley number while the size of flow separation zone is almost same for all pulsatile flow at high Womersley number. At time step t/T=0.25, for flow through mild stenosis, the size of flow separation zone is almost same for all the pulsatile flow condition. At the same time step, flow through severe stenosis, the size of flow separation zone is larger for simple pulsatile flow. At t/T=0.50, for flow through both mild and severe stenoses, the size of flow separation zone is larger for physiological pulsatile flow condition. At time step t/T=0.75, for flow through mild stenosis, the size of flow separation zone is larger for simple pulsatile flow condition. At the same time step, flow through severe stenosis, the size of flow separation zone is almost same for all the pulsatile flow conditions. Size of the flow separation zone always increases with increase in Reynolds number for all pulsatile flow conditions. The chances of atheromatous plaque formation increases with the increase in Reynolds number and thereby lead to grow more severe stenosis at the post stenotic zone. Size of the flow separation zone always increases with increase in percentage of restriction. For the flow through mild stenosis, with increase in Womersley number, the strength of the flow separation zone decreases at every time step. For the flow through severe stenosis, the strength of the flow separation zone decreases with increase in Womersley number at the time steps of t/T=0.25 and t/T=0.5 for each pulsatile flow conditions. Therefore, possibility of plaque deposition is higher for low value of Womersley number for the case of severe stenosis at time steps of t/T=0.25 and t/T=0.5. The strength of the flow separation zone increases with increase in value of Womersley number at the time steps t/T=0 and t/T=0.75 for flow through severe stenosis in all considered pulsatile flow conditions.

The peak WSS for realistic pulsatile flow condition is much higher than the peak WSS with either of the simple pulsatile flow condition or physiological pulsatile flow condition. The damaging chance of artery wall and subsequently chance of

initiation of atherosclerosis are more for realistic pulsatile flow condition. The Peak wall shear stress always increases with increase in Reynolds number for all pulsatile flow conditions. The peak wall shear stress increases with the increase in percentage of restriction for all considered pulsatile flows. The peak WSS slightly decreases with increase in Womersley number. The damaging chance of artery wall is less for higher Womersley number.

At low Womersley number, the lowest magnitude of maximum low WSS occurs at simple pulsatile flow and the highest magnitude takes place in case of realistic pulsatile flow. But, at high Womersley number, the lowest magnitude of maximum low WSS is noticed for realistic pulsatile flow. The chance of progression of the disease, atherosclerosis is high for realistic pulsatile flow condition at low Womersley number. The chance of progression of the atherosclerosis, in terms of the mass transportation across the arterial wall and long staying time for platelet endothelium interaction, is high for both simple and physiological pulsatile flows at high Womersley number. The maximum low WSS always increases with increase in Reynolds number, percentage of restriction and Womersley number separately while other conditions remain unchanged for all the pulsatile flow conditions. The chances of progression of the atherosclerosis increase with increase in Reynolds number, percentage of restriction and Womersley number for all considered pulsatile profiles.

The first peak OSI value is low for realistic pulsatile flow. The realistic pulsatile flow is always less prone to the disease atherosclerosis for each combination case of Reynolds number, percentage of restriction and Womersley number. The first peak OSI also increases with increase in Reynolds number, percentage of restriction and Womersley number for all types of pulsatile flow. The recirculation length for realistic pulsatile flow is very small in comparison to other two types of pulsatile flow. The chance of development of atherosclerosis is least for realistic pulsatile flow condition among all the considered flow conditions. The recirculation length always increases with increase in Reynolds number, percentage of restriction and Womersley number. The chances of atheromatous plaque deposition at the inner wall increase with increase in Reynolds number, percentage of restriction and Womersley number for all pulsatile flow conditions.

Our own developed numerical code may be considered as a useful predictive tool for study of the pulsatile flow through stenosed artery. It is noteworthy to mention here that the outcomes of present work may enrich the knowledge in the area

of cardiovascular disease (CVD) and could also be utilized for better design of medical tool to detect early atherosclerosis as well as severity of atherosclerosis. The systematic study of pulsatile flow may help the medical people to take better decision upon the treatment management of atherosclerosis such as exercise, medication, surgery etc.

NOMENCLATURE

D	Diameter of the artery, [m]
R	Radius of artery, [m]
L	Total length of computational domain, [m]
L_i	Length of computational domain before stenosis, [m]
L_s	Length of stenosis, [m]
L_{si}	Length of upstream stenosis, [m]
L_{se}	Length of downstream stenosis, [m]
L_e	Length of computational domain after stenosis, [m]
h_f	Height of stenosis
u_z	Velocity in z-direction, [ms^{-1}]
u_r	Velocity in r-direction, [ms^{-1}]
U	Average velocity in r-direction at inlet, [ms^{-1}]
μ	Dynamic viscosity, [kg $m^{-1}s^{-1}$]
ρ	Density, [kg m^{-3}]
υ	Kinematic viscosity, [ms^{-2}]
T	Time period of the pulsatile cycle, [s]
t	Time, [s]
p	Static pressure, [Nm^{-2}]
Re	Reynolds Number $= \frac{\rho UD}{\mu}$

Wo	Womersley number $= \frac{D}{2}\sqrt{\frac{2\pi}{\upsilon T}}$
p_w	Wall pressure
τ_w	Wall shear stress (WSS), [Nm^{-2}]
PWSS	Peak wall shear stress
LWSS	Low wall shear stress
TAWSS	Time-averaged wall shear stress
OSI	Oscillatory shear index
PR	Percentage of restriction
r_e	Grid refinement ratio
R_e	Convergence ratio
GCI	Grid convergence index
F_s	Factor of safety
A_c	Asymptotic range of convergence
p_e	Order of accuracy
r, z	Cylindrical co-ordinates
1-1	Inlet
2-2	Exit

Superscripts

*	Dimensionless terms

LIST OF FIGURES

LIST OF TABLES

CHAPTER 1: INTRODUCTION

1.0 INTRODUCTION

1.1 Motivation

The heart, blood and blood vessels are the vital components in a human cardiovascular system. The heart acts as a pump and it delivers oxygenated blood to the body and deoxygenated blood to the lungs. The valves, which are located at the entrances and exits to the ventricles, close and open intermittently with each beat of the heart. Thus the heart causes the blood flow rate to oscillate from zero to very high rates. The blood flows out from the heart through the aorta. All of the major branches of arteries from the aorta carry oxygenated blood to all parts of the body. In order to perform the task of pumping blood, the heart muscle itself needs a plentiful supply of oxygen-rich blood. That oxygen-rich blood is supplied through a network of coronary arteries.

A stenosis is a narrowing or restriction of the inside area (or lumen area) of the artery, usually caused by atherosclerosis. The most common cardiovascular disease is arthrosclerosis. Atherosclerosis occurs as a result of the buildup and infiltration of plaque in artery walls. The plaque is made up of fat, cholesterol, calcium, and other substances found in the blood. Over time, the buildup plaque hardens and then it narrows the artery. The Fig.1.1 shows the normal artery and how artery is narrowed due to plaque development inside the artery wall. From the said figure, it is clearly understandable that the normal artery has no plaque deposition on the artery wall. For the case of narrowed artery, the flow is restricted through the lumen area of artery by the event of the plaque deposition. Atherosclerosis is a chronic degenerative condition of arteries responsible for significant cardiovascular morbidity and mortality. Atherosclerosis can affect any artery in the body, including arteries in the heart, brain, arms, legs, pelvis, and kidneys. As a result, different diseases, coronary heart disease, carotid artery disease, peripheral artery disease and chronic kidney disease, may develop based on which arteries are affected. Atherosclerosis is potentially harmful because the reduced lumen area may cause blood to develop clots, resulting in the formation of embolus or thrombus. The high resistance to blood flow due to existence of stenosis inside artery does not allow

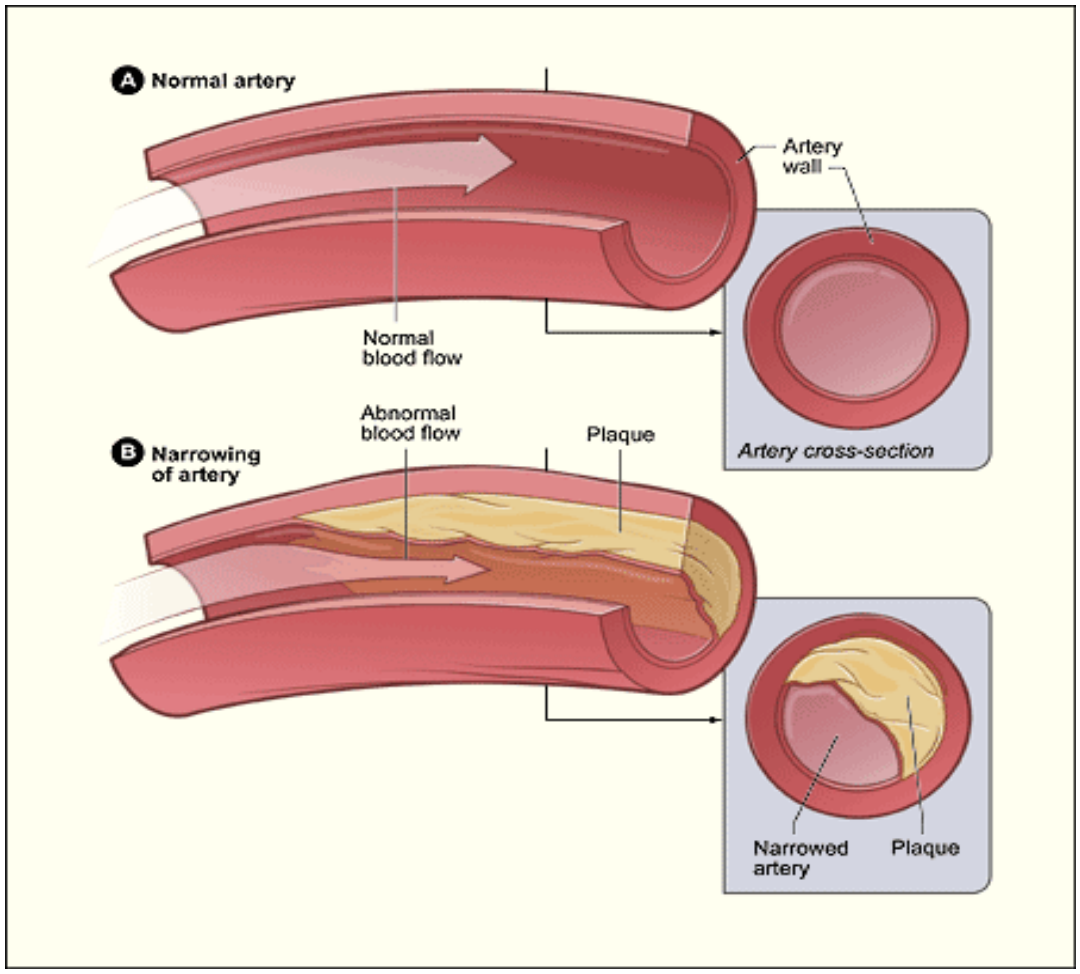

Figure 1.1: Plaque buildup in a healthy artery (NHLBI, 2013)

adequate blood supply to peripheral tissues (Guyton, 1976). Acute clinical conditions, myocardial infarction, stroke and gangrene, may result from the disease, arthrosclerosis (Raines, 1972). Myocardial infarction is a condition when a portion of the heart muscle becomes damaged because of interruption of blood supply to heart muscle by atherosclerotic plaque formation, acute thrombosis. Stroke is a condition when the blood supply to portions of the brain is suddenly reduced by cerebral arterial plaque formation or embolus. Gangrene is a condition when the blood supply to a peripheral tissue mass is reduced due to arterial plaque formation and when the tissue dies.

According to National Heart Lung and Blood Institute, atherosclerosis usually doesn't cause any sign and any symptom until it severely narrows or totally blocks an artery. Many people don't know that they are living the disease, atherosclerosis. They

come to know only when they have a medical emergency, such as a heart attack or stroke. Atherosclerosis can lead to various complications like myocardial infarction, stroke, ulceration, thrombosis and aneurysm. Thus the atherosclerosis affects the human life span and quality of life of a large segment of population. Understanding of the development of atherosclerosis is of critical importance. World Health Organization (2013) reported that an estimated 17.5 million people died from CVDs (Cardio Vascular Disease) in 2012, representing 31% of all global deaths. Of these deaths, an estimated 7.4 million were due to coronary heart disease and 6.7 million were due to stroke. Premature mortality in terms of years of life lost because of cardio vascular disease in India was increased by 59%, from 23.2 million in the year of 1990 to 37 million in the year of 2010, (Prabhakaran et al. 2016).

To counter the problem, early detection of cardiovascular disease and treatment of the disease are necessary with a systematic way. The pharmacologic treatment can be used instead of expensive and complicated surgical procedures. This is only possible when early detection of the development of atherosclerotic lesions can be done. For successful prevention, diagnosis and treatment of cardio vascular disease, a deep understanding of the hemodynamic of the cardiovascular system in disease conditions is needed. The diagnosis of arterial disease is frequently related to the effect of the arterial disease on the pressure, flow patterns and stresses, and their deviations from what is normally found in circulation. The behavior of flow characteristics related to blood flow in arterial stenosis bears some important aspects due to engineering interest as well as feasible medical applications.

In the last few decades, many researchers have studied the influence of blood flow characteristics on the initiation, progression and formation of atherosclerosis. Much of the works on arterial blood flow characteristics has been investigated by means of in vivo experiments in humans and animals and in vitro experiments in hydraulic circulatory models. Computational fluid dynamics have also been used to model the stenosed arterial flow to study the various flow characteristics of arterial blood flow. In the literature, physiological experimental studies are limited by the complexity of in vivo experiments to study the effects of flow characteristics on the atherosclerosis. Whereas the numerical approach often uses simplified models in comparisons to the realistic conditions. This is why; the general agreement of the mechanisms responsible for plaque formation has not yet been reached. In addition, in a large number of cases, the presence of plaques in arteries is asymptomatic. The

prediction of initiation and formation of atherosclerosis remains a complex question to elucidate, not only because of the interaction of numerous phenomena involved in this process (biological, chemical, and mechanical) but also because of the large time scale on which atherosclerosis formed.

At small reduction in radius of artery due to blockage, no symptoms can be felt by human being carrying this disease. When the symptom is felt, the reduction of the radius of artery becomes high, which is detected by angiography. To remove this restriction, angioplasty is advised by the doctors because the disease may not be cured with the help of medicine therapy. Motivation on the study of pulsatile blood flow through a stenosis with different degree of stenosis is felt by the need in obtaining a better understanding on the impact of flow phenomena on initialization, progression and formation of atherosclerosis. It is hoped that such analysis may provide the comparative necessary data to achieve a better understanding of the basic fluid mechanical phenomena in the arterial circulation system. This may help to enhance the knowledge of hemodynamic, cardiovascular response, and the rational design of prosthetic devices and other modifications of vascular systems.

1.2 Role of Fluid Flow Characteristics on Atherosclerosis

From the literatures, it is evident that fluid flow characteristics have significant impact on the initiation, progression and formation of atherosclerosis in the artery wall. The important flow characteristics are wall pressure, streamline contour for representing recirculation zone, peak wall shear stress, low wall shear stress and oscillatory shear index to represent oscillation in wall shear stress.

The wall pressure, the significant fluid flow characteristic, has important role on the development of atherosclerotic plaque. According to Gessner (1973), in the regions of low pressure, a suction action exerted on the endothelium surface eventually causes the layer to be selectively separated from adjacent tissue. This tearing action is considered to cause damage, in turn, of the endothelium and adjacent wall layers, with subsequent thickening of the intimae and eventual plaque development.

The recirculation zone in the post stenotic region is also considered to be an important phenomenon for the formation and propagation of atherosclerosis. As reported by Tu et al. (1992), the physiological significance of the recirculation zone is such a way that the bloodstream stagnates locally in this area and allows platelets and

fibrin to form a mesh at the inner wall. The lipid particles become trapped in the mesh of inner wall and these eventually coalesce to form atheromatous plaque. Thus this may tend to accumulate to cause a more severe stenosis.

The most important fluid dynamic characteristic is the wall shear stress (WSS), which induces a micro environment of interaction between blood and endothelial layer. Since the magnitude of wall shear stress is proportional to the blood viscosity and flow velocity gradient normal to the surface, and acts in a direction parallel to the local velocity at the wall, it is difficult to measure this stress directly in vivo or in vitro. The wall shear stress is generally computed from the local velocity distribution near the wall. This peak wall shear stress damages the artery wall and has also been postulated as a possible initiating factor in atherosclerosis, (Fry, 1968, 1969).

The low wall shear stress causes the progression of atherosclerosis. Low shear stress in the separation region is considered to be related to the mass transportation across the arterial wall and long "dwell time" for platelet endothelium interaction, (Caro et al. 1971).

Low mean shear stress and marked oscillations in the direction of wall shear stress may be critical factors in the development and localization of atherosclerotic plaques. There is also a strong correlation between endothelial dysfunction and temporally oscillating shear stress. A laser Doppler velocimetry study involving pulsatile flow through a model human carotid bifurcation revealed that while plaques grow in regions of low WSS, atherosclerosis development is enhanced by oscillations in wall shear stress. There has a close correlation between intimal thickening and oscillations in wall shear stress. The oscillation in wall shear stress is characterized by an oscillatory shear index (OSI) has been noted by Ku et al. (1985).

1.3 Literature Review

Understanding of flow dynamics and flow disorders due to flow restriction has important practical applications in branches of engineering and also in human cardiovascular system. There are large numbers of investigations which have led to understand of the flow disorders due to stenosis related to many theoretical and experimental studies. The most important research questions are how fluid flow characteristics influence the initiation, localization and formation of atherosclerosis. The other research questions on the study of pulsatile flow through stenosed artery are

about the geometry of stenosis, the sizes of stenosis, the flow parameters and how they are related to the atherosclerosis. What the assumptions may be considered to minimize the complexity of the study are also another research questions. To address the questions, numerous experimental works as well as numerical works have been highlighted chronologically to have a better understanding of the present study.

1.3.1 Experimental studies

There are many of experimental studies carried out by different researchers to study the flow fields having restriction in the flow path. In this sub-section, some important experimental studies have been discussed as below.

Young and Tsai (1973) have investigated experimentally the effects of a cosine shaped stenosis on the steady flow and unsteady flow through a locally constricted tube. They have used axisymmetric and non-axisymmetric models having different area ratio and length of constrictions. They have performed the experiment for the Reynolds numbers varying from approximately 100-5000, area ratios of 56% and 89% considering blood as a Newtonian fluid. They have observed that the pressure falls sharply at the constriction and after the constriction pressure recovery takes place over a length. The dimensionless pressure drop increases with the increase in Reynolds number. Laminar flow separation has been observed at low Reynolds number. The flow becomes locally unstable with the increase in the Reynolds number. They have noted that the pressure drop across stenosis also increases with increase in percent of stenosis and length of stenosis. In their experiment, they have measured the reattachment length and finally they have noted that the reattachment length increases with increase in Reynolds number and decreases with increase in length of stenosis. They have demonstrated that for severe constrictions, the reattachment point is primarily controlled by the area reduction rather than the length of stenosis.

Seeley and Young (1976) have investigated experimentally the pressure drop for different length of stenosis, percentage of stenosis, eccentricity of stenosis, multiple stenoses across an artery with rectangular constriction. They have considered the flow as steady and variation of Reynolds number from 0 to 1000 with 60%, 75%, 85% and 90% area reduction for the non-dimensional stenosis length of 0.5, 1.0, 2.0, 4.0 and 7.8. From their analysis, it is revealed that the non-dimensional pressure drop due to stenosis increases with percentage of restriction and length of stenosis, and increases with Reynolds number. They have also demonstrated that the eccentricity of

the lumen constriction has little effect on the pressure drop with severe stenoses. In case of two stenoses in series, they have observed that if the distance separating the two stenoses is sufficiently large, the pressure drop can be obtained by a simple summation of the pressure drops due to the two individual stenoses. This magnitude of pressure drop decreases with the decrease in distance between the two stenoses.

Azuma and Fulkushima (1976) have done experimental study on the disturbances of blood flow through contoured shaped stenotic blood vessels. They have investigated the effect of Reynolds number on the streamline patterns. In case of axisymmetric constriction, they have observed that at low Reynolds number, the fluid particles moves smoothly near the wall at the divergent part of constriction zone and also found no separation fluid flow at low Reynolds number. The separate of streamline from the wall begins at a divergent part of the constriction while Reynolds number of flow increases. They have noted that the magnitude of the flow separation increases with the decrease in Reynolds number of flow. They have also demonstrated that the reattachment point moves downstream and the separation point moves upstream with the increase in Reynolds number of flow. Further increase in Reynolds number reduces the stability of the wake vortex and caused the shear layer between the main stream and the separated region to fluctuate. They have also noted that vortices form consecutively at the shear layer and shed downstream at higher Reynolds number.

Ahmed and Giddens (1984) have carried out their extensive experimental work by laser Doppler anemometry on pulsatile flow through a straight tube with axisymmetric constrictions of 25, 50 and 75% area reduction. The pulsatile flow condition in the circulatory system was sinusoidal in the range of the Reynolds number 100 to 1000, with the mean Reynolds number of 600 and the frequency parameter of 7.5. They have observed that there exists turbulence at the post stenotic zone for the higher degree of stenosis and Reynolds number. They have also expressed that depending upon the degree of stenosis and the Reynolds number, the flow field contains disturbances of a discrete oscillation frequency of a turbulent nature.

Ojha et al. (1989) have used photo-chromic tracer methods for their experiment. They have measured velocity profile experimentally for the pulsatile flow through different symmetrical constricted tubes for different degrees of blockage. They have studied the flow patterns in tubes with mild to moderate degrees of vessel

constriction considering a 2.9 Hz sinusoidal flow superimposed on a steady flow. The considered Womersley number, mean Reynolds number and modulation Reynolds number are 7.5, 575 and 360 respectively. They have investigated spatial and temporal wall shear stress near the reattachment point.

Liepsch et al. (1992) have carried out an experiment to study the flow behavior in four models of cylindrical stenosis for rectangular shaped constriction with percentage of restrictions of approximately 21%, 45%, 49% and 72% under steady flow condition. During their study, they have considered Re varying from 150 to 920 and a stenosis length of 24 mm. To achieve fully developed flow at inlet, they have considered the non-dimensional inlet length as about 57.85. In their experiment, they have measured pressure drop and reattachment length. Their results have showed that there is no significant change in the magnitude of pressure drop across stenosis of the models with percentage of restrictions of 21%, 45% and 49%. The pressure drop is significant at 72% restriction, especially for higher Reynolds number. They have also computed the non-dimensional wall pressure drop across stenosis, which shows that the said pressure drop increases with percentage of restriction and decreases with Reynolds number. They have observed that at low percentage of restriction of 22%, the flow remains laminar in both the pre and post stenotic regions with recirculation zones close to the stenosis, and the reattachment length increases with the increase in Reynolds number in their considered range of Reynolds number of 920. In case of percentage of restrictions of 45%, 49% and 72%, the reattachment length increases upto certain value of Reynolds number (this value of Reynolds number for 45% restriction model is 500, Reynolds number for 50% restriction model is 350 and Reynolds number for 72% model is 100), then this length decreases with increase in Reynolds number.

1.3.2 Numerical studies for steady flow

Numbers of numerical studies considering steady flow at inlet of modeled artery having stenosis have been done to investigate the flow characteristics having effect on the disease, atherosclerosis. In this sub-section, some significant numerical studies for steady flow have been discussed as below.

Deshpande et al. (1976) have investigated numerically on streamlines, vorticity distribution, flow separation, pressure drop across stenosis, and shear stress for steady laminar flow of a Newtonian fluid through axisymmetric cosine shaped

constrictions in a rigid tube. They have considered the flow with Reynolds number ranging from 0 to 2000 and area reduction ranging from 56% to 89%. They have concluded that the non-dimensional wall pressure drop increases with increase in area reduction and stricture length, but decreases with increase in Reynolds number. From their analysis, it can be revealed that qualitative and quantitative variations of centre line pressure and the wall pressure are more or less same. They have mentioned that both the centre line pressure and wall pressure drop increase with the increase in Reynolds number. Pressure recovery has been observed after stenosis zone. From their study, it is observed that maximum wall shear stress increases with percentage of restriction and Reynolds number, which decreases with increase in stricture length. This maximum value of wall shear stress shifts upstream with increase in Reynolds number.

The pressure and flow patterns for steady, laminar, Newtonian and isothermal flow conditions for several models of stenosed vessels with different constriction ratios of 50%, 75% and 90% for Reynolds numbers of 10, 100 and 200 has been numerically analyzed by Wille (1980). The Navier–Stokes equations are solved by finite element method considering the fluid as incompressible, homogeneous and Newtonian. He has investigated the effect of the shape of the constriction by changing the shape of the stenosis model with a right angle constriction. Out of his two considered models, one is a rectangular constriction and the other one is rounded geometry. He has observed that for moderate and low constriction ratios, the pressure gradient increases slowly with increase in constriction ratio. For high constriction ratios, a small change in the constriction ratio will change the pressure markedly. He has noted that the pressure gradient increases with the increase in Reynolds numbers. From the study, it is revealed that vortex size at the downstream of the stenosis increases with the increase in Reynolds number and stenotic severity. The magnitude of high shear stress has been observed at the upstream portion of the stenosis. The low shear zone is found at the downstream of the constriction where the vortex is situated. From his numerical result for constriction of 75% and Reynolds number of 100 with right angle constriction and round constriction, it has been noted that the shape of the stenosis is having less importance with respect to pressure, and flow patterns.

Ahmed and Giddens (1983) have examined the velocity field and the flow pattern in the neighborhood of axisymmetric cosine shaped constrictions in rigid tubes

using laser Doppler anemometry and flow visualization. The flow conditions at the upstream of stenoses of 25, 50 and 75% area reductions with non-dimensional stricture length of 2.0 are steady, and Reynolds number is in the range of 500-2000. The entrance length of the tube have been taken sufficiently long (96 times of diameter) to ensure full development of the upstream flow. They have estimated wall shear stresses from the near wall velocity gradient. Subsequently the post stenotic flow disturbances are studied by demonstrating a quantitative description of disturbance in velocity. The results indicate that there exists turbulence at the post static zone for the higher degree of stenosis and Reynolds number. It is also expressed that depending upon the degree of stenosis and the Reynolds number, the flow field contains disturbances of a discrete oscillation frequency of a turbulent nature.

The flow behaviour through an artery with cosine shaped stenosis for the area reduction of 64% has been studied numerically by Tandom and Rana (1995). They have considered the fluid model consisting of three layer fluid having purely viscous fluid in the plasmatic layer near the wall, a central core of aggregated cells and an annular layer of a bi-viscous fluid layer in between two layers. In their study, blood flow has been considered to be steady and laminar, and fluid to be non-Newtonian and incompressible. They have considered no-slip boundary conditions at wall, and the normal gradient of the axial velocity and the transverse velocity to be zero at the line of symmetry. The governing non-linear coupled partial differential equations for motion and continuity for two dimensional axisymmetric steady flow have been solved by using finite element method. The velocity fields, separation and reattachment points, and the distribution of pressure and wall shear stress have been discussed in their numerical work for the Reynolds numbers of 15, 30 and 45. From their study, they have observed relatively high velocity at the throat of the stenosis, and the magnitude of the non-dimensional peak velocity increases with Reynolds number. The wall shear stress attains a maximum value on the throat and then it decreases to a minimum value away from the stenosis. The magnitude of peak wall shear stress at the throat and the low shear stress in the region downstream of the stenosis, increases with Reynolds number. From the pressure distribution, it is noted that the pressure decreases in the proximal part of the stenosis and attains a minimum value at the throat, and then recovers at the diverging section. The magnitude of adverse pressure gradient increases with increasing value of Reynolds number.

Ang and Majumdar (1997) have developed a three dimensional mathematical model of blood flow through a vessel with an asymmetric stenosis (cosine shaped). They have studied the model for varying Reynolds numbers ranging from 100 to 1000 and for varying percentage of restriction, 53%, 65%, 77% and 89% areal occlusions. The Navier–Stokes and continuity equation have been solved by Finite Volume technique for steady flow. They have considered no slip boundary condition at the arterial wall, velocity profile at the inlet to be parabolic, and zero pressure and free exit velocity at the outlet. To get parabolic inlet velocity, they have considered the inlet length of computation domain to be 20 times of vessel diameter. They have investigated the pressure drop, velocity profiles and wall shear stress for their corresponding Reynolds numbers and area occlusions. From the pressure drop curves, it is noted that the magnitude of non-dimensional pressure drop decreases with increase in Reynolds number and the same increases with the increase in area occlusion. The nature of wall shear stress curves are also observed to be similar like the nature of wall shear stress characteristics for axisymmetric stenosis studied by Despande et al. (1976), Tu et al. (1992) and Mishra et al. (1993).

Pontrelli (2001) has carried out a simulation of the blood flow through a bell shaped stenosed artery by considering a shear-thinning model. He has considered steady, two dimensional, axisymmetric flow with fixed 50% degree of stenosis. He has solved the momentum equation numerically by finite difference scheme followed by vorticity-stream function formulation. He has investigated the flow pattern with distribution of pressure and shear stress at the wall. He has studied comparatively all the results with Newtonian case. From the observation on the streamlines, he has noted that the reattachment point moves further downstream of stenosis for the case of the consideration of non-Newtonian fluid.

Gupta and Agrawal (2015) have investigated wall shear stress and oscillatory shear index of the blood flow through a geometrically realistic stenosis both experimentally and numerically. They have considered blood flow as steady. They have developed a computational model of an irregular stenotic descending aorta. The governing equations have been solved using finite volume or finite-difference techniques in the generalized body-fitted coordinates system. They have demonstrated that the developed wall shear stress at the stenotic zone for the irregular stenosis model is different from the regular stenosis. For the irregular stenotic case, the

oscillations of wall shear stresses at the post-stenotic zone are very strong in comparison to the regular stenosis case.

1.3.3 Numerical studies for pulsatile flow

Many investigators have done numerical studies considering blood flow as pulsatile in nature at inlet of modeled artery having stenosis and they have also compared the flow characteristics for pulsatile flow. In this sub-section, important aspects of various significant numerical studies for pulsatile flow have been presented as below.

Cheng et al. (1972, 74) have numerically studied the growth of vortex and local pressure variation in the vicinity of square wall obstacles for percentage of restriction of 25% and stricture length of 0.25 in plane conduits for steady, oscillatory and pulsatile laminar flow. In their study, they have considered the working fluid as Newtonian and they have carried out the simulation for the axisymmetric flow. They have revealed that the shear stress and vorticity become very large in the vicinity of the corners of the hump at certain times during the oscillation cycle and also observed the large pressure drop across a severe stenosis.

The blood flow patterns through normal, stenosed and aneurysmal arteries, and bifurcations are studied numerically by Wong et al. (1991). The shape of stenosis is trapezoidal with 45% and 75% area reductions. In their analysis, they have considered the flow Reynolds number varying from 125 to 750. They have solved the continuity and Navier–Stokes equations by Finite element Method for both steady and pulsatile flow. Blood has been considered to be incompressible Newtonian fluid, flow to be laminar and isothermal, and the vessel wall as rigid. They have studied the velocity vectors, streamlines and pressure contours. From the analysis, they have concluded that the recirculation zone increases with increase in Reynolds number and degree of stenosis.

Tu et al. (1992) have investigated both steady and physiological pulsatile flows through stenosed artery considering a single smooth axisymmetric cosine shaped constriction with 25%, 50% and 75% stenoses (by area) at Reynolds numbers of 100, 200 and 500. For the unsteady flow, they have studied on two cases of physiological pulsatile flow with different Womersley numbers. They have noted that the flow separation occurs at the downstream of the throat section for 50% and 75% stenosis and it reattaches subsequently at some distal location. They have noted that

the size of recirculation zone increases with the increase in Reynolds number and degree of stenosis, and decreases with the increase in stricture length. The magnitude of centerline pressure drop in the stenotic zone increases with increase in Reynolds number, degree of stenosis and stricture length. In cases of wall shear stress, they have noticed a sharp peak value of wall shear stress at the throat of stenosis and then negative value in the separation region. They have found that the magnitude of peak wall shear stress at the stenosis zone increases with increase in Reynolds number and degree of stenosis but decreases with stricture length.

Misra et al. (1993) have studied numerically the behavior of blood flow through an arterial segment having a mild cosine shaped stenosis. They have considered axisymmetric, laminar and unsteady flow of blood through a circulatory cylindrical arterial segment with non-Newtonian fluid. From their study it is revealed that the magnitude of wall shear stress increases with increase in size of stenosis.

He and Ku (1994) have studied unsteady entrance flow through a straight tube by numerically solving the Navier-Stokes equations using a spectral element method and quantified the effect of variations in Womersley parameter on the entrance length for a pulsatile flow. They have considered a sinusoidal inlet flow waveform with Reynolds number of 200 and a range of Womersley parameters from 1.8 to 12.5. They have observed the variations in the entrance length during the pulsatile cycle and the amplitude of entrance length variation decreases with an increase in the Womersley parameter.

Rathish Kumar and Naidu (1996) have unconditionally considered the wall of the vessel to be rigid and flow to be axisymmetric in their study for femoral and iliac arteries. To support their reason for the consideration of rigid wall, they have mentioned that the neglect of wall distansibilities is not a serious drawback, because the said arteries are mildly elastic and relative change in the diameter of the arteries is in order of 10% (McDonald, 1974). Therefore, it is believed by them that the magnitude of the inaccuracy introduced by assuming a fixed diameter is very less.

Siouffi et al. (1998) have presented a study of a post-stenotic velocity flow field corresponding to the oscillatory, pulsatile physiological flow waveforms and too much emphasis is placed on the analysis of the experimental velocity-profile patterns. They have proved that beyond the influence of the flow parameter such as the Reynolds number and frequency parameter, the velocity profile (hence the wall shear stress) highly depends on the wave form.

Zendehbudi and Moayeri (1999) have compared the velocity distributions, streamline contours and wall shear stresses for physiological flow and simple pulsatile flow through an axisymmetrical cosine shaped rigid stenosed artery with 61% area reduction. They have performed the relevant numerical computations considering the blood as Newtonian fluid and flow as laminar. The non-dimensional mass and linear momentum equations in cylindrical co-ordinates have been solved by using the SIMPLER algorithm of Patankar (1980). Apart from that, they have also computed the non-dimensional pressure drop across the cosine shaped stenosis with 56% area reduction (PR=33.33) for steady flow with Reynolds number varying from 50 to 250 to validate their results with the experimental results obtained by Young and Tsai (1973). They have noted the good agreement between their computed results and the results of Young and Tsai (1973).

Bath and Kamn (1999) have carried out a Finite Element analysis to observe fluid structure interaction of pulsatile flow through a compliant stenotic artery for an axisymmetric model of the flow and vessel. They have observed an increase in the pressure drop and wall shear stress associated with the flow for an increase in degree of stenosis. They have also noted that an increase in the inner wall hoop stress and the compressive stresses on the lesions, as well as additional decrease in vessel area occur during peak flow period.

Buchanan et al. (2000) have studied rheological effect on pulsatile laminar flow and found that those rheological properties may affect the wall shear stress quantitatively to some extent, which may be considered not to be appreciable. Most of the researchers have finally concluded from their studies that recirculation regions considered being an important parameter as a greater promise in identifying a stenosed vessel and the knowledge of temporal variations in the pressure gradient across a vessel may serve as an effective tool in identifying a block in a vessel.

Stroud et al. (2000) have investigated the blood flow in the presence of significant plaque deposits in a stenotic vessel and evaluated the influence of factors such as stenosis morphology and surface irregularity on the flow through that vessel. In their analysis, they have considered the fluid as incompressible and Newtonian fluid and Reynolds numbers in the range of 200 to 1200 and percentage of restrictions of 25%, 50% and 75%. They have solved the three dimensional Navier-Stokes equations using a finite volume technique for unsteady flows in the stenotic vessels. They have observed that the maximum shear stress occurs at the throat zone of

stenosis. Finally they have predicted that surface irregularity, stenosis aspect ratio and the shape of the pulsatile waveform all have considerable influence on the flow field.

Long et al. (2001) have obtained numerical solution assuming a physiological pulsatile flow through different models of stenosis, artery as rigid tube, laminar flow and Newtonian fluid. They have found that during the systolic deceleration phase there is a formation and development of flow separation zones in the poststenotic region. they also shown the influences of the severity and geometry of the stenosis and the pulse waveform of the flow on the poststenotic.

Lee and Xu (2002) have analyzed flow behavior of pulsatile flow through trapezoidal shaped 45% stenosed (by area) cylindrical tube considering the fluid to be incompressible and Newtonian. They have used two separate commercial code CFX 4.2 and ABAQUS7 for the analysis. They have investigated velocity profiles, wall shear stress for the rigid and compliant tube. From their wall shear stress representation, it is obvious that the wall shear stress curves for rigid and compliant tube are more or less identical.

Varghese and Frankel (2003) have modeled numerically pulsatile turbulent flow in stenotic vessels using the Reynolds-averaged Navier-Stokes equation approach. They have used commercially available computational fluid dynamics code (CFD), FLUENT, for these studies. Using their models, they have noted that a wall shear stress peak at the throat of the stenosis with minimum values observed distal to the stenosis where flow separation occurred.

Liu et al. (2004) have performed numerical simulations through different cosine shaped stenotic models of tapered arteries. In their study, they have considered the percentage of restrictions in the range between 25% and 65% approximately and Reynolds number of 396. They have also considered arterial wall as rigid and flow to be laminar, pulsating and two dimensional axisymmetric with fully developed velocity profile at inlet. They have solved incompressible Navier-Stokes equations numerically by using the finite difference method considering blood as a Newtonian fluid. The non-dimensional length of computational domain has been considered to be 10 with 200×35 non-uniform grid points. From their analysis, they have concluded that stenosis disturbs the flow field at its vicinity, especially at the throat and downstream, and leads to the formation of a flow separation region in the post-stenotic region. They have also revealed that the tapering of the artery does not

change the flow pattern, and the peak value of the wall shear stress for the tapered artery is bigger than that without tapering.

Sherwin and Blackburn (2005) have studied steady and pulsatile flow in a smooth axisymmetric 75% stenotic tube, using a combination of three-dimensional stability analysis and direct numerical simulation. They have considered two types of non-reversing pulsatile waveforms which satisfy the Womersley solution for straight tubes. The first waveform contained a mean and single harmonic and the second waveform contained a mean and two harmonics. They have found that the two-harmonic waveform, which had a higher peak-to-mean ratio is more stable than the single-harmonic waveform at the same reduced velocity.

The effect of non-Newtonian (Carreau model) behavior of blood on pulsatile flows in stenotic arteries is investigated by Amorsnamankul et al. (2006). The inner layer of arterial walls is modelled as a porous medium and human blood is considered as a incompressible fluid. They have used two different models, the Newtonian model and the non-Newtonian Carreau model. In their study, stenosis severity ranges from 25% to 80%. They have observed that the blood pressure increases very significantly in the upstream zone of stenotic artery as the degree of stenosis area severity increases both for non-Newtonian and Newtonian behaviour of blood. It is also evident from their results that the pressure drop at the stenosis zone at each percentage of restriction considering separately blood as Newtonian and non-Newtonian fluids does not vary.

Misra and Shit (2006) have developed a mathematical model for studying the non-Newtonian flow of blood through a bell-shaped stenosed arterial segment. They have considered blood flow as steady, fully developed laminar and one dimensional flow. They have noticed that the resistance of flow and the skin-friction increase as the stenosis height increases.

Ortiz et al. (2006) have performed a numerical simulation of physiological pulsatile waveform through axisymmetric stenosed arteries. They have described the physiological pulsatile waveform by the first five harmonic of Fourier series. They have investigated the velocity field and wall shear stress for different time phase of a cardiac cycle and for different sizes of stenosis. They have showed that the reversal flow and wall shear stress vary according with cardiac cycle and with constriction severity.

Lee et al. (2007) have carried out numerical simulations for laminar sinusoidal pulsating flow in a tube with smooth single constriction. A second-order finite volume method has been developed to solve the fluid flow governing equations on a non-staggered non-orthogonal grid. They have investigated the effects of the Reynolds number, the Womersley number, the pulsatile amplitude, the constriction ratio and the constriction length on fluid flow in constricted tube. They have observed that the peak wall vorticity increases with the increase of Reynolds number, the pulsating amplitude and the constriction ratio. The constriction length does not put a significant impact on the flow instantaneous streamline behaviors compared with other parameters. However, the peak wall vorticity increases monotonically with the decrease of the constriction length.

Ooi et al. (2007) have studied the pulsatile flow through an axisymmetric stenosed artery numerically to investigate how the wall shear stress (WSS) is affected by varying levels of stenosis contractions and pulse periods (reduced velocity). They have found that the distribution and strength of the WSS is closely correlated with the position of the vortex ring formed at the stenosis. Each vortex ring generates high WSS at the stenosis walls and this high WSS propagates downstream with the vortex ring. As the vortex ring convects downstream, it loses its strength due to viscous effects and WSS decreases in magnitude. In general, the strength of the vortex ring increases with increasing stenosis levels which leads to higher WSS values on the walls. The effect of smaller pulse period is to reduce the distance between the vortex rings, thus increasing the spatial variation of WSS along the stenosed artery.

Hasan and Das (2008) have studied numerically the sinusoidal fluctuated pulsatile laminar flow through stenotic artery assuming blood to be viscous, incompressible and Newtonian. They have investigated the effect of pulsation, stenosis severity, Reynolds number and Womersley number on the flow behavior. They have observed that the peak wall vorticity increases with the increase of stenosis sizes and Reynolds number.

Lee et al. (2008) studied the flow around a plaque grown in a human carotid bifurcation. They found, in addition to vortex formation downstream of the stenosis, high WSS on the stenosis during the systole, and high spatial gradient of WSS in the region of flow separation.

Gay and Zhang (2009) have numerically studied the blood flow through healthy, stenosed and stented carotid arteries with the aim of identifying

hemodynamic factors in the initiation, growth, and the potential of leading to severe occlusions of a diseased artery. They have observed a high wall shear stress at the stenosis throat, a low and oscillating wall shear stress downstream of the stenosis, and a high residence time immediately downstream of the stenosis.

Layek et al. (2009) have carried out a numerical simulation of the unsteady viscous flow in the neighborhood of an overlapping constriction under laminar flow conditions with the motivation for modeling blood flow through a local occlusion of artery formed due to arterial disease considering the flowing blood as incompressible and Newtonian with variable blood viscosity. They have employed the finite-difference technique with staggered grid distribution to solve the governing equations. They have found that the recirculation regions are formed in the downstream of the overlapping constriction. It has been noticed that the arterial wall shear stress, pressure distribution and flow rate in particular, in the constricted site, are significantly altered. The peak value of wall shear stress decreases with increasing haematocrit parameter. The flow separation region increases with increasing haematocrit parameter. They have also considered the motion of the arterial wall and its effects on local flow dynamics are considered. The contribution of deformability of the arterial wall reduces the wall shear stress in comparison to the consideration of rigid wall.

Kinght et al. (2010) have done patient specific computation study to correlate the wall shear parameters and suggested TAWSS, OSI and RRT are the parameters to predict the areas of plaque formation.

Mandal et al. (2011) have investigated numerically the effect of symmetrical and asymmetrical bell-shaped stenoses on wall pressure drop, streamline contour, and rise in wall shear stress for the progression of the disease, atherosclerosis for both steady and pulsatile flow. They have found that the impact of wall pressure and peak wall shear stress on progression of disease is always high for asymmetrical shaped stenosis for both steady and pulsatile flow. The impact of pulsatile nature of flow on the aggravation of disease is observed to be higher at some time steps in comparison to steady flow.

Razavi et al. (2011) have investigated numerically the effect of stenosis sizes (30%-60%) on the blood flow in a stenosed carotid artery for Newtonian and non-Newtonian models under pulsatile flow condition. They have considered symmetric bell shaped Gaussian distribution profile for the geometry of stenosis. They have

observed that when the constriction area is greater, the radial velocity disturbs more, the larger recirculation zone generates at the downstream of the stenosis and wall shear stress value is higher at the throat of the stenosis**.**

Ryou et al. (2012) have analyzed and compared the flow characteristics of the healthy vessel and diseased vessel through computational fluid dynamics simulation and concluded that low TAWSS and high OSI are widely accepted indicators of plaque formation or the direction of plaque progression.

Mehrabi and Setayeshi (2012) have studied on the behavior of blood flow in the stenosed vessels using a numerical technique based on the finite difference method taking into account the transient periodic behaviour of the blood flow in cardiac cycles considering blood as an incompressible non-Newtonian fluid which is based on the power law viscosity model. Comparing the results obtained from three stenosed vessels with 30%, 50%, and 75% area severity, they have found that higher percent area severity of stenosis leads to higher extra pressure jumps and higher blood speeds around the stenosis site. Also, they have observed that the size of the stenosis in stenosed vessels does influence the blood flow.

Chaichana et al. (2012) have performed a computational fluid-dynamics analysis involving model plaque in left coronary arteries to investigate the effect of plaque on the hemodynamic of flow. They have investigated that the presence of plaque alters the pressure gradient, with higher gradients in the stenotic regions that may contribute to plaque rupture. They also have found that the plaque induces low velocity in the region surrounding the plaque and these low-flow regions are associated with low WSS, and may contribute to plaque progression.

Awazdi and Salehi (2012) have studied computationally on blood flow in a stenotic artery using a suitable cubic interpolation profile method. The governing equations of the blood flow were the stream function-vorticity equations and they have computed the results of flow variables such as shear stress distribution and recirculation flow for different level of severity of the disease for wide range of Reynolds numbers. They have investigated that the development of negative wall shear stress downstream the stenosis is the prime development of further atherosclerotic plaque.

Rikhteger et al. (2012) have performed computational fluid dynamics simulations to calculate the wall shear parameters considering blood as viscous, incompressible and Newtonian and the blood flow as transient replicating systolic and

diastolic phase. They have investigated the performance of average wall shear stress, average wall shear stress gradient, oscillatory shear index and relative residence time for the prediction of plaque development locations. They have suggested that low wall shear stress is necessary for plaque formation; its presence alone is not sufficient to predict future plaque locations and time dependent factors have to be taken into account as well.

Mandal et al. (2012) have investigated the blood flow in a bell-shaped constricted rigid tube, modeled as stenosed artery assuming the flow to be axi-symmetric, laminar and of oscillatory type. They have presented the governing equations of motion with the help of stream function-vorticity and solved numerically by finite-difference technique. They have found that the arterial wall shear stress reduced significantly and the peak value of the wall shear stress at the maximum area reduction is comparatively low for Newtonian fluid viscosity. They have also showed that the lengths of recirculation regions formed after the constriction are reduced for the shear-thinning blood viscosity model and also for its different material parameters.

Shahed et al. (2013) have carried out a numerical analysis to demonstrate the variation of two hemodynamic forces: wall shear stress and pressure in the flow field of stenotic artery considering 75% stenosis severity with axisymmetric cosine shaped stenosis. They have assumed wall of the vessel to be rigid. A sinusoidal pulsatile flow is assumed as inlet boundary condition. During the simulation both standard k-ω model of low Reynolds correction and standard k-ε model are used. They have observed that the peak wall shear stress is located proximal to the stenosis throat. They also have showed that the standard k-ε turbulence model illustrates oscillating wall shear stress downstream the stenosis throat throughout the time period. The pressure gradient at the throat is highest at peak flow condition. These factors contribute to further growth and rupture of plaques.

Biyue Liu (2013) has performed a computer simulation of the blood flow in a patient specific stenotic right coronary artery to investigate the phasic variation and the spatial distribution pattern of the wall shear stress on the lumen surface. The inlet boundary was imposed with a fully developed flow with a physiological human right coronary waveform and the fluid was laminar, non-Newtonian, viscous and incompressible. He has shown that the wall shear stress elevates in the stenotic region, reaches the maximum at the neck of the stenosis, and drops sharply in the post-stenosis region.

Dabagh et al. (2013) have investigated the local hemodynamic more precisely through the stenosed artery models using the histological images from longitudinal section of four diseased coronary arteries. They have applied pulsatile blood flow through the reconstructed stenosed coronary arteries. They have investigated and analyzed distinctive flow patterns appear in different stenosed regions corresponding to the specific geometry of any artery by means of computational fluid dynamics. They have showed that the stenosis affects the wall shear stress locally along the diseased arterial wall as well as other adjacent walls and the maximum magnitude of WSS is observed in the throat of stenosis, and the high oscillatory shear index (OSI) is observed along the stenosed wall and the high curvature regions.

Bit and Chattopadhyay (2014) have investigated numerically the hemodynamic flow in a stenosed flow with the degree of stenosis from 25% to 80%.. They have considered the flow as laminar and Pulsatile, the fluid a non-Newtonian. They have calculated wall shear stress, oscillatory shear index and wall pressure drop. They have showed that the all the hemodynamic characteristics depend on the degree of stenosis and the positioning and size recirculation bubbles vary with flow Reynolds number and the degree of stenosis.

Rabby et al. (2014) have done finite volume numerical simulation of unsteady, incompressible, and homogeneous blood flow in two-dimensional rigid models with double constrictions. They have considered cosine shaped stenosis and sinusoidal pulsatile laminar flow in the inlet of the pipe. They have compared flow field, flow induced wall pressure, and wall shear stress for Newtonian and non-Newtonian models in a rigid pipe with two axisymmetric shaped stenosis of different degree under pulsatile condition. They have observed the maximum shear stresses occur at the throat locations of both of the considered stenosis of 75% and 50% with a very oscillating manner. The highest value of WSS is found at the peak systolic phase while the lowest one occurs during peak diastolic phase. They have also concluded that the Newtonian fluid is having its characteristics of high wall shear stress, pressure loss, and the largest recirculation region at the throat locations of the stenosis than the non-Newtonian models.

Haque and Hasan (2015) have carried out a numerical simulation for blood flow through an eccentric arterial stenosis. They have considered degree of stenosis as 50% and Womersley number as 7.122. They have solved the governing equations by numerical method followed by finite element method. They have investigated the

effect of pulsatile flow waveform on the time-averaged wall shear stress, wall shear stress gradient and oscillatory shear index both at stenotic and post-stenotic zone. They have also demonstrated that the generated vortex rings at the post-stenotic region are different for different pulsatile flow waveform.

Mamun et al. (2016) have carried out a numerical simulation of physiological pulsatile flow to investigate velocity, wall pressure, streamline contour and wall shear stress distribution for both Newtonian fluid and non-Newtonian fluid. They have compared the numerical results for Newtonian model, carreau model and cross model. They have observed that the cross model gives better results than other model.

Kamangar et al. (2017) have numerically investigated the influence of shape of stenosis for pulsatile blood flow condition. They have considered various sizes of blockage from 70% to 90% by area for different geometries of stenosis such as elliptical, trapezium and triangular. They have observed the highest level of pressure drop and highest wall shear stress for the case of trapezoidal shaped stenosis.

Stiehm et al. (2017) have performed pulsatile CFD simulations considering the physiological environment of the coronary vessels. They have considered Womersley number as 2.065 to describe the pulsatile character of flow. They have concluded that the steady state simulations are also valid for hemodynamic analyses while time-averaged values are only considered. They have also performed two different transient CFD-simulations using a physiologic waveform and a sinus inlet condition. They have investigated time averaged wall shear stress for hemodynamic analyses.

From the above review of literatures, this is understood that the researchers have studied the blood flow through an artery in different directions. Many investigators have considered blood flow as steady as well as pulsatile, and laminar as well as turbulent. Different shapes of stenosis, such as rectangular, trapezoidal, semicircular, cosine curved, bell shaped, have been considered by the investigators for their study. The researchers have also studied the different degrees of stenosis or percentage of restrictions. The artery wall has been considered as rigid. They have studied the flow characteristics for different values of Reynolds number and also for different values of Womersley number.

1.4 Objectives of present work

Although many investigators have contributed to the understanding for study of blood flow through stenosed artery as mentioned in above literature reviews, the

knowledge in this field is still inadequate. Very few have considered the realistic shaped stenosis and physiologically realistic flow parameters. A systematic study of hemodynamic parameters has not been yet studied to investigate through stenosed artery, especially to study the effects of Reynolds number, Womersley number and percentage of restriction on the flow characteristics like wall pressure drop, recirculation zone, streamline contour, peak wall shear stress, low wall shear stress and oscillatory shear index in terms of initiation, progression and formation of the cardiovascular disease, atherosclerosis.

Keeping in mind the review of literatures, the present work is focused to carry out a systematic numerical study on the effects of different pulsatile flow profiles through axisymmetric bell shaped stenosis for various geometries of stenosis with respect to percentage of restriction and for flow parameters such as Reynolds number and Womersley number on fluid flow characteristics. The flow characteristics are wall pressure, stream line contour representing recirculation zone, peak time-averaged wall shear stress, low time-averaged wall shear stress and oscillatory shear index. In this thesis, an attempt has been made to study numerically on the flow characteristics of pulsatile flow through bell shaped stenosed artery at the stenotic zone and post-stenotic zone for the Reynolds numbers ranging from 50 to 200, Womersley numbers ranging from 5 to 12.5 and the percentage of restriction ranging from 30% to 70% (by diameter). Three different pulsatile profiles, i.e., simple pulsatile profile, physiological pulsatile profile and realistic pulsatile profile, have been considered at the inlet of considered geometries of the modeled artery. The objective of the present work also includes investigation of the impact of the flow characteristics on the possibilities of initiation, progression and formation of the disease, atherosclerosis with respect to Reynolds numbers, percentage of restriction and Womersley numbers.

CHAPTER 2: NUMERICAL MODELING

2.0 NUMERICAL MODELING

2.1 Model of Stenosed Artery

The shape of stenosis does not obey any rule of geometry. The realistic shape may be like the Gaussian (bell shaped), or cosine or sinusoidal geometry of constriction. In the present work, an axially symmetric but radially asymmetric stenosis has been considered. The curvature of the stenosis is chosen as bell shaped Gaussian distribution profile.

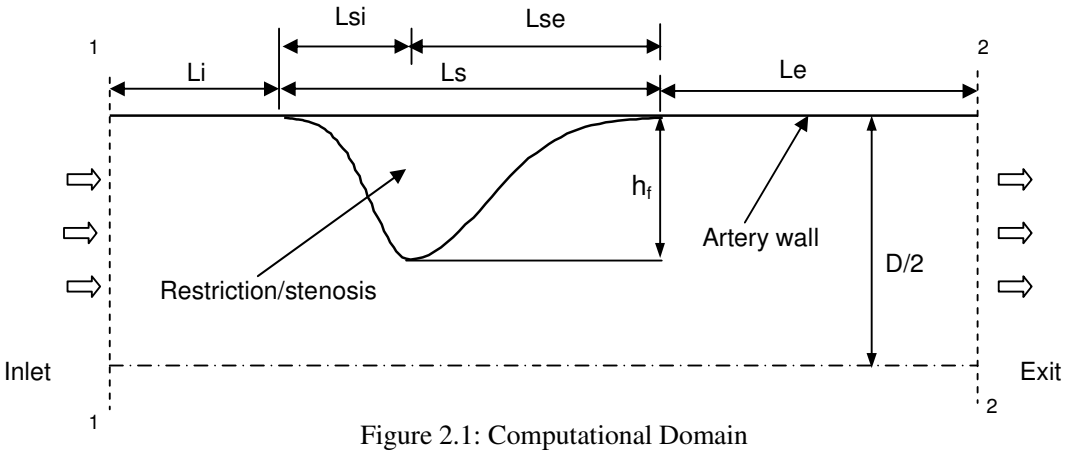

Figure 2.1: Computational Domain

The proposed schematic diagram of the computational domain is illustrated in Fig.2.1. This bell-shaped stenosis (Mishra and Shit, 2006) geometry is modeled mathematically as the following equation.

$$r = 0.5 - h_f \exp\left(-\frac{4m^2 z^2}{L_s^2}\right) \qquad (2.1)$$

Where, m is a parametric constant, which defines shape of stenosis. In the present study the value of m is considered as 1. Currently, the best indicator for surgical treatment of atherosclerosis is the degree of stenosis. In clinical medicine, degree of stenosis or percentage of restriction is commonly defined as percentage occlusion by diameter, (Wootton and Ku, 1999), followed by the equation (2.2).

$$PR = \frac{D - (D/2 - h_f)}{D} \times 100\% \qquad (2.2)$$

From the studies of different researchers, it is understood that when the flow passes through a stenosed artery, flow decelerates and eddies are formed at the downstream of the stenosed restriction. The deposition of plaque is more likely to occur in this post-stenotic zone. For the said reason, this may be considered that the height of stenosis (i.e. h_f) increases with increase in percentage of restriction. Without changing the distance between the start of stenosis and throat of stenosis (i.e. L_{si}), this is considered that the distance between the throat of stenosis and end of stenosis (i.e. L_{se}) increases with increase in percentage of restriction. In this present work, the increment of the distance between the throat of stenosis and end of stenosis is equal to increment of height of stenosis for all considered variation in percentage of restrictions. These variations of shape in percentage of restriction and stenosis length have been shown in Fig.2.2.

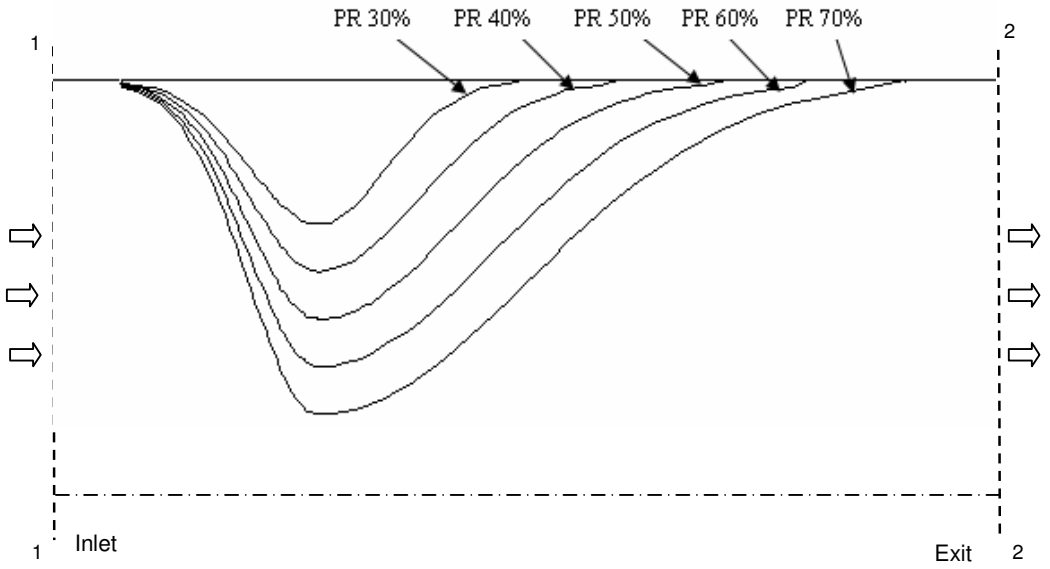

Figure 2.2 Stenosis Models for Different Percentage of Restrictions

In this work, percentage of restrictions has been considered to be 30%, 40%, 50%, 60% and 70% by diameter. The dimensions of stenosis height and stenosis diameter for different stenosis models, in terms of different percentage of restrictions, in the computational domain are shown in Table 2.1.

Table 2.1: Dimensions of Stenosis Models with Different Percentage of Restrictions

Dimensions	PR 30%	PR 40%	PR 50%	PR 60%	PR 70%
h_f	0.15	0.2	0.25	0.3	0.35
D	1	1	1	1	1
L	200	200	200	200	200
L_i	49.9	49.9	49.9	49.9	49.9
L_s	0.2	0.25	0.3	0.35	0.4
L_{si}	0.1	0.1	0.1	0.1	0.1
L_{se}	0.1	0.15	0.2	0.25	0.3

2.2 Assumptions

The realistic arterial flow is so complicated that it is not feasible to consider all factors with currently available resources and knowledge. So far, almost all the theoretical and experimental research activities have been carried out under different simplified assumptions. In the present work, the numerical solutions are obtained under the conditions of homogeneous, incompressible and Newtonian fluid through axially symmetric rigid stenosis. The blood flow has been considered as two-dimensional, laminar and pulsatile flow.

It has been known that the blood usually behaves as a Newtonian fluid in large arteries, especially at moderate to high shear rates (Ku, 1997, Pedley 1980; Fung 1997). Cho and Kensey, 1991, Tandom et al., 1993 and Tu and Deville, 1996 have showed the wall pressure drop at the contricted area and the wall shear stress of blood flow due to consideration of blood as Newtonian fluid are more or less asymptotic with the same due to consideration of blood as non-Newtonian fluid. Ishikawa et al. (1998) have noted that with the consideration of non-Newtonian property, the strength of the vortex and the vortex size are slightly different from that of consideration of Newtonian property in the analysis. Therefore, the assumption of Newtonian blood in this study may be regarded as an acceptable approximation.

The assumption of rigid boundary does not seriously affect the results in most cases, since the development of atherosclerosis in arteries causes a considerable reduction in the elastic property of its wall (Liu 2004). However, the effects of elasticity on the results are very small, so that an assumption of rigid tube flow is

reasonable (Ku, 1997). The interaction between the elastic arterial wall and the flowing blood has a significant impact on the fluid flow dynamics. Thus the consideration of rigid wall of artery in the model is an approximation.

According to some experiments (Khalifa et al., 1981, Solzbach et al., 1987), the maximum Reynolds number, which can sustain the axisymmetric flow, is about 500 for stenotic flow. It is also to be noted that the arteries are not straight throughout the artery network. Thus the assumption of axially symmetric flow is only an approximation.

The blood flow in the blood vessel, especially, the flow in narrow rigid tube, is normally considered as laminar flow (Ganong, 2001). For flow through human artery, physiological flow range of Reynolds number is from100 to 400 (Andersson et al., 2000 and Back and Banerjee, 2000), which is considered to be in the laminar zone.

Diameter of real blood cell in blood flow is about 8×10^{-4} cm. If the blood vessel diameter is greater than 10^{-3} cm, the homogeneity assumption is valid. Since the diameter of arteries in human varies from 0.05-0.3 cm, the individuality of red blood cells may be ignored, (Lee and Fung, 1970).

2.3 Governing Equations

For axisymmetric flow of incompressible and Newtonian fluids with constant fluid properties, the continuity and Navier-Stokes equations in two-dimensional cylindrical co-ordinates (r,z) can be written in the differential conservation form as follows:

Continuity equation:

$$\frac{1}{r}\frac{\partial(ru_r)}{\partial r}+\frac{\partial u_z}{\partial z}=0 \qquad (2.3)$$

r-direction momentum equation:

$$\frac{\partial u_r}{\partial t}+u_r\frac{\partial u_r}{\partial r}+u_z\frac{\partial u_r}{\partial z}=\frac{1}{\rho}\frac{\partial p}{\partial r}+\frac{\mu}{\rho}\left[\frac{\partial}{\partial r}\left(\frac{1}{r}\frac{\partial(ru_r)}{\partial r}+\frac{\partial^2 u_r}{\partial z^2}\right)\right] \qquad (2.4)$$

z-direction momentum equation:

$$\frac{\partial u_z}{\partial t}+u_r\frac{\partial u_z}{\partial r}+u_z\frac{\partial u_z}{\partial z}=-\frac{1}{\rho}\frac{\partial p}{\partial z}+\frac{\mu}{\rho}\left[\frac{\partial}{\partial r}\left(\frac{1}{r}\frac{\partial(ru_z)}{\partial r}+\frac{\partial^2 u_z}{\partial z^2}\right)\right] \qquad (2.5)$$

The following dimensionless variables are defined to obtain the governing equations, (2.3), (2.4) and (2.5) in the non-dimensional form;

Lengths: $r^* = r/D$, $z^* = z/D$, $L^* = L/D$, $t^* = t/T$.

Velocities: $u_r^* = u_r/U$, $u_z^* = u_z/U$

Pressure: $p^* = p/\rho U^2$.

The non dimensional equations are:

$$\frac{1}{r^*}\frac{\partial\left(r^* u^*_r\right)}{\partial r^*} + \frac{\partial u^*_z}{\partial z^*} = 0 \qquad (2.6)$$

$$\frac{1}{\pi}\frac{W_o^{\,2}}{\mathrm{Re}}\frac{\partial u^*_r}{\partial t^*} + u^*_r\frac{\partial u^*_r}{\partial r^*} + u^*_z\frac{\partial u^*_r}{\partial z^*} = -\frac{\partial p^*}{\partial r^*} + \frac{2}{\mathrm{Re}}\left[\frac{\partial^2 u^*_r}{\partial r^{*2}} + \frac{\partial^2 u^*_r}{\partial z^{*2}} + \frac{1}{r}\frac{\partial u^*_r}{\partial r^*}\right] \qquad (2.7)$$

$$\frac{1}{\pi}\frac{W_o^{\,2}}{\mathrm{Re}}\frac{\partial u^*_z}{\partial t^*} + u^*_r\frac{\partial u^*_z}{\partial r^*} + u^*_z\frac{\partial u^*_z}{\partial z^*} = -\frac{\partial p^*}{\partial r^*} + \frac{2}{\mathrm{Re}}\left[\frac{\partial^2 u^*_z}{\partial r^{*2}} + \frac{\partial^2 u^*_z}{\partial z^{*2}} + \frac{1}{r}\frac{\partial u^*_z}{\partial r^*} - \frac{u^*_z}{r^{*2}}\right] \qquad (2.8)$$

Where Wo is the Womersley number, which is defined by equation (2.9) and Re is the Reynolds number, which is defined by equation (2.10)

$$W_o = R\sqrt{\frac{\omega}{\nu}} \qquad (2.9)$$

$$\mathrm{Re} = \frac{\rho U D}{\mu} \qquad (2.10)$$

Where ω is the radial frequency $2\pi/\mathrm{T}$. From equation (2.9), the Womersley number can be interpreted as the ratio of unsteady force to viscous force. The Womersley number is an indicator of the main frequency of the pulsatile flow. In this work, four different values of Womersley number as 4, 7.5, 10 and 12.5 from different physiological conditions of the body have been considered in this study (Caro et al., 1978 and Tutty, 1992). In this work, the Reynolds number is considered as 50, 100, 150 and 200 respectively.

2.4 Boundary Conditions

For numerical modeling of laminar pulsatile flow, it is sufficient to consider Equations 2.6, 2.7 and 2.8 along with the necessary boundary conditions. For incompressible fluid, the velocity boundary conditions need to be specified all along

the domain boundary. Four different boundary conditions have been applied to the considered problem of this work. The boundary conditions are stated as bellows.

1. On the solid wall of artery, both the components of velocity are zero because no-slip and impregnability conditions on the solid surface have been applied. These may be expressed mathematically as follows:-

$u_r^* = 0,\ u_z^* = 0$

2. At the inlet, axial velocity has been applied as pulsatile flow condition (types of considered pulsatile flow have been specified in next sub-section 2.5)

$u_z^* = specified$,

and the transverse velocity has been set to zero, i.e.

$u_r^* = 0$.

3. At the exit, fully developed flow condition has been assumed and hence gradients have been set to zero, i.e.

$\partial u_z^* / \partial z^* = 0,\ \partial u_r^* / \partial z^* = 0$

4. On the plane or axis of symmetry, the symmetry boundary conditions have been imposed. The normal gradient of the axial velocity and the transverse velocity have been set to zero at the line of symmetry, i.e.

$\partial u_z^* / \partial r^* = 0,\ u_r^* = 0$.

2.5 Different Pulsatile Flows through Artery

Different pulsatile flow profiles are observed in the human arteries depending upon position in arterial network, condition of human body (e.g. physical exertion) and also individual to individual (Mills et. al, 1970, McDonald, 1974, Zendehbudi and Moayeri, 1999 and Long et. al., 2001).

In most of the experimental and numerical studies for blood flow through artery, researchers have assumed a simple harmonic waveform at inlet of the stenosis model (Cassanova and Giddens, 1978, Ahmed and Giddens, 1984, Ojha et al., 1989, Buchanan et al., 2000 and Lee and Xu, 2002). In this present work, the first considered pulsatile flow condition (profile-I) represents simple pulsatile flow, which is defined by the following equation (2.11).

Profile-I (simple pulsatile flow):

$u^*_z = 1 + \sin \omega t^*$ (2.11)

The flow with two-harmonic waveforms having a higher peak to mean velocity ratio is more stable than the flow with single harmonic waveform. This waveform is probable physiological pulsatile flow profile at a downstream location in the arterial system (Sherwin and Blackburn, 2005). In this present work, the second considered pulsatile flow condition (profile-II) represents physiological pulsatile flow, which is defined by the following equation (2.12).

Profile-II (physiological pulsatile flow):

$$u^*_z = 1 + 0.75\sin\omega t^* - 0.75\cos 2\omega t^* \qquad (2.12)$$

The third profile represents realistic pulsatile flow condition (profile-III), which is observed in the human right coronary artery (Wiwatanapataphee et al., 2006). The profile-III is defined by the following equation (2.13).

Profile-III (realistic pulsatile flow):

$$\begin{aligned} u^*_z = {} & 1 + 0.29244\cos(\omega t^* + 4.027) - 0.5908\cos(2\omega t^* + 6.509) + \\ & 0.2726\cos(3\omega t^* + 1.913) + 0.1980\cos(4\omega t^* + 1.461) + 0.1124\cos(5\omega t^* + 0.074) \end{aligned} \qquad (2.13)$$

The variations of axial velocities for different profiles have been shown in Fig.2.3.

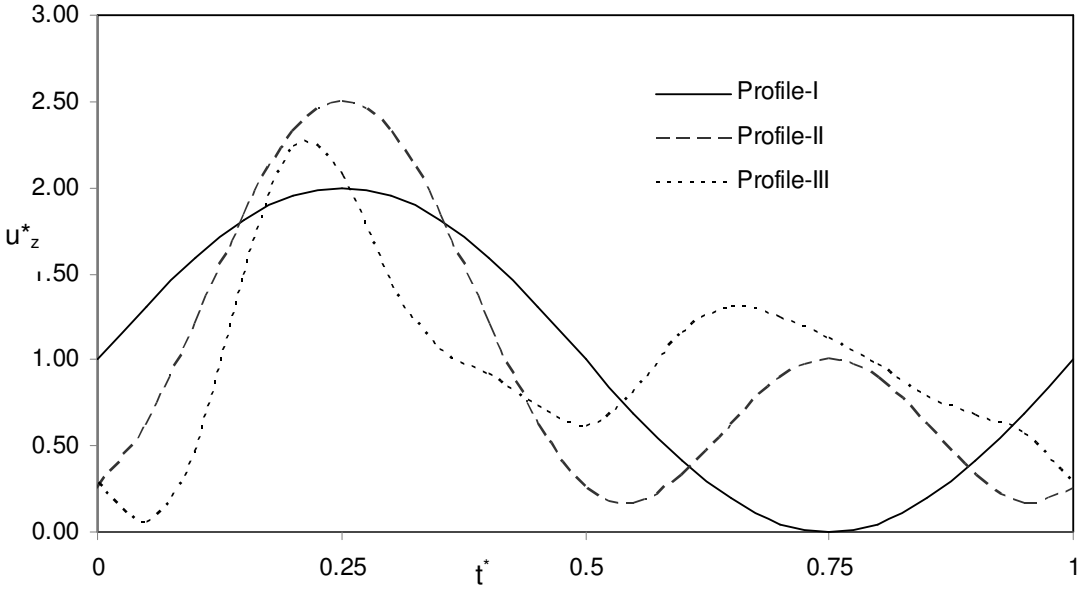

Figure 2.3: Distribution of axial velocities for different pulsatile profiles

2.6 Numerical Simulation

The discretized forms of the governing equations (2.6), (2.7) and (2.8) have been obtained by a control volume formulation in non-uniform staggered grid. The equations have been solved numerically by the in-house CFD code developed using integral approach of the finite volume method following SIMPLER (Semi-Implicit Method for Pressure Linked Equations Revised) algorithm (Patankar, 1980).

The distributions of grid nodes have been considered in both coordinate direction allowing higher grid node concentrations in the region close to the wall and restriction. The third-order upwind scheme has been used for advective part. The discretized equations have been solved iteratively using line-by-line Tri-diagonal Matrix Algorithm (TDMA) with Alternate Direction Implicit (ADI) scheme. The convergence of the iterative scheme has been achieved when the normalized residuals for mass and momentum equations summed over the entire calculation domain has fallen below 10^{-7}.

The size of numerical mesh in i and j direction for the computational domain has been fixed as 448 x 48 after grid independence test, which has been given in next sub-section 2.7.

Numerical calculations are performed according to the following steps:

1. Started with a guessed velocity field.
2. Coefficients for the momentum equations are calculated and hence pseudo velocities are calculated.
3. Coefficients of the pressure equation are calculated and the pressure equation is solved to obtain the pressure field.
4. With the obtained pressure field, the momentum equations are solved and the velocity field is obtained,
5. Steps 2 – 4 are repeated until the convergence criterion is satisfied.
6. The above calculations are repeated at each time step for several periods and the results obtained for each period are compared to those for the previous period. A periodic solution is obtained when the variables calculated at different points and at different times over two successive periods become almost identical.

2.7 Grid Independence Test

Richardson extrapolation (Richardson et al., 1927) has been applied to calculate a higher-order estimate of the flow fields from a series of lower-order

discrete values (F_1, F_2,…, F_n). For the case of grid independence study, the value estimated from the Richardson extrapolation is the value that would results if the cell grid size tended to zero, (h→0). The extrapolation is made from the results of at least two different grid solutions. A minimum of three grid solutions is required for the grid independence study (Stern et al.: 2001). Roache (1994) generalized Richardson extrapolation by introducing the p_e^{th}-order methods, which is defined by equation (2.14).

$$F_{h=0} = F_1 + \frac{F_1 - F_2}{r_e^{\,p_e} - 1} \qquad (2.14)$$

In this study, the grid refinement ratio r, is constant and has been adopted as 2. According to Stern et al. (2001), the order of accuracy can be estimated by using the following equations (2.15 and 2.16).

$$p_e = \frac{\ln(\frac{\varepsilon_{32}}{\varepsilon_{21}})}{\ln(r_e)} \qquad (2.15)$$

Where $\varepsilon_{i+1,i} = F_{i+1} - F_i$ (2.16)

To evaluate the extrapolated value from above equations, the convergence conditions of the solutions must be first confirmed. The feasible convergence conditions are as bellow;

1. Monotonic convergence; $0<R_e$
2. Oscillatory convergence; $R_e<0$
3. Divergence; $R_e>1$

Where R_e is the convergence ratio and it is determined by the equation (2.17).

$$R_e = \frac{\varepsilon_{21}}{\varepsilon_{32}} \qquad (2.17)$$

The Grid Convergence Index (GCI) provides a uniform measure of convergence for grid refinement studies (Roache, 1994). It is based on estimated fractional error derived from the generalization of Richardson extrapolation. The GCI value represents the resolution level and how much the solution approaches the asymptotic value. The GCI for the fine grid solution can be written as following equation (2.18).

$$GCI_{i+i,i} = F_s \frac{\left|\varepsilon_{i+1,i}\right|}{F_i(r_e^{\,p_e} - 1)} \qquad (2.18)$$

From the recommendation of Wilcox (2006), the safety factor (Fs) has been selected for this study is 1.25.

For assessing the accuracy of calculations, the grid should be sufficiently refined such that the solution is in the asymptotic range of convergence. The asymptotic range of convergence is obtained by the following equation (2.19)

$$A_c = \frac{GCI_{32}}{r_e^{\,p_e} GCI_{21}} \qquad (2.19)$$

Table 2.2: Analysis Results for Case of M_1, M_2 and M_3 for Grid Independence Study

Flow Characteristic	F_1	F_2	F_3	R_e	P_e	GCI_{32}	GCI_{21}	A_c
Low WSS	-690.59	-662.47	-591.05	.394	1.34	8.69	3.28	1.046
Wall pressure Drop	29.35	27.66	24.44	.525	0.93	16.08	7.95	1.061
Recirculation length (from OSI)	9.15	8.65	7.85	.62	0.8	0.192	0.113	1.060

Three different mesh sizes, which are represented by *M*3 (112 x 12), *M*2 (224 x 24) and *M*1 (448 x 48), have been arranged according to their increasing degree of fineness. The corresponding grid levels are marked as 3, 2 and 1 respectively. Where, grid level 1 represents the finest grid while level 3 represents the coarsest grid. The grid dependent parameters, that have been compared, are maximum low wall shear stress and wall pressure drop and length of recirculation (calculated from OSI value). The detailed analysis results using the above technique have been presented in Table 2.2 for physiological pulsatile flow (profile-II) with PR = 50%, Re=100 and Wo = 10**.** The analysis results show that the calculated results using mesh size as 448 x 48 are in the condition of monotonic convergence as well as in asymptotic range of accuracy.

The corresponding values of the Richardson's Extrapolated data of the exact solution of the considered parameters, as the grid size theoretically approaches zero value, have also been computed and listed in Table 2.3.

Table 2.3: Results of Grid Independence Test for PR=50%, Re=100 and Wo =10

Mesh Size (r, z)	M_3 (112x12)	M_2 (224x24)	M_1 (448x48)	Richardson's Extrapolated data
Max. WSS low	-591.05	-662.47	-690.59	-699.96
Error	108.91	37.49	9.3733	
% Error	15.55%	5.36%	1.34%	
WP Drop	24.44	27.66	29.35	29.91
Error	5.47	2.25	0.5633	
% Error	18.29%	7.52%	1.88%	
Length of recirculation (from OSI)	7.95	8.65	9.15	9.33
Error	1.48	0.73	0.1833	
% Error	15.86%	7.82%	1.96%	

Using these exact values of the above parameters, the absolute and the relative errors of the numerical solutions on all the three grid levels have been determined. It is obvious from the table that the errors monotonically converge towards zero and are only 1.34% error for maximum low WSS, 1.88% error for the wall pressure drop and 1.96% error for the recirculation length, respectively, when the grid level 1 is adopted. Accordingly, the mesh size selected for this present numerical simulation is 448 ×48 (i,j).

2.8 Validation of numerical code

This is well recognized that the first step of the numerical analysis is the present numerical results must be validated with the some experimental and analytical solutions with comparable flow situations. In this present study, pulsatile (i.e., unsteady) laminar flow through restricted artery (i.e., restricted tube) has been considered. So the present numerical results must be validated with the previous experimental and analytical solutions of unsteady laminar flows in restricted tube. To validate the developed numerical code for this thesis work, at first, the comparisons have been made between the exact analytical solution of Womersley and the result of

the present numerical simulation taking the same flow situation. The Womersley number and the mean Reynolds number have taken as 10 and 200, respectively. The sinusoidal pulsatile flow waveforms (i.e., $u_z^*=1+\sin\omega t^*$) has been considered for this code validation case. The Womersley velocity profile (Womersley 1955; Taylor et al. 1998) for the axial component of velocity is,

$$u(r,t)=\frac{2B_0}{\pi R^2}\left[1-\left(\frac{r}{R}\right)^2\right]+\sum_{n=1}^{N}\left\{\frac{B_n}{\pi R^2}\left[\frac{1-\dfrac{J_o\left(W_{on}\dfrac{r}{R}i^{3/2}\right)}{J_o\left(W_{on}i^{3/2}\right)}}{1-\dfrac{2J_1\left(W_{on}i^{3/2}\right)}{W_{on}i^{3/2}J_o\left(W_{on}i^{3/2}\right)}}\right]\right\}e^{in\omega t} \quad (2.20)$$

Where, R is the radius of the cylinder, J_O and J_1 *are* Bessel functions of the first kind of order 0 and 1 respectively, and $W_{on}=R\sqrt{(n\omega)/\upsilon}$ is Womersley number, where υ is the kinematic viscosity. The pulsatile flow has been simulated over sufficiently long time to obtain a periodic solution, namely the solution that has not changed measurably from one cycle to the next cycle. The Fig. 2.4 shows the comparison between the axial velocity distribution obtained from the present numerical code and the exact solution of Womersley at four different time steps (namely, t^*=0.125, 0.375, 0.625 and 0.875) for the sinusoidal pulsatile flow waveforms. Figure.2.4 shows a good agreement in the results of the present numerical code and the analytical solutions of Womersley.

The present numerical results have been also compared with the experiments of Ojha et al. (1989) for the purpose of validation of the results of present numerical code. The geometry used in this validation is a 45% stenosis with the trapezoidal profile. The considered inlet waveform is a sinusoidal pulse with mean Re of 575 and an amplitude variation of 360, as shown in the equation (2.21).

$$u^*_z = 575 + 360\ \sin(\omega t^* + 2.23) \quad (2.21)$$

The Womersley number for this pulse has been taken as 7.5 and discretized into 69 time steps. The inlet boundary condition has been considered to be fully developed axial velocity profile. The inlet centerline velocity variation versus time, obtained from the simulation results, has been compared with the same of Ojha et al. (1989)

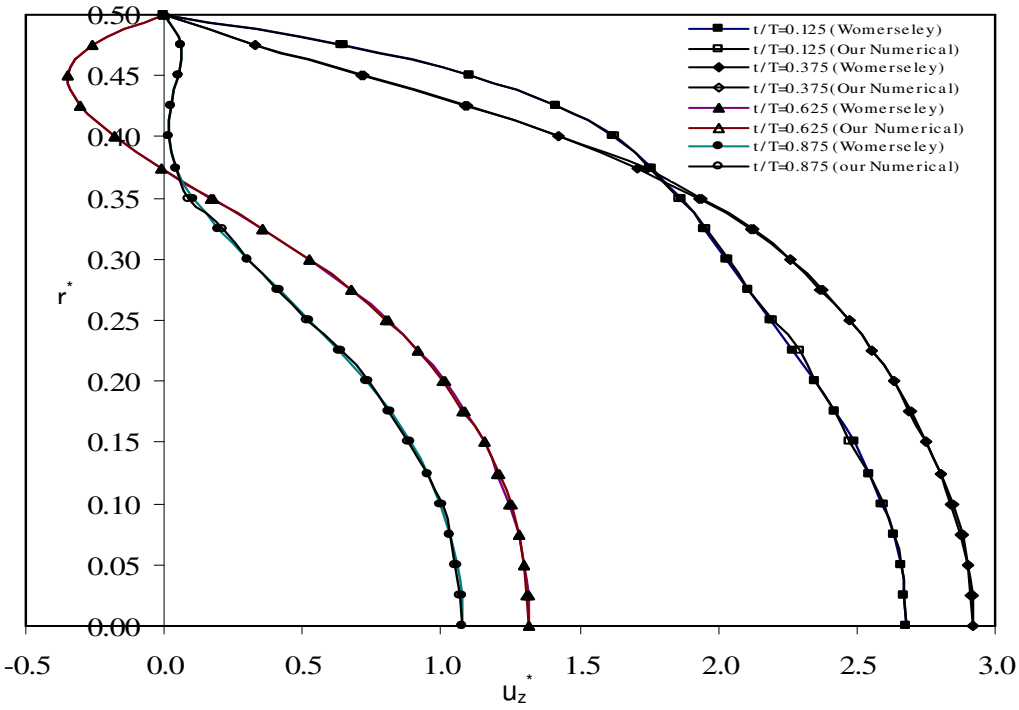

Figure 2.4: Axial velocities at different time step of the Womersley solution and the present numerical code at Re=200 and Wo=10 for Sinusoidal Profile

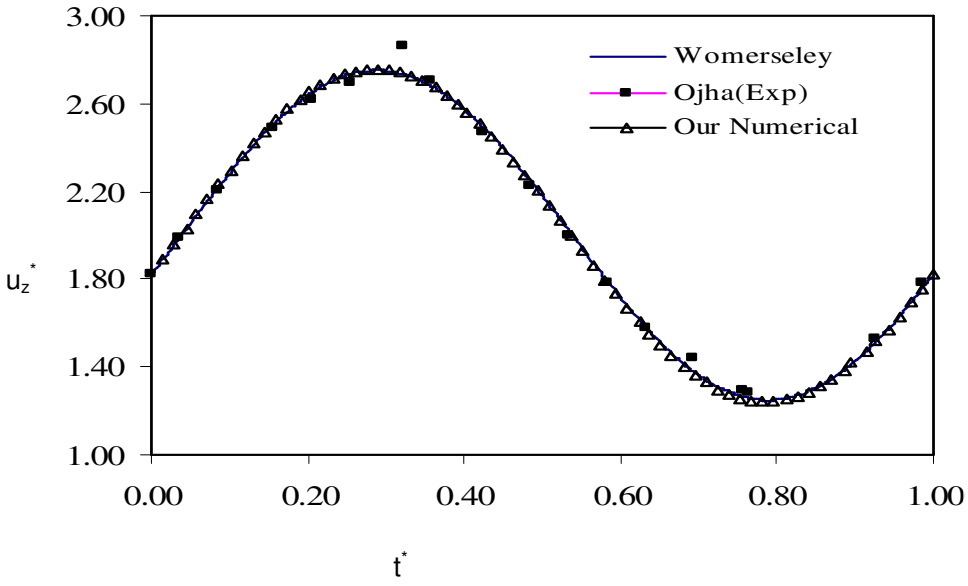

Figure 2.5: Distribution of inlet centerline velocities

and the same of Womersley solution in Fig.2.5. As can be seen from the figure, the inlet centerline velocities are similar throughout the pulse, except near the peak of the

pulse. This additional acceleration in the experimental input pulse causes slight discrepancies with the data.

The axial velocities for different location along axial direction in the post-stenotic region at different time steps, obtained from the simulation results, have also been compared with the same of Ojha et al. (1989) and the same of Womersley solution. Figure 2.6, 2.7 and 2.8 depict the comparison between the measured and computed velocity profiles at the three post stenotic regions (z^*= 1, z^*= 2.5 and z^*= 4.3) for different time steps (t^*= 0.225, t^*= 0.525 and t^*= 0.875). The said figures show that a good agreement between the predictions of present numerical code and experimental data which are found at different considered time steps and positions.

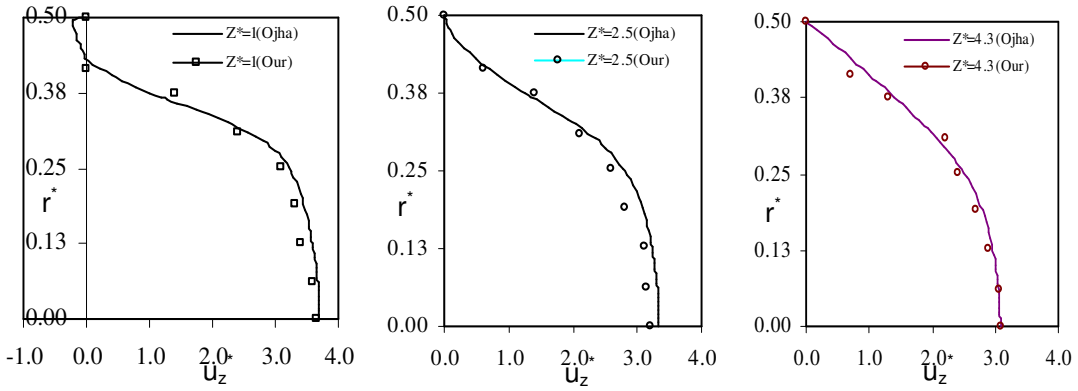

Figure 2.6: Axial velocity distributions for t^*= 0.225

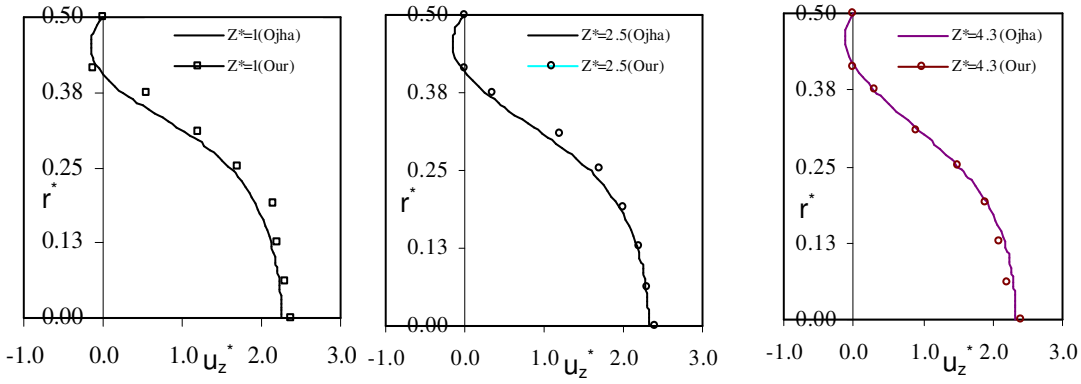

Figure 2.7: Axial velocity distributions for t^*= 0.525

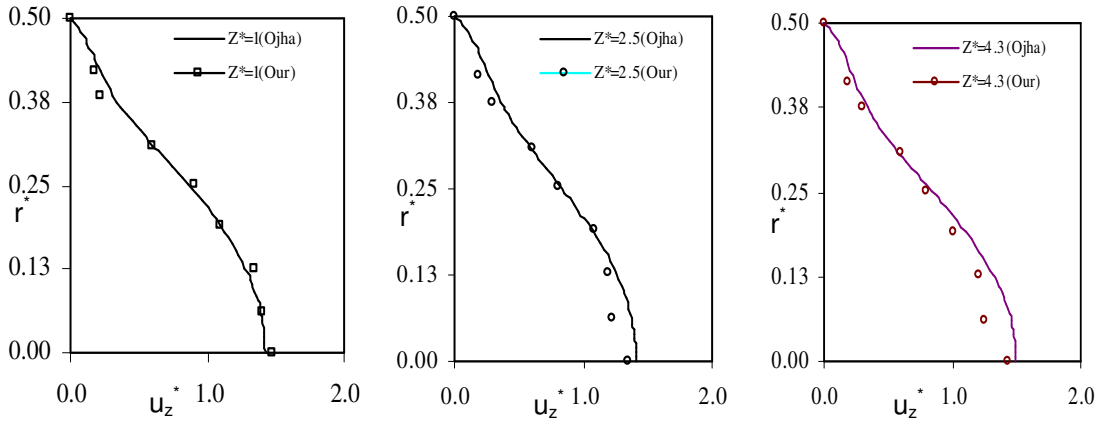

Figure 2.8: Axial velocity distributions for $t^* = 0.875$.

The modeling of stenosed artery for different percentage of restriction and pulsatile flow simulation of different flow parameters and other features of fluid flow characteristics have been elaborately discussed in this chapter. Following these procedural steps, simulated results have been presented in the subsequent chapter with different focuses.

CHAPTER 3: RESULTS AND DISCUSSION

3.0 RESULTS AND DISCUSSION

In this chapter, the systematic numerical analysis of flow characteristics of pulsatile flow through bell shaped stenosed artery has been carried out for simple pulsatile profile and then the flow characteristics of three different pulsatile profiles, simple pulsatile, physiological pulsatile and realistic physiological pulsatile, have been compared from the outcomes of the various numerical simulations for the Reynolds numbers (Re) ranging from 50 to 200, percentage of restrictions (PR) ranging from 30% to 70% and Womersley numbers (Wo) ranging from 5 to 12.5. The study employs computational fluid dynamics to analyze the flow characteristics, wall pressure (WP), streamline contour, peak wall shear stress (PWSS), low wall shear stress (LWSS), oscillatory shear index (OSI). The objective of the flow characteristics is to achieve concise and useful knowledge about disturbed blood flow and clearly elucidate the effects of the flow field. As mentioned, it is proved that hemodynamic parameters play important roles in access and progression of arterial diseases, mainly, atherosclerosis. Wall pressure, wall shear stress and oscillatory shear index are the most important hemodynamic parameters which are frequently used in disturbed blood flow for assessment of initiation, progression and development of the arterial disease, arthrosclerosis. Values of wall pressure and wall shear stress are timed-averaged for one cardiac cycle and the qualitative and quantitative comparisons of the flow characteristics are made for different cases. Time-averaged and non-dimensional hemodynamic parameters are considered in this work.

The time-averaged wall pressure is defined as follows:

$$\overline{p_w^*} = \frac{1}{T}\int_0^T p_w \, dt \qquad (3.1)$$

In Eq. (3.1) the wall pressure is expressed as time-averaged of the flow field normal force exerts on the arterial wall per unit area.

The wall shear stress is defined as follows:

$$\overline{\tau_w^*} = \frac{1}{T}\int_0^T \tau_w \, dt \qquad (3.2)$$

In Eq. (3.2) the wall shear stress is expressed as time averaged of the flow field force exerts on the arterial wall per unit area.

Oscillatory shear index (OSI) characterizes the transient nature of vascular flow fields. This index quantifies the pulsatility and the main direction of the flow. It varies between 0 and 0.5 and is effective at locating points of time-averaged separation and reattachment. The maximum of OSI shows the location of time-averaged reattachment point in flow pattern. The OSI is defined as follows in Eq. (3.3):

$$OSI = \frac{1}{2}\left[1 - \frac{\left|\int_0^T \tau_w \, dt\right|}{\int_0^T |\tau_w| \, dt}\right] \qquad (3.3)$$

3.1 Effect of Reynolds Number for Simple Pulsatile Flow

In this section, a series of numerical simulations of model bell shaped stenosed artery considering simple pulsatile flow have been carried out and the effect of Reynolds numbers on the flow characteristics, e.g. wall pressure, streamline contour, WSS and OSI in each case have been investigated.

The viscosity of blood and diameter of the conduit of blood flow depends on the physiological condition of the different patients and location of artery in the arterial system. Thus Reynolds numbers are different for different patient and different arteries to be concerned. In this section, our main interest is now to study the effects of Reynolds number on flow characteristics particularly on arterial wall pressure, stream line contours, wall shear tress and oscillatory shear index. The validated own developed numerical code is used to simulate the flow characteristics for simple pulsatile flow with Womersley number 5 and 12.5 through a constricted artery with 30% and 70% diametric occlusion. Four Reynolds numbers (Re=50, 100, 150 and 200) have been typically considered for studying the effect of Reynolds numbers on the flow characteristics. The effect of Reynolds numbers is investigated on the flow characteristics such as streamline contour, WP, PWSS, LWSS and OSI typically for four different combination cases separately. The first case is for mild stenosis (PR 30%) with low pulsality of blood flow (Wo 5), the second case is for mild stenosis (PR 30%) and high pulsality of blood flow (Wo 12.5), the third case is a

for severe stenosis (70%) and low pulsality of blood flow (Wo 5) and the fourth case is for severe stenosis (70%) and high pulsality of blood flow (Wo 12.5) respectively.

3.1.1 Wall pressure

The wall pressure plays an important role in the progression of the arterial diseases. The effects of Reynolds number on the wall pressures have been investigated for all the combination cases of mild stenosis, severe stenosis, high pulsality of flow and low pulsality of flow respectively. The variation of the time-averaged wall pressure along the axial direction of the considered arterial length is shown for different Reynolds numbers for the case of Wo 5 and PR 30% in Fig.3.1 The figure shows that the wall pressure drops gradually from entry to exit of the considered length of the artery for all considered Reynolds numbers. The general trend of the curves of Fig. 3.1 is noted to be decreasing in nature of the wall pressure throughout the considered length. It is a common phenomenon of a fluid flowing

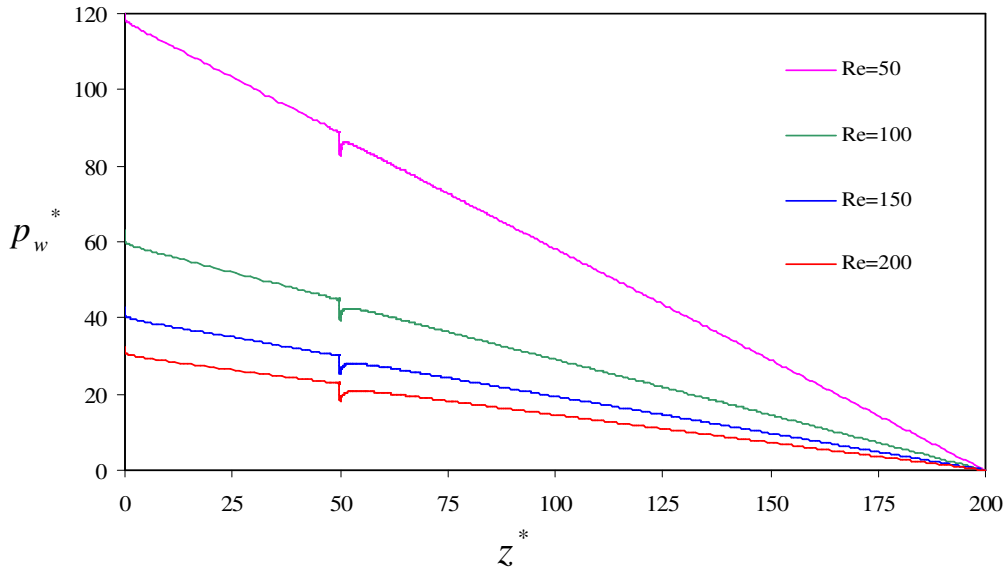

Figure 3.1: Variation of wall pressure along axial direction for the considered length for different Re for PR 30% and Wo 5

through a pipe or channel to have the decreasing tendency of the fluid pressure due to friction throughout the length of tube. There is a sudden pressure drop as flow approaches the throat of the stenosis and the wall pressure raises slightly after the throat of the stenosis. The minimum wall pressure corresponds to the maximum mean velocity of the fluid flow. The flow area decreases as the flow approaches the throat of the stenosis from the entry of the stenosis and again the flow area increases as the

flow approaches to the exit of the stenosis. The flow area has minimum magnitude at the throat of the stenosis. According to the continuity of the flow for an incompressible fluid, the mean velocity of the flow is inversely proportional to the flow area. Thus the maximum mean velocity of the throat corresponds to the minimum pressure at the throat of the stenosis. After sharp falling at the stenosis zone, the wall pressure partially recovers at the downstream due to conversion of kinetic energy to pressure energy at the divergence section of stenosis. It does not reach its original value because of an irrecoverable loss due to viscous effect. The figure also depicts that the variation of wall pressure at the stenosis zone for the different Reynolds numbers 50, 100, 150 and 200. There is no significant difference in the patterns of the pressure drop or rise and in the magnitude of the pressure drop for all considered Reynolds numbers. The maximum pressure drop at the stenosis zone is 6.43 for Re=50 and the same is4.84 for Re=200. The time averaged minimum pressure at the throat of stenosis is 82.46 and 17.98 for Re=50 and Re=200 respectively. The effect of Reynolds numbers on the wall pressure for the case of mild stenosis with high pulsality of flow has been studied further. The distribution of the

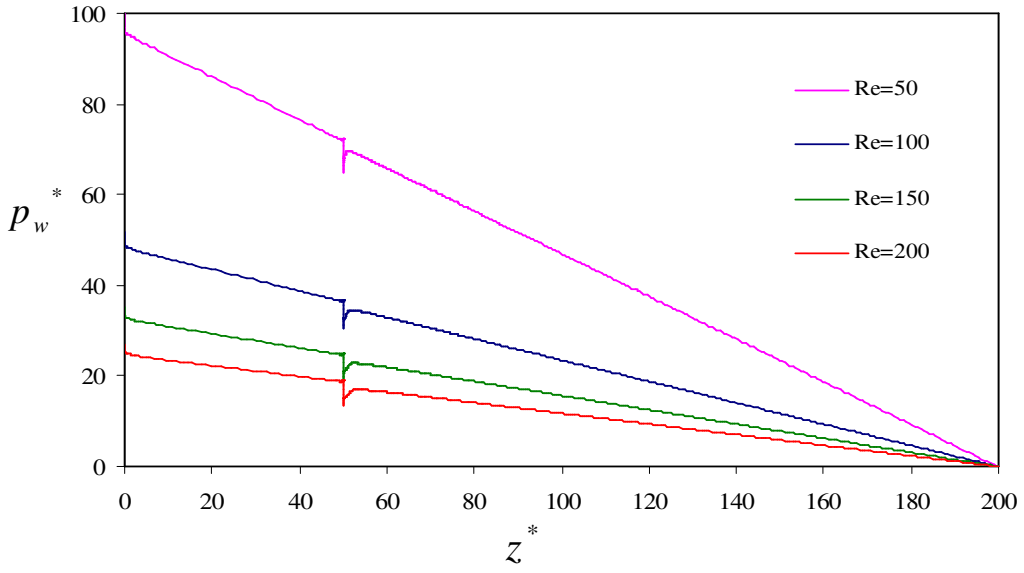

Figure 3.2: Variation of wall pressure along axial direction for the considered length for different Re for PR30% and Wo12.5

time-averaged wall pressure along axial direction of the considered length of artery for the case of Wo 12.5 and PR 30% for varying Reynolds numbers is shown in Fig.3.2. The pressure distribution pattern is same as the previous case. The maximum pressure drop at stenosis zone is 7.36 for Re=50 and the same is 5.36 for Re=200. The

time averaged minimum pressure is 64.85 and 13.51 for Re=50 and Re=200 respectively. The effect of Reynolds number on the wall pressure is also studied for the case of severe stenosis with low pulsality of flow. The distribution of the time-averaged wall pressure along axial direction throughout the considered length of the artery is shown for varying Reynolds number for Wo 5 and PR 70% in Fig.3.3. The wall pressure distribution pattern is also same as the both previous cases of mild stenosis. The maximum pressure drop is 242.77 for Re=50 and 242.93 for Re=200. The time averaged minimum pressure is -22.92 and -87.87 for

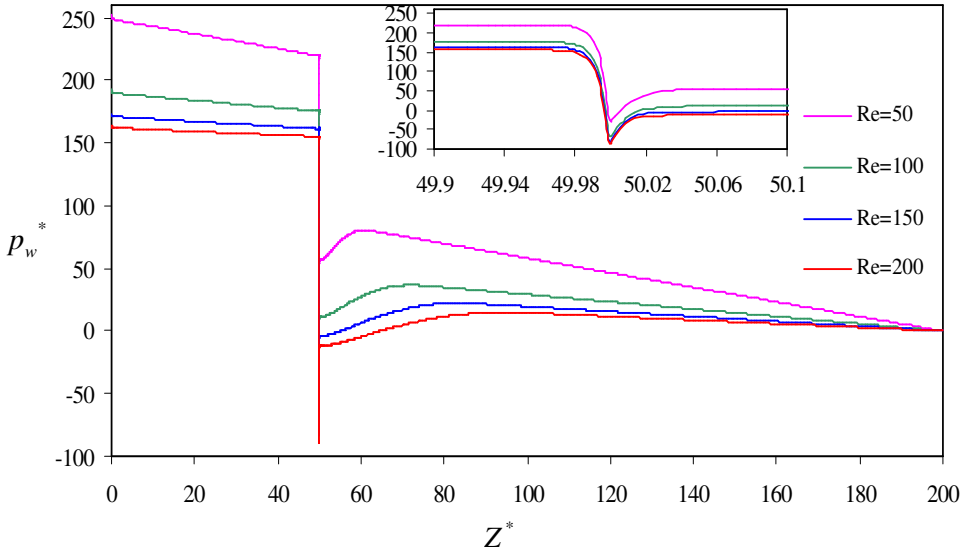

Figure 3.3: Variation of wall pressure along axial direction for the considered length for different Re for PR70% and Wo5

Re=50 and Re=200 respectively. Since no appreciable impact of Reynolds number on the variation of wall pressure at the stenosis zone is observed, the effect of Reynolds number on the wall pressure is studied for the case of severe stenosis with high pulsality of flow. The distribution of the time-averaged wall pressure along axial direction throughout the considered length of the artery is shown for Wo 12.5 and PR 70% for different Reynolds number in Fig.3.4. The maximum pressure drop is 244.07 for Re=50 and 244 for Re=200. The time averaged minimum pressure is -40.45 and -92.14 for Re=50 and Re=200 respectively. From the study on the effect of Reynolds number on wall pressure for all the combination cases, it is understood that the effect of Reynolds number is not so significant, but the magnitude of pressure drop decreases with increase in Re for all the cases. As can be seen from the figures the non-dimensional wall pressure drop decreases with increase in Reynolds number.

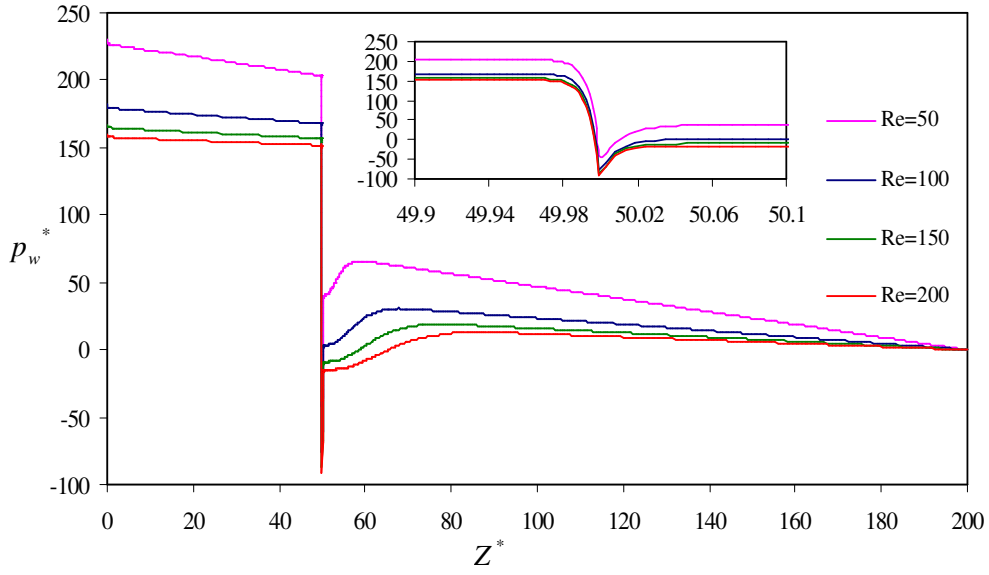

Figure 3.4: Variation of wall pressure along axial direction for the considered length for different Re for PR70% and Wo12.5

This inverse relation is happened because the pressure is non-dimensionalized as $p^* = p/\rho U^2$ in the mathematical formulation to solve the governing equations. At the throat of the stenosis i.e. when the blood flow converges, the pressure energy of flow converts to kinetic energy. As the Reynolds number of flow increases, the blood has a tendency to separate from the wall and the blood is less adhere to the artery wall. Thus the wall pressure has minimum magnitude at the throat of stenosis for higher Reynolds number and consequently the wall pressure drop is more for higher Reynolds number. From the overall study of the effect of Reynolds number on wall pressure, the wall pressure drop does not changes significantly for varying Re but the time average minimum pressure increases with increase in Re. Since low pressure at the stenosis zone correlates the tearing action of endothelium layer with subsequent thickening of plaque the chances of tearing action and plaque deposition increase with increase in Reynolds number for any particular combination case of mild stenosis, severe stenosis, low pulsality of flow and high pulsality of flow.

3.1.2 Streamline contour

From the study on the wall pressure in the previous section, it is understood that the flow field in the neighborhood of stenosis of an artery, especially throat of the stenosis and distal to the stenosis, is of great attention to fluid dynamics because of its relationship to localized arterial stenosis. To understand certain changes in the flow

structure as the Reynolds number changes, it is useful to consider the variations in the streamlines during one flow cycle (t/T=0.0-1.0). Time levels are chosen at points to clearly show the formation of flow separation zone, growth, expansion, and strength of the vortexes in the local stenosis of the artery. At first, the streamline contours are investigated for varying Reynolds numbers at different time steps for the case of mild stenosis and low pulsality of flow. The Fig.3.5 shows the streamline contours considering different Reynolds numbers (50, 100, 150 and 200) for different time steps, beginning of the systolic flow or forward flow (t/T=0.0), peak systolic flow phase (t/T=0.25), end of systolic flow (t/T=0.5) and peak diastolic flow or reverse flow (t/T=0.75) respectively for the case of PR 30% and Wo 5. The streamline contours indicate the area of flow separation as shown in the figure. The streamline separates from the wall just after the stenosis for every case. The negative pressure gradient termed as favorable pressure gradient enables blood flow through artery. The negative pressure gradient counteracts the retarding effect due to viscosity in the boundary layer. When the blood flow is passed through the stenosis, the pressure drops suddenly from the entry of the stenosis to the throat of the stenosis and the pressure recovers at the exit of the stenosis. Thus positive pressure gradient termed as adverse pressure gradient generates at the distal to the stenosis. The separated flow occurs at the downstream of the stenosis due to adverse pressure gradient. A permanent flow separation is found at the downstream of the stenosis, regardless of the time period as shown in the figures. The strength of the separated flow increases the flow approaches one time steps to next step. At the peak diastolic phase (t/T=0.75), the flow field cannot accommodate to the rapid changes of flow, a vortex ring is formed at the downstream of the stenosis for all considered Reynolds number as shown in Fig.3.5d. When the Reynolds number of flow increases the inertia force of flow dominates. With the increase of Reynolds number of flow, the flow at the post-stenotic zone is more perturbed. This is happened because at the higher Reynolds number, the kinetic energy of blood generated from the dissipation energy by the fluid on the fluid flow is not as much absorbed by the viscous force of flow. The size of the vortex ring for Reynolds number 200 is largest among all considered Reynolds numbers at the peak diastolic phase. This is also revealed that that the strength of the separated flow or the size of the flow separation zone increases with increase in value of Reynolds number for all the time steps. The Fig.3.6 shows the streamline contours considering different Reynolds numbers (50, 100, 150 and 200) for different time

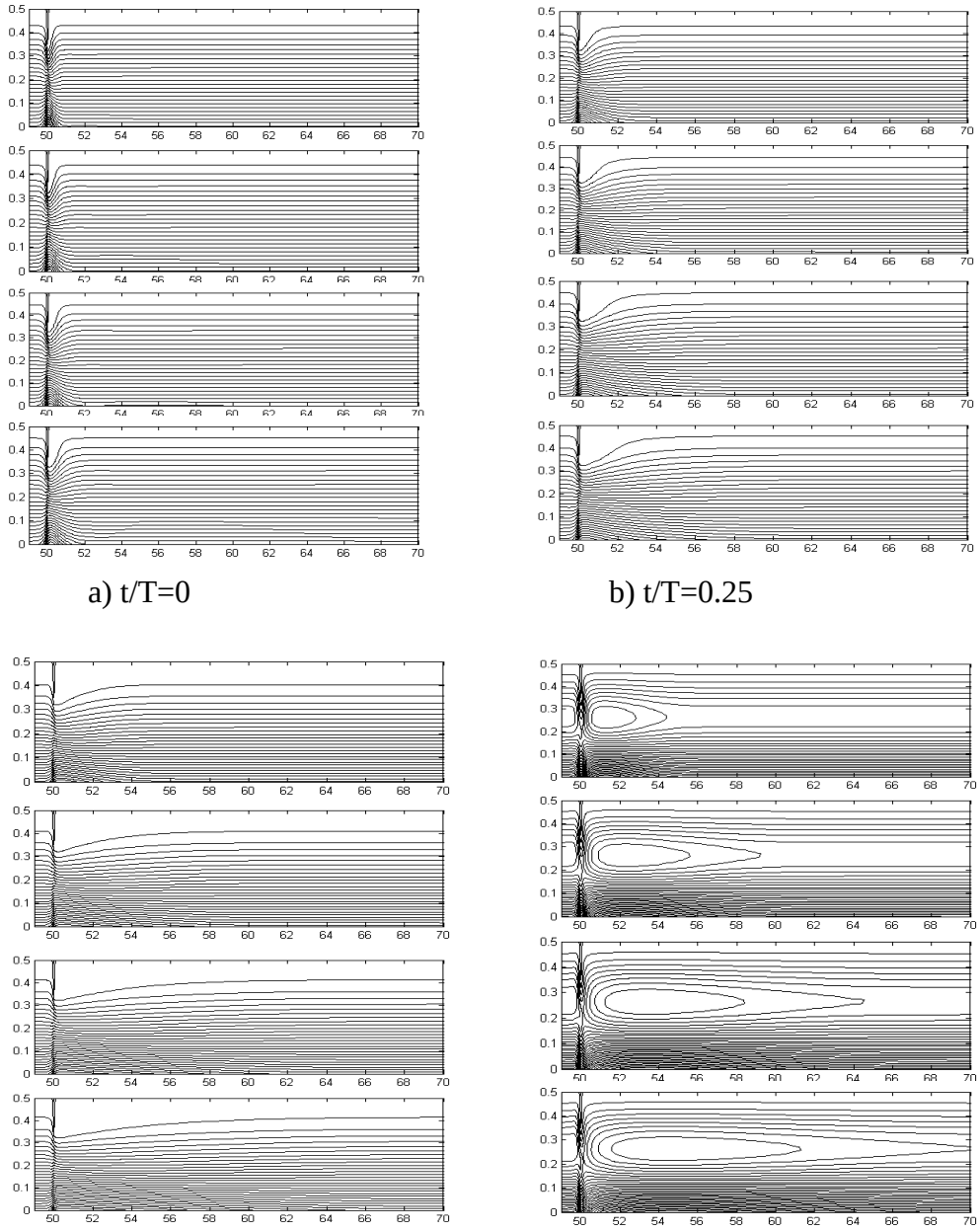

a) t/T=0 b) t/T=0.25

c) t*=0.50 d) t*=0.75

Figure 3.5: Streamline contours for Re 50, Re 100**,** Re150 and Re 200 (top to bottom) for PR 30% and Wo 5 at time step a) t/T=0, b) t/T=0.25, c) t/T=0.50 and d) t/T=0.75

steps, t/T=0.0, t/T=0.25, t/T=0.5 and t/T=0.75 respectively for the case of mild stenosis (PR 30%) and high pulsality of flow (Wo 12.5). The small vortex ring is formed at time level of peak systolic phase for higher Reynolds numbers (Re=150 and 200) as shown in Fig.3.6b. The vortex ring is always formed at the vicinity of stenosis for all considered Reynolds numbers at the beginning of diastolic phase and at the peak diastolic phase as shown in Fig.3.6c and Fig.3.6d. When the value of Re is

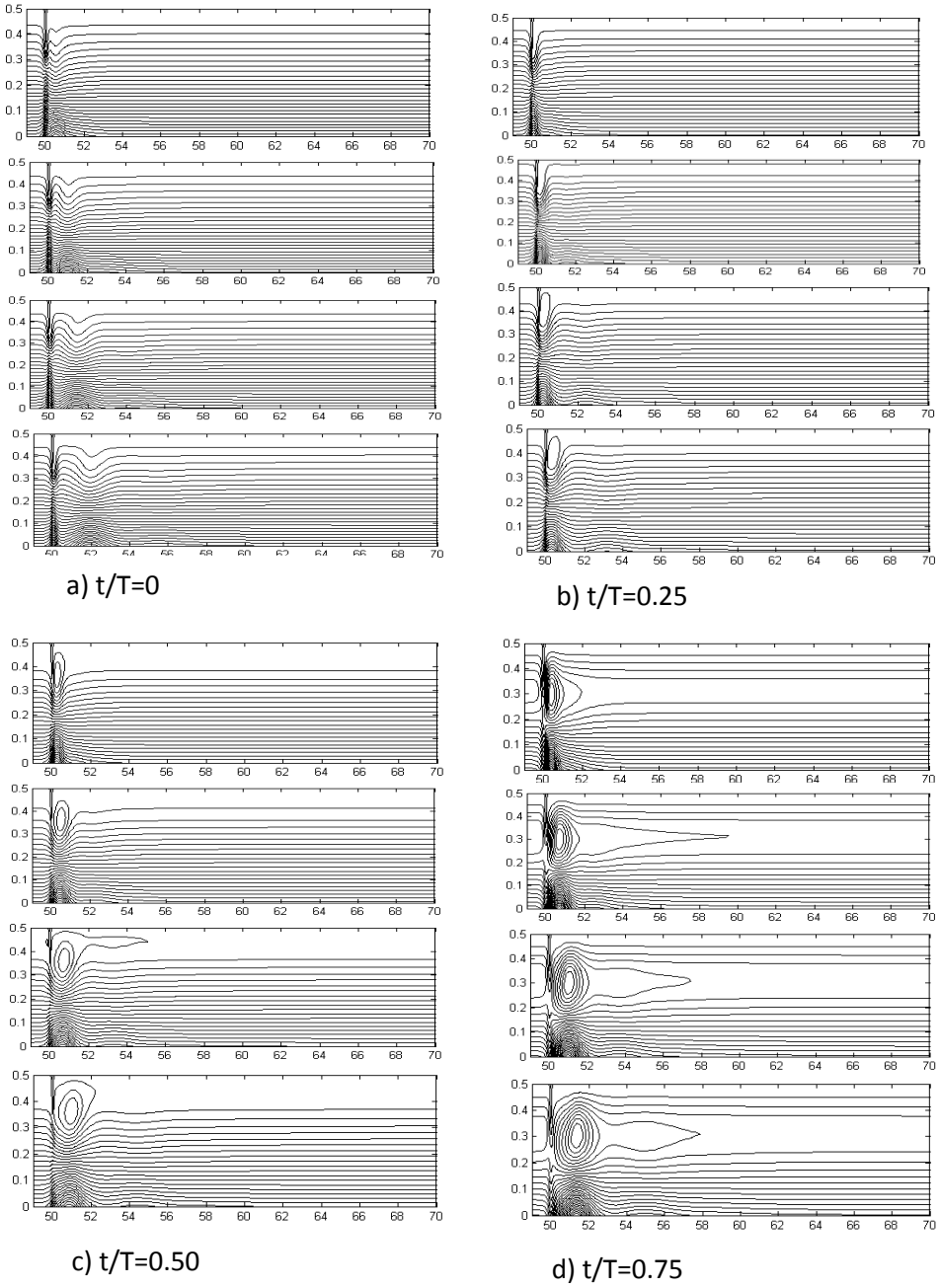

Figure 3.6: Streamline contours for Re 50, Re 100**,** Re150 and Re 200 (top to bottom) for PR 30% and Wo 12.5 at time step a) t/T=0, b) t/T=0.25, c) t/T=0.50 and d) t/T=0.75

increased, the strength of the flow separation as well as vortex formation is grown as depicted in the figures. Now the effect of Reynolds number on the streamline contours is investigated for the case of severe stenosis and low pulsality of flow. Figure.3.7 shows the streamline contours considering different Reynolds numbers (50, 100, 150 and 200) for different time steps, t/T=0.0, t/T=0.25, t/T=0.5 and t/T=0.75 respectively for the case of PR 70% and Wo 5. When the flow is restricted more and the flow frequency is less, i.e. the case of PR 70% and Wo 5, the vortex is formed at all the

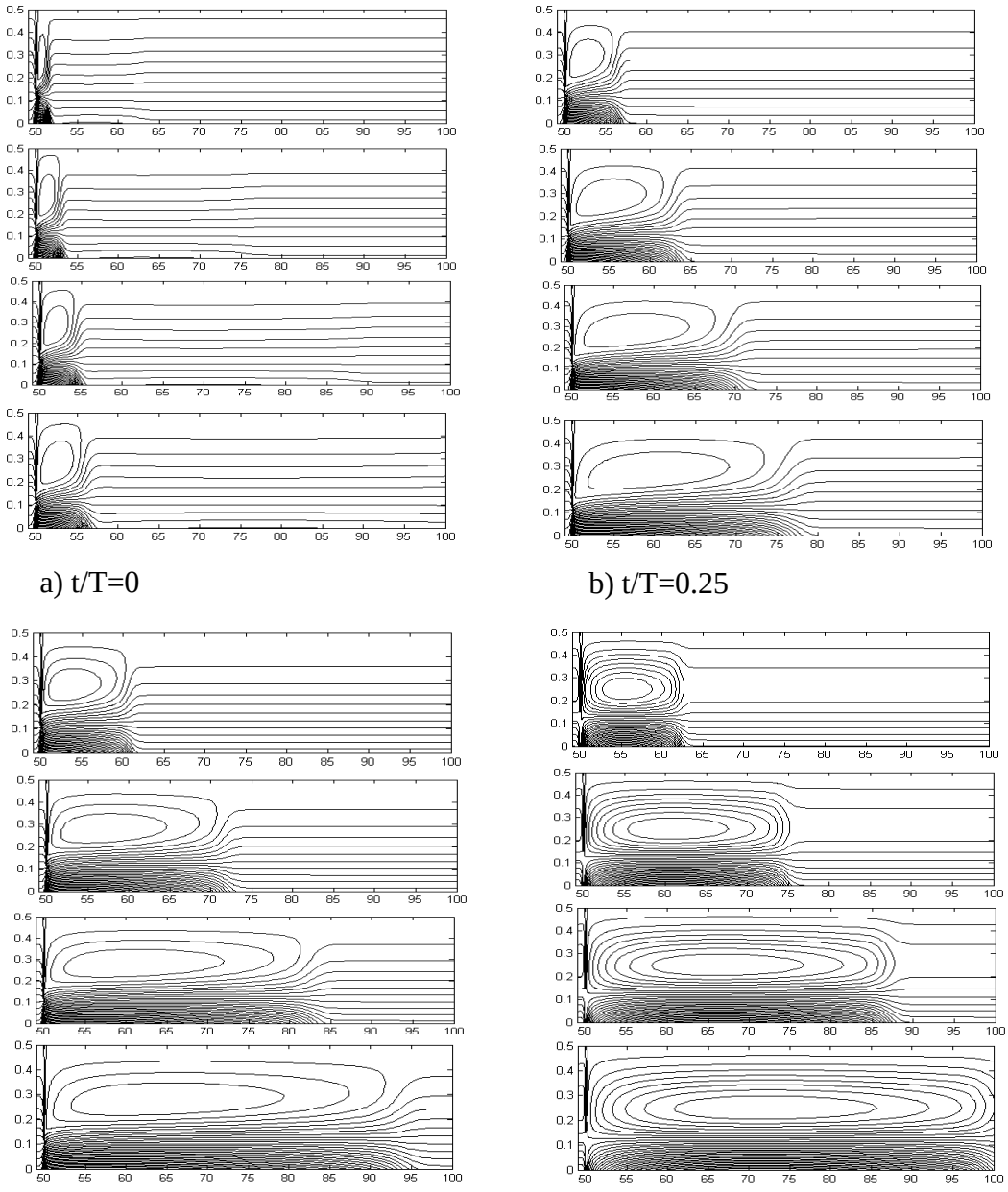

a) t/T=0 b) t/T=0.25

c) t/T=0.50 d) t/T=0.75

Figure: 3.7: Streamline contours for Re 50, Re 100**,** Re150 and Re 200 (top to bottom) for PR 70% and Wo 5 at time step a) t/T=0, b) t/T=0.25, c) t/T=0.50 and d) t/T=0.75

time phase for all considered Reynolds numbers. The strength of the vortex increases as the flow move from beginning of systolic phase to peak diastolic phase. The strength of the vortex also increases as the value of Re increases. Figure.3.8 shows the streamline contours considering different Reynolds numbers (50, 100, 150 and 200) for different time steps, t/T=0.0, t/T=0.25, t/T=0.5 and t/T=0.75 respectively for the case of PR 70% and Wo 12.5. The larger flow separation zone as well as formation of vortex is observed in this case at all the time phase for all considered Reynolds

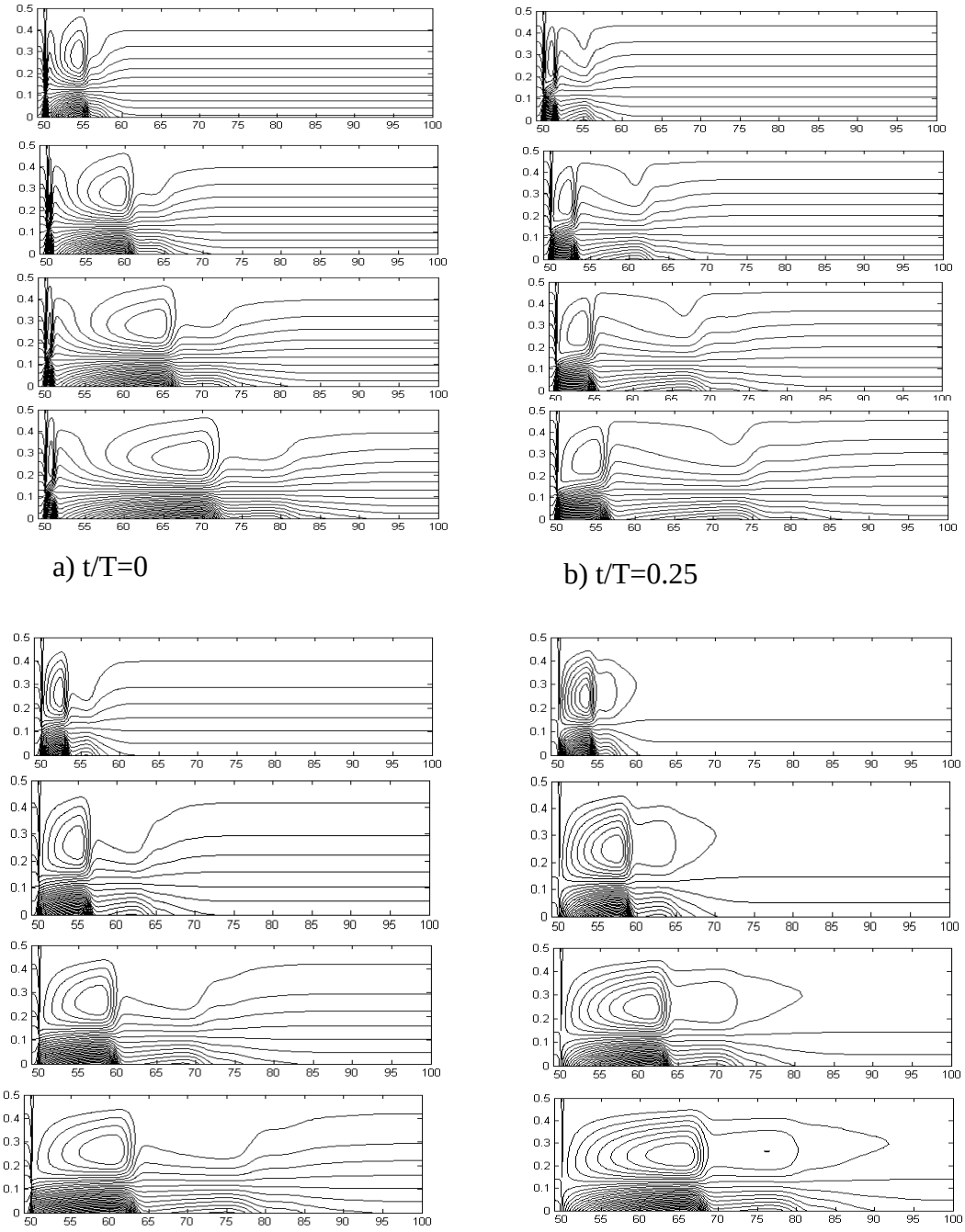

a) t/T=0 b) t/T=0.25

c) t/T=0.50 d) t/T=0.75

Figure 3.8: Streamline contours for Re 50, Re 100**,** Re150 and Re 200 (top to bottom) for PR 70% and Wo 12.5 at time step a) t/T=0, b) t/T=0.25, c) t/T=0.50 and d) t/T=0.75

numbers. The boundary layer thickness is very high at the time phase of peak diastolic phase shown in Fig.3.8d. In this case, the strength of the vortex also increases with increase in value of Reynolds number. From the overall study on the effect of Reynolds number on the instantaneous streamline patterns, it is understandable that

there is an increased flow separation zone for peak diastolic phase for a particular value of Reynolds number for any combination case of PR and Wo. The possible reason may be the minimum flow rate at that time instant of the cardiac cycle, leading to very low inertia strength with more or less same strength of diffusion. The strength of the flow separation zone always increases with increase in value of Re for any particular time phase and any combination case of PR and Wo. The major flow disturbance occurs at higher Reynolds number. This is known that the recirculation zone allows lipid particles and fibrin to form atheromatous plaque. Therefore, this phenomenon increases with the increase in Reynolds number and thereby leads to grow more severe stenosis at the post stenotic zone.

3.1.3 Peak wall shear stress and low wall shear stress

From the study on wall pressure and streamline contour in the previous sections, it is felt that the study of the shear stress in the arterial wall in the vicinity of a stenosis is important as it might help us to explain the cause of post-stenotic dilatation and to investigate the causes behind development and progression of arterial stenosis. Wall shear stress is directly proportional to the velocity gradient. Blood flow velocity changes in the stenosis zone and post-stenotic zone as the flow pressure gradient changes. It is understood from previous studies that the maximum velocity gradient exists at the throat of the stenosis and minimum velocity gradient exists at the post stenotic zone. Therefore, it is very important to notice the wall shear distribution in the stenotic zone as well as post stenotic zone. At first, the case of mild stenosis and low pulsality of flow is considered to understand the effect of Reynolds numbers on the wall shear stress. The variation of the time-averaged WSS along axial direction in the stenotic zone is shown for Wo 5 and PR 30% in Fig.3.9 to show the effect of Reynolds number on peak wall shear stress. It is revealed that the nature of variation of the time-averaged WSS is almost similar for all the considered Reynolds numbers. It is noted that TAWSS increases rapidly as the flow approaches the stenosis or restriction and reaches a peak value near the maximum restricted area. Then at the downstream of the stenosis, wall shear stress decreases rapidly to zero and then it becomes of negative magnitude. As the spatial and temporal magnitude of axial velocity increases with increase in Reynolds number, the flow rate is higher for higher Reynolds number of flow. The higher flow rate increases the velocity gradient in the artery wall and thus wall shear stress at the throat of the artery reaches at higher

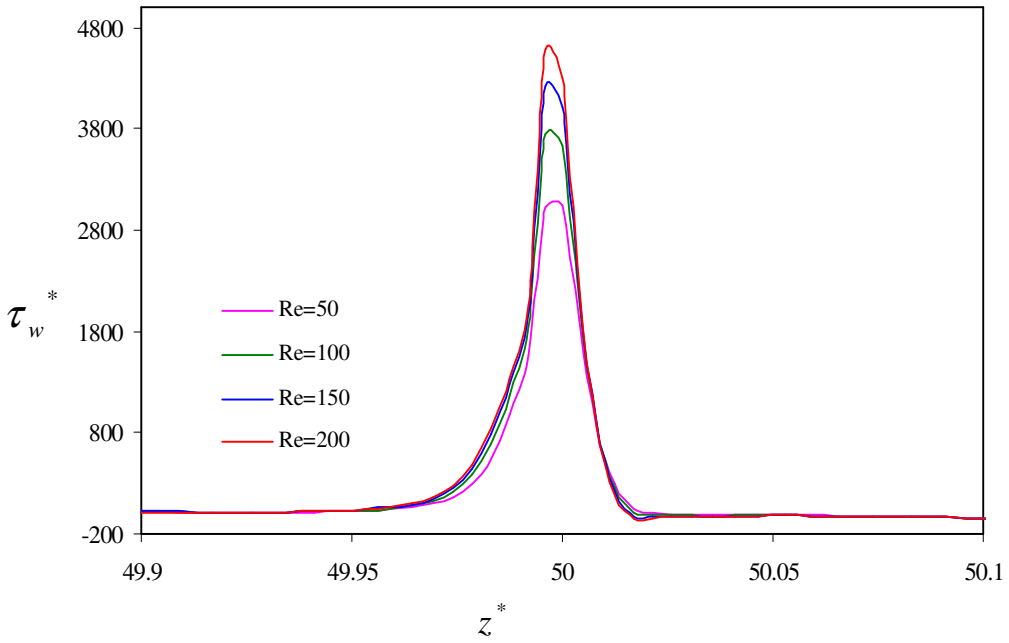

Figure 3.9: Variation of PWSS at stenotic zone along axial direction for different Re for PR30% and Wo5

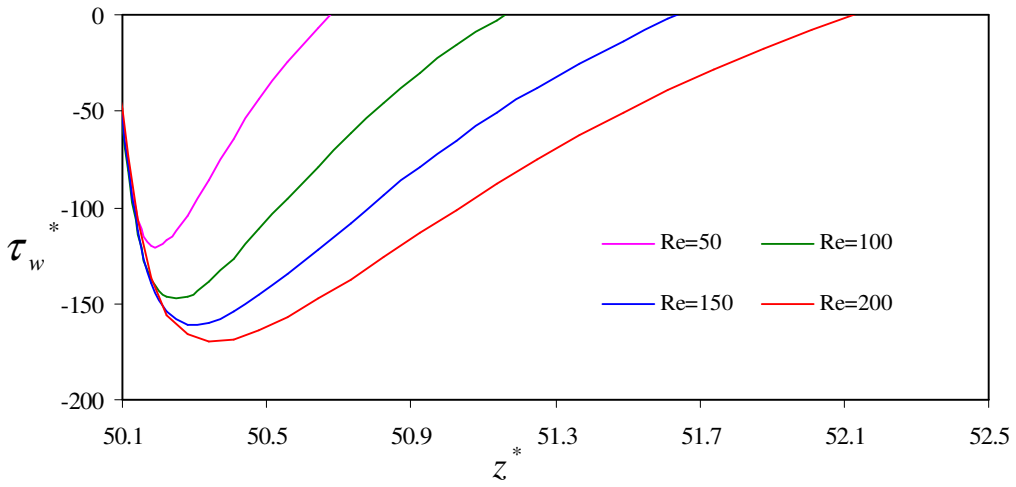

Figure 3.10: Variation of LWSS at post-stenotic zone along axial direction for different Re for PR30% and Wo5

value for higher Reynolds number. From the figure, it is also observed that the magnitude of peak wall shear stress increases with increase in Reynolds number. The PWSS for Re=200 is 1.5 times greater than the PWSS for Re=50. Figure.3.10 shows the variation of wall shear stress along axial direction at the post-stenotic zone to show the effect of Reynolds number on the low wall shear stress. It is noticed that the region just immediate after stenosis is prone to very low wall shear stress, irrespective

of Reynolds number of the flow. This is linked to the existence of recirculation zone at downstream of stenosis. The figure depicts that the wall shear stress changes its direction from positive to negative when the flow leaves the stenosis and from negative to positive at the downstream flow after stenosis. There are two points of zero wall shear stress. The time averaged wall shear stress zero means the velocity gradient is zero. Thus there are two points of flow stagnation. The first one is flow separation point and the second one is flow reattachment point. From the figure, it is observed that the reattachment length increases with increase in value of Re. It is also observed that the magnitudes of maximum low wall shear stress increase with increase in Reynolds number and the area under low wall shear stress also increases with increase in Reynolds number. At the higher Reynolds number, the adverse pressure gradient as well as the size of the recirculation zone is more, which leads to higher magnitude of peak of low wall shear stress with higher area of low wall shear stress zone. The maximum low WSS for Re=200 is 1.45 times greater than the maximum low WSS for Re=50. The variation of the time-averaged WSS along axial direction in the stenotic zone is shown in Fig.3.11 to show the effect of Re on peak TAWSS for the case of high pulsality of flow (Wo 12.5) and mild stenosis (PR

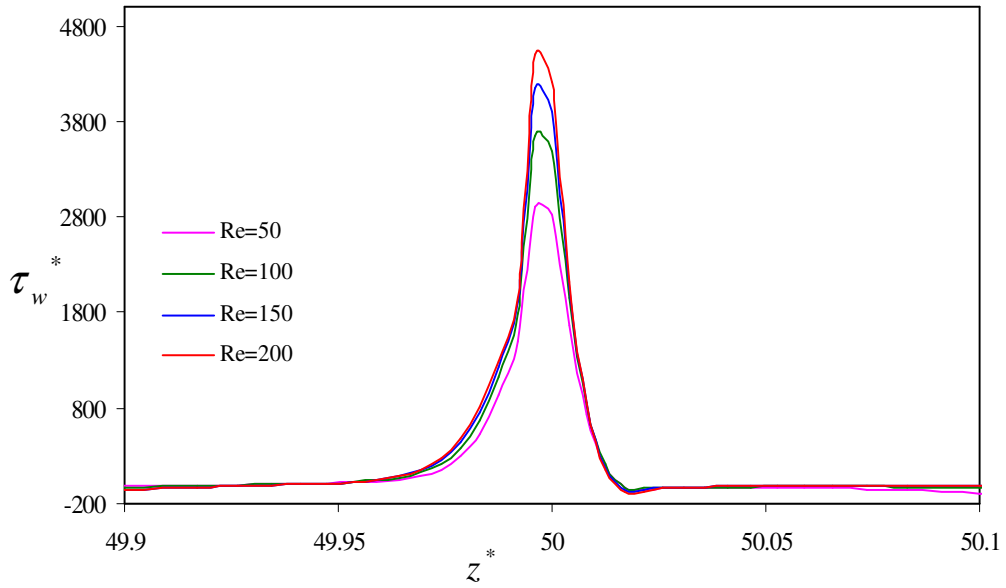

Figure 3.11: Variation of PWSS at post-stenotic zone along axial direction for different Re for PR30% and Wo12.5

30%). The distribution pattern of WSS is almost same as the previous case and the magnitude of peak wall shear stress also increases with increase in Reynolds number.

The PWSS for Re=200 is 1.49 times greater than the PWSS for Re=50. The Fig.3.12 illustrates the variation of wall shear stress along axial direction at the post-stenotic zone to show the effect of Re on low wall shear stress for the case of Wo 12.5 and PR 30%. From the figure of low wall shear stress, it is observed that the magnitudes of

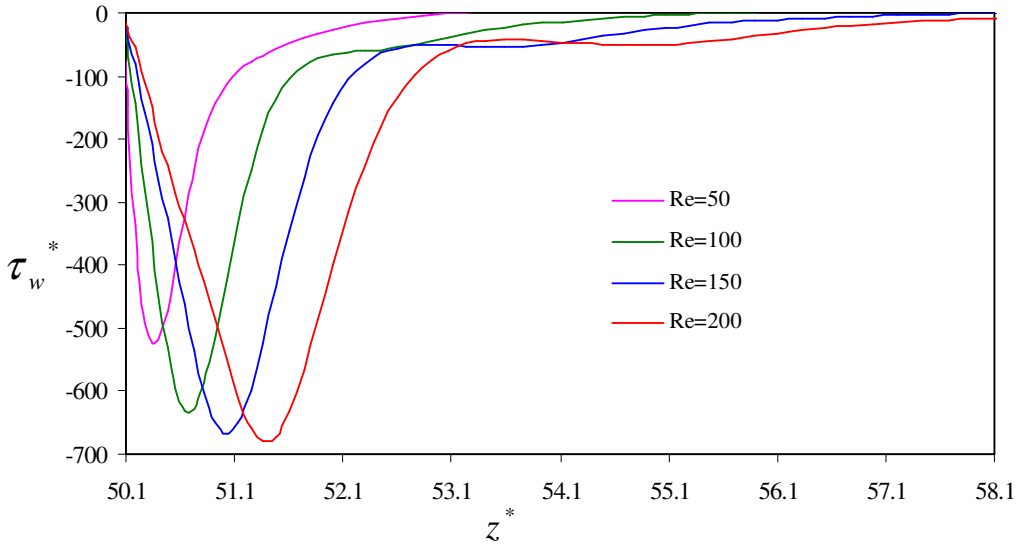

Figure 3.12: Variation of LWSS at post-stenotic zone along axial direction for different Re for PR30% and Wo12.5

maximum low wall shear stress and area for the low wall shear stress zone increase with increasing in Reynolds number. The reattachment length also increases with increase in Reynolds number for this case. The overall effect of Re on low WSS is

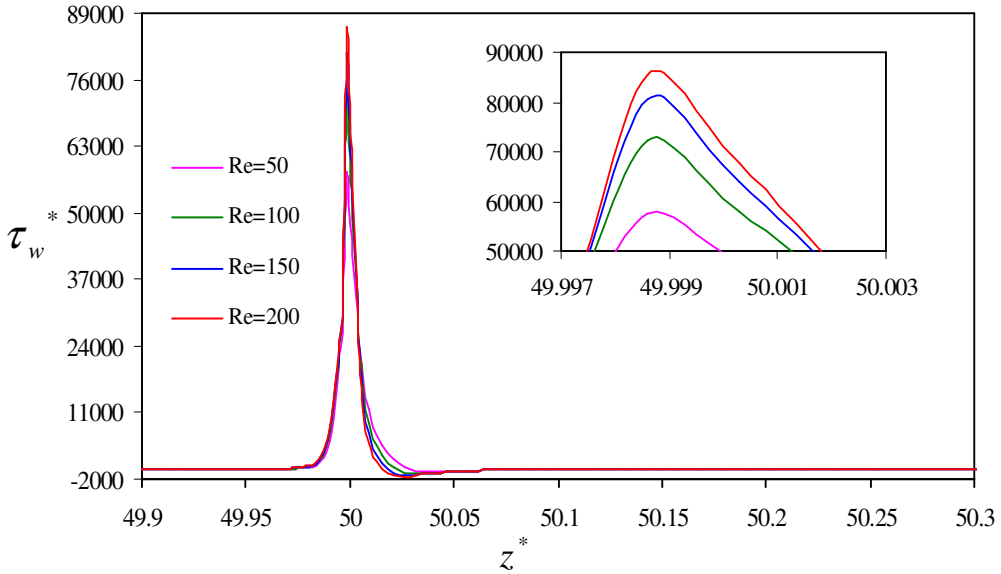

Figure 3.13: Variation of PWSS at post-stenotic zone along axial direction for different Re for PR 70% and Wo5

less in comparison to the previous case. The maximum low WSS for Re=200 is 1.31 times greater than the maximum low WSS for Re=50. Now the effect of Reynolds number on wall shear stress is investigated for severe stenosis with low pulsality of flow. The variation of the time-averaged WSS along axial direction in the stenotic zone is shown in Fig.3.13 for the case of Wo 5 and PR 70% to show the effect of Re on peak WSS. From the figure, it is investigated that the nature of distribution pattern of wall shear stress is similar as the previous cases and the magnitude of peak wall shear stress also increases with increase in Reynolds number. The magnitude of peak WSS is increased more for each Re while comparing with previous case due to more constriction of arterial flow. The PWSS for Re=200 is 1.48 times greater than the PWSS for Re=50. Figure 3.14 shows the variation of wall shear stress along axial

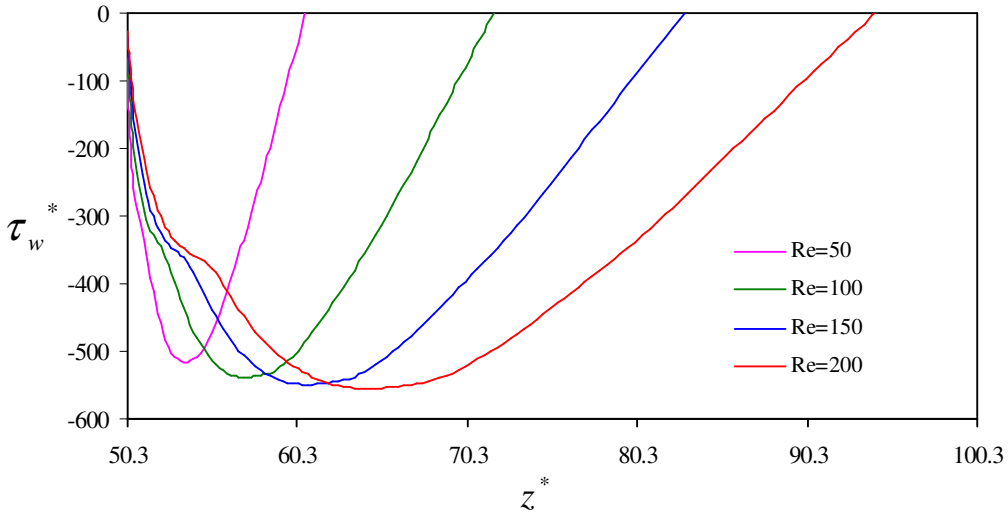

Figure 3.14: Variation of LWSS at post-stenotic zone along axial direction for different Re for PR70% and Wo5

direction at the post- stenotic zone to show the effect of Re on low wall shear stress for the case of Wo 5 and PR 70%. From the figure of low wall shear stress, it is observed that the area for the low wall shear stress zone increase with increase in Reynolds number but the effect of Re on maximum low WSS is almost negligible. The maximum low WSS for Re=200 is 1.08 times greater than the maximum low WSS for Re=50. The variation of the time- averaged WSS along axial direction in the stenotic zone to investigate the effect of Re on peak WSS is shown in Fig.3.15 for the case of Wo 12.5 and PR 70%. From the figure, it is observed that the nature of variation of WSS and the effect of Re on peak WSS is almost similar to the previous case, i.e. Wo 5 and PR 70%. The PWSS for Re=200 is 1.17 times greater than the

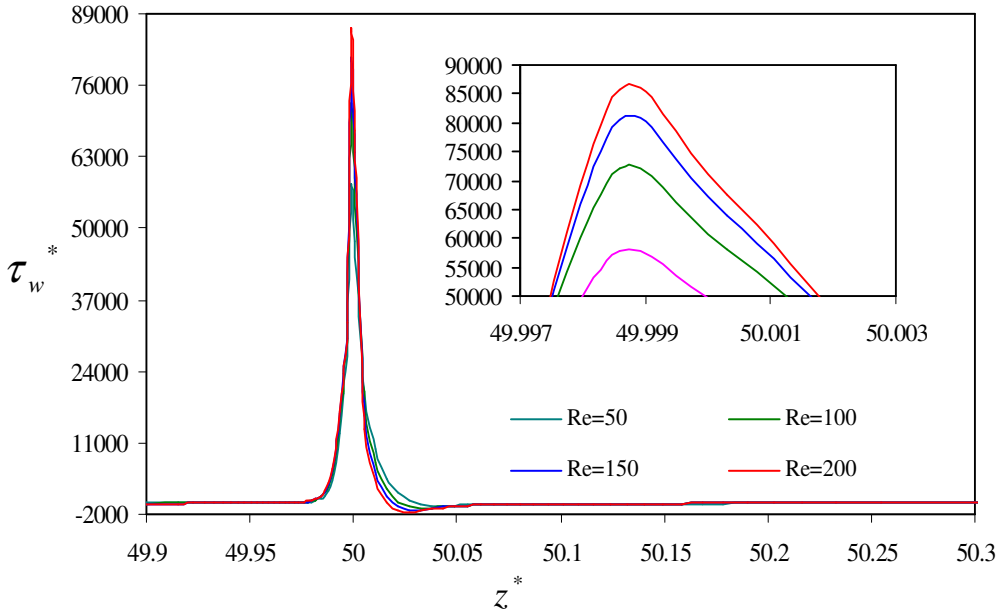

Figure 3.15: Variation of PWSS at post-stenotic zone along axial direction for different Re for PR70% and Wo12.5

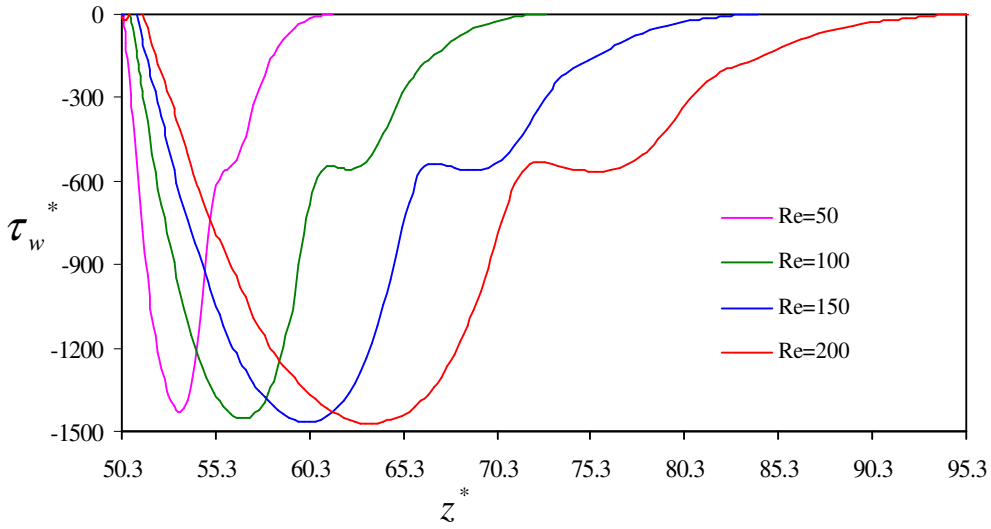

Figure 3.16: Variation of LWSS at post-stenotic zone along axial direction for different Re for PR70% and Wo12.5

PWSS for Re=50. Figure 3.16 depicts the variation of wall shear stress along axial direction at the post-stenotic zone to show the effect of Re on low wall shear stress for the case of Wo 12.5 and PR 70%. From the figure of low wall shear stress, it is observed that the magnitudes of maximum low wall shear stress changes minor with the changes in value of Re but the reattachment length increases with increasing in value of Reynolds number. The maximum low WSS for Re=200 is 1.03 times greater

than the maximum low WSS for Re=50. From the overall study of the effect of Reynolds number on the peak wall shear stress, it is attributed that the peak wall shear stress always increases with increase in Reynolds number for all combination case of percentage of restriction and Womersley number. As peak wall shear stress damages the vessel wall and causes intimae thickening, platelets aggregation and finally results in the formation of thrombus, the damaging chance is higher for higher value of Reynolds number. From the overall study of the effect of Reynolds number on the low wall shear stress, it is attributed that the magnitude of the maximum low WSS and the area under low wall shear stress always increases with increase in Reynolds number for all combination case of percentage of restriction and Womersley number. As low shear stress in the separation region is well thought-out to be associated to the mass transportation across the arterial wall and long staying time for platelet endothelium interaction the chances of formation of atherosclerosis due to the mass transportation across the arterial wall increases with increase in percentage of restriction.

3.1.4 Oscillatory shear index

During the study on instantaneous streamline patterns, it has been observed that the flow field always changes with the time steps of a cardiac cycle. The flow reversal is noticed at each time step and the pattern is different. The time-averaged wall shear stress is studied in the previous section. The time-averaged wall shear stress is estimated by integrating the instantaneous wall shear stress over a cycle time. Viewing on the instantaneous streamline patterns, it can be said that the instantaneous wall shear stresses are not same with varying times of a cardiac cycle at any particular location along the axial direction of arterial length. Thus there exists oscillatory wall shear stress in the blood flow. The oscillatory shear index defines the oscillatory motion of wall shear stress. In this sub section, the effect of Reynolds number on the OSI is investigated for all the combination case of mild stenosis, severe stenosis, low pulsality of flow and high pulsality of flow. The distribution pattern of the OSI along axial direction of arterial length in the stenotic zone and post stenotic zone is shown in Fig.3.17 for the case of Wo 5 and PR 30% to investigate the effect of Reynolds number on oscillatory wall shear stress. It is observed from the figure that the OSI has two maximum values for each of all the considered Re flow, one closely after midpoint of stenosis and another one far from the midpoint. As can seen at the

mathematical definition of OSI, it is cleared that OSI reaches its maximum value when the instantaneous wall stress at each time step of a cardiac cycle align at the same direction or remains at the same sign. Near the midpoint, the velocity gradient is high and the instantaneous wall shear stress reaches its peak value for each time step and thus OSI increases at this location. At the reattachment point, instantaneous

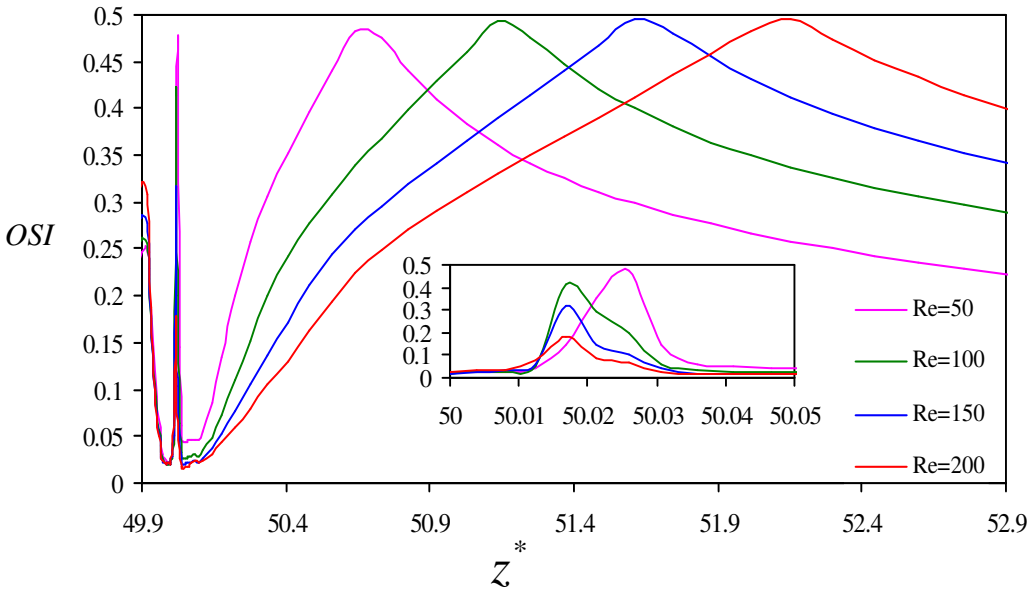

Figure 3.17: Variation of OSI along at stenotic and post stenotic zone axial direction for different Re for PR30% and Wo 5

wall shear stress, which remains in the negative direction, changes the sign. OSI again reaches its maximum value at the point of reattachment point. Therefore, the location of second maximum OSI magnitude coincides with the location of time-averaged reattachment point. Time-averaged reattachment points for all considered Reynolds numbers are clearly estimated by both WSS and OSI graphs. The axial location for which WSS reaches to zero value (Fig.3.10) or the location of second maximum value of OSI (Fig.3.17) shows the time-averaged reattachment point for each Reynolds number. The time-averaged reattachment point reflects the interaction of viscous and inertial forces and it differs for all considered Reynolds numbers as shown in figure. From the study, it is revealed that the longest time-averaged reattachment point (z*=52.15) appears at Re=200 and the shortest time averaged reattachment point (z*=50.64) is belonging to Re=50. At the stenosis zone the maximum value of OSI increases with decrease in value of Re. The possible reason may be explained as that at higher Reynolds number, the flow rate is higher. As the inertia force increases, the

core flow gets little time to complete more flow reversals at the artery wall at the

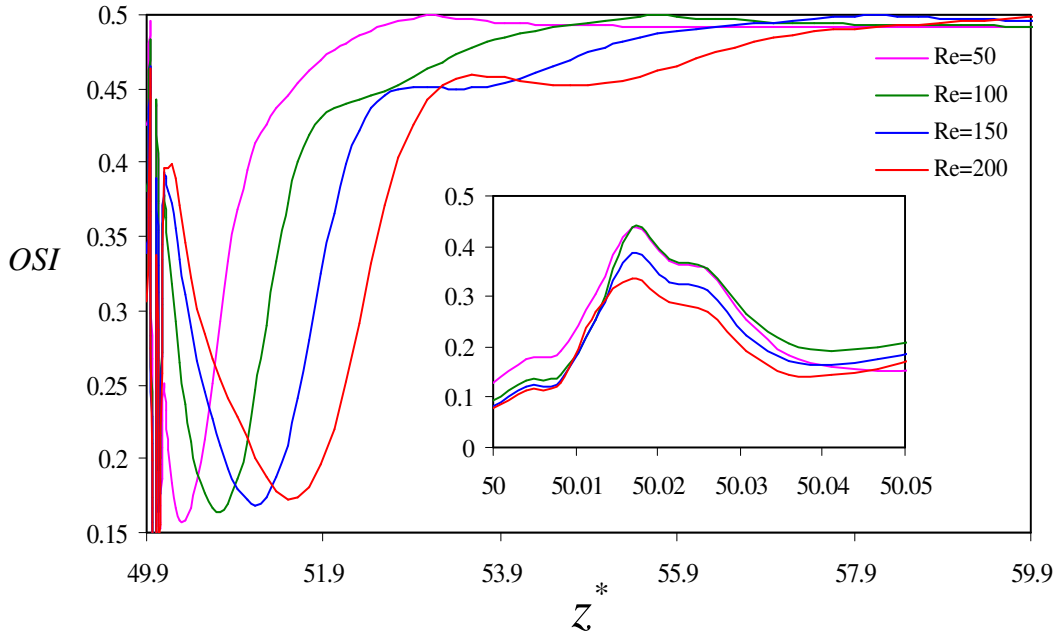

Figure 3.18: Variation of OSI along at stenotic and post stenotic zone axial direction for different Re for PR30% and Wo 12.5

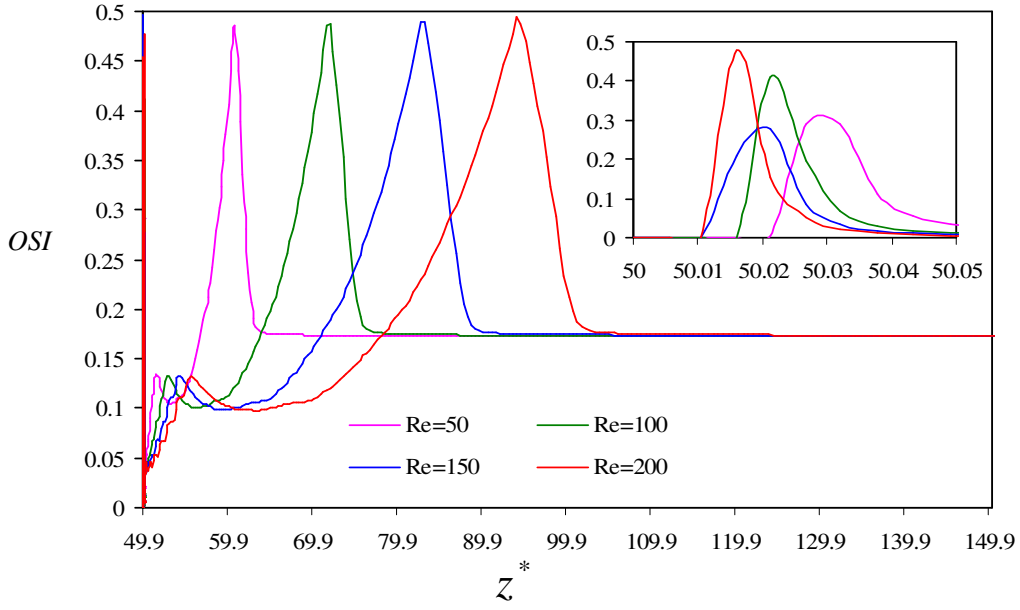

Figure 3.19: Variation of OSI along at stenotic and post stenotic zone axial direction for different Re for PR70% and Wo 5

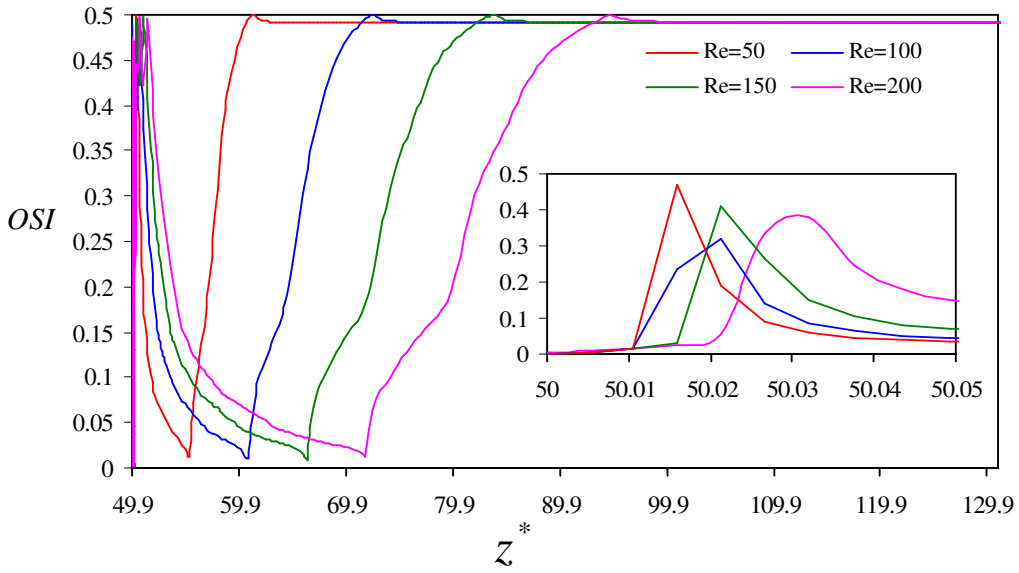

Figure 3.20: Variation of OSI along at stenotic and post stenotic zone axial direction for different Re for PR70% and Wo 12.5

stenotic zone and wall shear stress is less fluctuating in nature. At the downstream of stenosis, the dissipation of energy by the fluid on the flow is more for higher Reynolds number. The formed vortex oscillates more with time at the post stenotic zone for higher value of Reynolds number and the size of the formed vortex is also larger for higher Reynolds number. This is why, a large region of OSI is observed at higher value of Reynolds number. The variation of the OSI along axial direction in the stenotic zone and post stenotic zone is shown in Fig.3.18 for the case of Wo 12.5 and PR 30% for varying Reynolds numbers. For this case the OSI has also two maximum, one closely after midpoint of stenosis and the other one far from the midpoint. The both of the reattachment length and the maximum OSI value at stenosis zone increase with increase in value of Re. The effect of Re on OSI at the stenosis zone is not so prominent. It is also revealed that the longest time-averaged reattachment point (z*=59.88) appears at Re=200 and the shortest time averaged reattachment point (z*=53.07) is belonging to Re=50. The variation of the OSI along axial direction in the stenotic zone and post stenotic zone is shown in Fig.3.19 for the case of Wo 5 and PR 70% for varying Reynolds numbers. There is a noticeable increase of OSI at the stenotic zone and the effect of Re on the OSI is also obvious. At the stenotic zone, the OSI values are 0.29 and 0.48 for Re=50 and Re=200 respectively. The reattachment length increases with increase in value of Re as shown

in the figure. The longest time-averaged reattachment point (z*=94.11) appears at Re=200 and the shortest time averaged reattachment point (z*=60.89) is belonging to Re=50. The variation of the OSI along axial direction in the stenotic zone and post stenotic zone is shown in Fig.3.20 for the case of Wo12.5 and PR 70% for varying Reynolds numbers. In this case, there is a noticeable increase of OSI at the stenotic zone as the previous case. The effect of Re on the OSI at the stenotic zone is not so marked. In this case, the reattachment length also increases with increase in value in Re. the longest time-averaged reattachment point (z*=95.11) appears at Re=200 and the shortest time averaged reattachment point (z*=61.48) is belonging to Re=50. The reverse flow is associated with the development of atherosclerosis, which in turn is related to the degeneration of the arteries wall. High OSI along with low wall stress is the crucial factors in the development and formation and localization of the atherosclerosis. From the overall study of the effect of Reynolds number on the oscillatory shear index, it may be mentioned that higher value of Re always increases the chances of the development and localization of the disease of the atherosclerosis.

3.2 Effect of Percentage of Restriction for Simple Pulsatile Flow

In this section, a series of numerical simulations of model bell shaped stenosed artery considering simple pulsatile flow have been carried out and the effect of percentage of restriction on the flow characteristics, e.g. wall pressure, streamline contour, WSS and OSI in each case have been investigated.

The percentage of restriction or degree of stenosis estimates the extent of blockage of arterial flow in an artery. The percentage of restriction has an important effect on the hemodynamic flow characteristics. The validated numerical code is used to simulate the hemodynamic parameters for simple pulsatile flow through stenosed artery with all combination case of low Reynolds number (Re=50), high Reynolds number (Re=200), low Womersley number (Wo=5) and high Womersley number (Wo=12.5), The effect of percentage of restriction is investigated on the flow characteristics for four different cases. Five diametric occlusions (PR=30%, 40%, 50%, 60% and 70%) have been considered for studying the effect of percentage of restriction on the flow characteristics. The numerical simulation results is employed to study the effects of percentage of restriction on flow characteristics particularly on arterial wall pressure, stream line contours, wall shear tress and oscillatory shear index.

3.2.1 Wall pressure

In this subsection, the effect of percentage of restriction on the wall pressure is studied for the all the combination case of low Reynolds number, high Reynolds number, Low Womersley number and high Womersley number respectively. At first, the effect of percentage of restriction on wall pressure is investigated for the case of low Reynolds number and low Womersley number. The distribution of time-averaged wall pressure along the axial direction throughout the considered arterial length is shown in Fig. 3.21 for Re 50 and Wo 5. The figure depicts the effect of percentage of restriction on the wall pressure along the axial direction. The wall pressure gradually decreases from upstream of flow to downstream of flow for all the percentage of

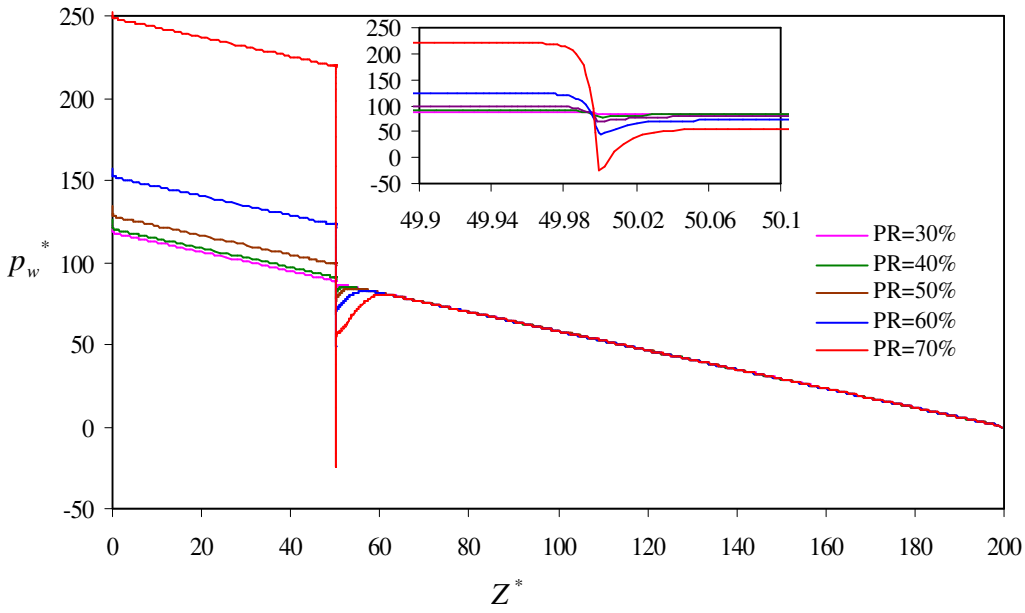

Figure 3.21: Variation of wall pressure along axial direction for the considered length and at the stenotic zone for different PR for Re 50 and Wo 5

restriction. There is a sharp pressure drop at the location of stenosis and then the wall pressure recovers with the partial pressure losses. The magnitude of wall pressure drop increases with the increase in percentage of restriction as can be seen in the figure. These phenomena can be explained with our considered bell shaped stenosis models. If the percentage of restriction increases, height of the stenosis at the throat section increases, and the length of the stenosis, from beginning of stenosis to throat of stenosis, does not change. As the height of stenosis at throat section increases the flow area at throat section decreases. The conversion of pressure energy to kinetic energy at the throat section is more for higher percentage of restriction and thus the

pressure drops more at the throat section. Furthermore, it is observed that the pressure recovery at end of the stenosis decreases with increase in percentage of restriction. The probable reason of this phenomenon can be clarified with varying diffuser angle in the diverging section of stenosis. When percentage of restriction increases, both of height and length of stenosis in the diverging section increases. As can be seen in the Table 2.1, the percentage increase of length is more than the percentage increase of height while percentage of restriction increases. So the diffuser angle decreases with increase in percentage of restriction. As we know that percentage of pressure recovery at diffuser section increases with increase in the diffuser angle till the advent of diffuser stall. Thus the pressure recovery in the diverging section of stenosis

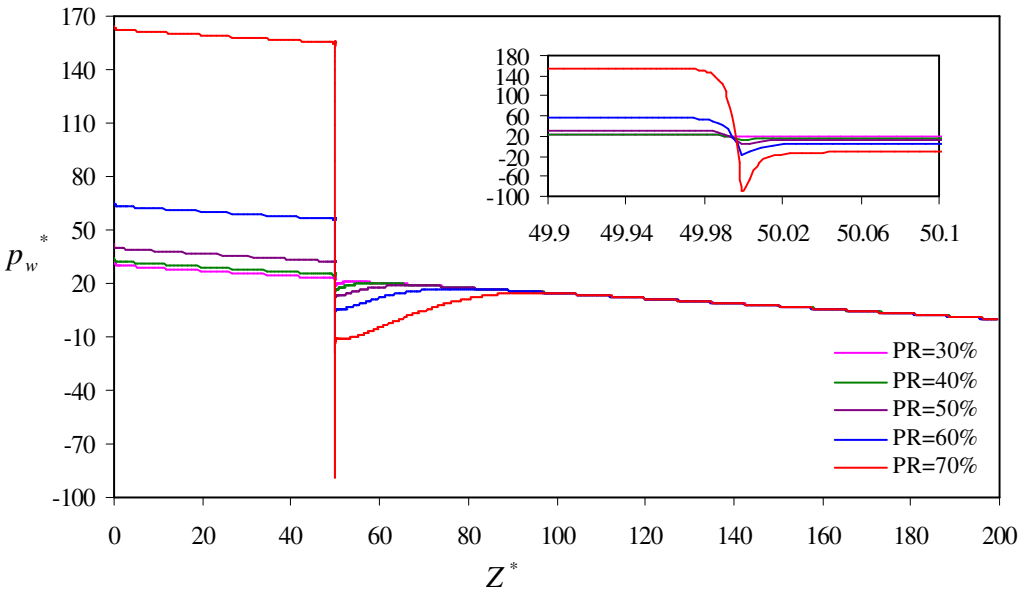

Figure 3.22: Variation of wall pressure along axial direction for the considered length for different PR for Re 200 and Wo 5

decreases with increase in percentage of restriction. The wall pressure drop is 6.43 for PR= 30% and 236.23 for PR=70%. The minimum time averaged pressure is observed for PR 70% and the value is -16.44. Now the effect of percentage of restriction on wall pressure is studied for the high Re flow with low Womersley number. The distribution of time-averaged wall pressure along the axial direction throughout the considered arterial length is shown in Fig. 3.22 for Re 200 and Wo 5. The wall pressure distribution pattern is same as previous case. The magnitude of wall pressure drop increases with increase in Percentage of restriction. The percentage of pressure recovery decreases as percentage of restriction increases, same as the previous case. The wall pressure drop is 4.84 for PR= 30% and 242.94 for PR=70%. The minimum

time averaged pressure is observed for PR 70% and the value is -87.87. The distribution of time-averaged wall pressure along the axial direction throughout the considered arterial length is shown in Fig. 3.23 for different percentage of restriction

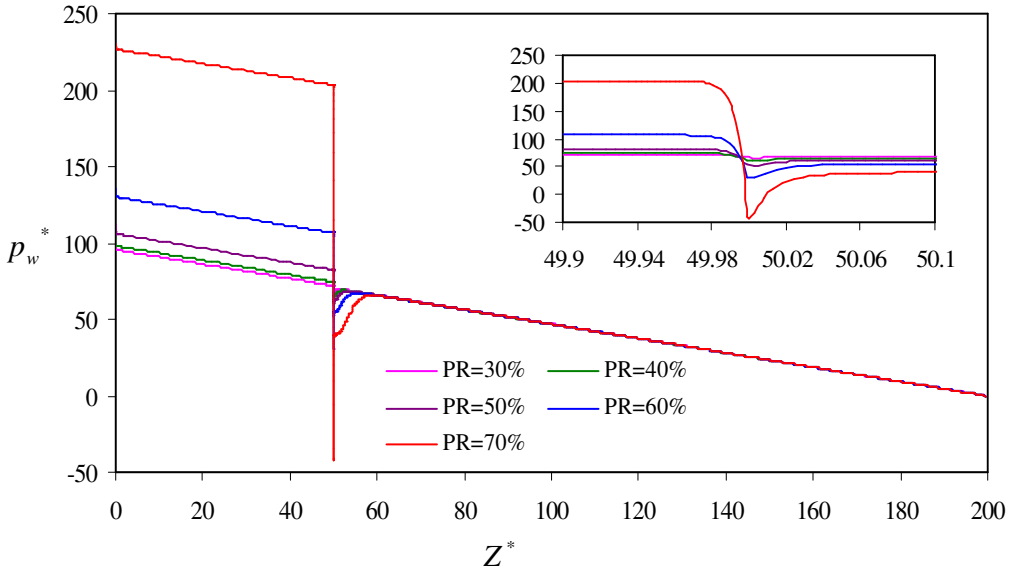

Figure 3.23: Variation of wall pressure along axial direction for the considered length and at the stenotic zone for different PR for Re 50 and Wo 12.5

for Re 50 and Wo 12.5. In this case, the distribution of wall pressure is also same as previous cases. The wall pressure drop increases with increase in percentage of restriction, and the percentage of pressure recovery decreases as percentage of restriction increases. The wall pressure drop is 7.41 for PR= 30% and 244.08 for PR=70%. The minimum time averaged pressure is observed for PR 70% and the value is -40.45. Finally the effect of percentage of restriction on wall pressure for varying percentage of restriction is investigated for the case of high Reynolds number and high Womersley number. The distribution of time-averaged wall pressure along the axial direction throughout the considered arterial length is shown in Fig. 3.24 for varying percentage of restriction for Re 200 and Wo 12.5. The wall pressure drop also increases with increase in PR and the percentage of pressure recovery also decreases as percentage of restriction increases. The wall pressure drop is 5.27 for PR= 30% and 244.01 for PR=70%. The minimum time averaged pressure is observed for PR 70% and the value is -92.14. From overall study of the effect of PR on the wall pressure it is understandable that there is a significant effect of PR on wall pressure. The wall pressure drop extensively increases with increase in percentage of restriction. This pressure drop at the stenosis zone increases slowly for mild to

moderate stenosis, whereas from moderate to severe stenosis condition, this pressure drop increases markedly. As the variable wall pressure, i.e. sudden drop of wall pressure and recovery, can damage and weaken the internal wall of the artery, the

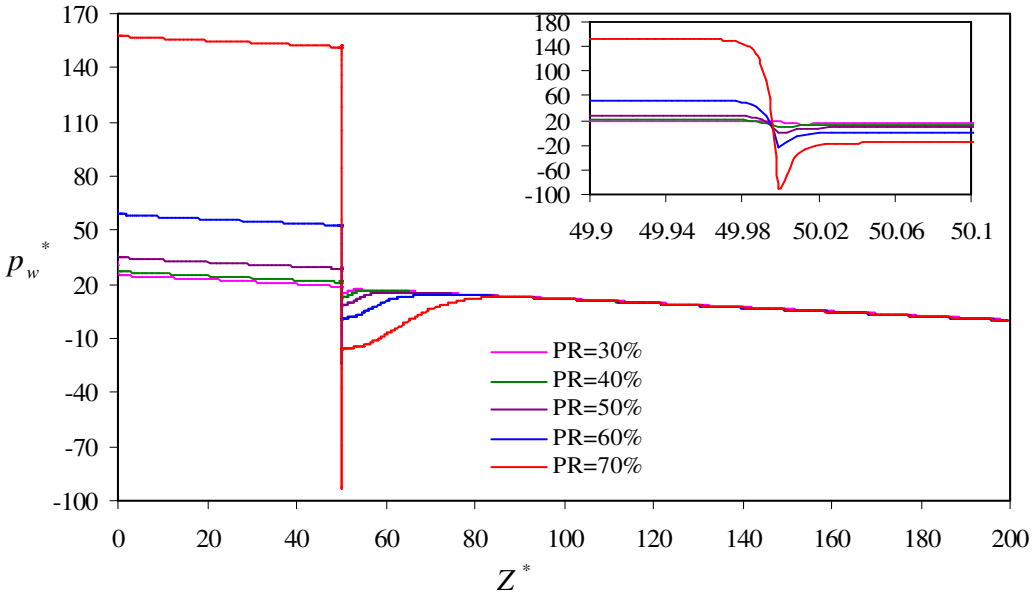

Figure 3.24: Variation of wall pressure along axial direction for the considered length and at the stenotic zone for different PR for Re 200 and Wo 12.5

chances of artery wall damage increases with higher percentage of restriction. The time averaged minimum wall pressure increases with increase in PR for all considered cases. As the low pressure at the stenosis zone correlates the tearing action of endothelium layer with subsequent thickening of plaque the chances of tearing action and plaque deposition increase with increase in percentage of restriction for any particular combination case of low Reynolds number flow, high Reynolds number flow, low pulsality of flow and high pulsality of flow.

3.2.2 Streamline contour

To understand certain changes in the flow structure when the degree of stenosis or percentage of restriction changes, it is useful to consider the variations in the streamlines during one cardiac flow cycle (t/T=0.0-1.0). Figure 3.25 shows the streamline contours considering different percentage of restrictions (30%, 40%, 50%, 60% and 70%) for different time steps, beginning of the systolic flow or forward flow (t/T=0.0), peak systolic flow phase (t/T=0.25), end of systolic flow (t/T=0.5) and peak diastolic flow or reverse flow (t/T=0.75) respectively for the case of low Reynolds

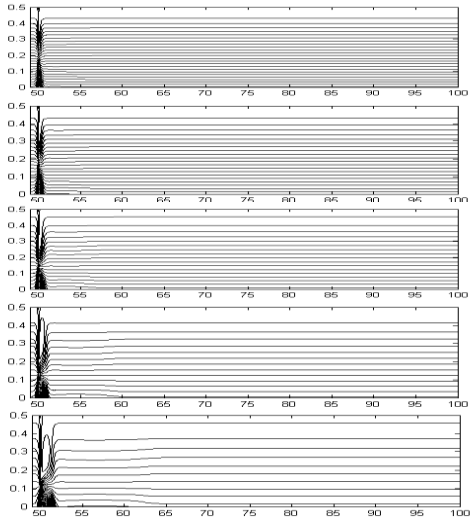

a) t/T=0

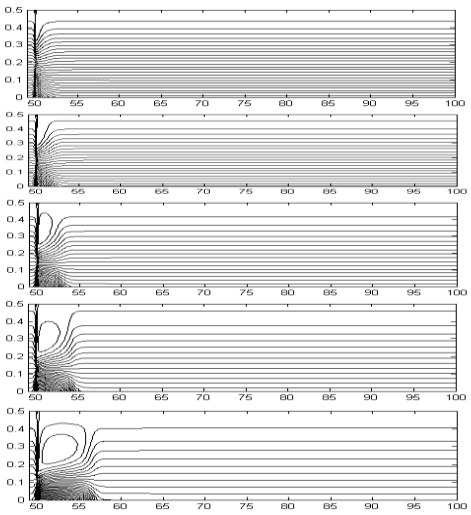

b) t/T=0.25

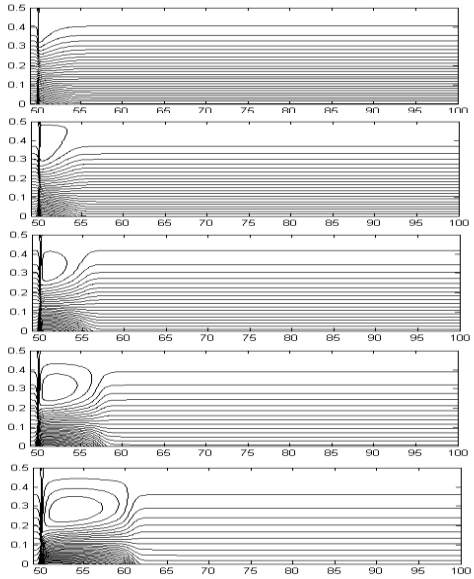

c) t/T=0.50

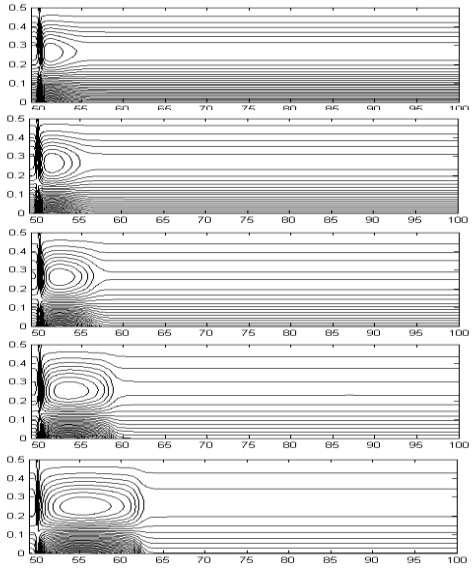

d) t/T=0.75

Figure 3.25: Streamline contours for PR 30%, PR 40%**,** PR 50%, PR 60% and PR 70% (top to bottom) for Re 50 and Wo5 at time steps a) t/T=0, b) t/T=0.25, c) t/T=0.50 and d) t/T=0.75

number (Re 50) and low Womersley number (Wo 5). From the figure, it is clear that there is always flow separation at the downstream flow. The flow separation is caused by excessive momentum loss in the boundary layer near artery wall at the post-stenotic zone. The figures also show that the strength of the separated flow increases with increase in value of percentage of restriction for all the time steps. This is happened because of enhancement of kinetic energy at the throat with increase in percentage of restriction. The generated kinetic energy partially diffuses in the diverging section of stenosis and the flow with high kinetic energy leaves from the

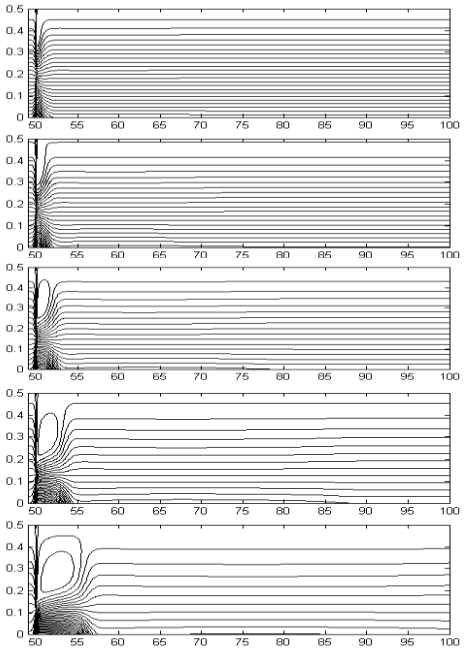

a) t/T=0

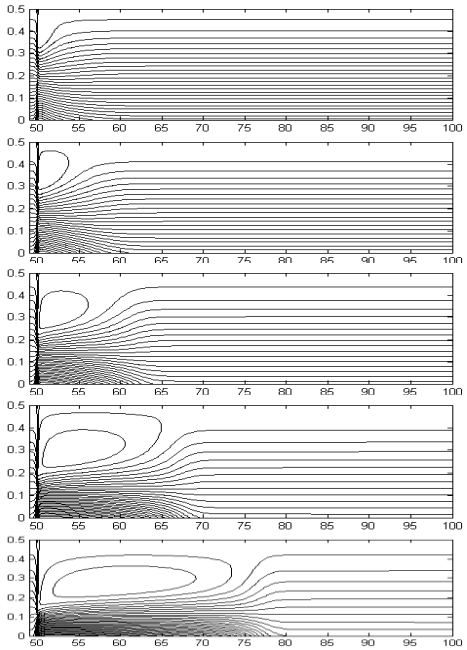

b) t/T=0.25

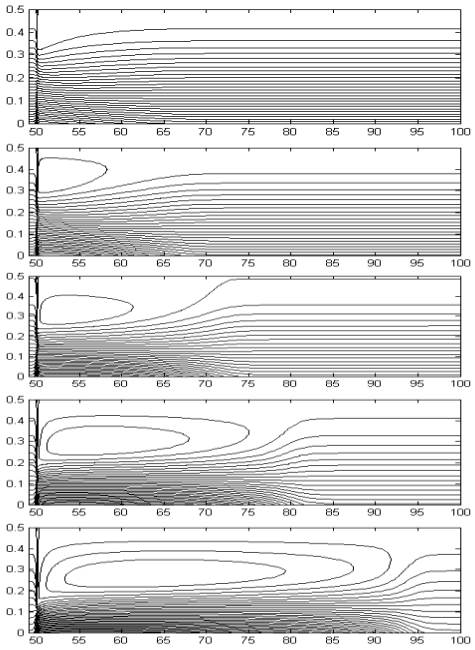

c) t/T=0.50

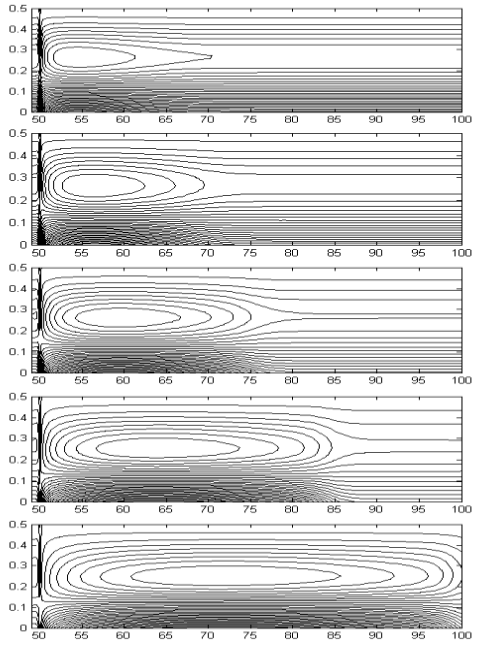

d) t/T=0.75

Figure 3.26: Streamline contours for PR 30%, PR 40%**,** PR 50%, PR 60% and PR 70% (top to bottom) for Re 200 and Wo5 at time step a) t/T=0, b) t/T=0.25, c) t/T=0.50 and d) t/T=0.75

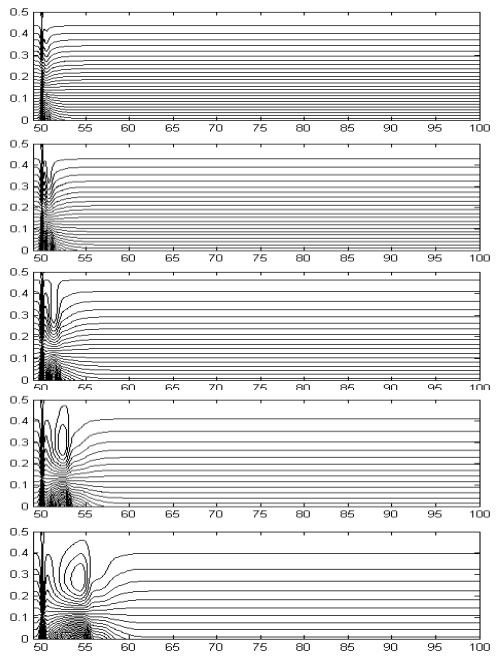

a) t/T=0

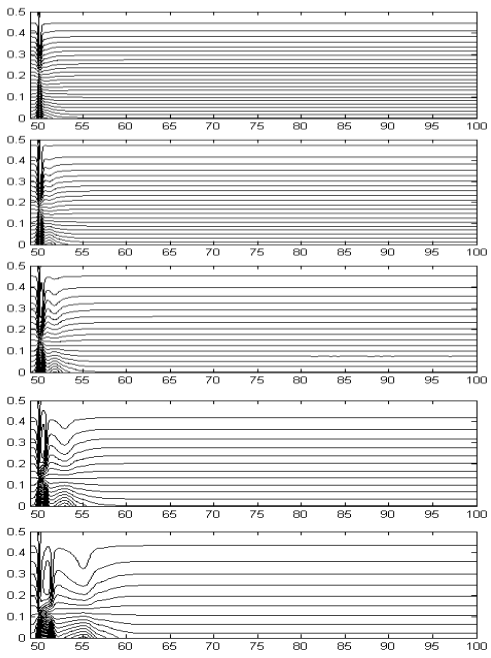

b) t/T=0.25

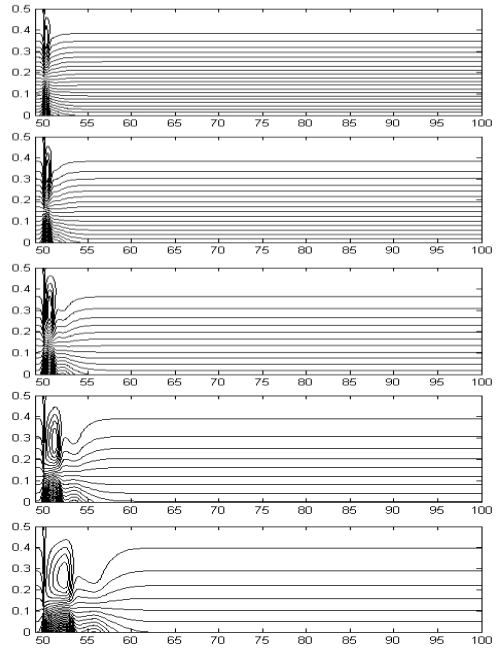

c) t/T=0.50

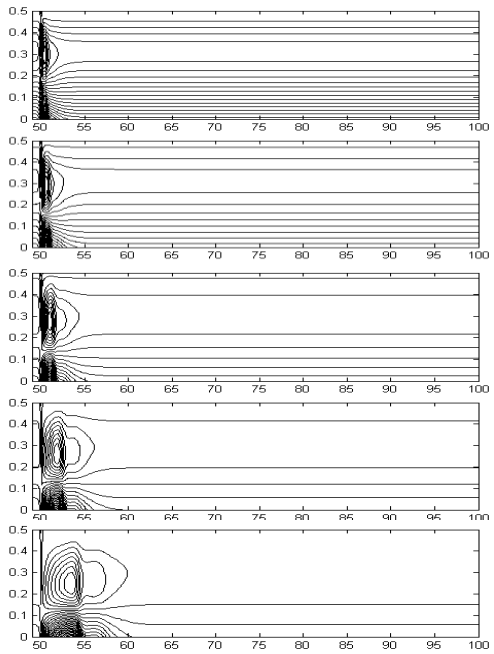

d) t/T=0.75

Figure 3.27: Streamline contours for PR 30%, PR 40%**,** PR 50%, PR 60% and PR 70% (top to bottom) for Re 50 and Wo12.5 at time step a) t/T=0, b) t/T=0.25, c) t/T=0.50 and d) t/T=0.75

exit of stenosis. This high kinetic energy cannot be accommodated by the flow field, leads to more perturbated flow. Thus the stronger flow separation as well as vortex ring takes place for higher percentage of restriction. The vortex ring is formed at the neighborhood of stenosis at the post-stenotic zone for only higher value of percentage

of restriction at the time steps, t/T=0, t/T=0.25 and t/T=0.5 and for all the considered percentage of restrictions at peak diastolic phase (t/T=0.75) as shown in the figure. In this case, largest vortex is formed for Re=200 and t/T=0.75. The figures also depict that size of formed vortex increases with increase in percentage of restriction. The probable reason of flow separation and formation of vortex with respect to time steps has already been discussed in sub-section 3.1.2. The formation of vortex with respect to percentage of restriction can be explained with excessive adverse pressure gradient caused by high diffuser angle. The flow separation results in reverse flow due to excessive adverse pressure gradient. The reverse flow causes formation of vortex at the downstream of stenosis. The Fig.3.26 shows the streamline contours for varying percentage of restrictions for different time steps respectively for the case of high Reynolds number (Re 200) and low pulsality of flow (Wo 5). The phenomenon of flow disturbance is same as the previous case but the large flow separation zone as well as large vortex ring is observed in this case. The probable reason of the same may be the large inertia effect relative to viscous effect in the flow. The Fig.3.27 shows the streamline contours considering different percentage of restrictions for all considered time steps for the case of low Reynolds number (Re 50) and high pulsality of flow (Wo 12.5). The figures depict that size of the flow separation zone increases with increase in percentage of restrictions. The vortex ring is prominent in case higher PR for all the time steps. In this case, effect of inertia in the flow is less than viscous effect but the transient effect is more than the viscous effect. The vortex ring is prominent in case higher PR for all the time steps. The large flow separation zone is observed at the peak diastolic phase as shown in Fig.3.27d. The Fig.3.28 shows the streamline contours for different percentage of restrictions for all the time steps for the case of high Reynolds number (Re 200) and low pulsality of flow (Wo 12.5). Very large flow separation zone is observed for higher percentage of restrictions for all the time steps as depicted by the figures. The bigger vortex is generated at peak diastolic phase for higher PR. These phenomena have probably occurred because of the dominating effect of both of inertia and transient inertia dominating over viscous effect. The double vortex ring is also observed for PR 70% at the beginning of the systolic phase. From the overall study on streamline patterns, it is understood that the strength of the flow separation zone always increases with increase in percentage of restriction for any particular time phase and any combination case of Re and Wo.

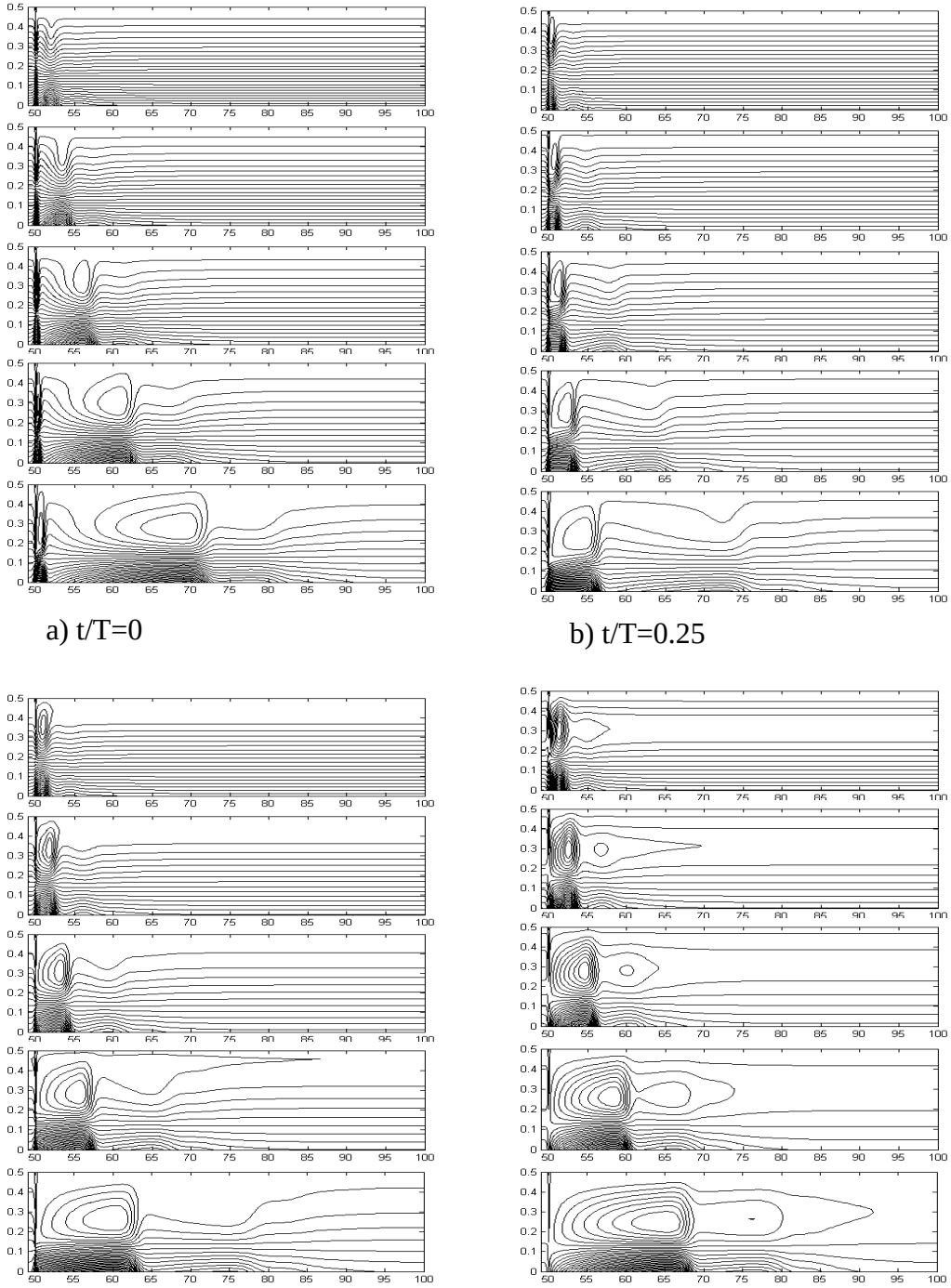

a) t/T=0 b) t/T=0.25

c) t/T=0.50 d) t/T=0.75

Figure 3.28: Streamline contours for PR 30%, PR 40%**,** PR 50%, PR 60% and PR 70% (top to bottom) for Re 200 and Wo12.5 at time steps a) t/T=0, b) t/T=0.25, c) t/T=0.50 and d) t/T=0.75

Therefore, major flow disturbance takes place at higher restrictions. Consequently the chance of plaque deposition increases with increase in percentage of restriction.

3.2.3 Peak wall shear stress and low wall shear stress

From the previous section, it is clearly understood that percentage of restriction has significant impact on the blood flow velocity changes in the constricted region and in the downstream of constriction region along the axial direction as well as transverse direction. It is very important to notice the wall shear distribution in the stenotic zone and in the post stenotic zone. The variation of the time-averaged WSS along axial direction in the stenotic zone is shown in Fig.3.29 for Wo 5 and Re 50 to show the effect of percentage of restriction on peak wall shear stress. It is revealed that the nature of variation of the time-averaged WSS is almost similar for all the

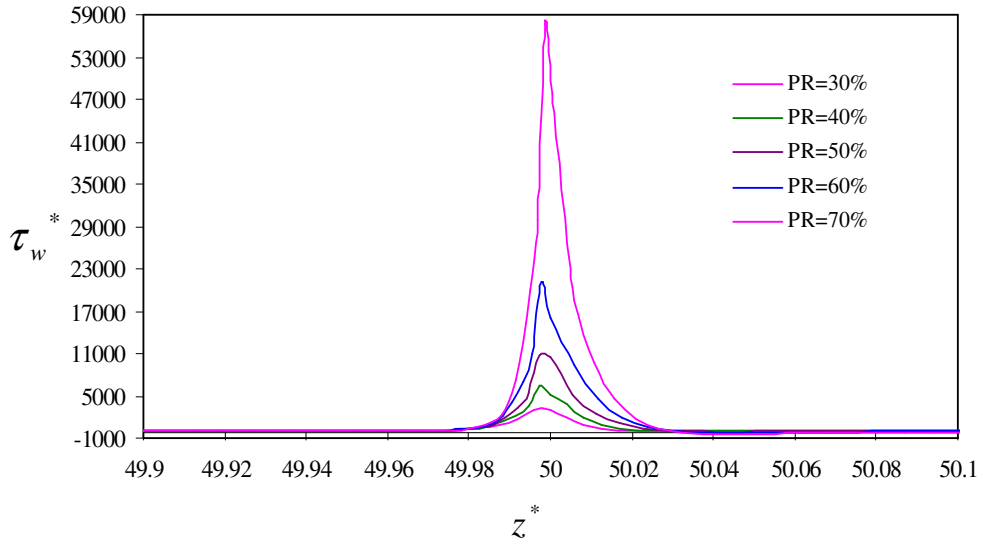

Figure 3.29: Variation of PWSS at stenotic zone along axial direction for different PR for Re 50 and Wo5

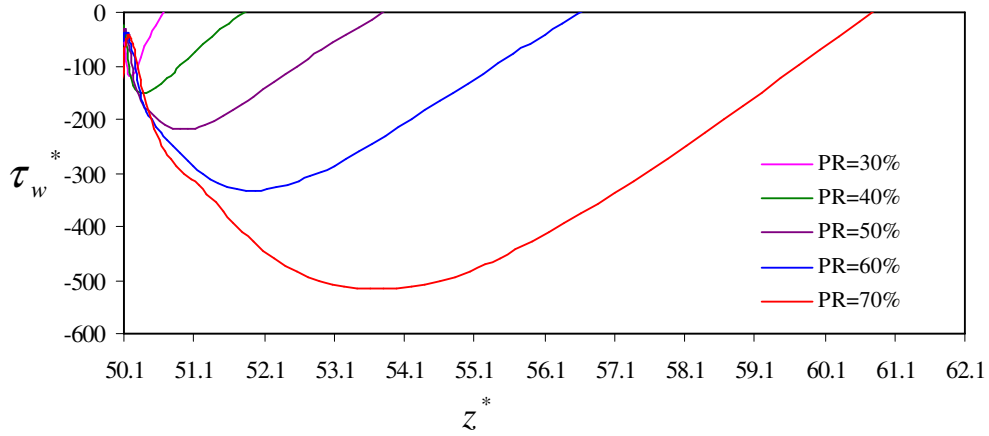

Figure 3.30: Variation of LWSS at post-stenotic zone along axial direction for different PR for Re 50 and Wo5

considered percentage of restrictions. Time-averaged wall shear stress increases sharply proximal to the throat of the stenosis and time-averaged wall shear stress decreases sharply distal to the throat. As the percentage of restriction increases, the converging angle increases and throat area wall shear stress rapidly reaches to zero magnitude and then it becomes negative in magnitude in the downstream of stenosis. The negative magnitude of wall shear stress implies a persistence of flow separation, which has been noticed in the streamline patterns presented in the previous section.

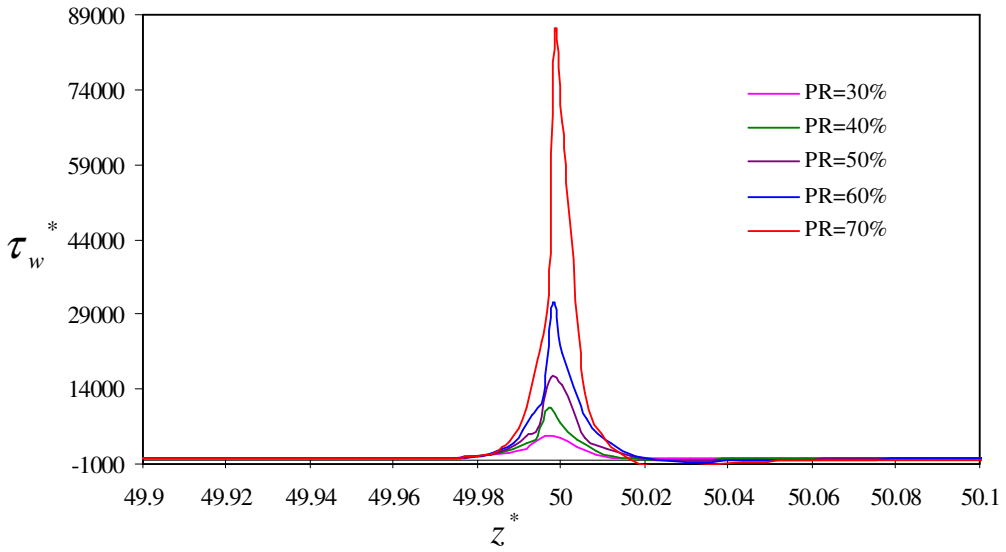

Figure 3.31: Variation of PWSS at stenotic zone along axial direction for different PR for Re 200 and Wo5

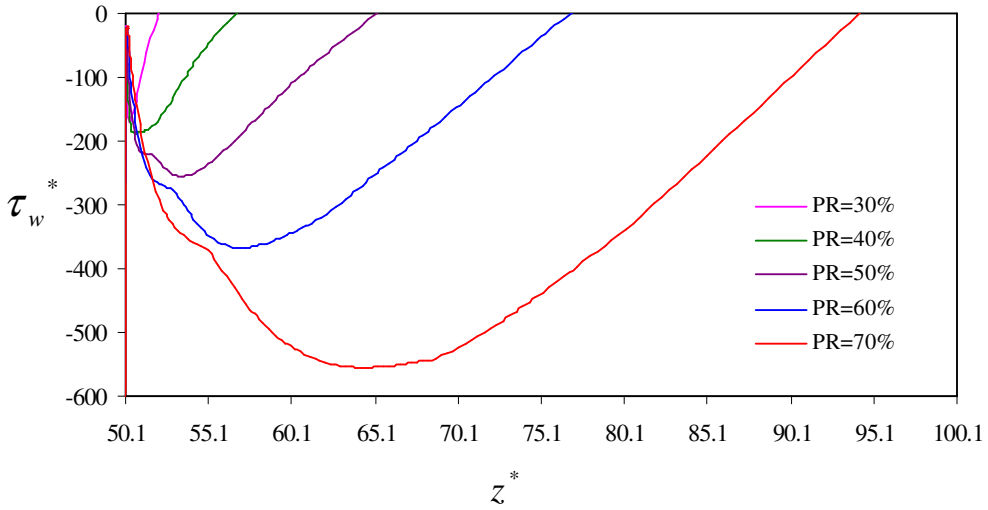

Figure 3.32: Variation of LWSS at post-stenotic zone along axial direction for different PR for Re 200 and Wo 5

Figure.3.30 depicts the variation of wall shear stress along axial direction at the post-stenotic zone to show the effect of percentage of restriction on the low wall shear stress for Re 50 and Wo 5. From the figure of low wall shear stress, it is observed that the magnitudes of maximum low wall shear stress and the area for the low wall shear stress zone increases with increase in percentage of restriction. At the higher percentage of restriction, the size of the recirculation zone is more, which leads to higher magnitude of peak of low wall shear stress with higher area of low wall shear stress zone. The maximum low WSS for PR=70% is 5.49 times higher than the maximum low WSS for PR=30%.

The variation of the time-averaged WSS along axial direction in the stenotic zone is shown for Wo 5 and Re 200 in Fig.3.31. It is found that the variation patterns of the time-averaged WSS are almost similar for all the considered percentage of restriction as can be seen in the previous case. The figure illustrates that the magnitude of peak wall shear stress increases with increase in percentage of restriction. The peak WSS for PR=70% is 13.59 times higher than the peak WSS for PR=30%. Figure.3.32 depicts the variation of wall shear stress along axial direction at the post-stenotic zone for Wo 5 and Re 200. From the figure of low wall shear stress, it is observed that the low wall shear stress decreases with increase in PR and the area under low wall shear stress increases with increase in PR. The maximum low WSS for PR=70% is 4.34 times higher than the maximum low WSS for PR=30%.

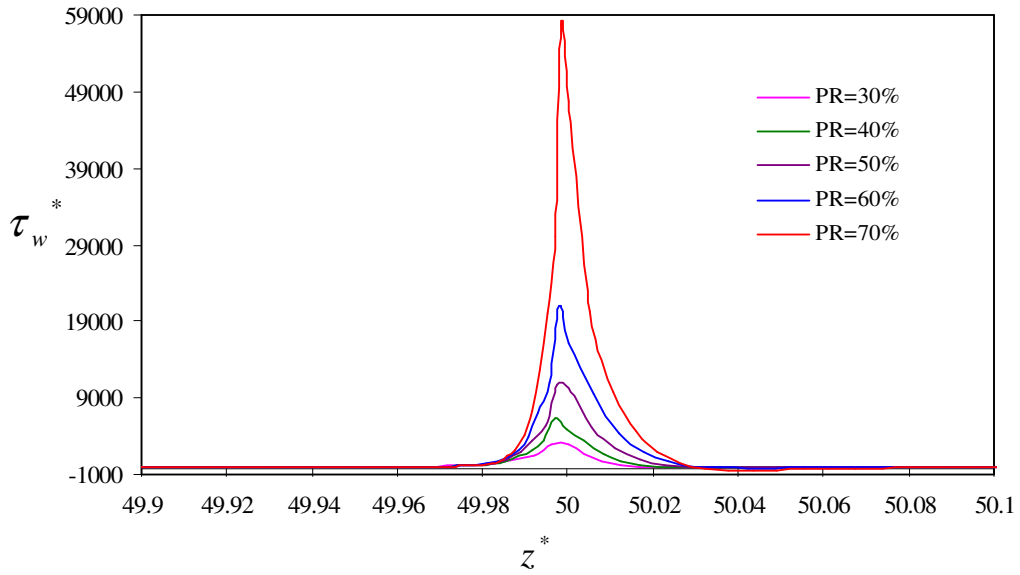

Figure 3.33: Variation of PWSS at stenotic zone along axial direction for different PR for Re 50 and Wo 12.5

The variation of the time-averaged WSS along axial direction in the stenotic zone is shown for Wo 12.5 and Re 50 in Fig.3.33 to show the effect of PR on peak wall shear stress. It is observed that the variation patterns of the time-averaged WSS are almost similar for all the considered percentage of restriction as the previous cases. The figure shows that the magnitude of peak wall shear stress increases with increase in percentage of restriction. The peak WSS for PR=70% is 10.95 times higher than the peak WSS for PR=30%. Figure.3.34 illustrates the variation of wall shear stress along axial direction at the post-stenotic zone to show the effect of PR on

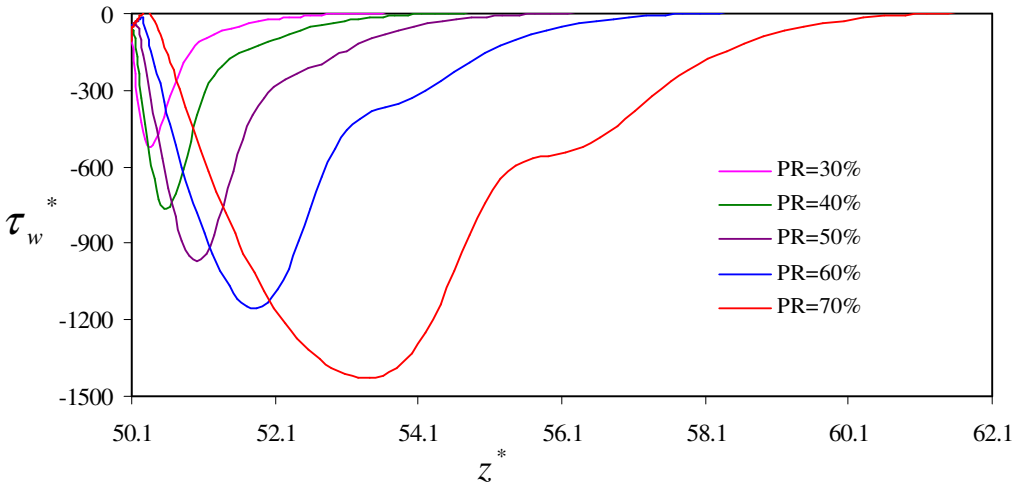

Figure 3.34: Variation of LWSS at post-stenotic zone along axial direction for different PR for Re 50 and Wo 12.5

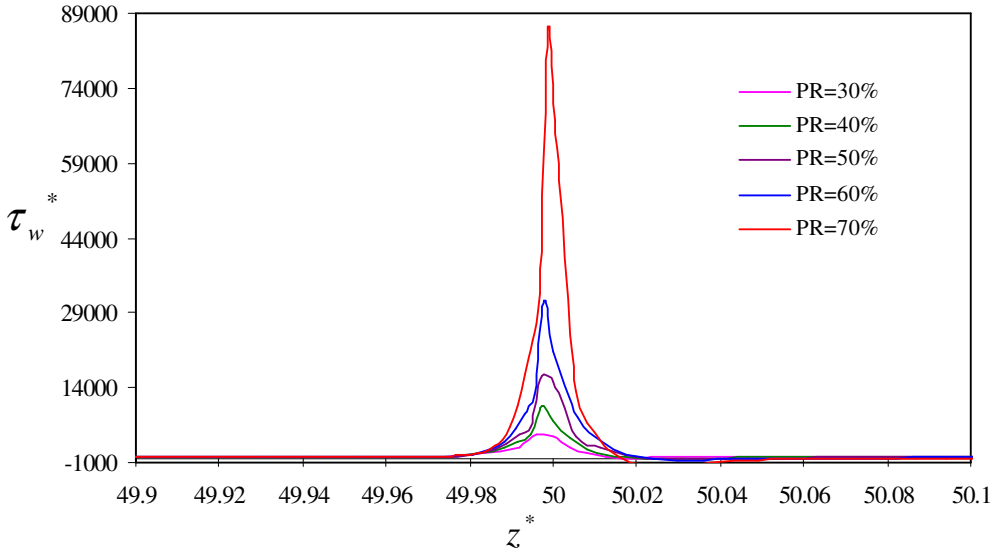

Figure 3.35: Variation of PWSS at stenotic zone along axial direction for different PR for Re 200 and Wo 12.5

the low wall shear stress for Wo 12.5 and Re 50. From the figure of low wall shear stress, it is observed that the low wall shear stress drops with increase in PR. The maximum low WSS for PR=70% is 2.54 times higher than the maximum low WSS for PR=30%. The area under low WSS also increases with increase in PR. The effect of PR on WSS is less in comparison to first and second cases.

The variation of the time-averaged WSS along axial direction in the stenotic zone is shown for Wo 12.5 and Re 200 in Fig.3.35 to show the effect of PR on peak wall shear stress. It is observed that the magnitude of peak wall shear stress increases with increase in percentage of restriction as the previous cases. The peak

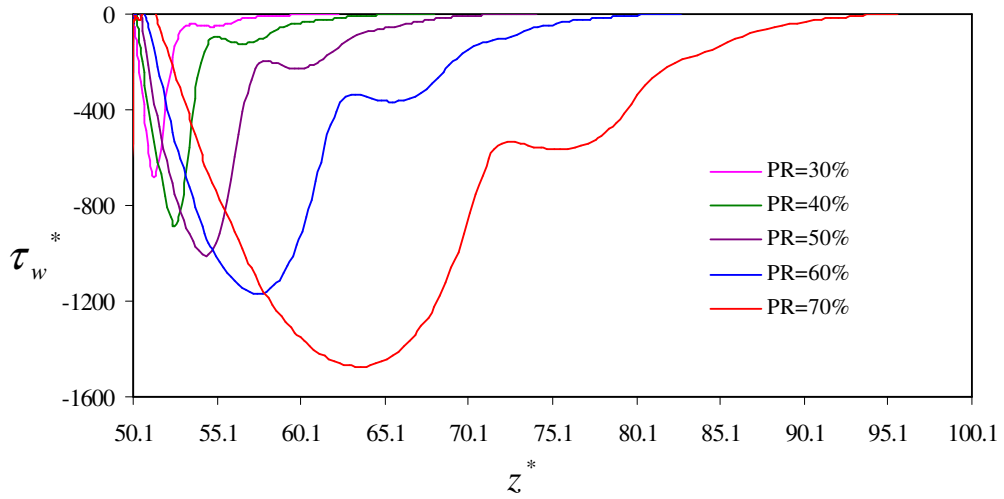

Figure 3.36: Variation of LWSS at post-stenotic zone along axial direction for different PR for Re 200 and Wo 12.5

WSS for PR=70% is 13.62 times higher than the PWSS for PR=30%. From the Fig.3.36, it is observed that both of magnitude of maximum low WSS and the area under low WSS increases with increase in percentage of restriction for the case of high pulsality of flow with high Reynolds number. The maximum low WSS for PR=70% is 2.21 times higher than the maximum low WSS for PR=30%. From the overall study on wall shear stress, it is noted that peak WSS along with both of the magnitude and the area under low WSS increase with increase in percentage of restriction. This region of low wall shear stress is a recirculation area and it may contribute to the progression of atherosclerosis. The acute high shear stress may cause endothelial dysfunction and thereby it may cause the chance for local plaque formation. From the overall effect on peak WSS and low WSS, it may be commented that the chances of both development and progression of the disease, atherosclerosis increase with increase in percentage of restriction.

3.2.4 Oscillatory shear index

In this sub section, the effect of percentage of restriction on the oscillatory shear index is investigated for all the combination case of high Reynolds number flow, low Reynolds number flow, low pulsatile flow and high pulsatile flow. At first, the variation of the oscillatory shear index along axial direction in the stenotic zone and post stenotic zone is shown in Fig.3.37 for the case of low Womersley number (Wo = 5) and low Reynolds number (Re = 50). From the figure, it is observed that the first peak OSI value just immediate after the throat of stenosis decreases with increase in percentage of restriction. The probable reason of this phenomenon is that the velocity gradient changes abruptly with the percentage of restriction but the

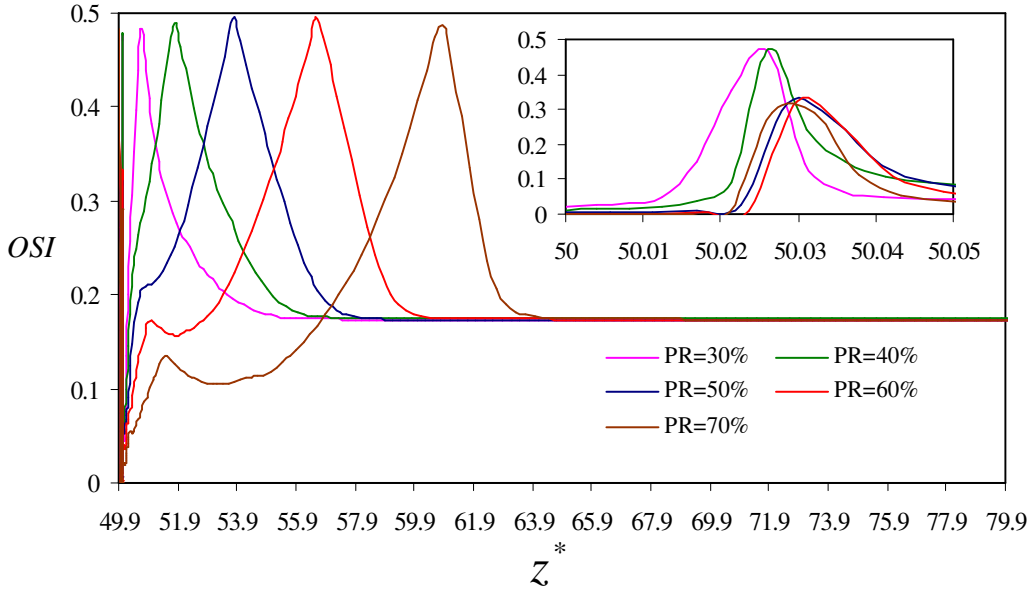

Figure 3.37: Variation of OSI along axial direction at stenotic and post stenotic zone for different PR for Re50 and Wo 5

oscillations in wall shear stress do not change proportionally for low Reynolds number flow with low Womersley number. The axial location of major oscillations in wall shear stress moves further downstream for higher percentage of restriction. Thus the point of first peak OSI shifts along the axial direction for the case of moderate and severe stenosis as can be observed in the said figure. The OSI value at stenotic zone is 0.32 for PR 70% and 0.48 for PR 30%. The reattachment length increases with increase in value of PR. The longest reattachment length is linked to the largest recirculation zone at the downstream of stenosis for higher percentage of restriction. This phenomenon is also observed in subsection 3.2.3 for the case of low wall shear

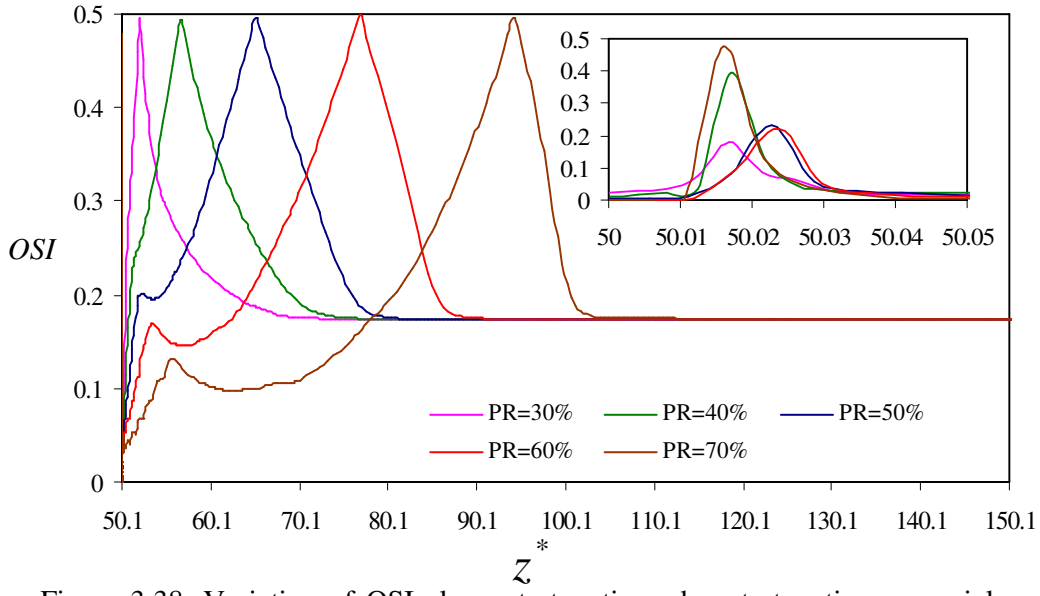

Figure 3.38: Variation of OSI along at stenotic and post stenotic zone axial direction for different PR for Re200 and Wo 5

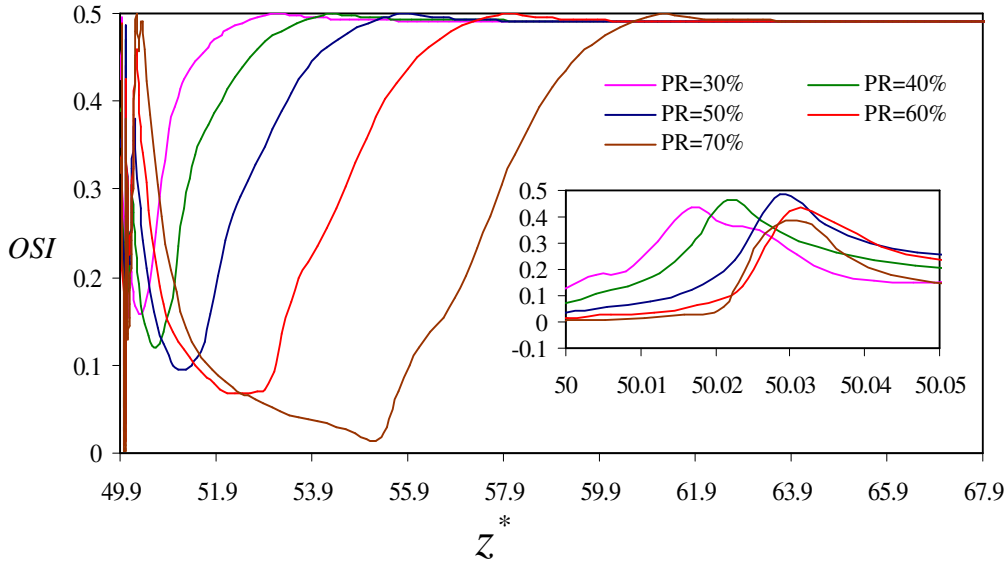

Figure 3.39: Variation of OSI along axial direction at stenotic and post stenotic zone for different PR for Re 50 and Wo 12.5

stress. The longest reattachment point (z*=60.89) is found for PR70% and the shortest reattachment point (z*=50.73) is found for PR30%. The variation of the OSI along axial direction in the stenotic zone and post stenotic zone is shown in Fig.3.38 for the case of low Womersley number (Wo = 5) and high Reynolds number (Re = 200). Shifting of first peak OSI along axial direction is noticed for moderate degree of

stenosis. The noticeable increment of OSI value is observed for PR=70% and the value is 0.48. The lowest peak OSI is 0.19 for PR=30%. This has happened because of domination of inertia force. The reattachment length increases with increasing of percentage of restriction. The longest reattachment point (z*=94.61) is found for PR70% and the shortage reattachment point (z*=52.15) is found for PR30%. The variation of the OSI along axial direction in the stenotic zone and post stenotic zone is shown in Fig.3.39 for the case of high Womersley number (Wo = 12.5) and low Reynolds number (Re =50). The increase of OSI value just immediate after the throat of stenosis is noticeable for all considered percentage of restrictions. The reason behind the observation is the dominated unsteady inertia force over the velocity gradient which changes with the changes in percentage of restriction. The shifting of peak OSI is observed for higher percentage of restriction from the figure. The highest and lowest values of the OSI at the stenotic zone are 0.44 and 0.39 for PR=30% and PR=70% respectively. The reattachment length also increases with increase of PR value. The longest reattachment point (z*=53.08) is found for PR70% and the shortest reattachment point (z*=61.19) is found for PR30%. The variation of the OSI along axial direction in the stenotic zone and post stenotic zone is shown in Fig.3.40 for the case of high pulsality of flow (Wo12.5) and high Reynolds number (Re 200). The marked rise of OSI value at the stenotic zone is observed for PR=70% and PR=40%

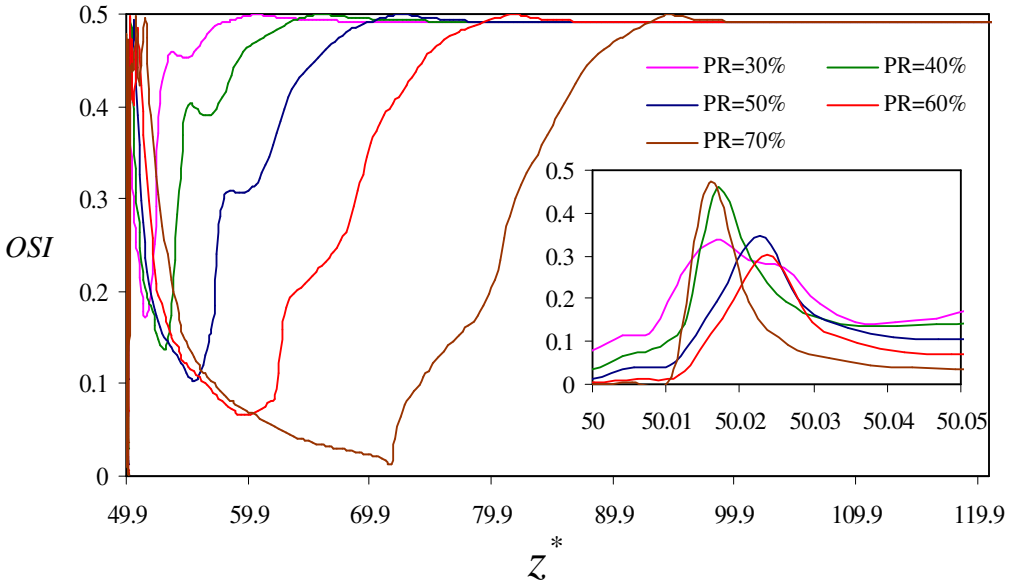

Figure 3.40: Variation of OSI along axial direction at stenotic and post stenotic zone for different PR for Re 200 and Wo 12.5

as shown in the figure and the estimated value is 0.47 and 0.46 respectively. The lowest peak OSI is 0.30 for PR=60%. The shifting of peak OSI is also observed for the case of moderate degree of stenosis. The increase or decrease of the value of first peak OSI does not obey the proportionality rule with the value of PR. The reattachment length also increases with increase in PR value as the previous case. The longest reattachment point (z*=95.11) is found for PR70% and the shortest reattachment point (z*=60.92) is found for PR30%. High oscillatory shear index value indicates high variation in wall shear stress over the duration of a cardiac pulse cycle and it is found in the regions of flow separation and recirculation. It is linked with the localization of atherosclerosis. High OSI along with low wall stress increases the chances of localization of atherosclerosis. The reattachment point in terms of OSI indicates the size of flow separation and it is linked to the formation of atherosclerosis. From the overall study on the effect of PR on OSI, it may be said that the flow with higher percentage of restriction is always prone to the disease atherosclerosis.

3.3 Effect of Womersley Number for Simple Pulsatile Flow

In this section, a series of numerical simulations of model bell shaped stenosed artery considering simple pulsatile flow have been carried out and the effect of Womersley numbers on the flow characteristics, e.g. wall pressure, streamline contour, WSS and OSI in each case have been investigated.

For a particular artery segment of a particular human being, Womersley number solely depends on pulsatile flow frequency. Womersley number increases or decreases with increase or decrease in pulsatile flow frequency respectively. Pulsatile flow frequency varies among different human beings. Pulsatile flow frequency also varies with different condition of human being such as physical exertion, emotional exertion, smoking, drinking alcohol, some types of illness etc. So it is important to understand the effect of Womersley number on blood flow characteristics for a better pathological interpretation. In this section, a simulation has been conducted for the hemodynamic parameters for simple pulsatile flow with Reynolds number 50 and 200 through a constricted artery with PR = 30% and PR = 70%. Four Womersley numbers (Wo =5, 7.5, 10 and 12.5) have been considered for studying the effect of Womersley numbers on the blood flow characteristics such as wall pressure, stream line contours, wall shear stress and oscillatory shear index respectively. The effect of Womersley

number is investigated on the blood flow characteristics for the four different cases, mild stenosis (PR=30%) with low Reynolds number flow (Re = 50), severe stenosis (PR = 70%) with low Reynolds number flow (Re = 50), mild stenosis (PR 30%) with high Reynolds number flow (Re = 200) and severe stenosis (PR70%) with high Reynolds number flow (Re = 200) separately.

3.3.1 Wall pressure

In this subsection, the effect of Womersley number on the wall pressure is studied for combination of low Reynolds number, high Reynolds number, Low Womersley number and high Womersley number. At first, the effect of Womersley number on wall pressure is observed for the case of mild stenosis (PR = 30%) and low Reynolds number (Re = 50). The distribution of time-averaged wall pressure along the axial direction throughout the considered arterial length is shown in Fig. 3.41 for PR= 30% and Re = 50 to investigate the effect of Womersley number on wall pressure.

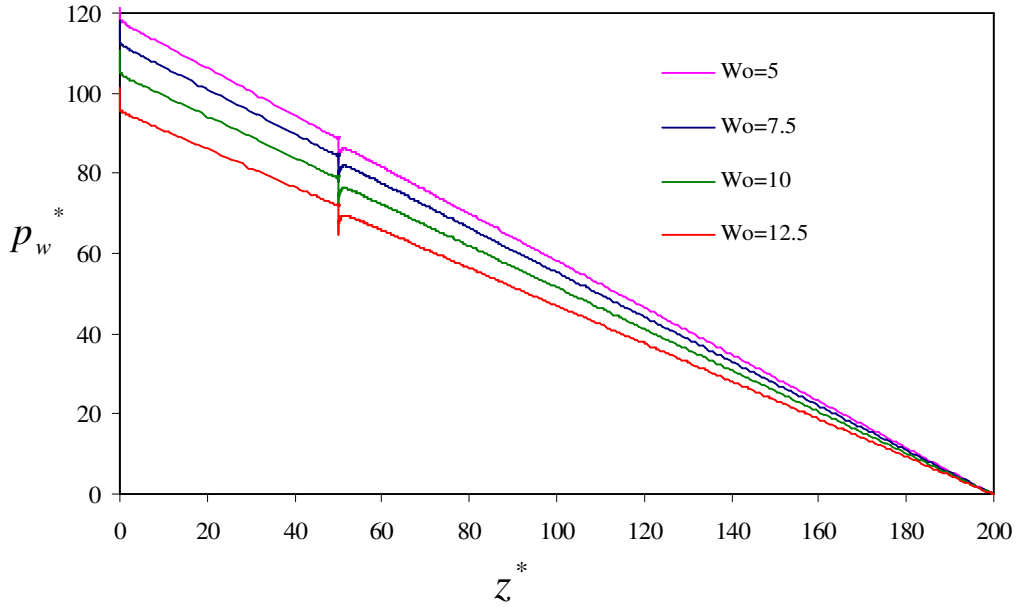

Figure 3.41: Variation wall pressure along axial direction of the considered length of artery for different Wo for PR30% and Re50

From the figure, it is observed that the wall pressure drop at the throat of the stenosis increases with increase in Womersley number. As the Womersley number of flow increases, the unsteady inertia force dominates. Therefore, the blood has a tendency to separate from the wall and the chance of adherence of blood to the artery wall is less

at higher Womersley number of flow. Thus the minimum wall pressure at the throat of stenosis is observed for higher Womersley number leading to the maximum wall pressure drop for higher Womersley number. The pressure drop is 6.43, 6.73, 7.04 and 7.36 for Wo 5, Wo 7.5, Wo 10 and Wo 12.5 respectively. The minimum time

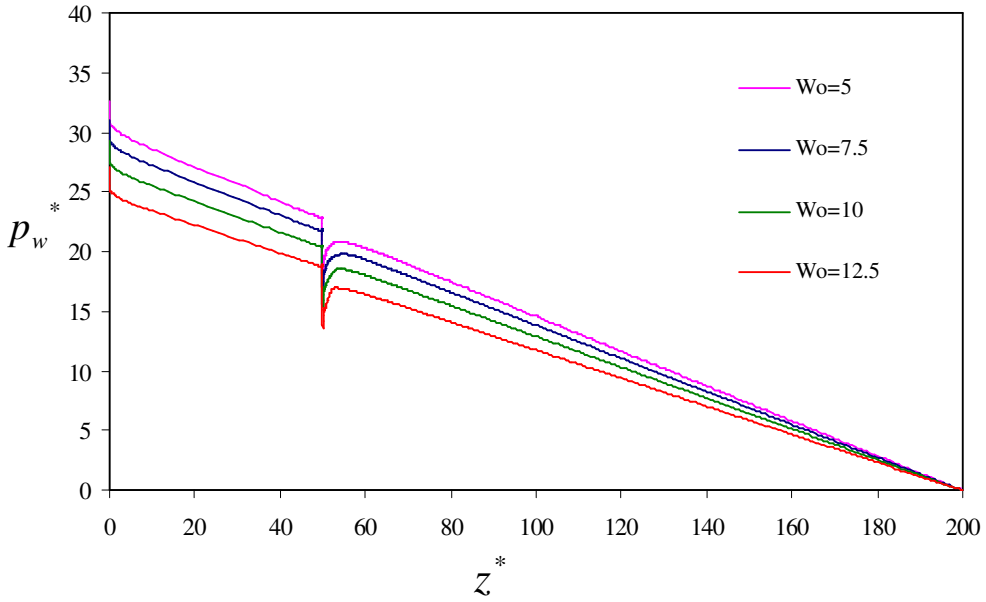

Figure 3.42: Variation of wall pressure along axial direction of the considered length of artery for different Wo for PR30% and Re200

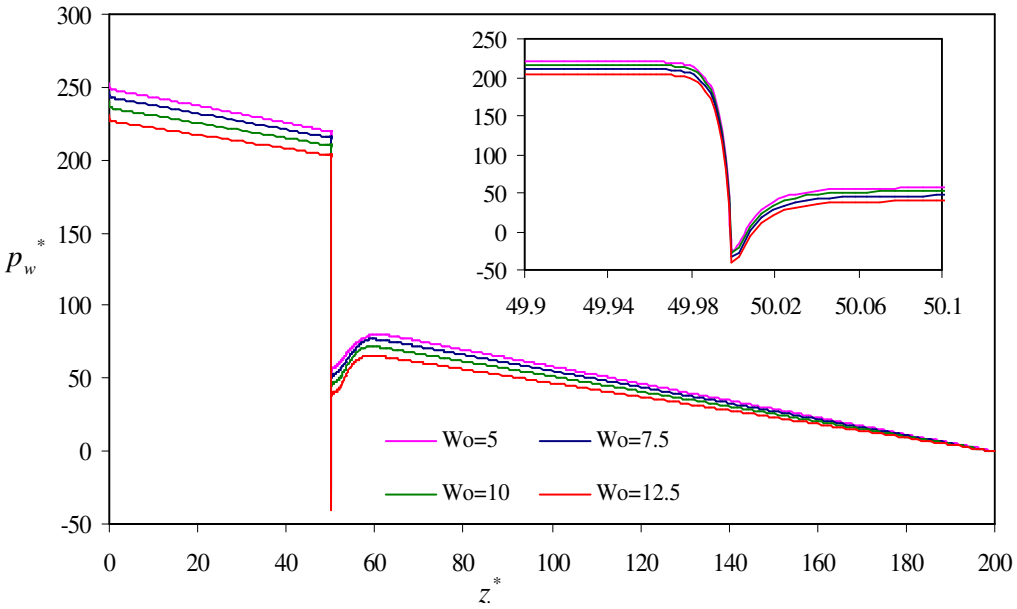

Figure 3.43: Variation of wall pressure along axial direction of the considered length of artery for different Wo for PR70% and Re50

averaged pressure at the throat of stenosis is 82.46, 77.84, 71.99 and 64.85 for Wo 5, Wo 7.5, Wo 10 and Wo 12.5 respectively. Once more, the effect of Womersley number on wall pressure is investigated for the case of mild stenosis with high Reynolds number. The distribution of time-averaged wall pressure along the axial direction throughout the considered arterial length is shown in Fig. 3.42 for PR 30% and Re 200 for the considered Womersley numbers. In this case, the wall pressure drop also increases with increase in Womersley number. The pressure drop is 4.83, 5.05, 5.21 and 5.36 for Wo 5, Wo 7.5, Wo 10 and Wo 12.5 respectively. The minimum time averaged pressure is 17.98, 16.75, 15.27 and 13.51 for Wo 5, Wo 7.5, Wo 10 and Wo 12.5 respectively. Again, the effect of Womersley number on wall pressure is investigated for the case of severe stenosis with low Reynolds number. The distribution of time-averaged wall pressure along the axial direction throughout the considered arterial length is shown in Fig. 3.43 for PR 70% and Re 50, like the earlier observation, the wall pressure drop increases with increase in Womersley number. The pressure drop is 242.77, 243.39, 243.77 and 244.07 for Wo 5, Wo 7.5, Wo 10 and Wo 12.5 respectively. The minimum time averaged pressure is -22.93, -27.71, -33.46 and -40.45 for Wo 5, Wo 7.5, Wo 10 and Wo 12.5 respectively. In case of severe stenosis with high Reynolds number, the distribution of time-averaged wall

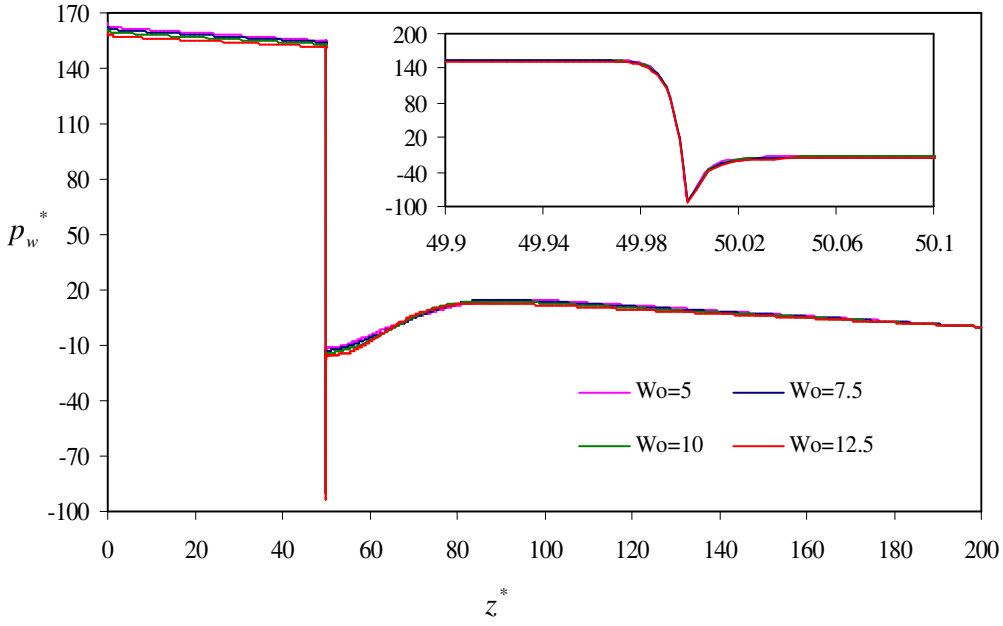

Figure 3.44: Variation of wall pressure along axial direction of the considered length of artery for different Wo for PR70% and Re200

pressure along the axial direction throughout the considered arterial length is shown in Fig. 3.44 for PR 70% and Re 200. Here also, the wall pressure drop increases with increase in Womersley number. The pressure drop is 220.24, 220.73, 220.99 and 221.15 for Wo 5, Wo 7.5, Wo 10 and Wo 12.5 respectively. The minimum time averaged pressure is -65.17, -66.44, -67.75 and -69.28 for Wo 5, Wo 7.5, Wo 10 and Wo 12.5 respectively. The overall observation from the exercise, it may be said that the pressure drop for any combination case of percentage of restriction and Reynolds number always increases with increase in the value of Womersley number. So the chance of artery wall damage is more for high value of Womersley number. The minimum time averaged wall pressure is always found in case of higher value of Womersley number. Therefore, the chance of development of atherosclerosis is more for higher Womersley number.

3.3.2 Streamline contour

The variation of streamline contour during one cardiac cycle is investigated to understand the flow fields at different Womersley numbers. Fig.3.45a shows the streamline contours of the flow through mild stenosis (PR 30%) with low Reynolds number (Re 50) at time step t/T=0, just beginning of the pulsatile flow, for typical considered Womersley numbers. The figure shows that the size of flow separation zone decreases as Womersley number increases. When Womersley number of flow increases, the unsteady inertia increases and thus flow rate increases. So the size of the flow separation zone decreases with increase in Womersley number for this case. The same phenomenon is observed for PR 30% with Re 200 at this time step as shown in Fig.3.45b. But the size of the flow separation zone increases with increase in Womersley number for both the cases of severe stenosis with Re 50 and Re 200 as shown in Fig.3.45c and Fig.3.45d respectively. The secondary vortex is also observed for higher Womersley number for the cases of severe stenosis. For the flow through severe stenosis, unsteady inertia increases with increase in Womersley number and the flow at the post-stenotic zone is more perturbed. At time step t/T=0.25, peak systolic phase, it is observed that the size of flow separation zone decreases as Womersley number increases for the flow through PR 30% with Re 50 as shown in Fig.3.46a. The same observation is noted for the cases of PR 30% with Re 200, PR 70% with Re 50 and PR 70% with Re 200 as can be seen in Fig.3.46b, Fig.3.46c and Fig.3.46d respectively. The streamline contours for various Womersley numbers for

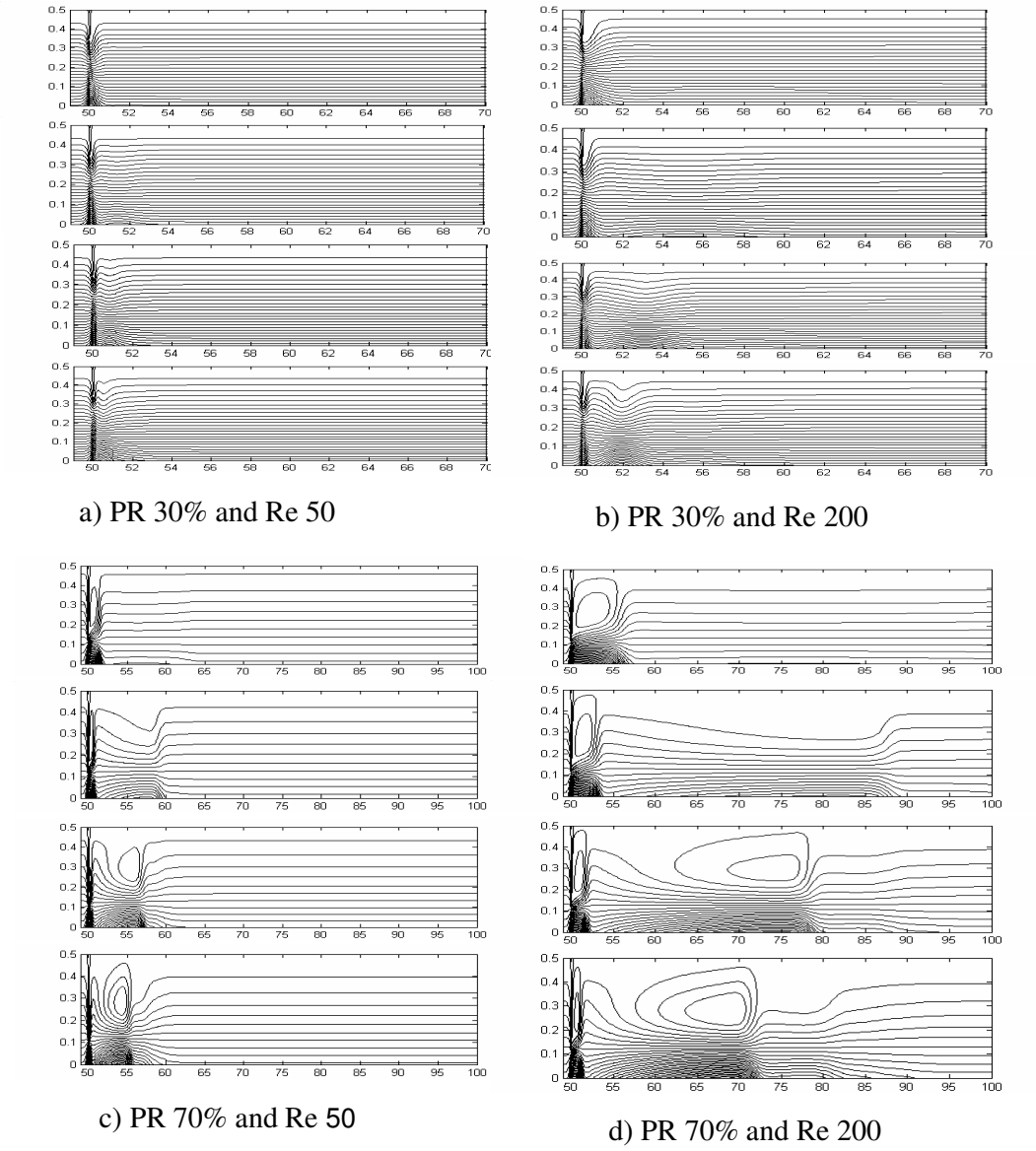

a) PR 30% and Re 50

b) PR 30% and Re 200

c) PR 70% and Re 50

d) PR 70% and Re 200

Figure 3.45: Streamline contours for Wo 5, Wo 7.5, Wo 10 and Wo 12.5 (top to bottom) at t*=0 for a) PR 30% and Re 50, b) PR 30% and Re 200, c) PR 70% and Re 50 and d) PR 70% and Re 200

flow through PR 30% with Re 50, PR 30% with Re 200, PR 70% with Re 50 and PR 70% with Re 200 are shown in Fig.3.47a, Fig.3.47b, Fig.3.47c and Fig.3.47d respectively at time step t/T=0.5. At t/T=0.5, the flow decelerates and size of the flow separation zone become larger than that of the case of previous time step. At this time step, both the generated vortex size and the flow separation zone size decrease with increase in Womersley number. At t/T=0.75, peak diastolic phase, the strength of vortex as well as the size of the flow separation zone decreases with increase in the value of Womersley number for PR 30% with Re 50 and Re 200 as depicted in

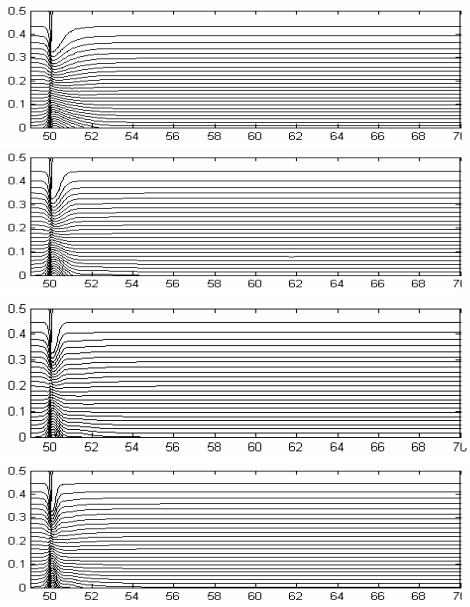

a) PR 30% and Re 50

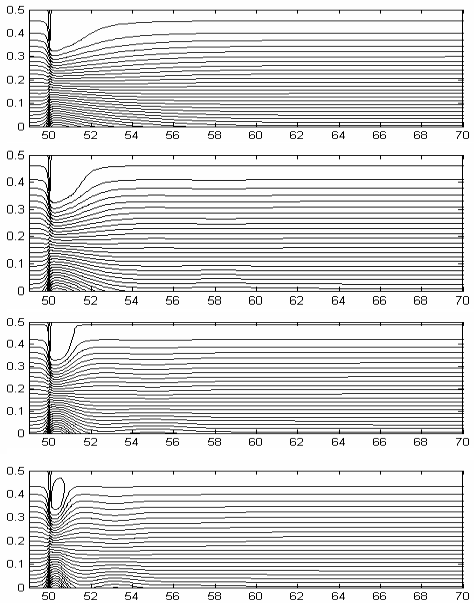

b) PR 30% and Re 200

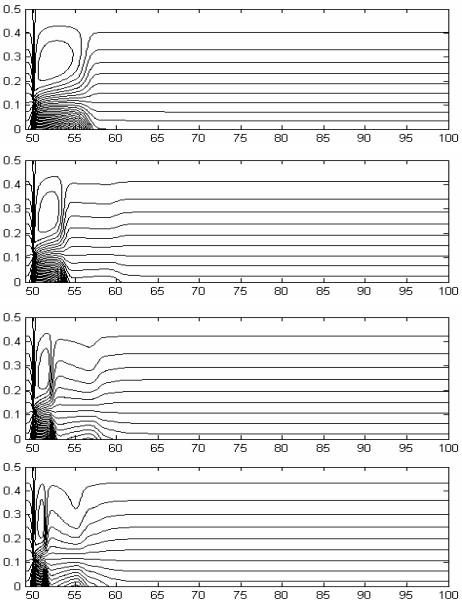

c) PR 70% and Re 50

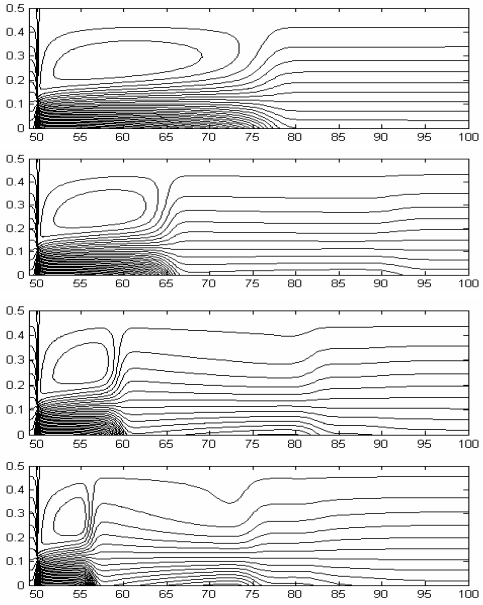

d) PR 70% and Re 200

Figure 3.46: Streamline contours for Wo 5, Wo 7.5, Wo 10 and Wo 12.5 (top to bottom) at t*=0.25 for a) PR 30% and Re 50, b) PR 30% and Re 200, c) PR 70% and Re 50 and d) PR 70% and Re 200

Fig.3.48a and Fig.3.48b respectively. But the Fig.3.48c and Fig.3.48d illustrate that the size of the flow separation zone increases with increase in the value of Womersley number for PR 70% with Re 50 and Re 200 respectively. From the overall study on streamlines for different Womersley numbers, it is noted that the strength of the flow

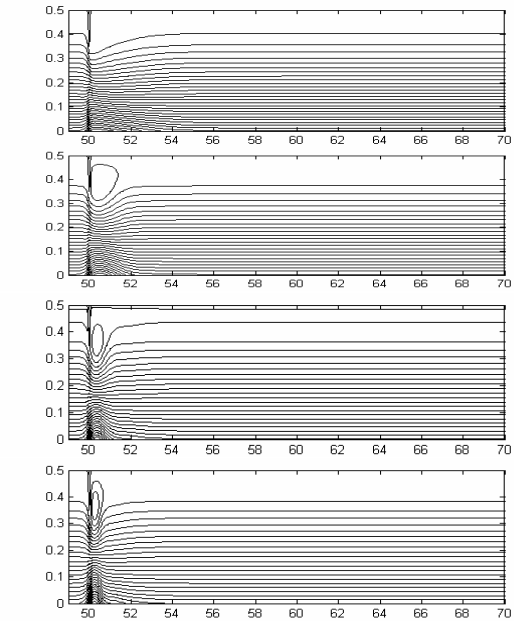

a) PR 30% and Re 50

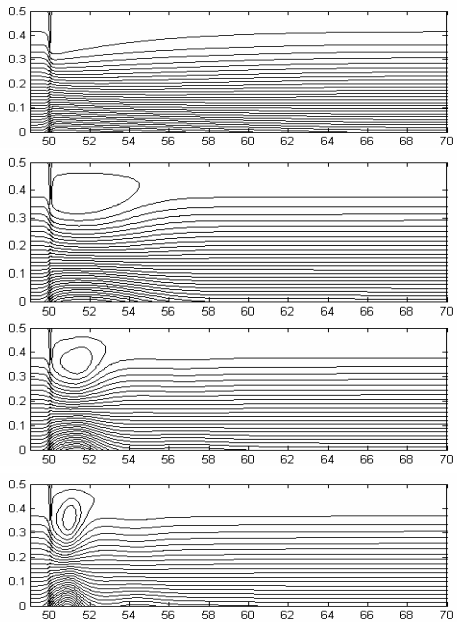

b) PR 30% and Re 200

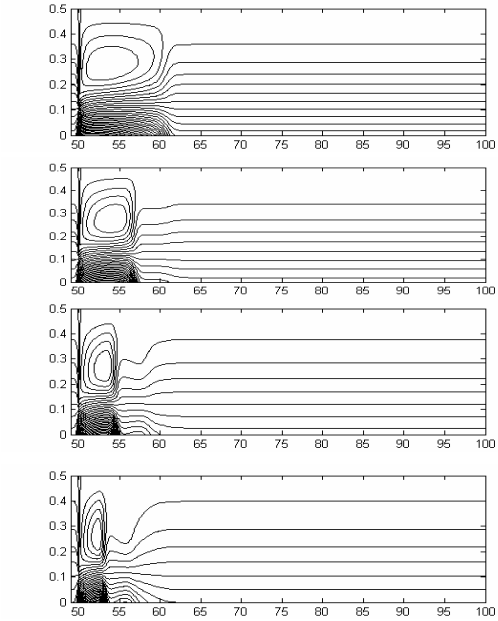

c) PR 70% and Re 50

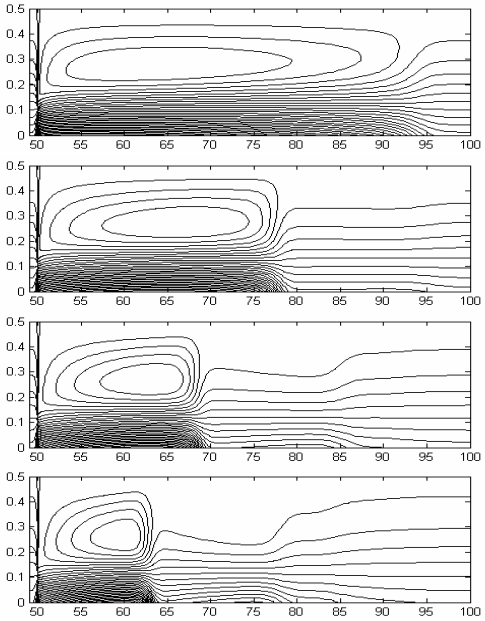

d) PR 70% and Re 200

Figure 3.47: Streamline contours for Wo 5, Wo 7.5, Wo 10 and Wo 12.5 (top to bottom) at t*=0.50 for a) PR 30% and Re 50, b) PR 30% and Re 200, c) PR 70% and Re 50 and d) PR 70% and Re 200

separation zone decreases with increase in value of Womersley number for the flow through mild stenosis at all the time steps. Therefore, possibility of plaque deposition is higher for low value of Womersley number for the case of mild stenosis at any time

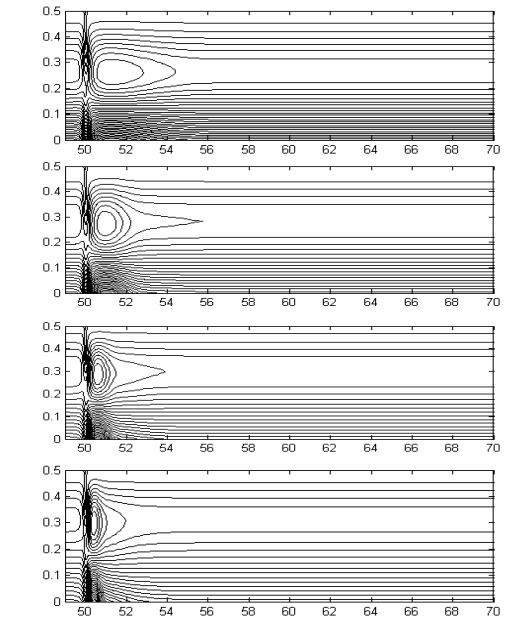

a) PR 30% and Re 50

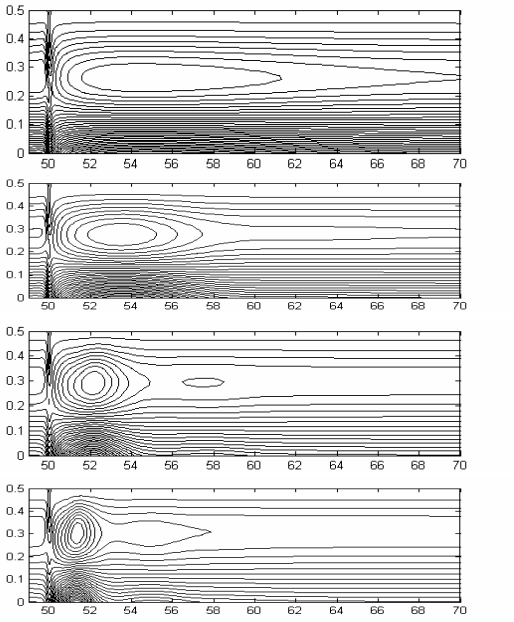

b) PR 30% and Re 200

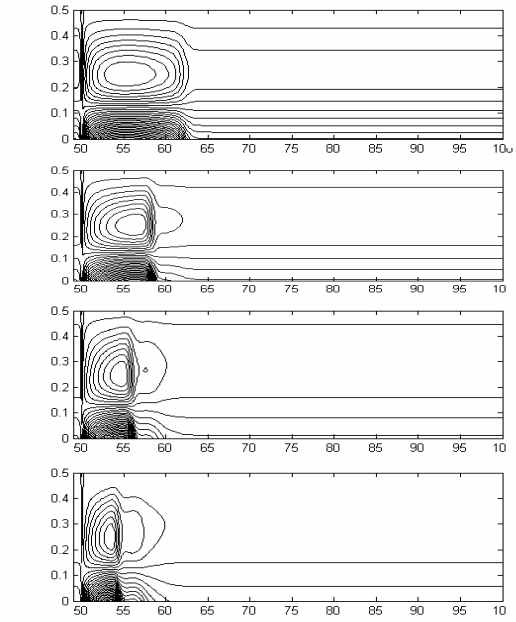

c) PR 70% and Re 50

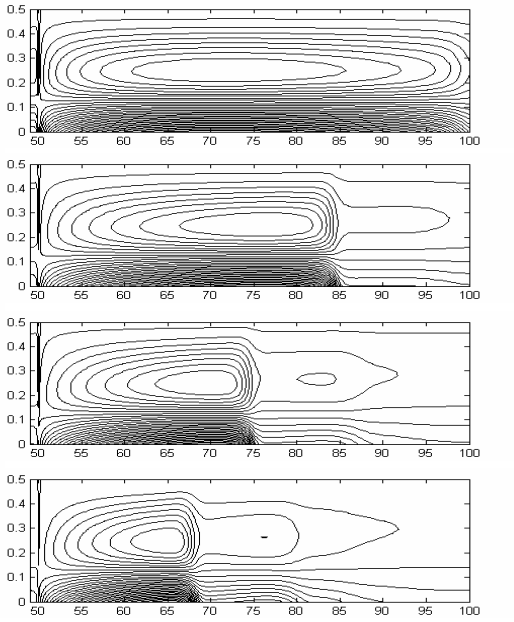

d) PR 70% and Re 200

Figure 3.48: Streamline contours for Wo 5, Wo 7.5, Wo 10 and Wo 12.5 (top to bottom) at t*=0.75 for a) PR 30% and Re 50, b) PR 30% and Re 200, c) PR 70% and Re 50 and d) PR 70% and Re 200

steps. For the flow through severe stenosis, the strength of the flow separation zone decreases with increase in value of Womersley number for the flow through severe stenosis at the time steps of t/T=0.25 and t/T=0.5. Therefore, possibility of plaque

deposition is higher for low value of Womersley number for the case of severe stenosis at these time steps. On the contrary, the strength of the flow separation zone increases with increase in value of Womersley number at the time steps t/T=0 and t/T=0.75. The possibility of plaque deposition is higher for high value of Womersley number for the case of severe stenosis at these time steps. The observation of secondary vortex at higher Womersley number for the case of severe stenosis may lead to conclusion regarding the chances of multiple depositions.

3.3.3 Peak wall shear stress and low wall shear stress

In this subsection, the effect of Womersley number on peak wall shear stress and low wall shear stress is investigated. At first, the effects of Womersley numbers on peak WSS and low WSS are investigated for the case of mild stenosis with low Reynolds number. The effect of Womersley number on peak WSS at stenotic zone for the case of PR 30% and Re 50 is shown in Fig. 3.49. It is found that the variation patterns of the time-averaged WSS are almost similar for all the considered

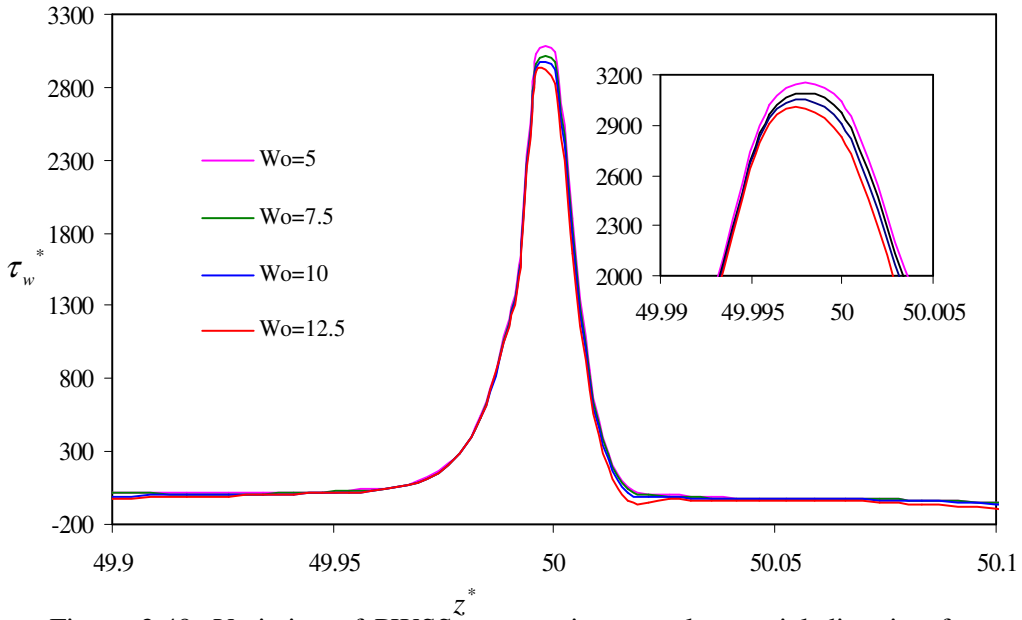

Figure 3.49: Variation of PWSS at stenotic zone along axial direction for different Wo for PR30% and Re 50

Womersley number. Here, peak WSS increases sharply as the flow approaches the throat of stenosis and reaches its peak value at the maximum restricted area. The wall shear stress decreases rapidly and reverses its sign at the downstream of the stenosis. There is no significant differences in magnitude of peak WSS for the considered

Womersley numbers. But the magnitude of peak WSS decreases with increase in the value of Womersley number as depicted in the figure. The probable cause of this phenomenon is larger unsteady inertial effect in respect to viscous effect at higher Womersley number. The peak WSS is 3048.29, 2974.40, 2913.82 and 2829.32 for Wo 5, Wo 7.5, Wo 10 and Wo 12.5 respectively. During the study of streamline contours for different Womersley numbers in the section 3.3.2, the flow separation zone and recirculation zone are found at the post-stenotic zone. Therefore, low WSS exists at the post stenotic zone. Figure.3.50 shows the effect of Womersley number on low WSS at post-stenotic zone for the case of PR 30% and Re 50. A sharp change is observed in low wall shear stress for different Womersley numbers. The probable reason behind this may be due to varying size of recirculation zone at different Womersley numbers. Both of the magnitude of maximum low WSS and the area under low WSS increase with increase in Womersley number. The magnitude of maximum low WSS is -117.20, -171.52, -341.98 and -524.70 for Wo 5, Wo 7.5, Wo 10 and Wo 12.5 respectively. The effect of Womersley number on peak WSS at

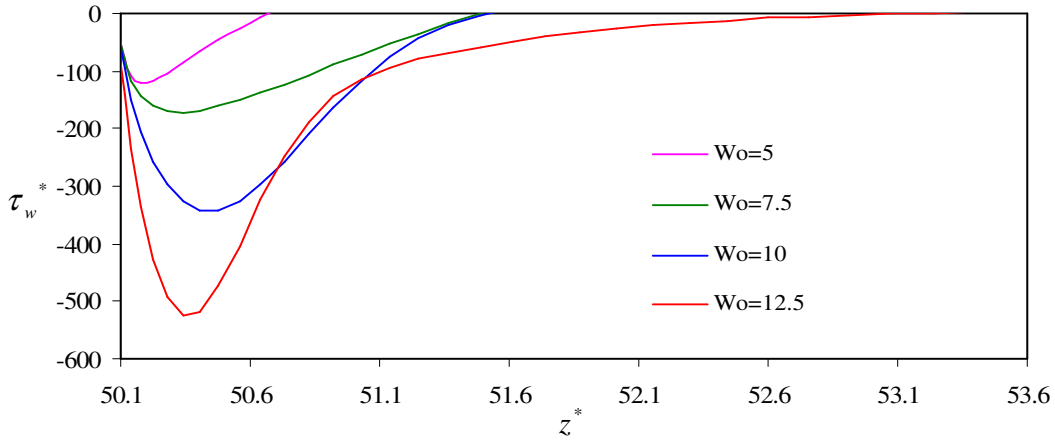

Figure 3.50: Variation of LWSS at post-stenotic zone along axial direction for different Wo for PR30% and Re 50

stenotic zone for the case of PR 30% and Re 200 is presented in Fig. 3.51. Like the previous observation on peak time averaged wall shear stress, in this case, the peak WSS is almost equal for all considered Womersley number and peak WSS decreases with increase in Womersley number. The noted magnitude of peak WSS is 3048.29, 2974.40, 2913.82 and 2829.32 for Wo 5, Wo 7.5, Wo 10 and Wo 12.5 respectively. Fig. 3.52 depicts the variation of low WSS at post-stenotic zone for the case of PR 30% and Re 200. In this case, the magnitude of maximum low WSS and the area

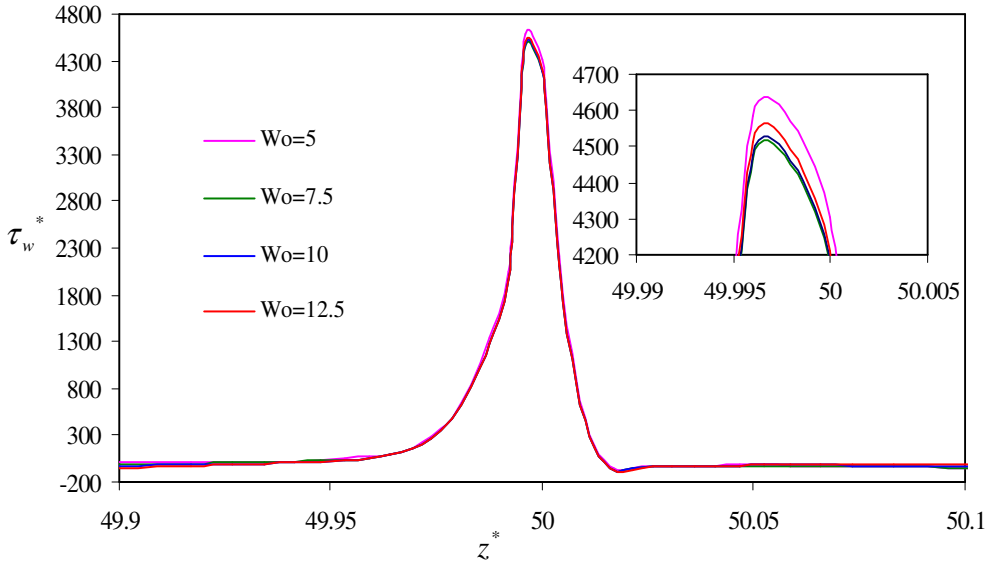

Figure 3.51: Variation of PWSS at stenotic zone along axial direction for different Wo for PR30% and Re200

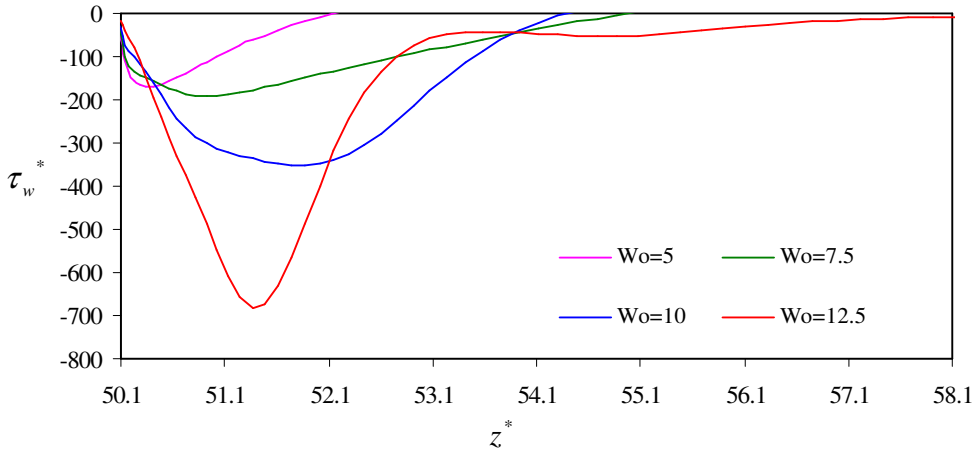

Figure 3.52: Variation of LWSS at post-stenotic zone along axial direction for different Wo for PR30% and Re200

under low WSS also increase with increase in Womersley number. The magnitude of maximum low WSS is -117.20, -171.52, -341.98 and -524.70 for Wo 5, Wo 7.5, Wo 10 and Wo 12.5 respectively. The effect of Womersley number on peak WSS at stenotic zone for the case of PR 70% with Re 50 is shown in Fig. 3.53. The peak WSS is almost equal for all considered Womersley numbers and peak WSS decreases with increase in Womersley number. The magnitude of peak WSS is 3048.29, 2974.40, 2913.82 and 2829.32 for Wo 5, Wo 7.5, Wo 10 and Wo 12.5 respectively. The effect

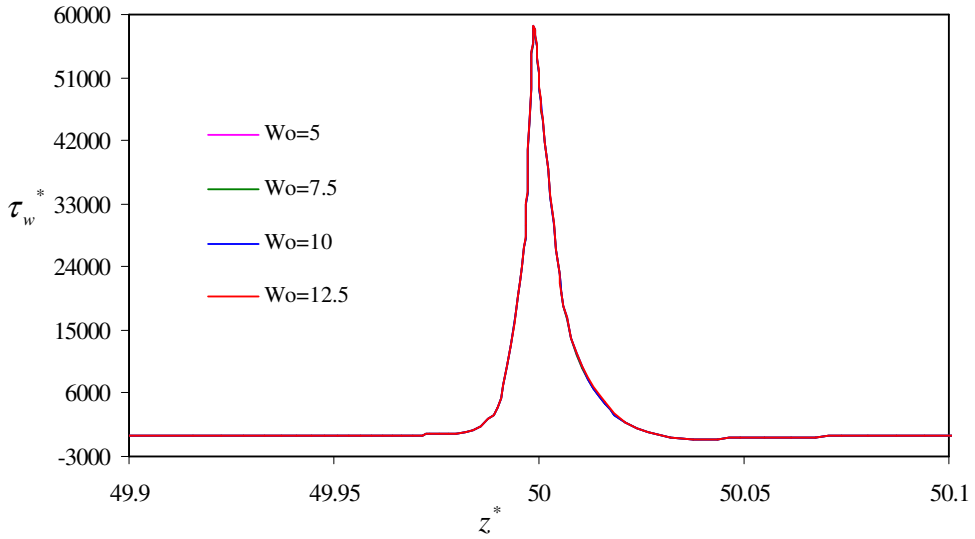

Figure 3.53: Variation of PWSS at stenotic zone along axial direction for different Wo for PR70% and Re 50

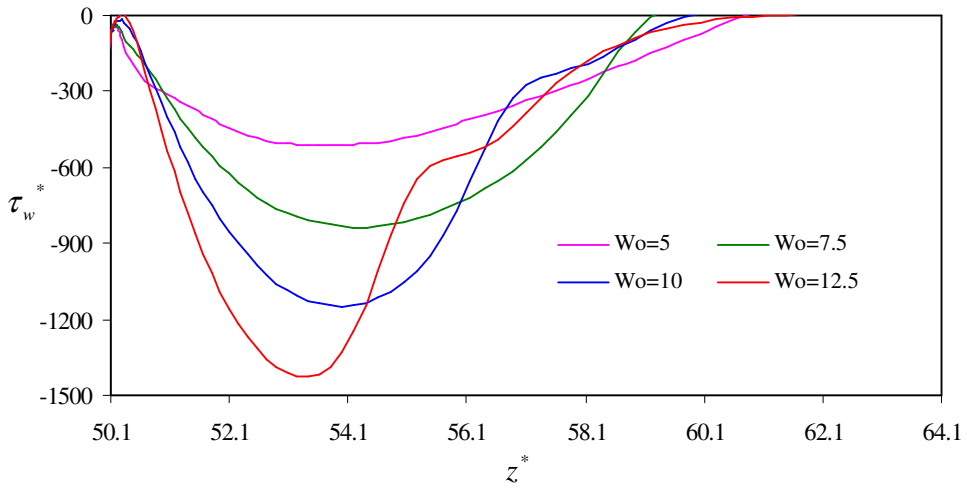

Figure 3.54: Variation of LWSS at post-stenotic zone along axial direction for different Wo for PR70% and Re 50

of Womersley numbers on low WSS at post-stenotic zone is shown in Fig. 3.54 for the case of PR 70% with Re 50. The magnitude of maximum low WSS and the area under low WSS increase with increase in Womersley number. The magnitude of maximum low WSS is -117.20, -171.52, -341.98 and -524.70 for Wo 5, Wo 7.5, Wo 10 and Wo 12.5 respectively. The effect of Womersley number on peak WSS at stenotic zone for the case of PR 70% with Re 200 is shown in Fig. 3.55. The peak WSS is almost equal for all considered Womersley numbers, which is same as the

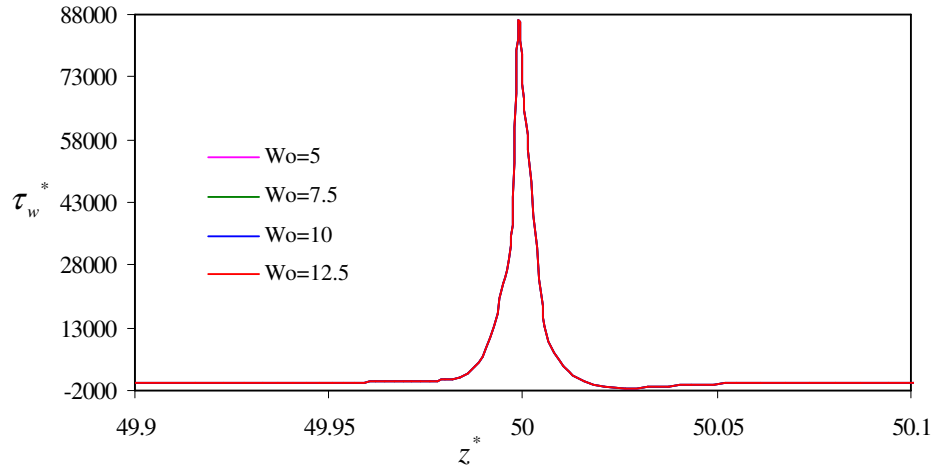

Figure 3.55: Variation of PWSS at stenotic zone along axial direction for different Wo for PR70% and Re200

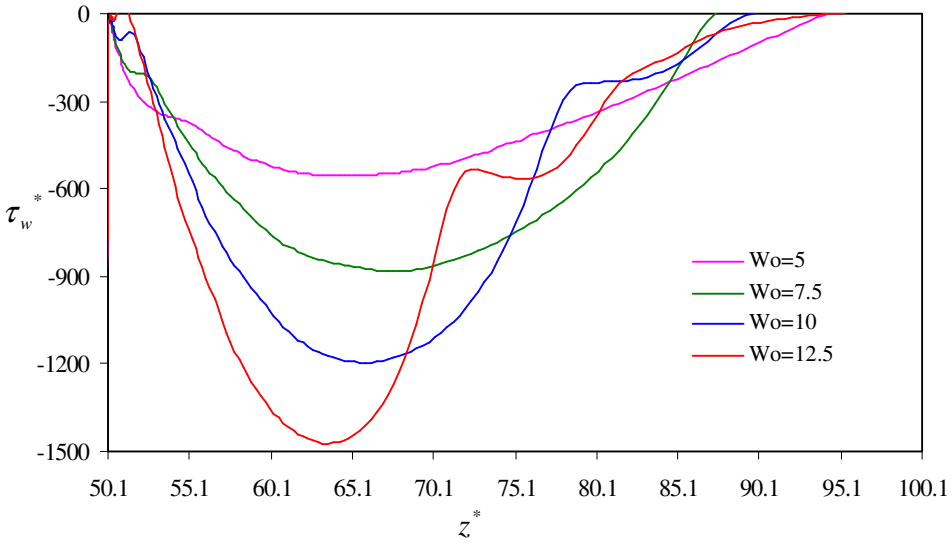

Figure 3.56: Variation of LWSS at post-stenotic zone along axial direction for different Wo for PR70% and Re200

earlier cases. The peak WSS is 3048.29, 2974.40, 2913.82 and 2829.32 for Wo 5, Wo 7.5, Wo 10 and Wo 12.5 respectively. The effect of Womersley number on low WSS at post-stenotic zone is shown in Fig.3.56 for the case of PR 70% with Re 200. The magnitude of maximum low WSS and the area under low WSS increase with increase in Womersley number. The magnitude of maximum low WSS is -117.20, -171.52, -341.98 and -524.70 for Wo 5, Wo 7.5, Wo 10 and Wo 12.5 respectively. From the overall study on WSS, it is understandable that there is negligible effect of Womersley number on peak wall shear stress. But there is high impact of Womersley

number on low wall shear stress. For all the considered cases, the magnitude of maximum low wall shear stress and area under low wall stress increase as Womersley number increases. Atherosclerosis occurs in sites of low shear stress because of low mass diffusion of lipids. Thus it may be said that the chances of formation of atherosclerosis increases with increase in Womersley number.

3.1.3.4 Oscillatory shear index

In this sub section, the effect of Womersley number on the oscillatory shear index is investigated for all the combination case of mild stenosis, severe stenosis, low Reynolds number flow and high Reynolds number flow. The variation of the OSI along axial direction in the stenotic zone and post stenotic zone is shown in Fig.3.57

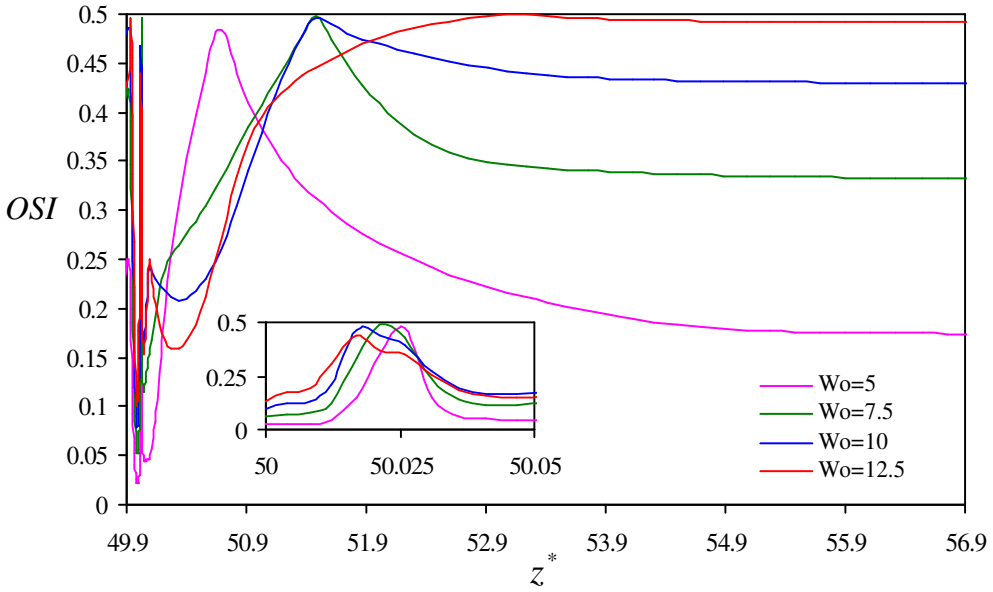

Figure 3.57: Variation of OSI at stenotic and post stenotic zone along axial direction for different Wo for PR30% and Re 50

for the case of PR 30% with Re 50. From the Figure, it is revealed that there is no prominent impact of Womersley numbers on oscillatory shear index. On viewing on the inset of the above figure, the high OSI is observed at the stenosis zone for all considered Womersley number and the peak value of OSI remains more or less same with the changes in Womersley number. This may happen because the zone just immediate after the throat of stenosis is of low inertial flow and the wall shear stress is more fluctuating in nature. The effect of unsteady inertia is not so prominent for flow through mild stenosis with low Reynolds number. The second peak OSI at the post stenosis zone is the reattachment point of flow separation as discussed earlier.

The reattachment length is 53.22 for Wo 12.5, 51.49 for Wo 10, 51.48 for Wo 7.5 and 50.61 for Wo 5. Now the effect of Womersley number on OSI is investigated for the second case, i.e. PR 30% with Re 200. The variation of the OSI along axial direction in the stenotic zone and post stenotic zone is shown in Fig.3.58 for the second case.

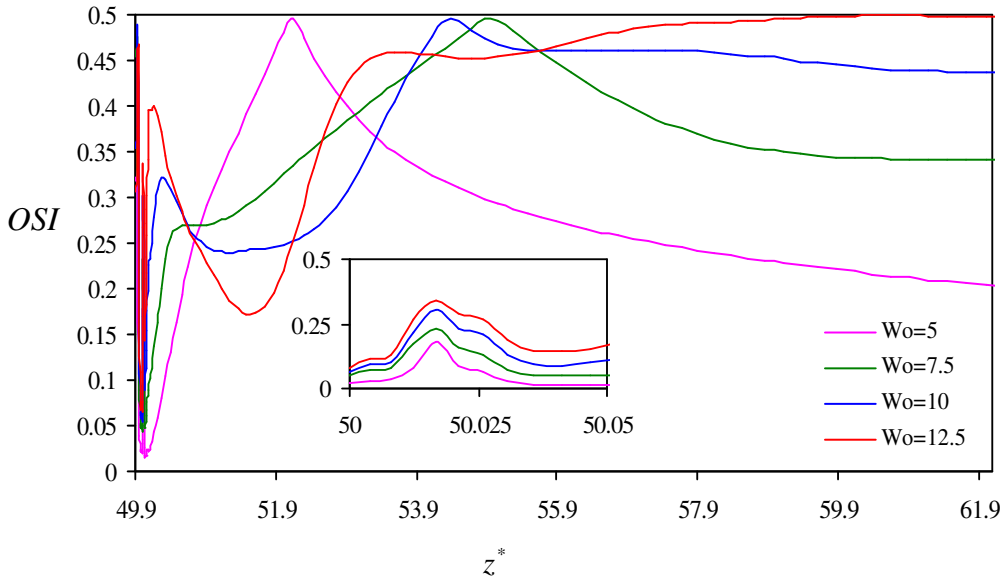

Figure 3.58: Variation of OSI at stenotic zone and post-stenotic zone along axial direction for different Wo for PR30% and Re200

The OSI is not so high at the stenotic zone for all considered Womersley number but the peak OSI at the stenosis zone increases with increase in Womersley number as shown in figure. In this case, the zone just immediate after the throat of stenosis is of high inertial flow and the wall shear stress is not so fluctuating in nature in comparison to the previous case. The effect of unsteady inertia is prominent for flow through mild stenosis with high Reynolds number. The second peak OSI points are localized significantly at different points with variation in Womersley number. The longest reattachment length is 59.88 for Wo 12.5 while other reattachment lengths are 54.30, 54.88 and 52.11 for Wo 10, Wo 7.5 and Wo 5 respectively. The variation of the OSI along axial direction in the stenotic zone and post stenotic zone is shown in Fig.3.59 for PR 70% with Re 50. The peak OSI at the stenosis zone increases with increase in Womersley number but there is a minor impact of Womersley numbers on the peak OSI. In the case of severe stenosis, the zone just immediate after the throat of stenosis is of high kinetic flow and thus wall shear stress is less fluctuating in nature. So the effect of Womersley number is minor. The second peak OSI points are

localized not so noticeably at the different points for different Womersley numbers. The reattachment length is 61.16 for Wo 12.5 while the same is 59.75 for Wo 10,

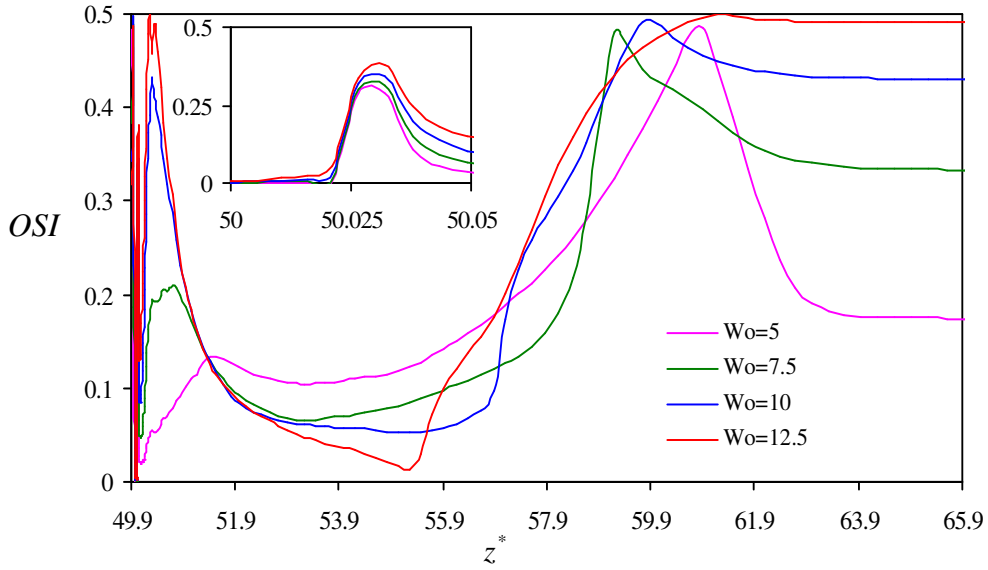

Figure 3.59: Variation of OSI at stenotic and post stenotic zone along axial direction for different Wo for Re 50 and PR70%

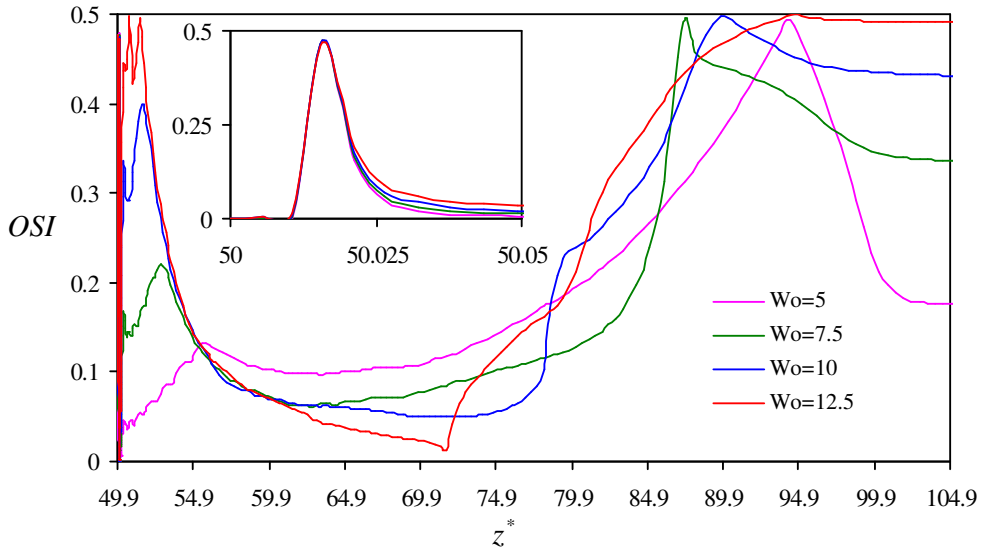

Figure 3.60: Variation of OSI at stenotic and post stenotic zone along axial direction for different Wo for Re200 and PR70%

59.20 for Wo 7.5 and 60.88 for Wo 5. Now the variation of OSI is observed for the case of PR 70% with Re 200 for the typical values of Womersley numbers. The

variation of the OSI along axial direction in the stenotic zone and post stenotic zone is shown in Fig.3.60 for this case. The peak value of OSI is very high at the stenosis zone for all considered Womersley numbers but there is no change of the peak OSI value with the changing in Womersley number. This may happen due to high inertia of flow at this zone. The high inertia of flow through severe stenosis is so dominated that the variation of Womersley number does not affect the first peak value of OSI. The second peak OSI points are localized considerably at the same point for all the considered Womersley numbers. The reattachment length is 94.58 for Wo 12.5, while the same is 94.09 for Wo 5, 87.36 for Wo 7.5 and 89.73 for Wo 10. From the overall study on OSI, it may be mentioned that the effect of Womersley number is not so significant. However, from the observation of the percentage increase of peak value of OSI just immediate after the stenosis zone, it may be mentioned that the chance of the development and localization of the disease, atherosclerosis, increases with increase in Womersley number. As far as the reattachment length estimated from OSI plots is concerned, the chance of atheromatous plaque deposition at the inner wall due to existence of recirculation zone increases with increase in Womersley number.

3.4 Comparisons on the Effect of Pulsatile Flow Profiles on Flow Characteristics

There is a variation of pulsatile flow profile when the blood flows through artery away from the heart. Again the pulsatile profiles are not identical among different human beings. Therefore, it is essential to study the effect of different pulsatile flow profiles on the blood flow characteristics such as wall pressure, streamline contour, wall shear stress and oscillatory shear index. In this section, a series of numerical simulations of model bell shaped stenosed artery have been carried out for typically three different pulsatile flow profiles such as simple pulsatile flow, physiological pulsatile flow and realistic pulsatile flow at the inlet of modeled stenosis geometry. The considered three pulsatile flow profiles are as follows;

Pulsatile flow profile-I (i.e. simple pulsatile flow):

$$u^*_z = 1 + \sin \omega t^*$$

Pulsatile flow profile-II (i.e. physiological pulsatile flow):

$$u^*_z = 1 + 0.75 \sin \omega t^* - 0.75 \cos 2\omega t^*$$

Pulsatile flow profile-III (i.e. realistic pulsatile flow):

$$u^*_z = 1 + 0.29244\cos(\omega t^* + 4.027) - 0.5908\cos(2\omega t^* + 6.509) +$$
$$0.2726\cos(3\omega t^* + 1.913) + 0.1980\cos(4\omega t^* + 1.461) + 0.1124\cos(5\omega t^* + 0.074)$$

As the detail study on the effect of Reynolds number, Womersley number and percentage of restriction for simple pulsatile flow is already made in the previous section, in this section, only two Reynolds numbers (Re 50 and Re 200), two Womersley number (Wo 5 and Wo 12.5) and two percentage of restriction (PR 30% and PR 70%) have been considered for comparisons of three different type of pulsatile flows. The results of three different pulsatile flows are compared by evaluating the effect of Reynolds number, Womersley number and percentage of restriction on the flow characteristics.

3.4.1 Wall pressure

The main interest is now to compare the arterial wall pressure of three different pulsatile flows (simple pulsatile flow, physiological pulsatile flow and realistic pulsatile flow) by evaluating the effect of Reynolds number, Womersley number and percentage of restriction on wall pressure. The variation of the time-averaged wall pressure along the axial direction of the considered arterial length is shown in Fig.3.61, Fig.3.62, Fig.3.63 and Fig.3.64 for all considered pulsatile flow conditions, Reynolds numbers, Womersley numbers and percentage of restrictions. The wall pressure at the outlet of the modeled artery has been set to zero for all considered cases. The figures help to visualize the exact scenario of blood pressure acted upon the artery wall for three different pulsatile flows with all different combination cases of Reynolds numbers, Womersley numbers and percentage of Restrictions. The wall pressure decreases gradually from inlet to outlet of the artery with a pressure drop at the throat of the stenosis for all the combination cases of each type of pulsatile flow, Reynolds number, percentage of restriction and Womersley number. The details of distribution of wall pressure along axial direction of length of artery have already been discussed in section 3.1. From the above figures, it can be mentioned that the time-averaged wall pressure drop varies with the changes of type of pulsatile profile for any combination case of Reynolds number, Womersley numbers and percentage of restriction. Table 3..1 depicts the values of time-averaged wall pressure drop for different combination cases of pulsatile profiles, Reynolds number, Womersley numbers and percentage of Restrictions. The wall pressure drop strongly gets affected by type of pulsatile flow. For all the combination cases of Re,

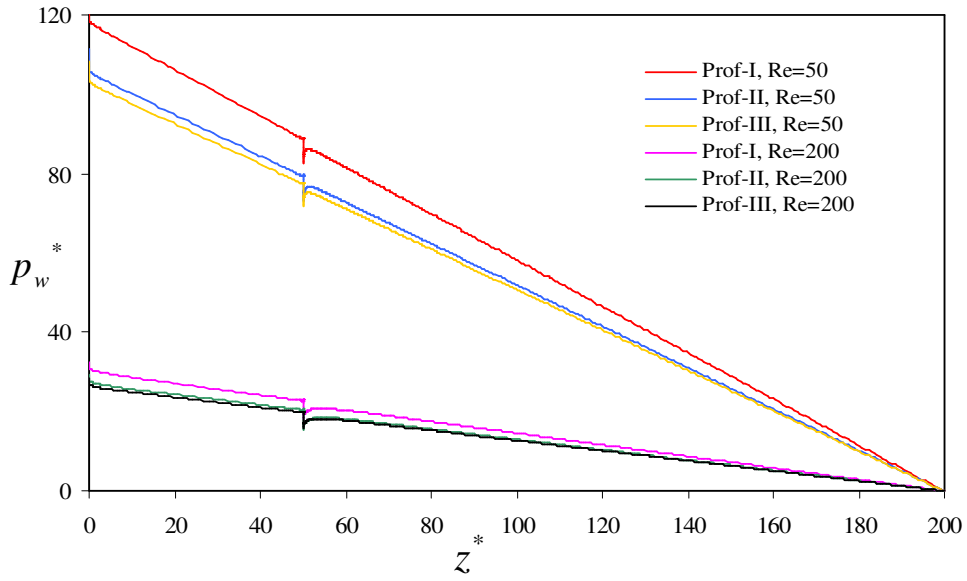

Figure 3.61: Variation of wall pressure along axial direction of considered length for different Re for PR 30% and Wo 5 for different pulsatile flows

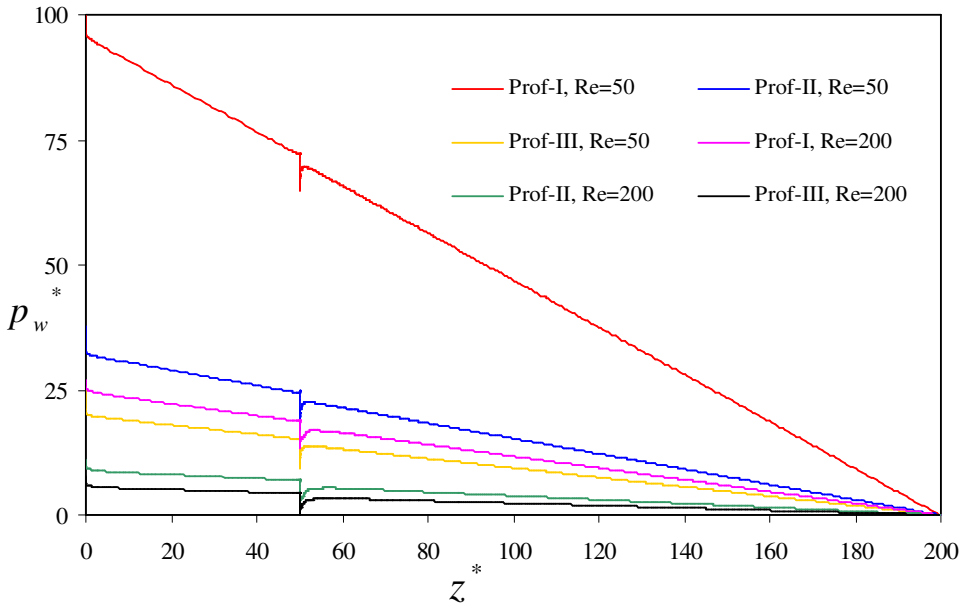

Figure 3.62: Variation of wall pressure along axial direction of considered length for different Re for PR 30% and Wo 12.5 for different pulsatile flows

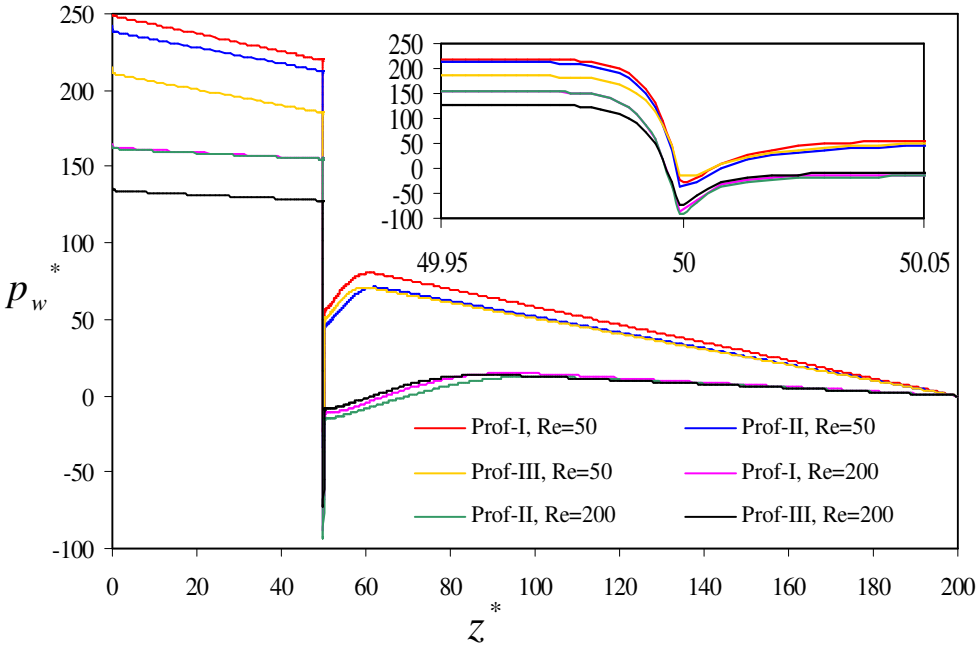

Figure 3.63: Variation of wall pressure along axial direction of considered length for different Re for PR 70% and Wo 5 for different pulsatile flows

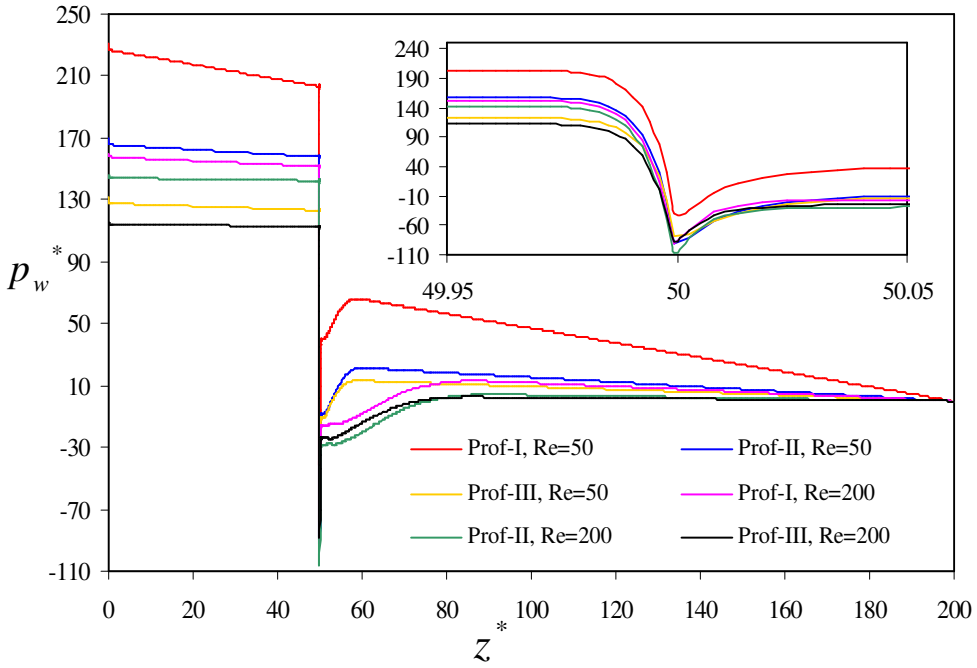

Figure 3.64: Variation of wall pressure along axial direction of considered length for different Re for PR 70% and Wo 12.5 for different pulsatile flows

Table 3.1: Time averaged wall pressure drop for different combination cases of pulsatile profiles, Reynolds number, Womersley numbers and percentage of Restrictions

Sl. No.	Combination case of profile type, Re, Wo and PR				Time-averaged wall pressure drop
	Profile type	Re	Wo	PR	
1	I	50	5	30%	5.38
2	II	50	5	30%	5.41
3	III	50	5	30%	4.92
4	I	200	5	30%	3.25
5	II	200	5	30%	3.29
6	III	200	5	30%	2.84
7	I	50	12.5	30%	6.65
8	II	50	12.5	30%	6.82
9	III	50	12.5	30%	5.83
10	I	200	12.5	30%	4.33
11	II	200	12.5	30%	4.41
12	III	200	12.5	30%	3.63
13	I	50	5	70%	221.13
14	II	50	5	70%	225.19
15	III	50	5	70%	183.06
16	I	200	5	70%	220.65
17	II	200	5	70%	224.56
18	III	200	5	70%	181.55
19	I	50	12.5	70%	221.81
20	II	50	12.5	70%	225.84
21	III	50	12.5	70%	183.48
22	I	200	12.5	70%	221.12
23	II	200	12.5	70%	224.80
24	III	200	12.5	70%	181.67

PR and Wo, the largest pressure drop is observed for physiological pulsatile flow (i.e. profile-II) while the realistic pulsatile flow (i.e. profile-III) has the least pressure drop. So the chances of tearing action on inner wall of artery and subsequent atherosclerotic plaque deposition are more for physiological pulsatile flow and less for realistic pulsatile flow. From the table, it is also noted that the wall pressure drop at the throat of stenosis decreases with increase in Reynolds number for all considered pulsatile flows at inlet. Thus the chance of plaque deposition increases with increase in Reynolds number for all considered type of pulsatile flows. Viewing on the table, it can also be mentioned that wall pressure drop increases prominently with increase in percentage of restriction for all three pulsatile flows. So plaque deposition chance is high for higher percentage of restriction. Further, it can be also pointed out that the effect of Womersley number on wall pressure drop is not so evidenced, but the wall pressure drop increases with increase in Womersley number. As a result, plaque deposition chance increases by increase in Womersley number of all the type of pulsatile flows.

3.4.2 Streamline contour

In this section, the details of flow fields are investigated for three different pulsatile flow conditions at four different times of a cardiac cycle such as t/T=0, t/T=0.25, t/T=0.50 and t/T=0.75.

At the beginning of the forward flow (t/T=0.0) of a cardiac cycle, the instantaneous streamline contours of three different pulsatile profiles are presented in Fig.3.65a for the case of mild stenosis (PR 30%) with Re 50 and Wo 5. The smaller flow separation is found for the simple pulsatile flow (profile-I) at this time step. This may happen because the simple pulsatile flow has the highest flow velocity among all three pulsatile flows at this time step, which can be seen in Fig.2.3 (presented in sub-section 2.5).

Fig.3.65b shows the instantaneous streamline contours for the case of mild stenosis with Re 200 and Wo 5 at this time step. In this case, the smaller flow separation zone is also found at the downstream of the stenosis for simple pulsatile flow condition. The strength of the flow separation increases with increase in Reynolds number for each type of pulsatile flow, which is noted by evaluating the above two figures, Fig.3.65a and Fig.3.65b. The probable cause of this phenomenon has already been discussed in sub-section 3.1.2.

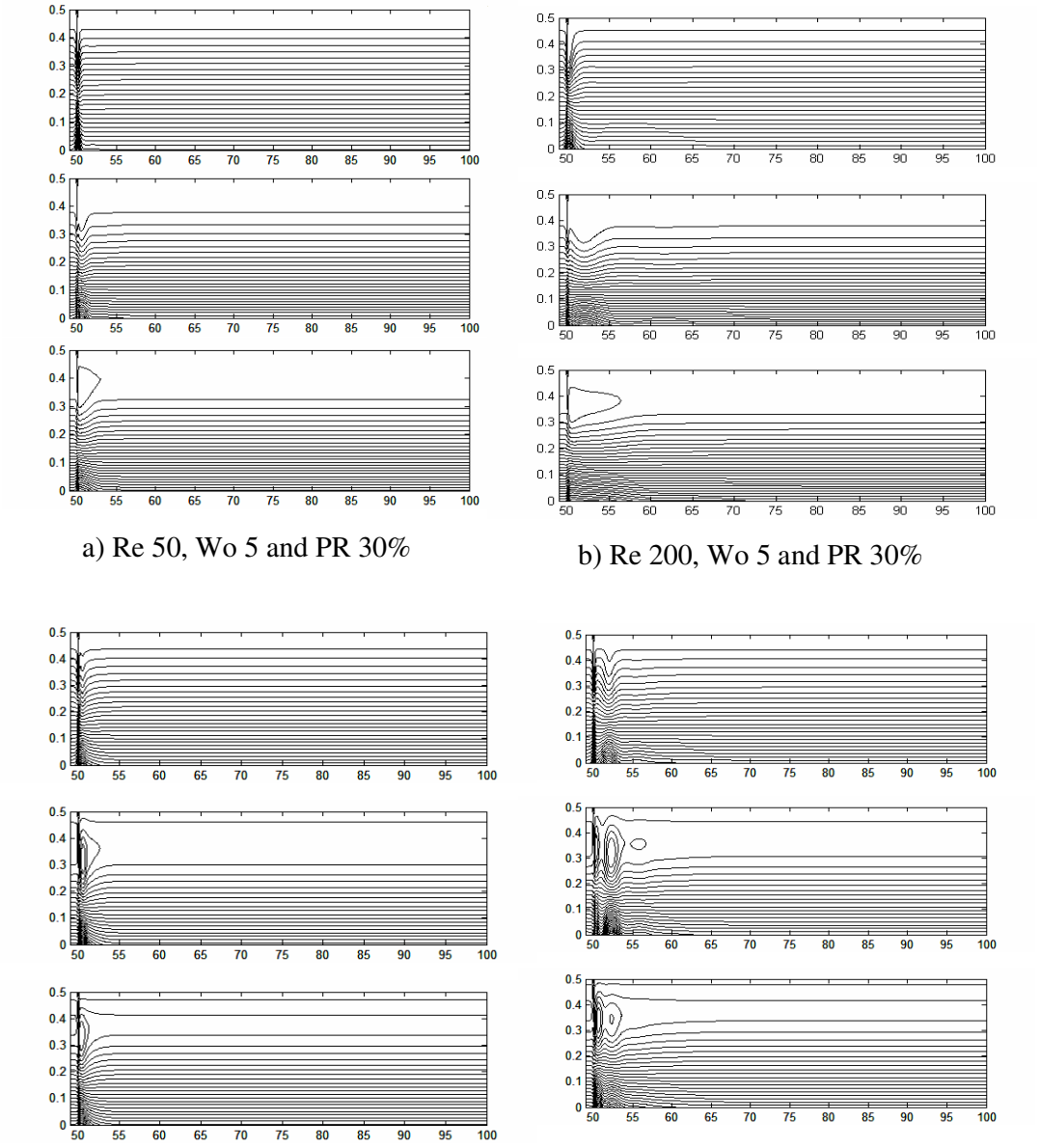

a) Re 50, Wo 5 and PR 30%

b) Re 200, Wo 5 and PR 30%

c) Re 50, Wo 12.5 and PR 30%

d) Re 200, Wo 12.5 and PR 30%

Figure 3.65: Streamline contours for profile-I, profile-II and profile-III (top to bottom) at time step t/T=0 for a) Re 50, Wo 5 and PR 30%, b) Re 200, Wo 5 and PR 30%, c) Re 50, Wo 12.5 and PR 30% and d) Re 200, Wo 12.5 and PR 30%

Figure 3.65(c-d) show the instantaneous streamline contours for mild stenosis with Re 50 and Wo 12.5 and for mild stenosis with Re 200 and Wo 12.5 respectively at t/T=0. The smaller flow separation is found for the simple pulsatile flow and the vortex ring has also been noticed in streamline contours of both of physiological and realistic pulsatile flows (profile-II and profile-III) for these cases of high Womersley

number (Wo = 12.5). Both the figures depict that the strength and size of the flow separation zone increase with increase in Reynolds number for each type of pulsatile flow. By studying Fig.3.65a and Fig.3.65c, and Fig.3.65b and Fig.3.65d separately, it is noted that the effect of Womersley number is minor. But flow separation zone size decreases with increase in Womersley number for all the considered profiles at this time steps (t/T=0) for mild stenosis. The observed phenomenon has already been explained in sub-section 3.3.2.

Now, the streamline contours are investigated for different pulsatile flow conditions for the case of severe stenosis at the time step, t/T=0. Fig.3.66 show the streamline contours for the case of PR 70% with Re 50 and Wo 5, PR 70% with Re 200 and Wo 5, PR 70% with Re 50 and Wo 12.5 and PR 70% with Re 200 and Wo 12.5 respectively at t/T=0. The larger flow recirculation zone is observed for the realistic pulsatile flow in comparison to other two types of flow conditions at lower value of Womersley number at this time step and the smaller flow separation is found for the simple pulsatile flow at this time step for severe stenosis with both high and low Reynolds numbers flow conditions. But, for the higher value of Womersley number, the size of recirculation zone does not change with the change in the type of pulsatile flow for severe stenosis with both high and low Reynolds number of flow. The probable reason of the observed phenomenon is that all types of pulsatile flow have minimum flow velocity with high unsteady inertia of flow because of high Womersley number, and the flow is more perturbed due to higher restriction of flow. From the above figures, it is may be said that an increase in the value of Reynolds number, with other unchanged conditions, an increase in the strength of the formed vortex as well as the flow separation zone size for each type of pulsatile flow has taken place. The probable explanation of this phenomenon has been stated in sub-section 3.1.2. The above figures also ensure that the strength of the flow separation zone increases with increase in the value of Womersley number for each type of pulsatile flow. The probable explanation of this phenomenon has been stated in sub-section 3.3.2.

By comparing all the streamline contours in Fig.3.65 and Fig.3.66 at this time step for different combination of considered cases, it is well understood that higher percentage of restriction leads to higher flow separation with formed vortex in the downstream of stenosis. The probable reason of this phenomenon has already been discussed in sub-section 3.2.2.

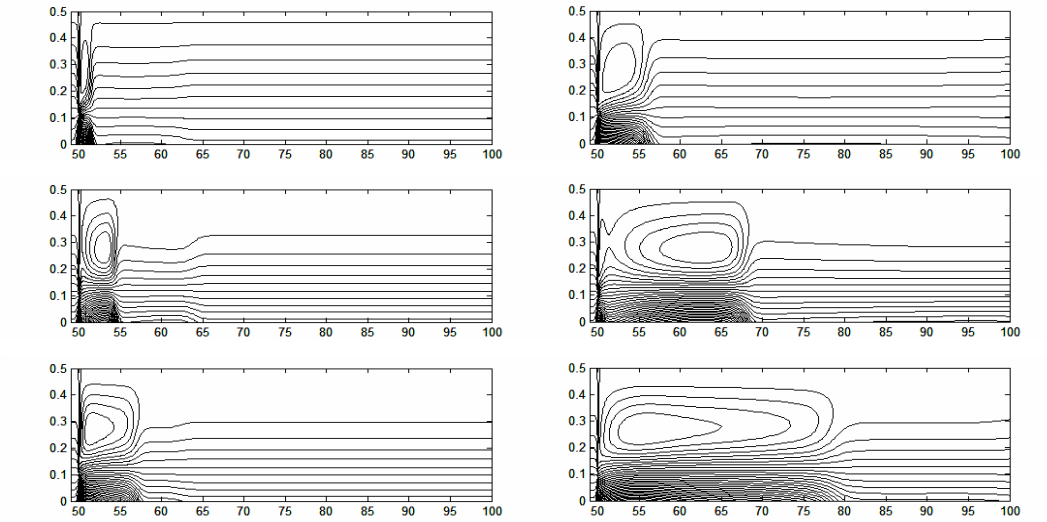

a) Re 50, Wo 5 and PR 70%

b) Re 200, Wo 5 and PR 70%

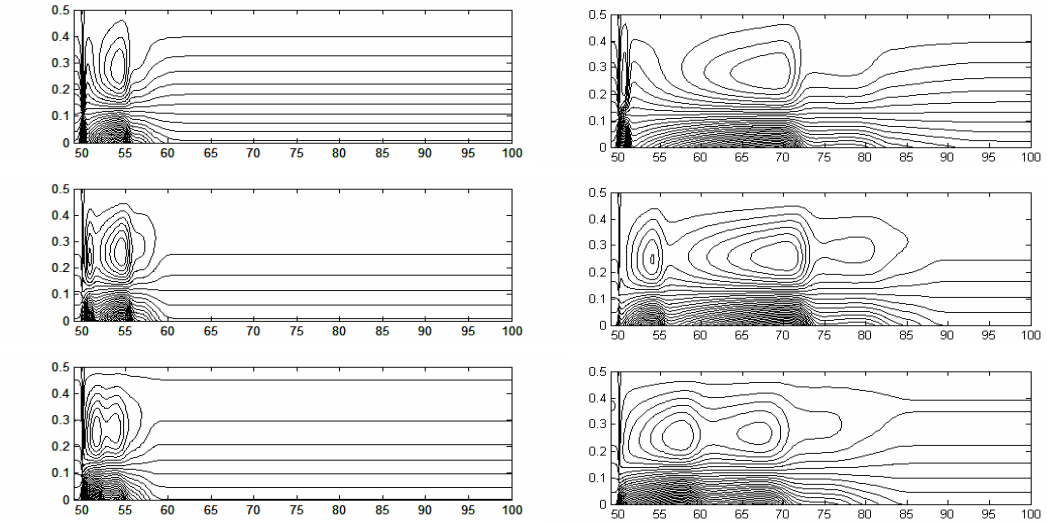

c) Re 50, PR 70% and Wo12.5

d) Re 200, PR 70% and Wo12.5

Figure 3.66: Streamline contours for profile-I, profile-II and profile-III (top to bottom) at time step t/T=0 for a) Re 50, Wo 5 and PR 70%, b) Re 200, Wo 5 and PR 70%, c) Re 50, Wo 12.5 and PR 70% and d) Re 200, Wo 12.5 and PR 70%

It is known that areas of flow separation are prone to the development of atherosclerotic plaque in the inner wall of artery. For the case of mild stenosis, the chance of atherosclerosis is more for physiological and realistic pulsatile flows at t/T=0 in comparison to the case of simple pulsatile flow. For the case of severe stenosis, the chance of atherosclerosis is more for realistic pulsatile flow with lower

Womersley number. But for higher Womersley number at t/T=0, the chance of atherosclerosis is more or less same for all considered flow profile conditions. For both mild stenosis and severe stenosis cases, the increase in Reynolds number leads to more chance of atherosclerosis for all the type of pulsatile flows at this time step while other condition remain unaltered. For the case of mild stenosis, chances of atherosclerosis decrease with increase in the value of Womersley number for all type of pulsatile flows at the considered time step. But increase in Womersley number directs the more chance of atherosclerosis at time steps t/T=0. It may be also commented that chances of development of atherosclerotic plaque at the inner wall of artery increase with increase in percentage of restriction for all considered types of pulsatile flow.

From Fig.2.3, presented in sub-section 2.5, this may be stated that the flow reaches the peak systolic flow for both simple pulsatile flow and physiological pulsatile flow at time step t/T=0.25. In case of realistic pulsatile flow condition, the peak systolic flow takes place just before time step, t/T=0.25. The streamline contours of three different pulsatile flow conditions for the case of PR 30% with Re 50 and Wo 5 is shown in Fig.3.67a. No significant difference is found in size of flow separation for three different types of pulsatile flow conditions. This may happen because the flow through mild stenosis is less perturbed for all the pulsatile flow conditions.

The streamline contours of three different pulsatile flow conditions for the case of PR 30% with Re 200 and Wo 5 is shown in Fig.3.67b. In this case, no significant difference is also found in size of flow separation for three different types of pulsatile flow conditions. From the above said two figures, it may stated that the effect of Reynolds number on flow separation is very small at this time step for the case of mild stenosis for all considered type of pulsatile flow conditions. This has happened because pulsatile flows have maximum flow velocities at this time step and flow through mild stenosis is less perturbed.

The streamline contours of three different pulsatile flow conditions for the case of PR 30% with Re 50 and Wo 12.5 and PR 30% with Re 200 and Wo 12.5 are shown in Fig.3.67(c-d) respectively. Like previous cases, in these cases of mild stenosis, no significant difference is also found in size of flow separation for three different types of pulsatile flow conditions. The effect of Reynolds number on flow separation is very small. From Fig.3.67a and Fig.3.67b, and Fig.3.67c and Fig.3.67d separately, it is observed that the flow separation zone size decreases with increase in

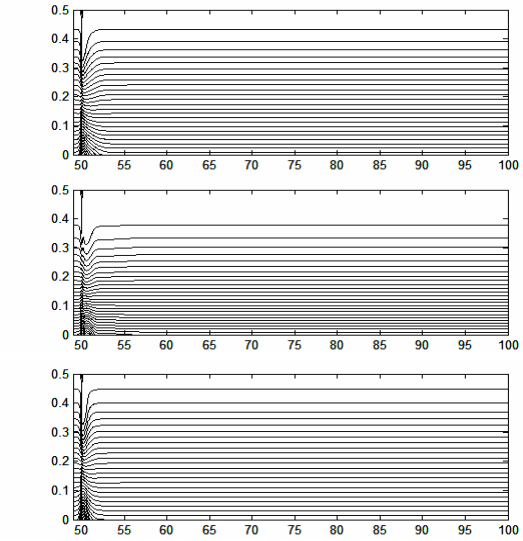

a) Re 50, Wo 5 and PR 30%

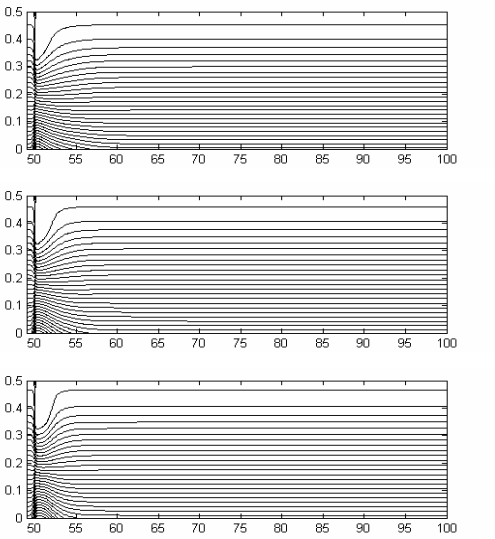

b) Re 200, Wo 5 and PR 30%

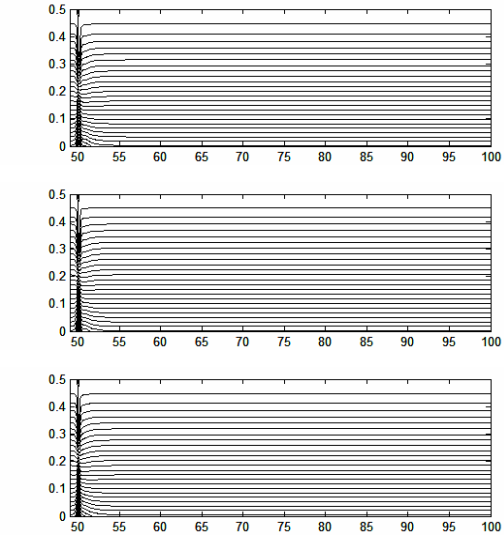

c) Re 50, Wo 12.5 and PR 30%

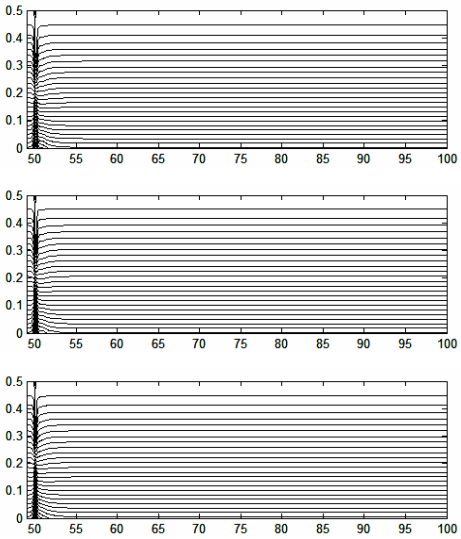

d) Re 50, PR 30% and Wo 12.5

Figure 3.67: Streamline contours for profile-I, profile-II and profile-III (top to bottom) at time step t/T=0.25 for a) Re 50, Wo 5 and PR 30%, b) Re 200, Wo 5 and PR 30%, c) Re 50, Wo 12.5 and PR 30% and d) Re 200, Wo 12.5 and PR 30%

the value of Womersley number for all considered type of pulsatile flow conditions at this time step for mild stenosis case. The probable explanation of this phenomenon has already been discussed in sub-section 3.3.2.

The Fig.3.68 holds the instantaneous streamline contours created by three different pulsatile flow conditions for the case of PR 70% with Re 50 and Wo 5, PR

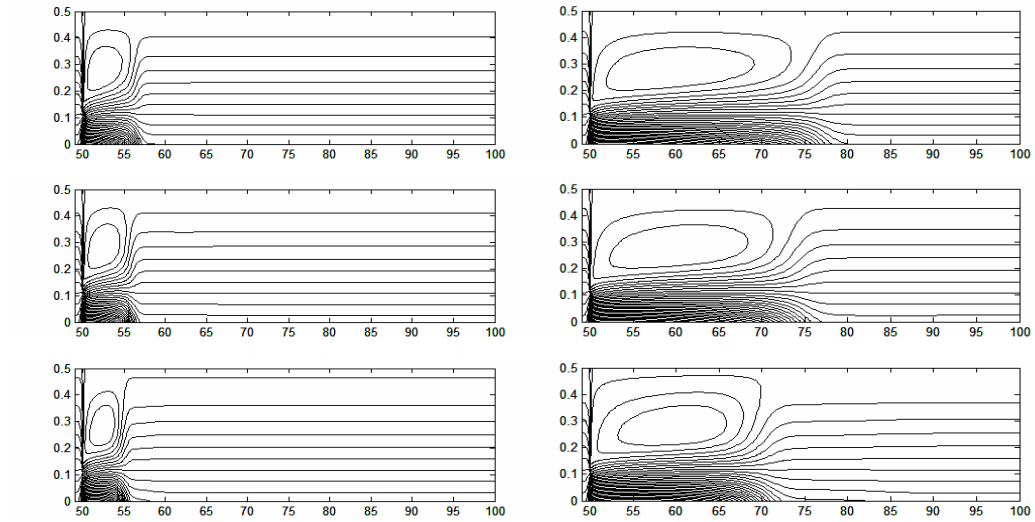

a) Re 50, Wo 5 and PR 70%

b) Re 200, Wo 5 and PR 70%

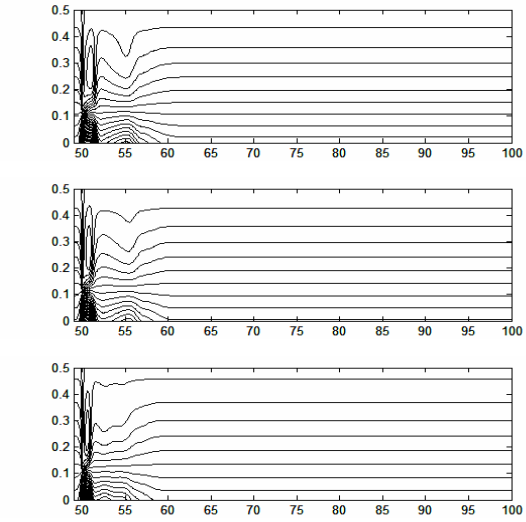

c) Re 50, Wo 12.5 and PR 70%

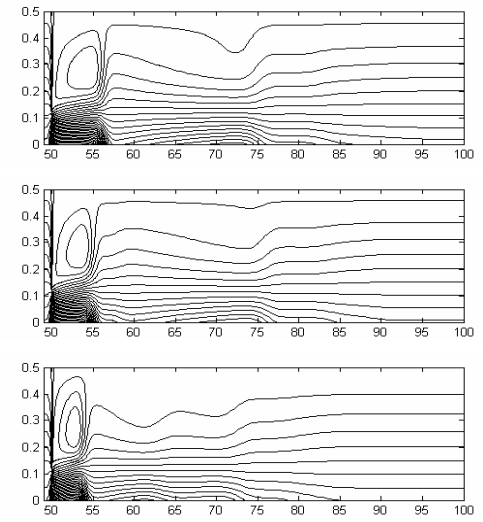

d) Re 200, Wo 12.5 and PR 70%

Figure 3.68: Streamline contours for profile-I, profile-II and profile-III (top to bottom) at time step t/T=0 for a) Re 50, Wo 5 and PR 70%, b) Re 200, Wo 5 and PR 70%, c) Re 50, Wo 12.5 and PR 70% and d) Re 200, Wo 12.5 and PR 70%

70% with Re 200 and Wo 5, PR 70% with Re 50 and Wo 12.5 and PR 70% with Re 200 and Wo 12.5 respectively. The streamlines demonstrate the larger flow recirculation zone creates for the simple pulsatile flow while the smaller flow recirculation zone creates for the realistic pulsatile flow. This has happened because simple pulsatile flow condition has lowest flow velocity and realistic pulsatile flow condition has highest flow velocity. In this case of severe stenosis, flow recirculation

zone size increases with increase in Reynolds number in this time step for all the considered pulsatile flow conditions. Like the previous case of mild stenosis, at this time step, flow recirculation zone size decreases with increase in Womersley number.

From the evaluation of all the streamline contours presented in Fig.3.69 at this time step, it is clearly understood that size of flow separation zone increases with increase in percentage of restriction. For the case of mild stenosis, the chance of atherosclerosis is more or less same for all pulsatile flow conditions at t/T=0.25. For the case of severe stenosis, the chance of atherosclerosis is more for simple pulsatile flow at t/T=0.25. For both mild and severe stenosis cases, the increase in Reynolds number leads to more chance of atherosclerosis for all the considered type of pulsatile flows. Chances of atherosclerosis decrease with increase in the value of Womersley number for all type of pulsatile flows at this time step for both mild stenosis and severe stenosis. At this point, it may be commented that chances of development of atherosclerosis increase with increase in percentage of restriction for all considered pulsatile flow conditions.

From Fig.2.3, presented in subsection 2.5, it may be opined that all three pulsatile flows decelerate at the time step, t/T=0.5. The physiological pulsatile flow holds the lowest flow rate and the simple pulsatile flow holds the highest flow rate at the said time step. The streamline contours for mild stenosis with Re 50 and Wo 5 are depicted in Fig.3.69a at this time step t/T=0.5 for all considered types of pulsatile flow. The largest flow separation zone along with a vortex ring is found in case of physiological pulsatile flow. This has happened because physiological pulsatile flow has lowest flow velocity at this time step.

The streamline contours for mild stenosis with Re 200 and Wo 5 for all considered pulsatile flow conditions at time step t/T=0.5 are illustrated in Fig.3.69b. In this case, the largest flow separation zone as well as a vortex ring has been found for physiological pulsatile flow. The above two figures depict that the size of the flow separation zone increases with increase in Reynolds number for all the considered pulsatile flows. The probable cause has already been explained at sub-section 3.1.2.

The streamline contours for mild stenosis with Re 50 and Wo 12.5 and mild stenosis with Re 200 and Wo 12.5 for all considered types of pulsatile flow condition are presented in Fig.3.69(c-d) respectively. Like the previous cases of this time step, for these two cases, the larger flow separation zone and a vortex ring are also found for physiological pulsatile flow. The size of the flow separation zone increases with

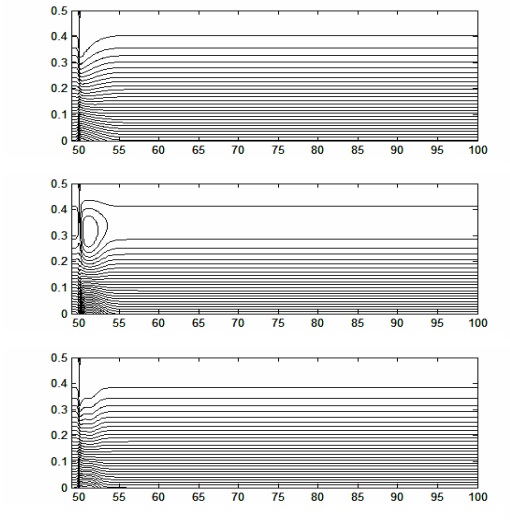

a) Re 50, Wo 5 and PR 30%

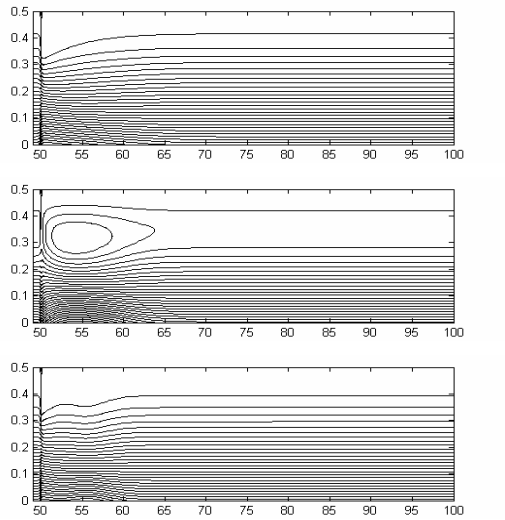

b) Re 200, Wo 5 and PR 30%

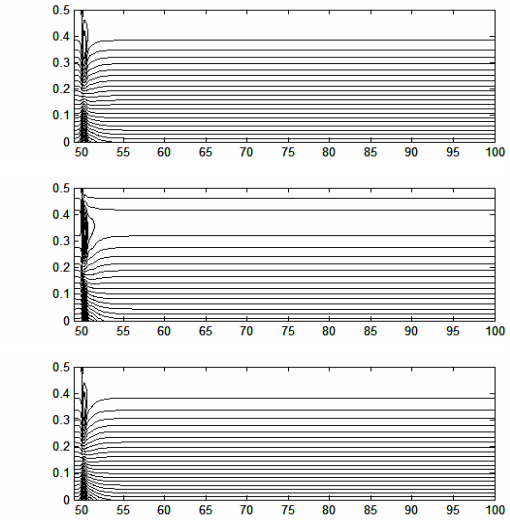

c) Re 50, Wo 12.5 and PR 30%

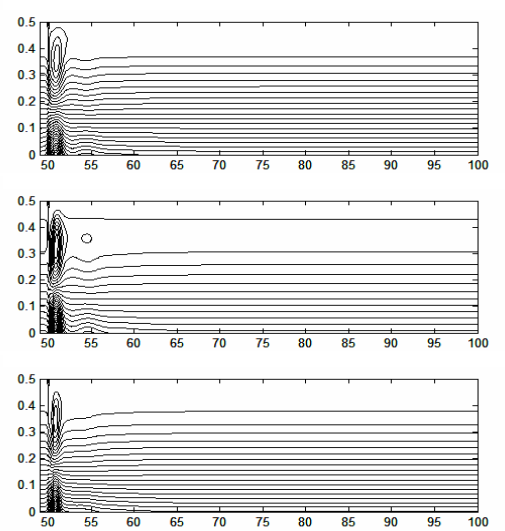

d) Re 200, Wo 12.5 and PR 30%

Figure 3.69: Streamline contours for profile-I, profile-II and profile-III (top to bottom) at time step t/T=0.50 for a) Re 50, Wo 5 and PR 30%, b) Re 200, Wo 5 and PR 30%, c) Re 50, Wo 12.5 and PR 30% and d) Re 200, Wo 12.5 and PR 30%

increase in Reynolds number for all considered pulsatile flow types. The figures also illustrate that flow recirculation zone size decreases with increase in Womersley number for the case of mild stenosis at this time step. The probable reason has already been explained at sub-section 3.3.2.

The Fig.3.70 shows the streamline contours for PR 70% with Re 50 and Wo 5, PR 70% with Re 200 and Wo 5, PR 70% with Re 50 and Wo 12.5 and PR 70% with

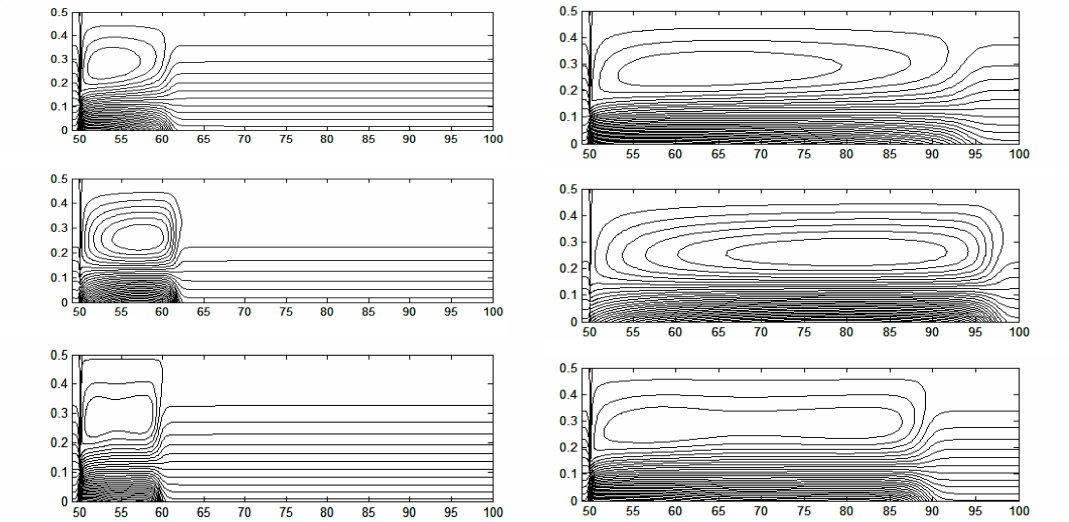

a) Re 50, Wo 5 and PR 70%

b) Re 200, Wo 5 and PR 70%

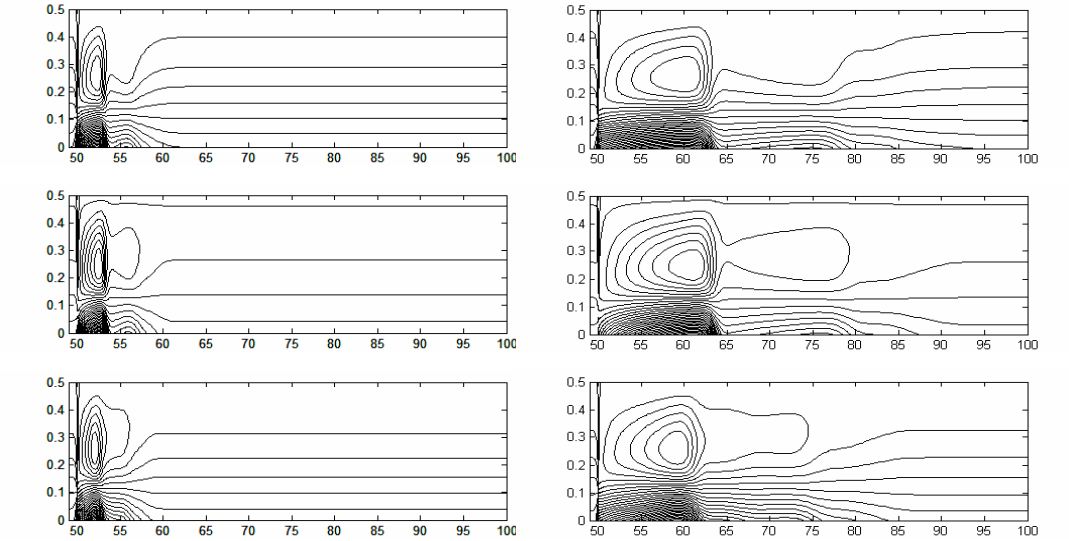

c) Re 50, Wo12.5 and PR 70%

d) Re 200, Wo12.5 and PR 70%

Figure 3.70: Streamline contours for profile-I, profile-II and profile-III (top to bottom) at time step t/T=0 for a) Re 50, Wo 5 and PR 70%, b) Re 200, Wo 5 and PR 70%, c) Re 50, Wo 12.5 and PR 70% and d) Re 200, Wo 12.5 and PR 70%

Re 200 and Wo 12.5 respectively for all considered pulsatile flow conditions at time step t/T=0.5. There are no significant differences in the size of flow separation zones for all considered pulsatile flow conditions at different considered combination cases of Reynolds number and Womersley number for the case of severe stenosis. This may happen because of high restriction of flow. The impact of Reynolds number is

prominent for all the pulsatile profiles for this case of severe stenosis. Both the flow separation zone size and generated vortex strength increase with increase in Reynolds number for all the considered pulsatile flows. From the above said figures, it is observed that the flow separation zone size decreases slightly with increase in Womersley number for severe stenosis for all considered pulsatile flow conditions.

From Fig.3.69 and Fig.3.70, this is observed that the larger flow separation zone along with a formed vortex ring has been found for all the considered pulsatile profiles for severe stenosis in comparison to the cases of mild stenosis condition. The explanation of this phenomenon has already been discussed in section 3.2.2.

The chance of atherosclerosis is more for physiological pulsatile flows at t/T=0.50 in comparison to the case of simple pulsatile flow and realistic pulsatile flow for both severe stenosis and mild stenosis. The chance of atherosclerosis is almost same for all considered pulsatile flow conditions for the case of severe stenosis. For both mild and severe stenoses, the increase in Reynolds number leads to more chance of atherosclerosis for all considered types of pulsatile flow at that time step. Chances of atherosclerosis decrease with increase in the value of Womersley number for all types of pulsatile flow at this time step for all considered combination cases. Chances of development of atherosclerotic plaque at the inner wall of artery increase with increase in percentage of restriction for all considered types of pulsatile flow.

From Fig.2.3 (presented in sub-section 2.5), at the time step, t/T=0.75, the flow reaches the peak diastolic flow for physiological pulsatile flow. In case of realistic pulsatile flow condition, the peak diastolic flow takes place just before time step, t/T=0.75. For simple pulsatile flow, flow rate has its minimum value at this time step. Figure.3.71a represents the streamline contours for all considered pulsatile flow conditions for PR 30% with Re 50 and Wo 5 at t/T=0.75. The said figure reveals that flow separation zone sizes for both physiological pulsatile and realistic pulsatile flows are more or less same at this time step. Comparatively large flow separation zone including a vortex at the downstream of stenosis is observed for the simple pulsatile flow. This has happened because the flow rate of simple pulsatile flow is very low while comparing with other two types of pulsatile flow.

The Fig.3.71b represents the streamline contours for PR 30% with Re 200 and Wo 5 at t/T=0.75 for all considered types of pulsatile flow. From the figure, it is seen that size of flow separation zone is larger for simple pulsatile flow at this time step. The above two figures demonstrate that the size of the flow separation zone increases

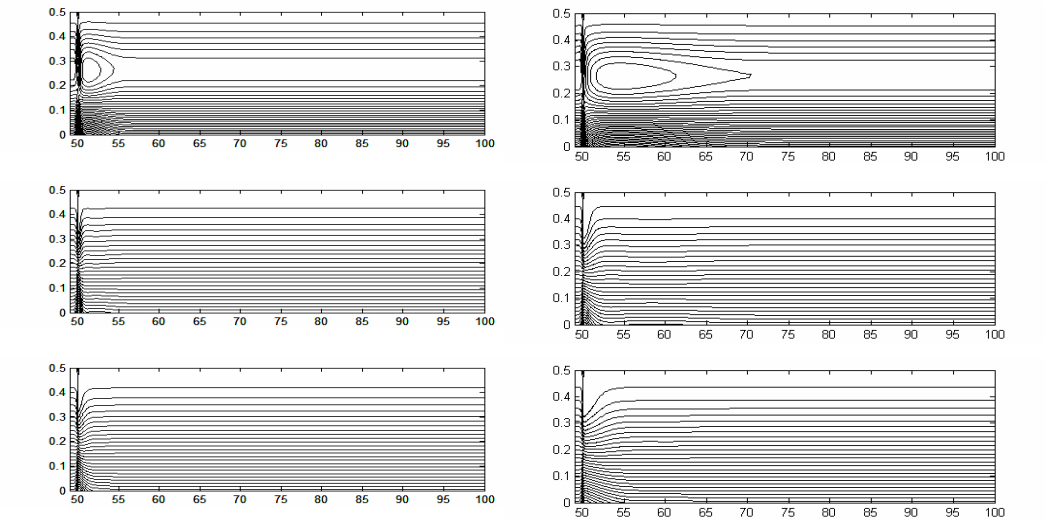

a) Re 50, Wo 5 and PR 30%

b) Re 200, Wo 5 and PR 30%

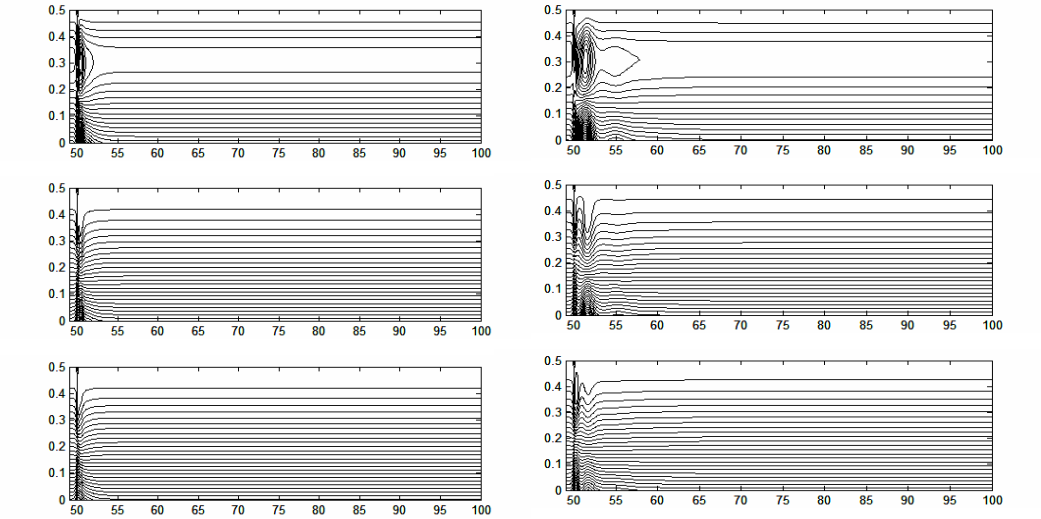

c) Re 50, Wo 12.5 and PR 30%

d) Re 200, Wo 12.5 and PR 30%

Figure 3.71: Streamline contours for profile-I, profile-II and profile-III (top to bottom) at time step t/T=0.75 for a) Re 50, Wo 5 and PR 30%, b) Re 200, Wo 5 and PR 30%, c) Re 50, Wo 12.5 and PR 30% and d) Re 200, Wo 12.5 and PR 30%

with increase in Reynolds number for all considered pulsatile flow conditions. The reason of this phenomenon has already been given in sub-section.3.1.2.

The streamline contours for all considered pulsatile flow conditions for PR 30% with Re 50 and Wo 12.5, and PR 30% with Re 200 and Wo 12.5 are presented in Fig.3.71(c-d) respectively at t/T=0.75. Like the previous cases of low Womersley number, the highest flow separation zone size is observed for simple pulsatile flow

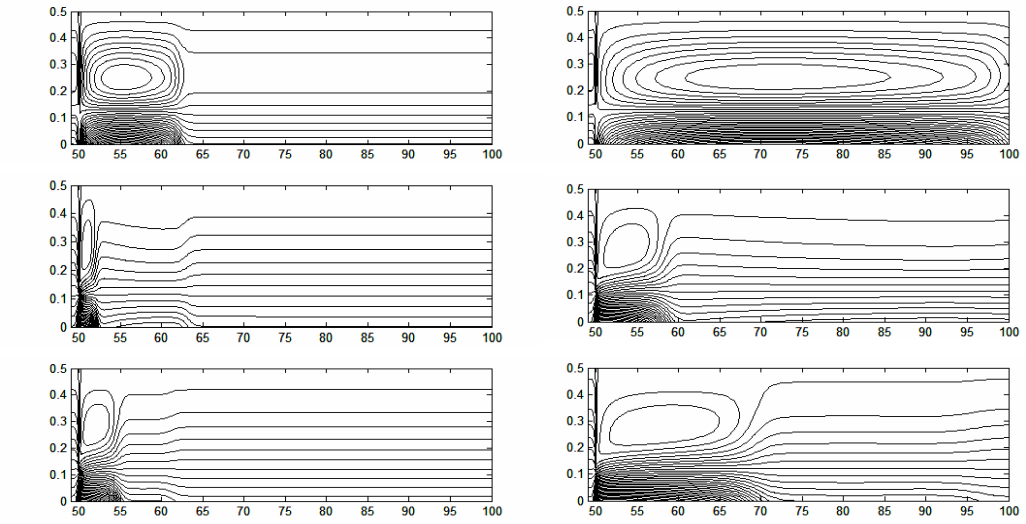

a) Re 50, Wo 5 and PR 70%

b) Re 200, Wo 5 and PR 70%

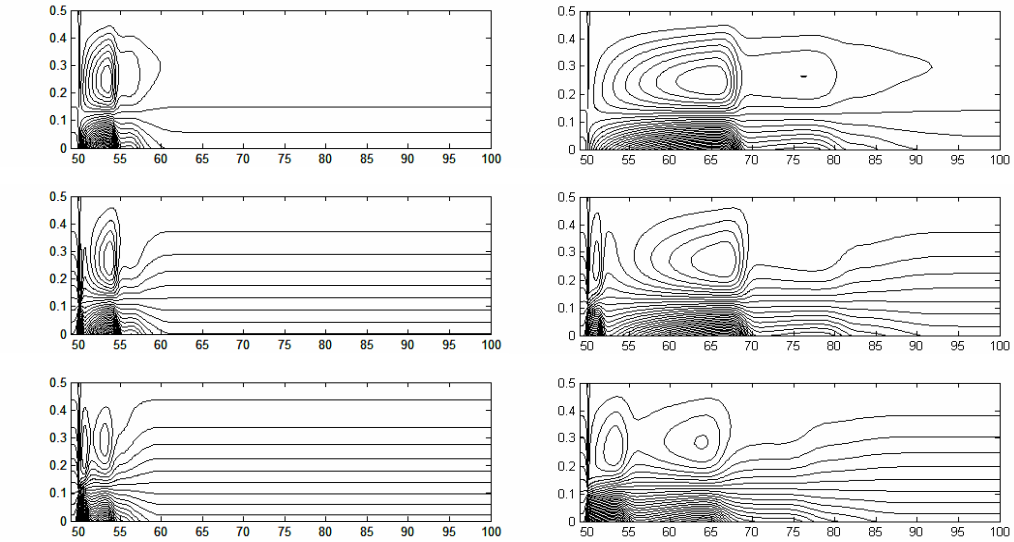

c) Re 50, Wo 12.5 and PR 70%

d) Re 200, Wo 12.5 and PR 70%

Figure 3.72: Streamline contours for profile-I, profile-II and profile-III (top to bottom) at time step t/T=0 for a) Re 50, Wo 5 and PR 70%, b) Re 200, Wo 5 and PR 70%, c) Re 50, Wo 12.5 and PR 70% and d) Re 200, Wo 12.5 and PR 70%

condition in these two cases of high Womersley number. The size of flow separation zone increases with increase in Reynolds number, as can be seen from figures. The figures also illustrate that the impact of Womersley number on streamline contours is very less, but flow separation zone size decreases with increase in Womersley number

for each type of pulsatile flow profile. The probable reason of this phenomenon has already been given in sub-section.3.3.2.

Now the streamline contours for PR 70% with Re 50 and Wo 5, PR 70% with Re 200 and Wo 5, PR 70% with Re 50 and Wo 12.5, and PR 70% with Re 200 and Wo 12.5 are presented in Fig.3.72 respectively at the same time step, t/T=0.75. From the said figures, it is observed that the larger flow separation zone as well as a vortex ring are found in case of simple pulsatile flow condition for the case of severe stenosis, similar to the previous case of mild stenosis. In this case, the size of the flow separation zone as well as the strength of vortex ring also increases with increase in Reynolds number for all the considered pulsatile flows. The flow separation zone size increases with increase in the value of Womersley number for the case of severe stenosis at this time step, as can be seen from the figures. The probable cause of this phenomenon has already been given in sub-section.3.3.2.

From the study of all streamline contours presented in Fig.3.71 and Fig.3.72, this is observed that the larger flow separation zone as well as a vortex ring is noted for all the considered pulsatile profiles for severe stenosis in comparison to the case of mild stenosis. The reason of this phenomenon has already been explained in sub-section 3.2.2.

From the overall study on streamline contours, this may be commented that the chance of atherosclerosis is more for simple pulsatile flow at t/T=0.75. For both mild and severe stenosis cases, the increase in Reynolds number leads to more chance of atherosclerosis for all the type of pulsatile flows at this time step while other conditions remain unaltered. The possibility of plaque deposition is higher for low value of Womersley number for the case of mild stenosis at this time step. But, the possibility of plaque deposition is higher for high value of Womersley number for the case of severe stenosis at this time step. Chances of development of atherosclerotic plaque increase with increase in percentage of restriction for all considered types of pulsatile flow.

3.4.3 Peak wall shear stress and low wall shear stress

In this section, peak wall shear stress distributions and low wall shear stress distribution are compared for three different pulsatile profiles by evaluating the impact of Reynolds number, percentage of restriction and Womersley number. At first, peak WSS distributions along axial length of artery for three different pulsatile

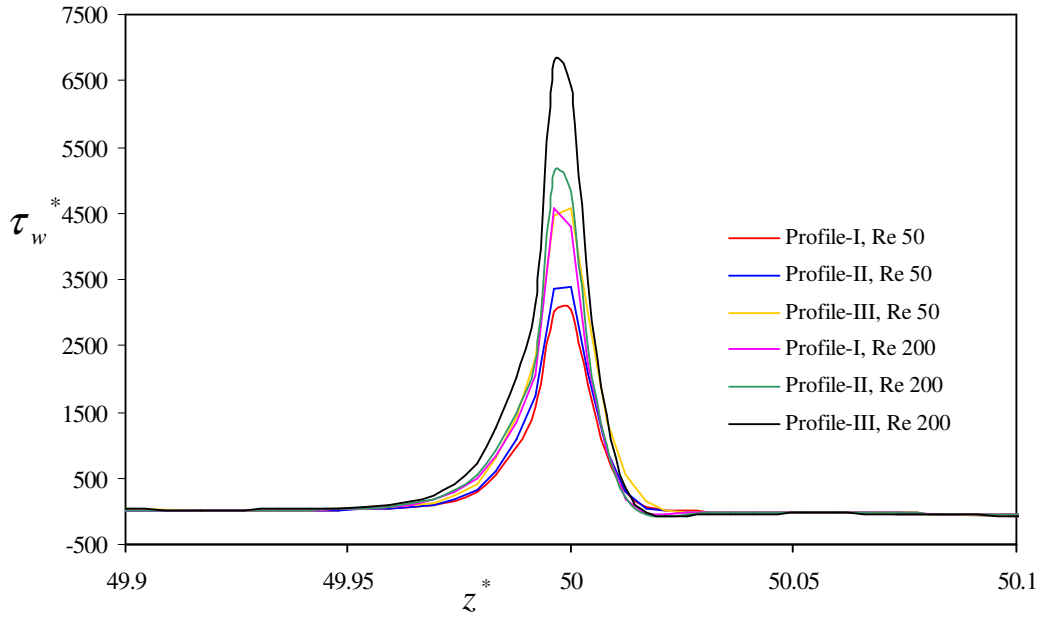

Figure 3.73: Variation of peak WSS at stenotic zone along axial direction for different Re for PR30% with Wo 5 for different pulsatile flows

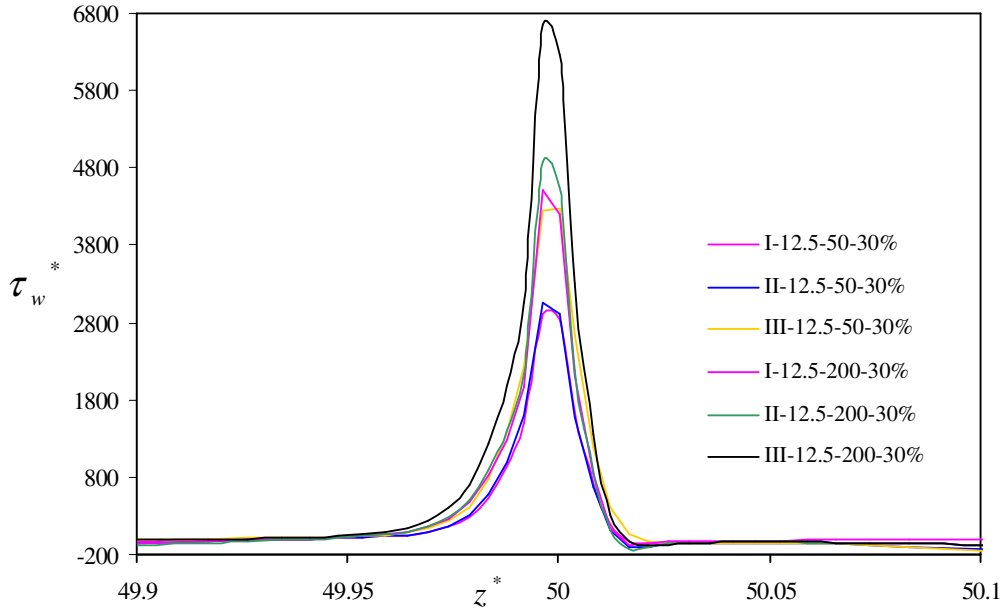

Figure 3.74: Variation of peak WSS at stenotic zone along axial direction for different Re for PR30% and Wo12.5 for different pulsatile flows

flows with all different considered cases of Reynolds numbers (Re 50 and 200), Womersley numbers (Wo 5 and 12.5) and percentage of Restrictions (PR 30% and 70%) in Fig.3.73, Fig.3.74, Fig.3.75 and Fig.3.76. From the said figures, it is observed that the variation patterns of WSS are almost similar for all the considered type of pulsatile flow conditions with any combination value of Reynolds number, percentage

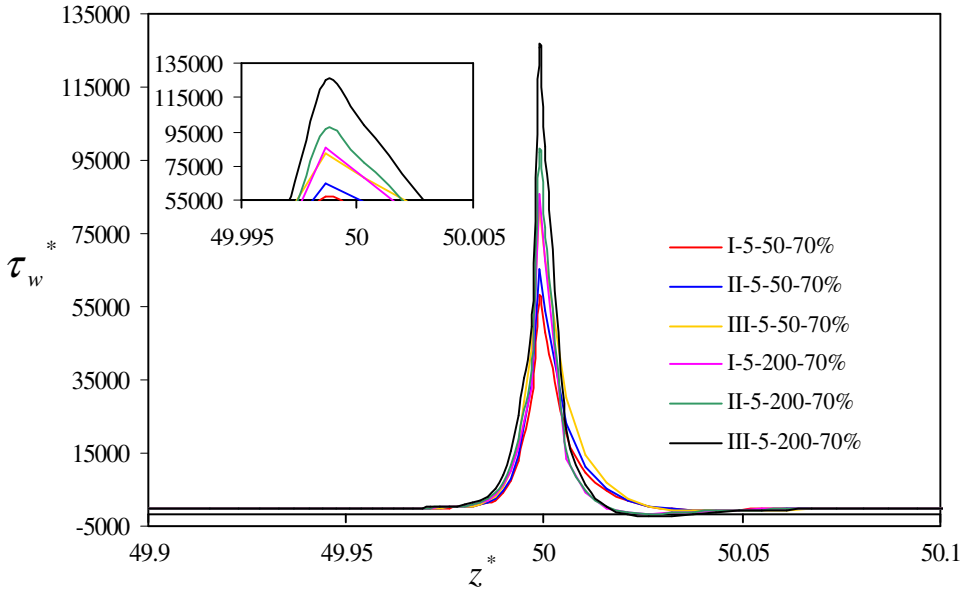

Figure 3.75: Variation of peak WSS at stenotic zone along axial direction for different Re for PR70% and Wo5 for different pulsatile flows

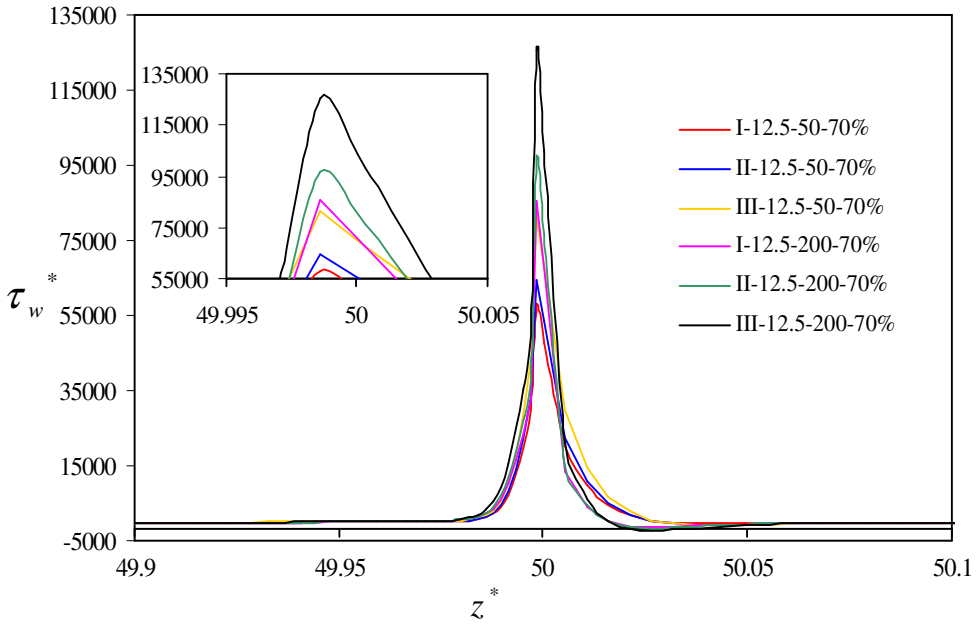

Figure 3.76: Variation of peak WSS at stenotic zone along axial direction for different Re for PR70% and Wo12.5 for different pulsatile flows

of restriction and Womersley number. The details of distribution of peak wall shear stress for simple pulsatile flow have already been discussed in the section 3.1 (Effect of Reynolds number for simple pulsatile flow). The magnitudes of peak time-averaged wall shear stress for all three pulsatile flows with different combination

cases of Reynolds number, Womersley numbers and percentage of restrictions are tabulated in the Table 3.2. On viewing the said table, the comparisons of peak wall shear stress magnitudes for different pulsatile flows can be assessed clearly. At any combination case of Reynolds number, percentage of restriction and Womersley number, the peak WSS for realistic pulsatile flow (i.e. profile III) is much higher than the peak WSS with either of the simple pulsatile flow (i.e. profile-I) or physiological pulsatile flow (i.e. profile-II) while the second highest peak wall shear stress is achieved by physiological pulsatile flow. As a result, the damaging chance of artery wall is more for physiological pulsatile flow. From the table, it is also observed that the peak WSS increases with increase in Reynolds number for all the considered type of pulsatile flows at any combination case of percentage of restriction and Womersley number. From the table, it can be commented that peak wall shear stress is greatly influenced by the percentage of restriction and it increases with the increase in percentage of restriction increases for all considered pulsatile flows with any combination of Reynolds number and Womersley number. Therefore, from the above observation, it may be remarked that the chance of artery wall damage enhances with increase in Reynolds number of flow or percentage of restriction of flow area while other conditions remain unchanged for all type of pulsatile flows. From the said figures and the table, it is noted that the impact of Womersley number is not so significant for all considered pulsatile flows at any combination case of Reynolds number and percentage of restriction, but the peak WSS decreases with increase in Womersley number. Thus the damaging chance of artery wall is less for higher Womersley number for all considered pulsatile flow conditions.

The variation of low time-averaged wall shear stress along axial direction of the considered arterial length is shown in Fig.3.77, Fig.3.78, Fig.3.79 and Fig.3.80 for all considered pulsatile flows with different combination of Reynolds numbers, Womersley numbers and percentage of restrictions. All the said figures depict that the wall shear stress changes its direction from positive to negative when the flow leaves the stenosis and from negative to positive at the downstream flow. The maximum low wall shear stress is estimated from earlier mentioned figures and tabulated in Table 3.2 for each of combination cases. From the table, it is observed that magnitudes of maximum low WSS are different for different pulsatile flows. At low Womersley number, lowest magnitude of maximum low WSS occurs at simple pulsatile flow and highest magnitude takes place in case of realistic pulsatile flow. But the

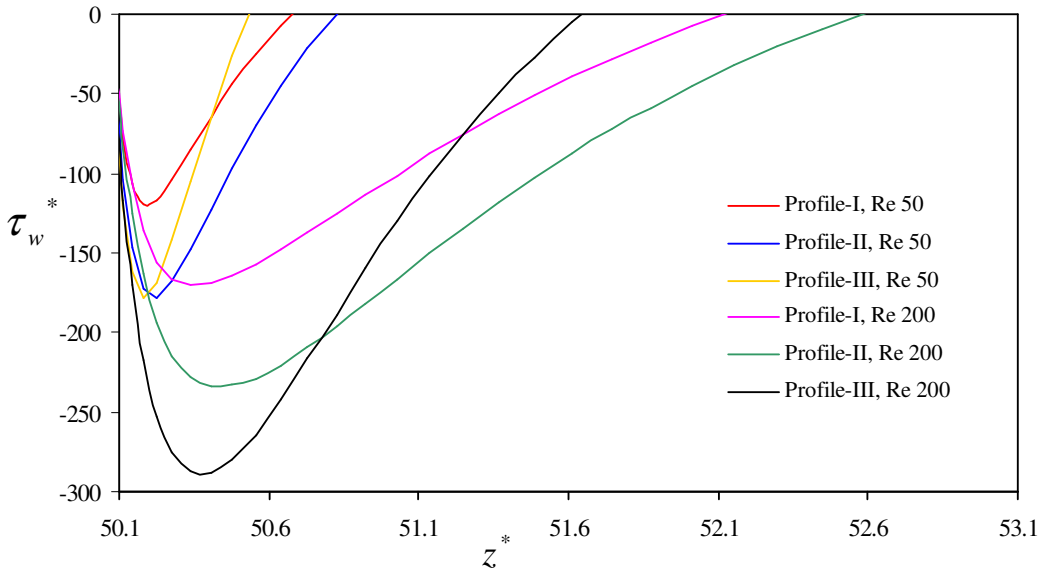

Figure 3.77: Variation of low WSS at post-stenotic zone along axial direction for different Re for PR30% and Wo5 for different pulsatile flows

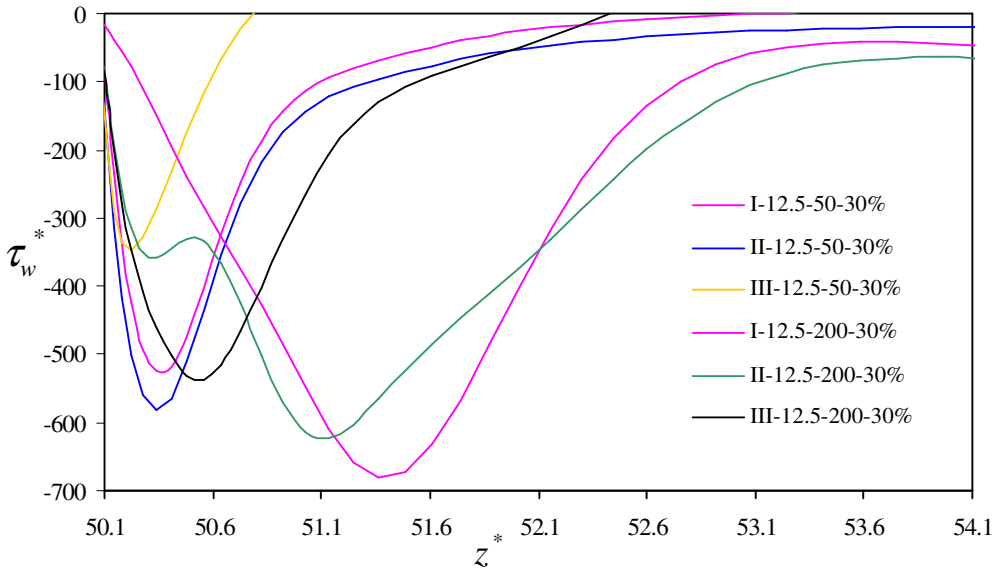

Figure 3.78: Variation of low WSS at post-stenotic zone along axial direction for different Re for PR30% and Wo12.5 for different pulsatile flows

lowest magnitude of maximum low WSS is noticed for realistic pulsatile flow at high Womersley number. As a result, it can be said that the chance of progression of the disease, atherosclerosis is high for pulsatile profile-III at low Womersley number. The chance of progression of the atherosclerosis is high for both simple and physiological pulsatile flows at high Womersley number. From the table, it may also be said that maximum low WSS always increases with increase in Reynolds number, percentage

of restriction and Womersley number separately while other conditions remain unchanged for all the pulsatile flows. Therefore, it may be mentioned that the chances of progression of the atherosclerosis increase with increase in Reynolds number, percentage of restriction and Womersley number for all considered pulsatile profiles.

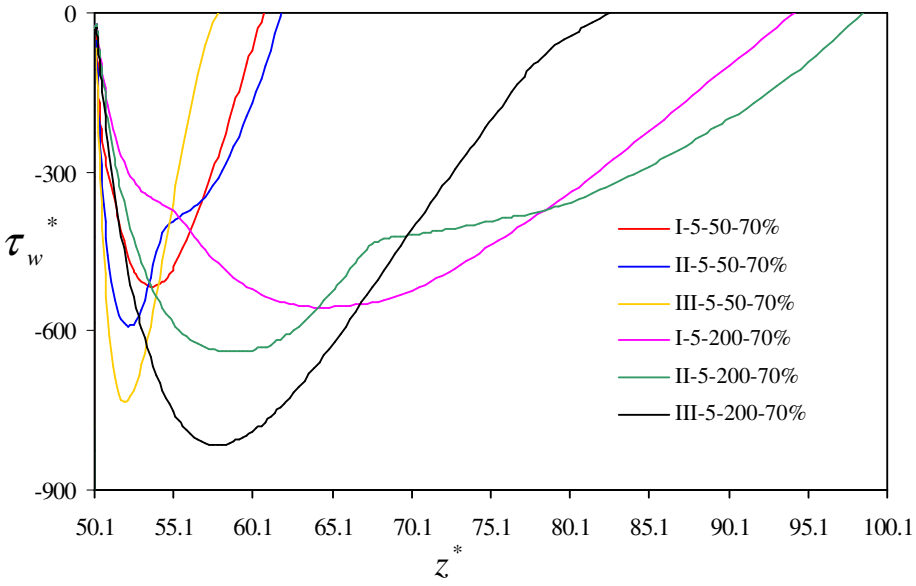

Figure 3.79: Variation of low WSS at post-stenotic zone along axial direction for different Re for PR70% and Wo5 for different pulsatile flows

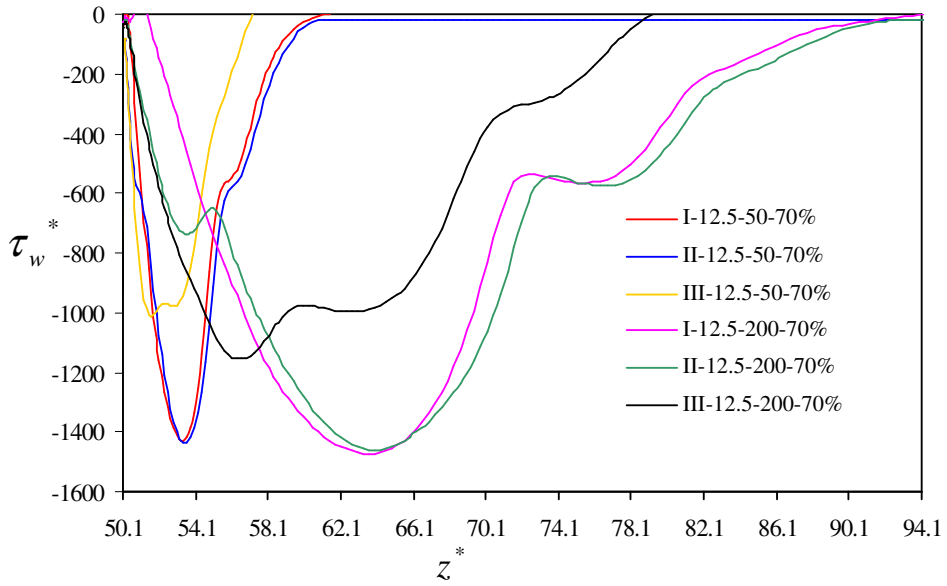

Figure 3.80: Variation of low WSS at post-stenotic zone along axial direction for different Re for PR70% and Wo12.5 for different pulsatile flows

Table 3.2: Peak TAWSS and maximum low TAWSS for different combination cases of pulsatile profiles, Reynolds number, Womersley numbers and percentage of Restrictions

Sl. No.	Combination case of profile type, Re, Wo and PR				Peak TAWSS	Maximum low TAWSS
	Profile type	Re	Wo	PR		
1	I	50	5	30%	3048.29	-119.74
2	II	50	5	30%	3373.76	-178.01
3	III	50	5	30%	4585.78	-178.53
4	I	200	5	30%	4584.02	-168.69
5	II	200	5	30%	5128.74	-233.64
6	III	200	5	30%	6788.11	-288.61
7	I	50	12.5	30%	2905.20	-524.70
8	II	50	12.5	30%	3050.92	-582.85
9	III	50	12.5	30%	4208.43	-348.41
10	I	200	12.5	30%	4510.10	-680.48
11	II	200	12.5	30%	4888.42	-624.14
12	III	200	12.5	30%	6655.42	-536.50
13	I	50	5	70%	57679.36	-515.58
14	II	50	5	70%	65161.31	-590.30
15	III	50	5	70%	82088.45	-734.15
16	I	200	5	70%	85636.94	-555.23
17	II	200	5	70%	97044.73	-639.10
18	III	200	5	70%	125640.45	-815.39
19	I	50	12.5	70%	57783.90	-1426.07
20	II	50	12.5	70%	64360.47	-1435.31
21	III	50	12.5	70%	81536.46	-1013.89
22	I	200	12.5	70%	85709.13	-1472.33
23	II	200	12.5	70%	96563.76	-1460.22
24	III	200	12.5	70%	125344.10	-1154.96

3.4.4 Oscillatory shear index

Looking on the instantaneous streamline patterns presented in the sub-section 3.4.2, it can be mentioned that the instantaneous wall shear stresses at any particular location along the axial direction of arterial length are not same for all the time steps of a cardiac cycle for each type of the considered pulsatile flow conditions with any combination of the considered cases of Reynolds number, percentage of restriction and Womersley number. Thus it is evident that there exists oscillatory wall shear stress in the flow through artery for all the considered combination cases of pulsatile flow conditions. In order to get a clear understanding on oscillatory wall shear stress conditions, oscillatory shear index at the stenotic and post-stenotic zone along the arterial length are analyzed for different pulsatile flow profiles.

The distribution pattern of the OSI along axial direction of arterial length in the stenotic zone and post stenotic zone is shown in Fig.3.81, Fig.3.82, Fig.3.83 and Fig.3.84 for all combination cases of three different pulsatile flow conditions with Reynolds number, percentage of restriction and Womersley number. The figure clearly indicates that the first peak OSI just immediate after throat of the stenosis and the location of time-averaged reattachment point i.e. second peak OSI at the downstream of stenosis are greatly influenced by the type of pulsatile flow profiles with all combinations of Reynolds number, percentage of restriction and Womersley number. The time-averaged reattachment length is measured located from the throat of stenosis of the considered modeled geometry. The first peak OSI values and the magnitudes of reattachment length for different combination cases are presented in the Table 3.3. The table clearly indicates that the largest recirculation length is achieved by physiological pulsatile flow and the second longest recirculation length is achieved by simple pulsatile flow. The recirculation length for realistic pulsatile flow is very small in comparison to other two types of flow for all the combination cases. Again, from the table, it is also observed that the first peak OSI value is comparatively low for realistic pulsatile flow for almost all the considered combination cases. Thus it may be said that the realistic pulsatile flow is always less prone to the disease atherosclerosis.

From the figures and table, it can be stated that the recirculation length always increases with increase in Reynolds number for all the combination cases of pulsatile flows. The peak OSI also increases with increase in Reynolds number for all types of pulsatile flow for the case of severe stenosis. The probable reason of this phenomenon

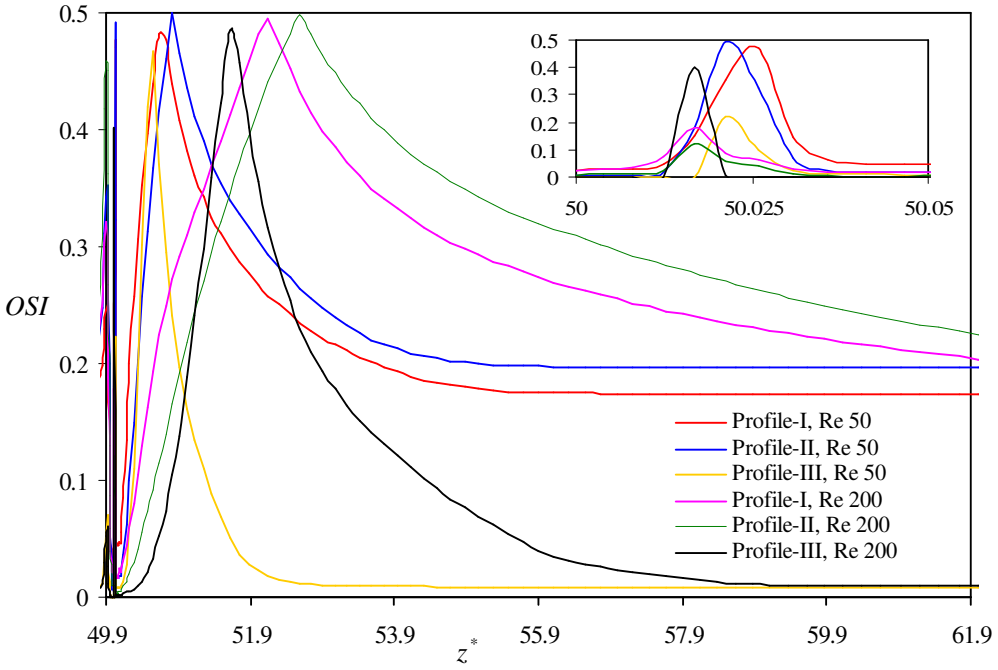

Figure 3.81: Variation of OSI at stenotic and post stenotic zone along axial direction for different Re for Wo5 and PR30% for different pulsatile flows

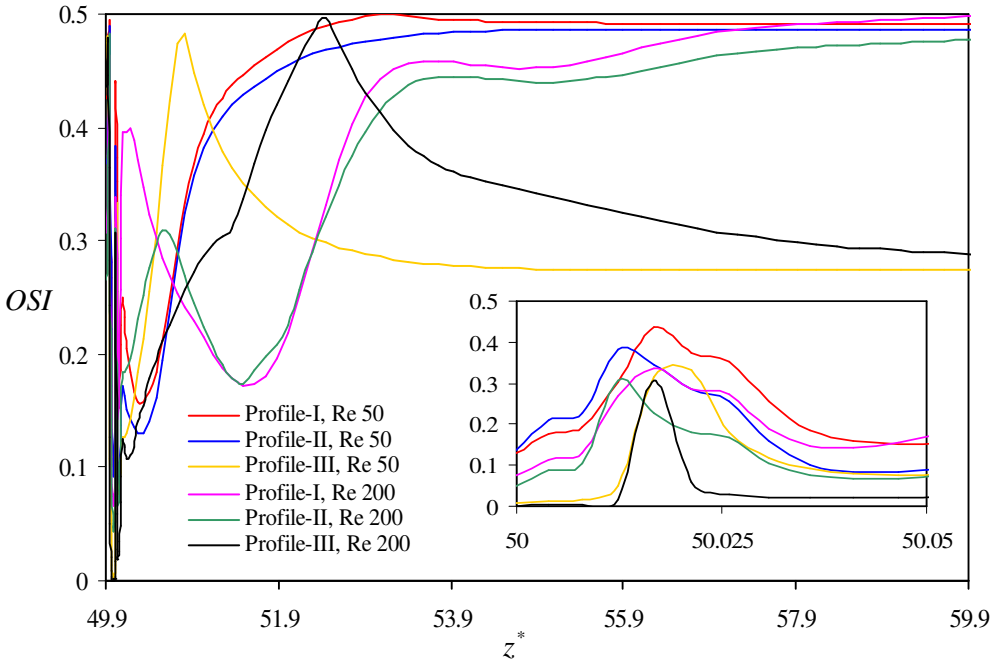

Figure 3.82: Variation of OSI at stenotic and post stenotic zone along axial direction for different Re for Wo12.5 and PR30% for different pulsatile flows

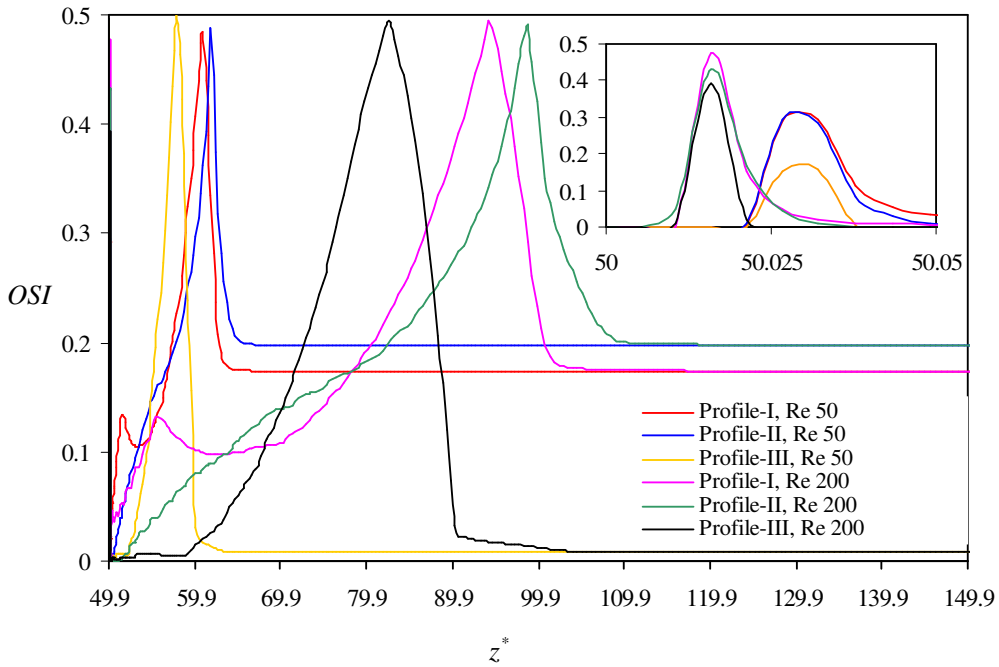

Figure 3.83: Variation of OSI at stenotic and post stenotic zone along axial direction for different Re for Wo5 and PR70% for different pulsatile flows

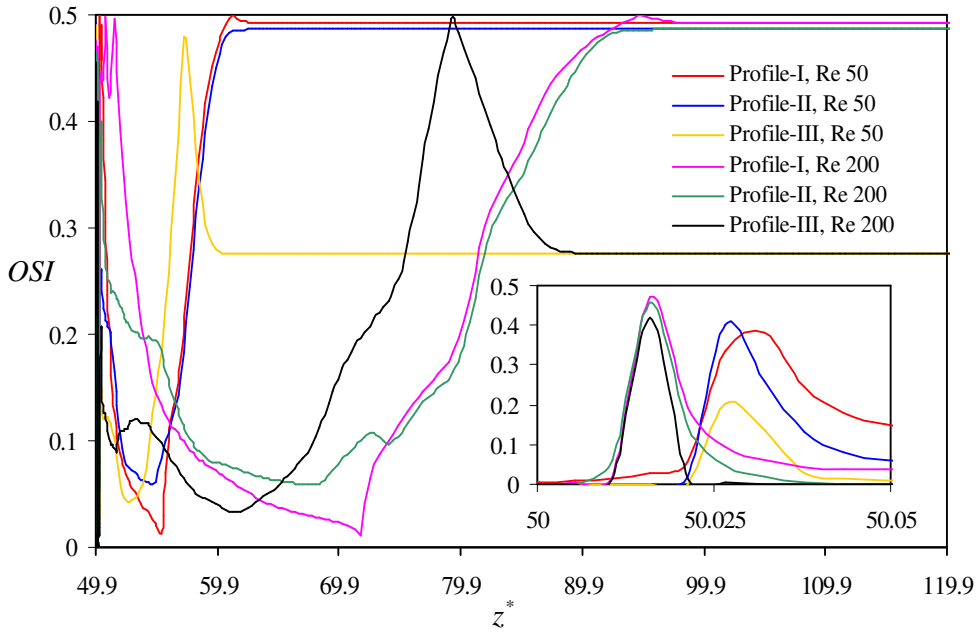

Figure 3.84: Variation of OSI at stenotic and post stenotic zone along axial direction for different Re for Wo12.5 and PR70% for different pulsatile flows

Table 3.3: First peak OSI and reattachment length for different combination cases of pulsatile profiles, Reynolds number, Womersley numbers and percentage of Restrictions

Sl. No.	Combination case of profile type, Re, Wo and PR				First peak OSI	Reattachment length
	Profile type	Re	Wo	PR		
1	I	50	5	30%	0.47	0.64
2	II	50	5	30%	0.49	0.83
3	III	50	5	30%	0.22	0.56
4	I	200	5	30%	0.18	2.15
5	II	200	5	30%	0.12	2.60
6	III	200	5	30%	0.40	1.61
7	I	50	12.5	30%	0.44	3.07
8	II	50	12.5	30%	0.38	6.11
9	III	50	12.5	30%	0.33	0.82
10	I	200	12.5	30%	0.33	10.49
11	II	200	12.5	30%	0.31	14.29
12	III	200	12.5	30%	0.31	2.44
13	I	50	5	70%	0.29	10.89
14	II	50	5	70%	0.29	11.78
15	III	50	5	70%	0.15	7.87
16	I	200	5	70%	0.47	44.11
17	II	200	5	70%	0.43	48.66
18	III	200	5	70%	0.39	32.36
19	I	50	12.5	70%	0.38	11.18
20	II	50	12.5	70%	0.40	12.39
21	III	50	12.5	70%	0.20	7.11
22	I	200	12.5	70%	0.47	44.61
23	II	200	12.5	70%	0.46	46.11
24	III	200	12.5	70%	0.42	29.33

has already been stated in sub-section 3.1.4. Therefore, from the overall observation, it may be commented that chance of formation of atherosclerosis is high for higher Reynolds number for all the pulsatile flows.

From Table 3.3, it can be said that the first peak OSI increases with increase in Womersley number for most of the cases. Thus it may be mentioned that the chance of the development and localization of the disease, atherosclerosis, increases with increase in Womersley number. The estimated reattachment length also increases with increase in Womersley number for all pulsatile flows. The probable reason of this phenomenon has already been discussed in sub-section 3.3.4. So the chance of plaque deposition at the inner wall of artery due to existence of recirculation zone increases with increase in Womersley number for all three pulsatile flows.

Increase or decrease of first peak OSI does not obey any proportionality rule with percentage of restriction, but higher percentage of restriction always leads to longer recirculation length for all combination cases. The probable cause of this phenomenon has already been explained in sub-section 3.2.4. Thus it may be concluded that restriction increases the chance of formation of atherosclerosis.

CHAPTER 4: CONCLUSIONS AND FUTURE SCOPE OF WORK

4.0 CONCLUSIONS AND FUTURE SCOPE OF WORK

4.1 Conclusions

In this present work, a numerical study of blood flow through different bell shaped stenosed arteries with five different percentage of restrictions (PR= 30%, 40%, 50%, 60% and 70% by diameter) has been carried out. Three flow profile conditions (simple pulsatile profile, physiological pulsatile profile and realistic pulsatile profile) have been considered and the profiles have been prescribed at inlet in each case. This study has also considered four different Reynolds numbers (Re=50, 100, 150 and 200) and four different Womersley numbers (Wo= 5, 7.5, 10 and 12.5) of flow. The different flow characteristics such as wall pressure, streamline contour, peak wall shear stress, low wall shear stress and oscillatory shear index, which are related to the initiation, progression and formation of the disease, atherosclerosis, have been analyzed in this thesis.

At first, a systematic study of simple pulsatile flow has been made on the effect of Reynolds number, percentage of restriction and Womersley number on the flow characteristics for different combination cases. After that, effect of different pulsatile blood flow conditions in stenosed artery has been studied to analyze the influence of different pulsatile flow conditions along with the effect of Reynolds numbers, percentage of restrictions and Womersley numbers on the key flow characteristics. The observations of results have been utilized to focus on the impact of the flow characteristics on the initiation, progression, formation and development of the disease, atherosclerosis.

The wall pressure drop strongly is influenced by types of pulsatile flow condition (simple pulsatile, physiological pulsatile and realistic pulsatile). For any combination case of Reynolds number, percentage of restriction and Womersley number, the largest pressure drop is observed for physiological pulsatile flow condition while the realistic pulsatile flow condition has the least pressure drop. The chances of atherosclerotic plaque deposition are more for physiological pulsatile flow and less for realistic pulsatile flow for each combination case of Reynolds number, Percentage of restriction and Womersley number.

For all Types of pulsatile flow condition, with an increase in Reynolds number, the wall pressure drop increases for each combination case of percentage of restriction and Womersley number. As a result, the chances of tearing action and plaque deposition increase with increase in Reynolds number for any particular combination case of mild stenosis, severe stenosis, low pulsality of flow and high pulsality of flow for all pulsatile flow conditions.

Wall pressure drop increases slowly for mild to moderate stenosis, whereas from moderate to severe stenosis condition, this pressure drop increases markedly for any particular combination case of mild stenosis, severe stenosis, low pulsality of flow and high pulsality of flow for all pulsatile flow conditions . As a result, the chances of plaque deposition increase with higher percentage of restriction for any combination case of low Reynolds number flow, high Reynolds number flow, low pulsality of flow and high pulsality of flow for all pulsatile flow conditions.

For all pulsatile flow conditions, for any combination case of percentage of restriction and Reynolds number, the effect of wall pressure is not so evidenced, but the wall pressure drop always increases with increase in Womersley number. So the chance of plaque development is more for high value of Womersley number for all pulsatile flow conditions for each combination case of severe stenosis, mild stenosis, high Reynolds number and low Reynolds number.

At the time step t/T=0, for flow through mild stenosis, the smaller flow separation zone is found for simple pulsatile flow condition while large flow separation zone is found for other two flow conditions. The chance of development of atherosclerosis is more for physiological and realistic pulsatile flows in comparison to simple pulsatile flow at the said time step for the case of mild stenosis. At time step t/T-0, for flow through severe stenosis, lager flow separation zone is found for realistic pulsatile flow at low Womersley number while the size of flow separation zone is almost same for all pulsatile flow at high Womersley number. At the step t/T=0, for the case of severe stenosis, the chance of development of atherosclerosis is more for realistic pulsatile flow with lower value of Womersley number and is more or less same for all pulsatile flow conditions for higher Womersley number.

At time step t/T=0.25, for flow through mild stenosis, the size of flow separation zone is almost same for all the pulsatile flow condition. At the same time step, flow through severe stenosis, the size of flow separation zone is larger for simple pulsatile flow. At t/T=0.25, the chance of development of atherosclerosis is more or

less same for all pulsatile flow conditions for mild stenosis and is more for simple pulsatile flow for severe stenosis.

At t/T=0.50, for flow through both mild and severe stnoses, the size of flow separation zone is larger for physiological pulsatile flow condition. The chance of development of atherosclerosis is more for physiological pulsatile flow at t/T=0.50 for both severe stenosis and mild stenosis.

At time step t/T=0.75, for flow through mild stenosis, the size of flow separation zone is larger for simple pulsatile flow condition. At the same time step, flow through severe stenosis, the size of flow separation zone is almost same for all the pulsatile flow conditions. At time step t/T=0.75, the chance of development of atherosclerosis is more for simple pulsatile flow for mild stenosis case and is almost same for all the pulsatile flow conditions for the case of severe stenosis.

Size of the flow separation zone always increases with increase in Reynolds number for each time phase for any combination case of percentage of restriction and Womersley number for all pulsatile flow conditions. The chances of atheromatous plaque formation increases with the increase in Reynolds number and thereby lead to grow more severe stenosis at the post stenotic zone for any particular combination case of mild stenosis, severe stenosis, low pulsality of flow and high pulsality of flow situations.

Size of the flow separation zone always increases with increase in percentage of restriction for every time phase and any combination case of Reynolds number and Womersley number for all pulsatile flow conditions. Consequently the chance of plaque formation increases with increase in percentage of restriction for each combination case of Reynolds number and Womersley number.

For the flow through mild stenosis, with increase in Womersley number, the strength of the flow separation zone decreases at every time step. The possibility of plaque deposition is higher for low value of Womersley number for the case of mild stenosis at any time step for all pulsatile flow conditions.

For the flow through severe stenosis, the strength of the flow separation zone decreases with increase in Womersley number at the time steps of t/T=0.25 and t/T=0.5 for each pulsatile flow conditions. Therefore, possibility of plaque deposition is higher for low value of Womersley number for the case of severe stenosis at time steps of t/T=0.25 and t/T=0.5.

The strength of the flow separation zone increases with increase in value of Womersley number at the time steps t/T=0 and t/T=0.75 for flow through severe stenosis in all considered pulsatile flow conditions. The possibility of plaque deposition is higher for high value of Womersley number for the case of severe stenosis at time steps t/T=0 and t/T=0.75.

At any combination case of Reynolds number, percentage of restriction and Womersley number, the peak WSS for realistic pulsatile flow condition is much higher than the peak WSS with either of the simple pulsatile flow condition or physiological pulsatile flow condition. Whereas, the second highest peak wall shear stress is found for physiological pulsatile flow condition. The damaging chance of artery wall and subsequently chance of initiation of atherosclerosis are more for realistic pulsatile flow condition for each combination case of Reynolds number, percentage of restriction and Womersley number.

The Peak wall shear stress always increases with increase in Reynolds number for all combination cases of percentage of restriction and Womersley number for all pulsatile flow conditions. Higher Reynolds number augments the chance of initiation of atherosclerosis in terms of damaging the endothelial cell due to high level of wall shear stress.

The peak wall shear stress increases with the increase in percentage of restriction for all considered pulsatile flows for each combination case of Reynolds number and Womersley number. The chance of artery wall damage becomes more with increase in percentage of restriction of flow area for all combination cases of Reynolds number and Womersley number for all type of pulsatile flows.

For all considered pulsatile flow conditions at any combination case of Reynolds number and percentage of restriction, the peak WSS slightly decreases with increase in Womersley number. The damaging chance of artery wall is less for higher Womersley number for all pulsatile flow conditions for each combination case of Reynolds number and Womersley number.

At low Womersley number, the lowest magnitude of maximum low WSS occurs at simple pulsatile flow and the highest magnitude takes place in case of realistic pulsatile flow. But, at high Womersley number, the lowest magnitude of maximum low WSS is noticed for realistic pulsatile flow. The chance of progression of the disease, atherosclerosis is high for realistic pulsatile flow condition at low Womersley number. The chance of progression of the atherosclerosis, in terms of the

mass transportation across the arterial wall and long staying time for platelet endothelium interaction, is high for both simple and physiological pulsatile flows at high Womersley number.

The maximum low WSS always increases with increase in Reynolds number, percentage of restriction and Womersley number separately while other conditions remain unchanged for all the pulsatile flow conditions. The chances of progression of the atherosclerosis increase with increase in Reynolds number, percentage of restriction and Womersley number for all considered pulsatile profiles.

Two peak value of OSI are found in stenotic and post-stenotic zone in case of the considered pulsatile flow conditions. The first peak OSI is found at just immediate after the throat of stenosis and the second one (i.e. reattachment point) at far downstream of post-stenotic zone.

The first peak OSI value is low for realistic pulsatile flow for almost all the considered combination cases of Reynolds number, percentage of restriction and Womersley number while it is compared to the simple pulsatile flow and physiological pulsatile flow. The realistic pulsatile flow is always less prone to the disease atherosclerosis for each combination case of Reynolds number, percentage of restriction and Womersley number.

The first peak OSI also increases with increase in Reynolds number, percentage of restriction and Womersley number for all types of pulsatile flow. The chance of localization of atherosclerosis is high for higher Reynolds number, percentage of restriction and Womersley number.

The recirculation length for realistic pulsatile flow is very small in comparison to other two types of pulsatile flow for all the combination cases Reynolds number, percentage of restriction and Womersley number. The chance of development of atherosclerosis is least for realistic pulsatile flow condition among all the considered flow conditions.

The recirculation length always increases with increase in Reynolds number, percentage of restriction and Womersley number. The chances of atheromatous plaque deposition at the inner wall increase with increase in Reynolds number, percentage of restriction and Womersley number for all pulsatile flow conditions.

Our own developed numerical code may be considered as a useful predictive tool for study of the pulsatile flow through stenosed artery. It is noteworthy to mention here that the outcomes of present work may enrich the knowledge in the area

of cardiovascular disease (CVD) and could also be utilized for better design of medical tool to detect early atherosclerosis as well as severity of atherosclerosis. The systematic study of pulsatile flow may help the medical people to take better decision upon the treatment management of atherosclerosis such as exercise, medication, surgery etc.

4.2 Future Scope of Work

The present work can be extended to investigate blood flow through arteries more realistic way. The arterial walls in real biological system are compliant, future simulation may include nonlinear and elastic boundary materials. In this thesis work, axisymmetric flow model has been considered. Consideration of asymmetrical condition may give more realistic results. Only one single stenosis has been considered in this study. Investigation of the effects of multiple stenoses in a single circular tube can be another interesting topic. In the present study, a laminar pulsatile flow is studied, however, in certain parts of the artery system, flow exhibits a turbulent behaviour. So a numerical study on the turbulent flow model for pulsatile flow may be carried out in the future. The blood is considered as Newtonian fluid in the present work. To get more correct results, non–Newtonian behaviour of the blood should be included in future study. In the present study of pulsatile flow through stenosed artery, the heat transfer analysis has not been done. So analysis on the effect of temperature dependent viscosity on the flow and heat transfer characteristics on the stenosed artery may be carried out in future study. The effect of asymmetric shape of the stenosis on skin friction, Nusselt number and size of the vortices may also be investigated in future.

REFERENCES

Ahmed, S. A. and Giddens, D. P., 1983, "Velocity measurements in steady flow through axisymmetric stenoses at moderate Reynolds numbers", Journal of Biomechanics, 16(7):505-516.

Ahmed, S. A. and Giddens, D. P., 1983, "Flow Disturbance measurements through a constricted tube at moderate Reynolds numbers", Journal of Biomechanics, 16(12):955-963.

Ahmed, S. A. and Giddens, D. P., 1984, "Pulsatile poststenotic flow studies with laser Doppler anemometry," Journal of Biomechanics, 17(9): 695–705.

Amornsamankul, S., Wiwatanapataphee, B., Wu, Y. H. and Lenbury, Y., 2006, "Effect of non-Newtonian behaviour of blood on pulsatile flows in stenotic arteries", International Journal of Biomedical Sciences, 1(1):306-1216.

Andersson, H. I., Halden, R. and Glomsaker, T., 2000, "Effects of surface irregularities on flow resistance in differently shaped arterial stenoses", Journal of Biomechanics, 33:1257-1262.

Ang, K. C. and Majumdar, J. N., 1997, "Mathematical modelling of three-dimensional flow through an asymmetric arterial stenosis", Mathl. Comput. Modelling, 25(1):19-29.

Azuma, T. and Fulkushima, T., 1976, "Flow patterns in stenotic blood vessel models", Biorheology, 13:337-355.

Azwadi, S. N. and Salehi M., 2012, "Prediction of flow characteristics in stenotic artery using cip schemec", S.N, International Journal of Mechanical and Materials Engineering, 7(1):101–106.

Back, L. H. and Banerjee, R. K., 2000, "Estimated flow resistance increase in a spiral human coronary artery segment", Journal of Biomechanical Engineering, 122:675-677.

Bathe, M. and Kamm, R. D., 1999, "A Fluid-Structure interaction finite element analysis of pulsatile blood flow through a compliant stenotic artery," J. Biomech. Eng., 121:361-369.

Bit, A. and Chattopadhyay, H., 2014, "Numerical investigations of pulsatile flow in stenosed artery" Acta of Bioengineering and Biomechanics, 16(4):33-44.

Buchanan Jr. J. R., Kleinstreuer, C. and Comer, J. K., 2000, "Rheological effects on pulsatile hemodynamics in a stenosed tube", Computers & Fluids, 29:695-724.

Caro, C. G., F-G, J. M. and Schroter, R. C., 1971, "Atheroma and arterial wall shear: observation, correlation, and proposal for a shear dependent mass transfer mechanism for atherogenesis", Proc R Soc Lond [Biol], 117:109-159.

Caro, C. G. Pedley, T. J., Schroter, R. C. and Seed, W. A., "The mechanics of the circulation, oxford medical", New York, NY, USA, 1978.

Cassanova, R. A. and Giddens, D. P., 1978, "Disorder distal to modeled stenoses in steady and pulsatile flow", journal of biomechanics, 11(10-12):441-453.

Chaichana T., Sun Z. and Jewkes J., 2012, "Computational fluid dynamics analysis of the effect of plaques on the left coronary artery", Comput Math Methods Med., 2012:1–9.

Cheng, L. C., Clark, M. E. and Robertson, J. M., 1972, "Numerical calculations of oscillating flow in the vicinity of square wall obstacles in plane conduits", Journal of Biomechanics, 5:467-484.

Cheng, L. C., Robertson, J. M. and Clark, M. E., 1974, "Calculation of plane pulsatile flow past wall obstacles", Computers & Fluids, 2:363-380.

Cho, Y. I. and Kensey, K. R., 1991, "Effects of the non-Newtonian viscosity of blood flows in a diseased arterial vessel, part-1: steady flows", Biorheology, 28:241-262.

Dabagh, M., Takabe, W., Jalali, P.,White, S. and Jo, H., 2013, "Hemodynamic features in stenosed coronary arteries: cfd analysis based on histological images",Journal of Applied Mathematics, Article ID 715407, 11 pages.

Deshpande, M. D., Giddens, D. P. and Mabon, R. F., 1976, "Steady laminar flow through modelled vascular stenoses", Journal of Biomechanics, 9(4):165-174.

Fry, D. L., 1968, "Acute vascular endothelial changes associated with increased blood velocity gradients". Circ. Res., 12:165-97.

Fry, D. L., 1969, "Certain histological and chemical responses of the vascular interface to acutely induced mechanical stress in the aorta of the dog", Circ. Res., 24(1):93-108.

Fung, Y. C. 1997 "Biomechanics: Circlulation", 2nd edn. Springer.

Ganong, William F., 2001, "Review of Medical Physiology", Appleton.

Gay, M. and Zhang, L. T., 2008, "Numerical studies of blood flow in healthy, stenosed, and stented carotid arteries", Int. J. Numer. Meth. Fluids, DOI: 10.1002/fld1966.

Gessner, F. B., September 1973, "Haemodynamic theories of atherogenesis", Circulation research, 3:259-266.

Gupta, A. K. and Agrawal, S. P., 2015, "Computational modeling and analysis of the hydrodynamic parameters of blood through stenotic artery" Procedia Computer Science, 57:403 – 410.

Guyton, A. C., 1976, "Textbook of medical physiology", 4th ed. W. B. Saunders Co., Philadelphia.

Hasan, A.B.M. T. and Das, D. K., 2008, "Numerical simulation of sinusoidal fluctuated pulsatile laminar flow through stenotic artery", Journal of Applied Fluid Mechanics, 1(2):25 -35.

Haque, M. R. and Hasan, A. B. M. T., 2015, "Flow characteristic in an eccentric arterial stenosis with variable pulsatile flow waveforms", Procedia Engineering, 105:902 – 910.

He, X. and Ku, D. N., 1996, "Pulsatile flow in the human left coronary artery bifurcation: average conditions", Journal of biomechanical engineering, 118: 74-82.

Ishikawa, T., Guimaraes, L. F. R., Oshima, S. and Yamane, R., May 1998, "Effect of non-Newtonian property of blood on flow through a stenosed tube", Fluid Dynamics Research, 22(5):251-264.

Kamangar, S., Badruddin, I.A., Badarudin, A., Ahamad N.A., Govindaraju, K., Nik-Ghazali, N., Salman Ahmed, N.J. and Yunus Khan, T.M., 2017, "The Influence of Geometrical Shapes of Stenosis on the Blood Flow in Stenosed Artery", Sains Malaysiana, 46(10): 1923–1933.

Khalifa, A. M. A. and D. P. Giddens, 1981, "Characterization and evolution of poststenotic flow disturbances", J. Biomechanics, 14(5):279-296.

Kinght, J., Olgac, U., Saur, S. C., Poulikakos, D. W., Cattin, P. C. and Kurtcuoglu, H. V., 2010, "Choosing the optimal wall shear parameter for the prediction of plaque location—A patient-specific computational study in human right coronary arteries", Atherosclerosis, 211:445-450.

Ku, D. N., Giddens, D. P., Zarins, C. K., and Glagoy, S., 1985, "Pulsatile flow and atherosclerosis in the human carotid bifurcation—positive correlation between plaque location and low and oscillating shear– stress", Arteriosclerosis, 5:293-302.

Ku., D. N., 1997, "Blood flow in arteries", Annu. Rev. Fluid Mech., 29:399-434.

Ku, D. N. and Wootton, D. M., 1999, "Fluid mechanics of vascular systems, diseases, and thrombosis", Annu. Rev. Biomed. Eng,1:299-329.

Layek, G. C., Mukhopadhaya, S. and Gorla, R. S. D., 2009, "Unsteady viscous flow with variable viscosity in a vascular tube with a double constriction", Int. J. Eng. Sci., 47:649-659.

Lee, J. S. and Fung, Y. C., 1970, "Flow in locally constricted tubes at low Reynolds number", J. appl. Mech., 37:9-16.

Lee, K. W. and Xu, X. Y., 2002, "Modelling of flow and wall behaviour in a mildly stenosed tube", Medical Engineering & Physics, 24:575-586.

Lee, S. E., Lee, S. W., Fischer, P. F., Bassiouny, H. S. and Loth, F., 2008, "Direct numerical simulation of transitional flow in a stenosed carotid bifurcation", J Biomech., 41:2551–2561.

Lee T. S., Liu, X., Li, G. C. and Low, H. T., 2007, "Numerical study on sinusoidal fluctuated pulsatile laminar flow through various constrictions", Commun Comput Phys, 2(1):99–122

Liepsch, D., Singh, M. and Lee, M., 1992, "Experimental analysis of the influence of stenotic geometry on steady flow", Biorheology, 29(4):419-31.

Liu, B., 2013, "The Wall shear stress of a pulsatile blood flow in a patient specific stenotic right coronary artery", Engineering, 5:396-399.

Liu, Guo-Tao., Wang, Xian-Ju., Ai, Bao-Quan. and Liu, Liang-Gang., August 2004, "Numerical study of pulsating flow through a tapered artery with stenosis", Chinese Journal of Physics , 42, No.4-1:401-409.

Long, Q., Xu, X. Y., Ramnarine, K. V. and Hoskins, P., October 2001, "Numerical investigation of physiologically realistic pulsatile flow through arterial stenosis", Journal of Biomechanics, 34(10):1229-1242.

MacDonald, D. A., 1979, "On steady flow through modelled vascular stenoses", J. of Biomechanics, 12:13-20.

Mamun, K., Ali, M. and Akhter, M. N., 2016, "Physiological non-Newtonian blood flow through single stenosed artery" Theoretical and Applied Mechanics, 43 (1):99–115.

Mandal, D. K. and Manna, N. K., 2011, "Influence of different bell-shaped stenoses on the progression of the disease, atherosclerosis", Journal of Mechanical Science and Technology, 25(8):1933-1947.

Mandal, M. S., Mukhopadhyay, S. and Layek, G.C., 2012, "Pulsatile flow of an incompressible, inhomogeneous fluid in a smoothly expanded vascular tube", International Journal of Engineering Science, 57:1–10.

McDonald, D. A., 1974, "Blood Flow in Arteries", Camelot, Baldwin Park, CA.

Mehrabi, M. and Setayeshi, S., 2012, "Computational fluid dynamics analysis of pulsatile blood flow behavior in modelled stenoses vessel with different severities", Math. Probl. Eng., 2012:1–13.

Misra, J. C., Patra, M. K., and Misra, S. C., 1993, "A non-Newtonian fluid model for blood flow through arteries under stenotic conditions", Journal of Biomechanics, 26(9):1129-1141.

Misra, J. C. and Shit, G. C., 2006, "Blood flow through arteries in a pathological state: a theoretical study", International Journal of Engineering Science, 44:662-671.

Mills, C. J., Gabe, I. T., Gault, J. H., et al., 1970, "Pressure-flow relationships and vascular impedance in man," Cardiovascular Research, 4(4):405–417.

National Heart, Lung and Blood Institute, http://www.nhlbi.nih.gov/health/health-topics/topics/atherosclerosis.

Ojha, M., Cobbold, C., Johnston, K. W. and Hummel, R. L., 1989, "Pulsatile flow through constricted tubes: an experimental investigation using photochromic tracer methods," J. Fluid Mech., 203:173-197.

Ooi, A., Blackburn, H. M., Zhu, S., Lui , E. and Tae, W., 2007, "Numerical study of the behaviour of wall shear stress in pulsatile stenotic flows", 16th Australasian Fluid Mechanics Conference, 82-86.

Ortiz, J. P., Bessa, K. L., Legendre, D. F. and Prado, R. H. A., 2006, "Physiological pulsatile waveform through axisymmetric stenosed arteries: numerical simulation", ABCM Symposium Series in Bioengineering,Vol1.

Pedley, T. J., 1980, "The Fluid mechanics of large blood vessels", Cambridge University Press

Patankar, S. V., 1980, "Numerical heat transfer and fluid flow", Hemisphere Publication.

Pontrelli, G., 2001, "Blood flow through an axisymmetric stenosis", Proc. of the Instn. Mech. Engrs, Part-H, Journal of Engineering in Medicine, 215(1):1-10.

Prabhakaran, D., Jeemon, P. and Roy, A., 2016, "Cardiovascular diseases in india: current epidemiology and future directions" Circulation.,133(16):1605-20

Rabby, M. S., Shupti, S. P. and Molla, M. M., 2014, "Pulsatile non-Newtonian laminar blood flows through arterial double stenoses", Journal of Fluids, 2014:1–13.

Raines, J. K., 1972, "Diagnosis and analysis of arteriosclerosis in the lower limbs from the arterial pressure pulse", Ph.D. Thesis, Massachusetts Institute of Technology, Cambridge

Rathish Kumar, B. V. and Naidu, K. B., 1996, "A pulsatile suspension flow simulation in a stenosed vessel", Mathl. Comput. Modelling, 23(5):75-86.

Razavi, A., Shirani, E. and Sadeghi, M. R., 2011, "Numerical simulation of blood

pulsatile flow in a stenosed carotid artery using different rheological models",

Journal of Biomechanics, 44:2021–2030.

Richardson, L. F. and Gaunt, J. A., 1927, "The deferred approach to the limit. Part I. Single lattice. Part II. Interpenetrating lattices." Philosophical Transactions of the

Royal Society of London. Series A, Containing Papers of a Mathematical or Physical Character, 226:299-361.

Rikhtegar F, Knight JA, Olgac U, Saur SC, Poulikakos D, Marshall W, Cattin PC, Alkadhi H, Kurtcuoglu V., 2012, "Choosing the optimal wall shear parameter for the prediction of plaque location—a patient-specific computational study in human left coronary arteries. Atherosclerosis", 221(2):432–7.

Roache, P. J., 1994, "Perspective: A method for uniform reporting of grid refinement studies." Journal of Fluids Engineering, 116(3):405-41

Ryou, H. S., Kim, S., Kim, S.W. and Cho, S. W., 2012, "Construction of healthy arteries using computed tomography and virtual histology intravascular ultrasound", Journal of Biomechanics, 45:1612–1618.

Seeley, B. D. and Young, D. F., 1976, "Effect of geometry on pressure losses across models of arterial stenoses", Journal of Biomechanics, 32:439-48.

Shahed, S.R., Ali, M. and Islam, M.Q., 2013, "Numerical analysis of hemodynamic forces through stenotic artery", J. Mech Eng, IEB, 43:41-47

Sherwin, S. J., & Blackburn, H. M. (2005). Three-dimensional instabilities and transition of steady and pulsatile axisymmetric stenotic flows, J. Fluid Mech., 533, 297–327.

Siouffi, M., Deplano, V. and Pelissier, R., 1998, "Experimental analysis of unsteady flows through a stenosis", Journal of Biomechanics, 31:11-19.

Solzbach, U., Wollschlager, H., Zeiher, A. and Just, H., 1987, "Effect of stenotic geometry on flow behaviour across stenotic models", Medical and Biological Engineering and Computing, 25:543-550.

Stern, F., Wilson, R. V., Coleman, H. W., and Paterson, E. G., 2001, "Comprehensive approach to verication and validation of cfd simulations part 1: Methodology and procedures" Journal of Fluids Engineering, 123(4):793-802.

Stiehm, M., Wüstenhagen, C., Siewert, S., Grabow, N. and Schmitz, K., 2017, "Numerical simulation of pulsatile flow through a coronary nozzle model based on FDA´s benchmark geometry", Current Directions in Biomedical Engineering, 3(2): 775–778.

Stroud, J. S., Berger, S. A. and Saloner, D., 2000, "Influence of stenosis morphology on flow through severely stenotic vessels: implications for plaque rupture", Journal of Biomechanics, 33:443-455.

Tandom, P. N., Rana, U. V. S., Kawahara, M. and Katiyar, V. K., 1993, "A model for blood flow through a stenotic tube", Int. J. Biomed. Comput., 32:61-78.

Tandon, P. N. and Rana, U. V. S., 1995, "A new model for blood flow through an artery with axisymmetric stenosis", International Journal of Bio-Medical Computing, 38:257-267.

Taylor, C. A., Hughes, T. J. R. and Zarins, C. K., 1998, "Finite element modeling of blood flow in arteries", Comput Methods Appl Mech Eng, 158:155–196

Tu, C., Deville, M., Dheur, L. and Vanderschuren, L., October 1992, "Finite element simulation of pulsatile flow through arterial stenosis", Journal of Biomechanics, 25(10):1141-1152.

Tu, C. and Deville, M., 1996, "Pulsatile flow of Non-Newtonian fluids through arterial stenoses", Journal of Biomechanics, 29(7):899-908.

Tutty, O. R., 1992, "Pulsatile flow in a constricted channel", J Biomech. Eng., 114:50-54.

Varghese, S. S. and Frankel, S. H., 2003, "Numerical modeling of pulsatile turbulent flow in stenotic vessels", Journal of Biomechanical Engineering, 125: 445-460.

Wilcox, D. C., 2006, "Turbulence modeling for CFD, 3rd Ed.", DCW Industries, Inc..

Wille, S. O., 1980, "Pressure and flow in arterial stenosis simulated in mathematical models", Appl. Math. Modelling, 4:483-488.

Wiwatanapataphee, B., Poltem, D. Wu, Y. H. and Lenbury, Y., 2006, "Simulation of pulsatile flow of blood in stenosed coronary artery bypass with graft," Mathematical Biosciences and Engineering, vol. 3(2):71–383.

Womersley, J. R., 1955, "Method for the calculation of velocity, rate of flow, and viscous drag in arteries when the pressure gradient is known", J. Physiol, 127:553-563.

Wong, P. K. C., Johnston, K. W., Ethier, C. R. and Cobbold, S. C., 1991, "Computer simulation of blood flow patterns in arteries of various geometries", Journal of

Vascular Surgery, 14(5):658-667.

Wootton, D. M. and Ku, D. N., 1999, "Fluid mechanics of vascular systems, diseases, and thrombosis", Annual Review of Biomedical Engineering, 1:299–329.

Young, D. F. and Tsai, F. Y., July 1973, "Flow characteristics in models of arterial stenoses-i. steady flow", Journal of Biomechanics, 6(4):395-410.

Young, D. F. and Tsai, F. Y., September 1973, "Flow characteristics in models of arterial stenoses-ii. unsteady flow", Journal of Biomechanics, 6(5):547-559.

Zendehbudi, G. R. and Moayeri, M. S., 1999, "Comparison of physiological and simple pulsatile flows through stenosed arteries", Journal of Biomechanics, 32: 959-969.